University of Southern Queensland

Faculty of Engineering and Surveying

Lateral Earth Pressure Problems involved with Cantilever Retaining Structures and Stability of those Structures

Presented By

Mr Scott Clayton

In fulfilment of the requirements of

Bachelor of Engineering

October 2014

ABSTRACT

Retaining walls provide support for vertical or near vertical grade changes, while also preventing erosion or down slope movement. The backfill is usually associated with an amount of surface strip load, thereby creating lateral pressure which acts onto the non yielding retaining wall. The purpose of this thesis is to calculate mathematically and graphically the lateral earth pressures and how stability of a retaining structure is influenced by these pressures. Calculations are made which will involve Rankine earth pressure theory and Coulomb earth pressure theory. It also involves determining whether there are any correlations between the two theories. Either Rankine's or Coulomb's theory is then taken further to investigate the bearing, sliding and overturning with various soil foundation and backfill material. One of these theories will be representing 64 cases, all unique and presenting varying geometries and soil materials, while backfill is considered inclined throughout. From this outline, the factor of safeties is determined in order to identify the most effective scenario.

The upper and lower bound are calculated in order to determine the material base factor of safety. A numerical approach involving software known as OptumG2 is undertaken in order to calculate a strength reduction factor, involving both the upper and lower bound values of each case. From this, a material base factor of safety will be calculated, and an indirect comparison will be concluded.

LIMITATIONS OF USE

The Council of the University of Southern Queensland, its Faculty of Health, Engineering & Sciences, and the staff of the University of Southern Queensland, do not accept any responsibility for the truth, accuracy or completeness of material contained within or associated with this dissertation.

Persons using all or any part of this material do so at their own risk, and not at the risk of the Council of the University of Southern Queensland, its Faculty of Health, Engineering & Sciences or the staff of the University of Southern Queensland.

This dissertation reports an educational exercise and has no purpose or validity beyond this exercise. The sole purpose of the course pair entitled "Research Project" is to contribute to the overall education within the student's chosen degree program. This document, the associated hardware, software, drawings, and other material set out in the associated appendices should not be used for any other purpose: if they are so used, it is entirely at the risk of the user.

CERTIFICATION OF DISSERTATION

I certify that the ideas, designs and experimental work, results, analyses and conclusions set out in this dissertation are entirely my own effort, except where otherwise indicated and acknowledged.

I further certify that the work is original and has not been previously submitted for assessment in any other course or institution, except where specifically stated.

Scott Clayton

0061010140

ACKNOWLEDGEMENTS

This research was carried under the principal supervision of Dr Kazem Ghabraie. I would like to thank Dr Kazem Ghabraie not just for his time and support, but most of all his guidance, allowing me to coordinate my project especially in writing this report.

Table of Contents

Lateral Earth Pressures

LIST OF FIGURES

LIST OF TABLES

NOTATIONS

b_1 = Width of stem: top

b_2 = Width of toe

b_3 = Width of stem: bottom

b_{min} = minimum width of the heel (m)

B_{min} = width of the base slab (m)

c' = cohesion

c_w = wall adhesion

e = eccentricity

F_o = Factor of Safety against overturning

F_b = Factor of Safety against bearing

F_s = Factor of Safety against sliding

g = gravity (m/s^2)

G_{b_1} = weight of stem (kN)

G_{b_2} = weight of footing (kN)

G_{s_1} = weight of soil above footing (kN)

G_{s_2} = weight of inclined soil (kN)

h = Wall stem height

h_1 = Toe embedment depth

h_2 = Height of base

H_1 = Wall height, (m)

H_2 = Virtual wall height, (m)

H_L = critical height determined from the lower bound theorem (m)

H_L = critical height determined from the lower bound theorem (m)

K_o = earth pressure coefficient

K_a = Active pressure coefficient

K_p = Passive pressure coefficient

K_s = rest, active or passive earth pressure coefficient

q = uniform surcharge pressure, (Pa)

M_o = sum of the moments of forces acting on the retaining wall

M_R = sum of the moments of forces resisting overturning

N_c, N_q, N_y = bearing capacity factors

p_p = passive pressure (Pa)

P_a = total active force (Pa)

P_p = total passive force (Pa)

P_{max} = maximum pressure acting at the base slab (Pa)

R = reaction on the failure plane

R_H = sum of all the horizontal forces acting on the wall

R_V = sum of all the vertical forces acting on the wall

q_u = ultimate bearing capacity

z = depth from surface (m)

z_{0w} = depth of a water filled crack (m)

α = Slope angle (°)

ϕ' = soil friction angle

θ = Slip line angle (°)

γ = unit weight, (kN/m^3)

γ_b = unit weight of backfill, (kN/m^3)

γ_f = unit weight of foundation, (kN/m^3)

γ_d = actual soil density after construction completion, (kN/m^3)

$\gamma_{d(\min)}$ = loosest soil density, (kN/m^3)

ρ = density (kg/m^3)

δ = Wall friction angle

σ_1 = major principle stress

σ_3 = minor principle stress

$\sigma_o{}'$ = vertical earth pressure, (Pa)

σ_a' = active pressure (Pa)

$\sigma_h{}'$ = horizontal earth pressure, (Pa)

σ_p' = horizontal principle stress

$\sigma_c{}'$ = Preconsolidation pressure

$\lambda_{cs}\lambda_{qs}\lambda_{ys}$ = shape factors

$\lambda_{cd}\lambda_{qd}\lambda_{yd}$ = depth factors

$\lambda_{ci}\lambda_{qi}\lambda_{yi}$ = inclination factors

ψ = inclination of the load on the foundation with respect to the vertical

ABBREVIATIONS

OCR	–	Overconsolidated Ratio
FoS	–	Factor of Safety
SFoS	–	Strength Based Factor of Safety
ULS	–	Ultimate Limit State
GEO	–	Failure of the Ground
LB	–	Lower Bound
UB	–	Upper Bound
ULS	–	Ultimate Limit State
GFRP	–	Glass Fiber Reinforced Plastic
SEM	–	Scanning Electron Microscopy
EDX	–	Energy Dispersive X-ray

1. INTRODUCTION

A retaining wall is a structure constructed to primarily hold back masses of soil known as backfill (horizontal or inclined). They provide support for vertical or near vertical grade changes, while also preventing erosion or down slope movement. The backfill is usually associated with an amount of surface strip load, thereby creating lateral pressure which acts onto the non-yielding retaining wall. Typical surface strip loads may include highways, building infrastructure, or railroads.

Surface strip loads will become in particular interest in the thesis, especially under circumstances where a rigid retaining wall is directly under its influence. The purpose of this thesis is to calculate mathematically and graphically the lateral earth pressures and how stability of a retaining structure is influenced by these pressures. The selected retaining wall which will be focused upon in this thesis includes the cantilever type structure.

Calculations will be made which will involve Rankine earth pressure theory and Coulomb earth pressure theory. It will also involve determining whether there are any correlations between these two theories. It is known that Rankine's theory considers the back of the retaining wall as frictionless, while Coulomb considers there to be friction between the retaining wall and backfill.

A numerical approach will involve software known as OptumG2 to determine the representation of the stresses experienced by the retaining wall and the influence it has on the backfill and foundations.

1.1 Risk Assessment

Risk is the determination of qualitative and quantitative value of risk related to a recognised hazard and a concrete situation. The *magnitude* of the potential loss, and the *probability* that the loss will occur are the two prime components of quantitative risk assessment. On the other hand, risk that is understood and tolerated is denoted the term '*acceptable risk',* usually because implementing a countermeasure for this type of risk would involve difficulty and/or cost which would exceed the expectation of loss.

Hazards

Wherever there is a hazard there is an associated risk factor, if the hazard is unavoidable then the risk may be minimised. In the office environment hazards are seen to be less significant then out in the manufacturing station, however, all types of hazards have the potential to cause serious consequences if not thoroughly analysed. A list of hazards and their associated risks have been identified below for an office work environment, they include:

- Poor posture – results from repetition of daily activities, can increase stress and strain. Can be caused by excessive duration in a seated position and/or incorrect setup of workstation. This risk is substantial; to reduce this risk regular exercise must be undertaken to stretch muscles. Three prime symptoms listed below which are caused by poor posture.
  - Stiff neck
  - Stiff shoulders
  - Back pain
- Eye strain – Results from extended use of the eyes, such as excessive computer use and/or poor lighting. This risk is significant, however symptoms are only short term (i.e. headaches and/or blurred vision), hence, will not cause eye damage.
- Glare – Results from direct light source which reflects light from the monitor. This hazard results in eye strain and fatigue. If the hazard is not removed then the risk is substantial. To remove the hazard blinds will need to be closed, clean monitor, or place screen at right angles to the light source.
- Carpal tunnel syndrome – Results from repetitive keyboard use which requires hand movements. The risk is very slight, however carpal tunnel syndrome tend to affect some individuals more than others. The symptoms include numbness, pins and needles, hand weakness, sore wrists, etc.

Each of these hazards can easily be controlled once identified. Risk assessment is a significant factor to consider when it concerns the threat to the environment, life or machine functionality.

1.2 Terminology

For simplicity, Figure 1 details a cross section of a cantilever retaining structure with common terminology and their typical locations.

The *stem* acts as a cantilever beams, it is imperative that it resist all lateral pressures caused by the soil which acts against it.

The *base slab (footing),* is structurally designed to withstand vertical pressures, therefore must transmit those pressures to the undisturbed soils.

The *key* is to resist lateral pressure and movement; it is an optional component within the design of the wall. Location of the key may be located anywhere along the base slab.

Backfill is soil material which is supported by the stem of the retaining wall. Backfill is usually associated with 'disturbed' soil material, and elevated to design level.

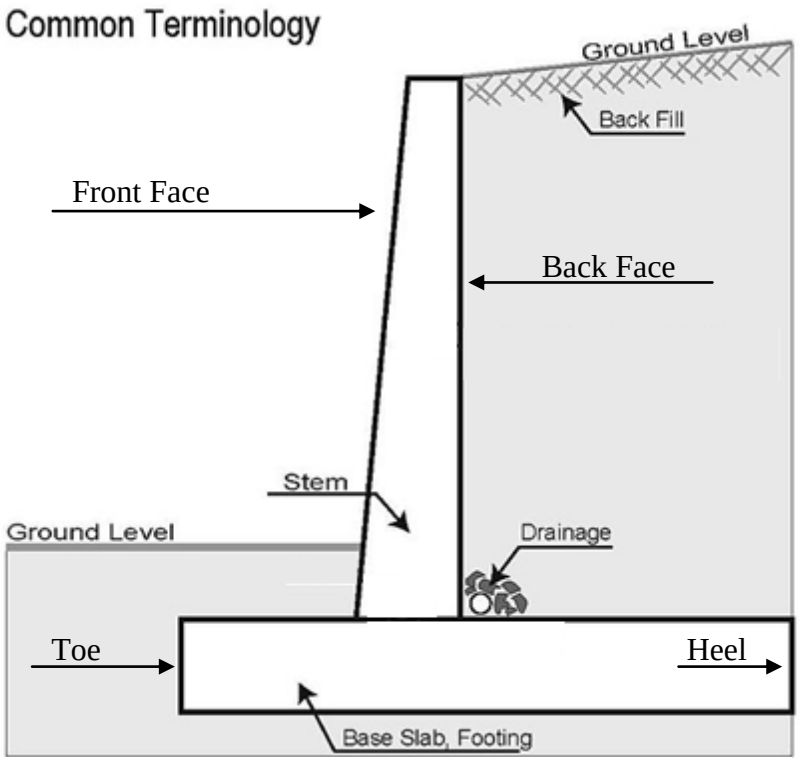

Figure 1- Cantilever retaining wall terminology (Denson, 2013)

The *back face* is the side of the stem which is in contact with the backfill for majority of the retaining walls height. The *front face* is the side of the stem which is exposed for majority of the retaining walls height.

The *toe* is the face of the base slab at the front side of the wall, while the *heel* is the face of the base slab on the back side of the wall.

Drainage is located within the backfill between the stem and the footing of the retaining wall; it is a method in reducing the amount of concentrated water within the backfill. If the drainage system fails then the water won't dissipate, this will lead to an additional lateral pressure which will act against the wall (Donkada & Menon 2012, para. 3).

1.3 Historical Background

The development of the cantilever retaining wall was induced after the Second World War, following techniques which involved reinforced concrete structures. These walls are designed to cantilever loads to the footing. In order to improve their stability against high loads the wall is usually installed with a counterfort on the back or the wall is buttressed on the footing. However, the *theory* behind cantilever was introduced by Galileo in the 16th century. Further study within this field continued within the 19th century by John Fowler and Benjamin Baker. In the 1880s the use of reinforced retaining walls were introduced (UMR, 2014).

1.3.1 *Coulomb*

The first significant contribution to the study of soil behaviour is dated back to 1776 when a French-physicist by the name of Charles-Augustin de Coulomb (1736 – 1806) published an article on wedge theory of earth pressure. It was Coulomb that introduced the concept that shear resistance of soil is made up of two components, i.e. cohesion and friction (Shroff & Shah 2003).

1.3.2 *Rankine*

The Rankine Theory was originally constructed by William Rankine (1820 – 1872) in 1857, when his theory was presented in calculating safe bearing capacity and earth pressure in foundations (Shroff & Shah 2003). The theory predicts at-rest, passive and active pressures when shear failure through-out the

soil mass is at the point of occurring. Rankine's analysis of earth pressure was continued on after his period of time by Resal (1910) and Bell (1915), their research included soil containing both friction and cohesion.

2. LATERAL EARTH PRESSURES

Lateral stress values involved in retaining structures depend primarily on the geometry of deformation. In detail, the lateral earth pressure depends on two factors, the stem of the retaining wall and the supported material. Earth pressure will vary accordingly to both magnitude and direction of the retaining wall stem, while also considering the cohesive strength and the internal friction of the supported material. The pressure distribution is typically triangular in shape, increasing the further the depth.

All soil materials are associated with a certain mass, more or less than others, and as a result all soil masses have internal stresses. However, the magnitudes of these stresses are directly influence by the properties of the surrounding geometry, quantity of soil material and any external loadings. A retaining wall must be structurally designed so the stresses applied by the soil mass are counteracted. In order for this, the retaining wall must provide a pressure equal and opposite to the pressures applied by the soil.

Rankine and Coulomb are based on five fundamental assumptions, they require:

- the backfill soil to be granular and cohesionless; it must contain very little or no fine grained soil particles (i.e. silt and clay);
- the soil is homogenous (i.e. contains no mixture of materials);
- the soil is isotropic, (i.e. equal stress-strain properties in all directions and no artificial reinforcement);
- no boundary conditions, that is, the wall and soil are considered semi-infinite and soil left undisturbed;
- drained soil conditions, so pore water pressure can be ignored.

2.1 At-Rest Earth Pressure

If the wall is static then the soil adjacent becomes in a state of static equilibrium (Braja & Khaled, 2014). In this case, in order to define the earth pressure coefficient, K_o, with soil having a unit weight of γ at depth z:

$$\frac{\sigma_h{}'}{\sigma_o{}'} = \frac{K_o \gamma z}{\gamma z} = K_o \qquad \text{Eq. 2.1}$$

Where:

σ_o' = vertical earth pressure; and

σ_h' = horizontal earth pressure.

Craig (2004) refers in his report that since the soil which experiences at-rest condition does not fail, then the horizontal and vertical stresses represented within the Mohr circle does not touch the failure envelope and the horizontal stress can't be mathematically calculated. Therefore, experimental procedures must be used. Figure 2 details the form of relationship between lateral pressure coefficient and lateral strain.

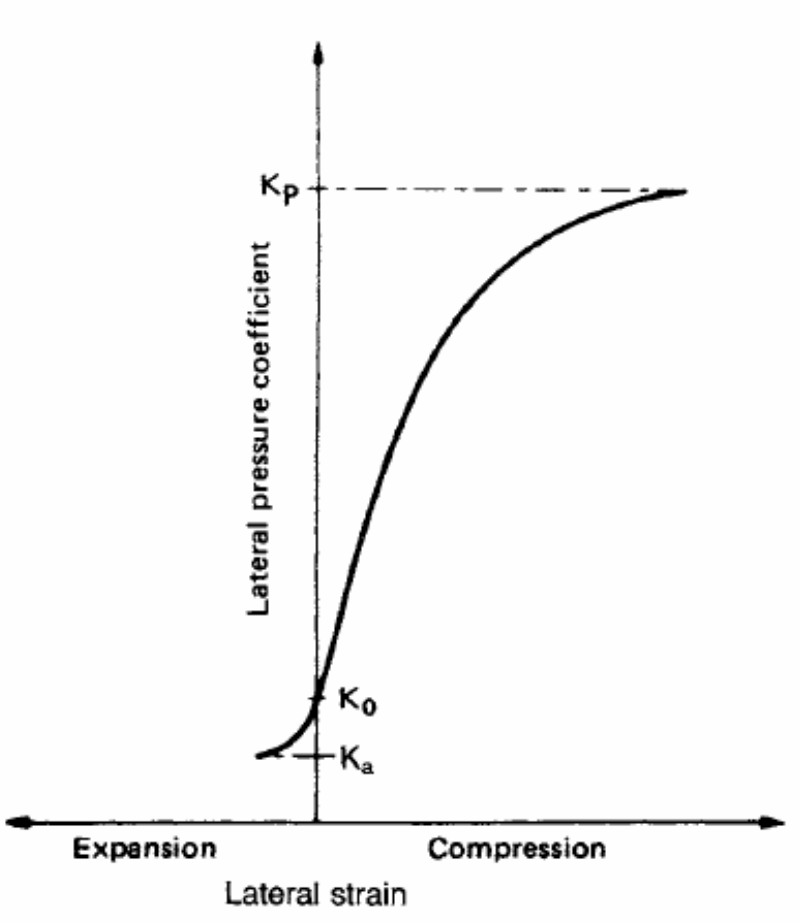

Figure 2 - Lateral strain and lateral pressure coefficient (Craig, 2004)

Alternatively, Jaky (1944) has represented a formula which is widely accepted for the normally consolidated soils, the coefficient of earth pressure at rest can be *estimated* by:

$$K_o = 1 - \sin\phi \qquad \text{Eq. 2.2}$$

Where:

$\phi =$ drained friction angle.

Eq. (2.2) is applicable only for calculations involving loose deposits (e.g. non-compacted sands), where only compaction is by gravity. However, when the soil becomes densified Eq. (2.2) does not represent accurate results (Sherif, Fang and Sherif 1984), as it induces additional horizontal stresses acting against the wall which is not considered within the given formula. This has been experimentally conducted by Sherif, Fang, and Sherif. Due to this predicament, a formula which resolves only around densified soil types has been recommended:

$$K_o = (1 - \sin\phi) + \left(\frac{\gamma_d}{\gamma_{d(\min)}} - 1\right)5.5 \qquad \text{Eq. 2.3}$$

Where:

$\gamma_d =$ actual soil density after construction completion

$\gamma_{d(\min)} =$ loosest soil density

Braja & Khaled remarks on the increase in the earth pressure coefficient between Eq. (2.2) and Eq. (2.3), due to over consolidation. Therefore, calculations involving over consolidation must be considered in order to minimise this difference between both formulas.

Hanna & Al-Romhein stated the significants of Wroth, Meyerhof and Mayne and Kulhawy's contribution, involving experiments which resulted in their recommendation of Eq. (2.4), which is a modification of Eq. (2.2). A quote from Wroth, Meyerhof and Mayne and Kulhawy's states 'formula provided good agreement with the experimental results of the coefficient of earth pressure at rest $K_{o(OC)}$ up to an OCR value of about 3.00. The theoretical values of Wroth were about 10% to 12% lower than the experimental values'. The formula which Hanna & Al-Romhein were referring to is empirical and considers the Overconsolidated Ratio (OCR):

$$K_{o(OC)} = (1 - \sin\phi')OCR^{\sin\phi' - 0.18} \qquad \text{Eq. 2.4}$$

Where;

$$OCR = \text{ Overconsolidated Ratio} = \frac{\text{Preconsolidation pressure, } \sigma_c'}{\text{Present effective overburden pressure, } \sigma_o'}$$

2.2 Rankine Earth Pressures Theory

Rankine's theory involves the consideration of the stress levels in the soil when the plastic equilibrium has been reached (Braja & Khaled, 2014). Rankine's method in distinguishing the stress levels at failure is represented by Mohr circle, this is achieved in a two dimensional plane, detailed in Figure 3.

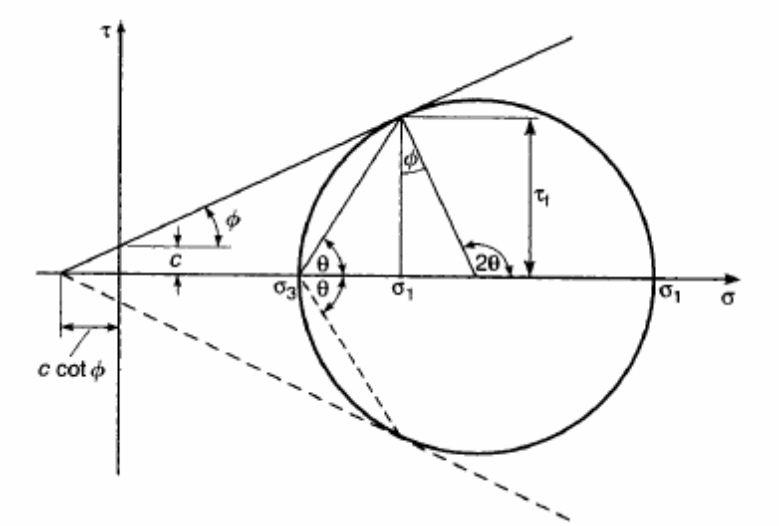

Figure 3 - Mohr Circle (Craig, 2004)

Where c and ϕ are the relevant shear strength parameters.

Using the failure envelope given in the Mohr circle and substituting the horizontal and vertical stresses for the minor and major principle stresses, Rankine was able to determine equations which calculated the active and passive pressure coefficients.

Shear failure occurs along a plane at an angle of $(45° + \phi/2)$ to the major principle plane. Theoretically, if a mass of soil is stressed that the principle stresses are in the same direction at every point, then there will be a network of failure planes. This is detailed in Figure 4.

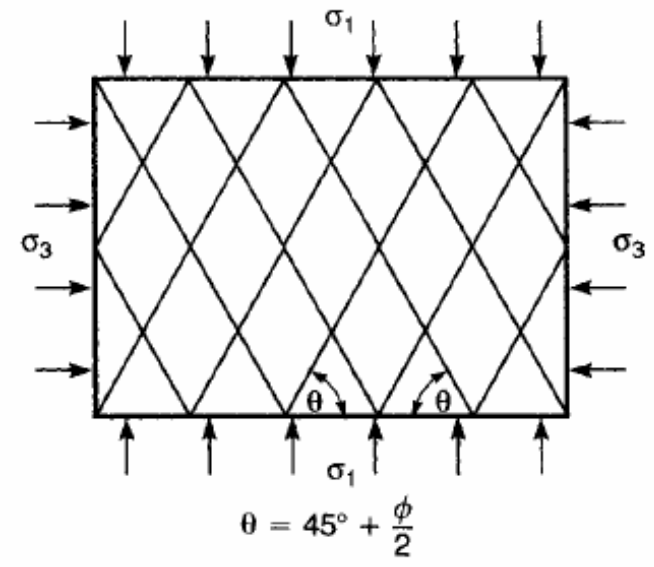

Figure 4 - Failure Plans: active case (Craig, 2004)

Now, let's to consider a semi-infinite mass of soil being restrained by a *frictionless* wall of semi-infinite depth between points AB, this is detailed in Figure 5. The soil is considered to be homogenous and isotropic. The relationship between active and passive soil conditions can be determined through the inclinations of the slip line; also detailed in Figure 5. Craig (2004) declares that when the horizontal stress is equal to the active pressure, then the soil is within the *active Rankine state*. In the active Rankine state the shear opposes the effect of gravity (Lambe, 1969), where there are two sets of shear lines (failure planes) inclined at an angle of $(45° + \phi/2)$ to the *horizontal* (Craig, 2004).

Craig (2004) also elaborates when the horizontal stress equals the passive pressure, then the soil is in a *passive Rankine state*. In the passive Rankine state

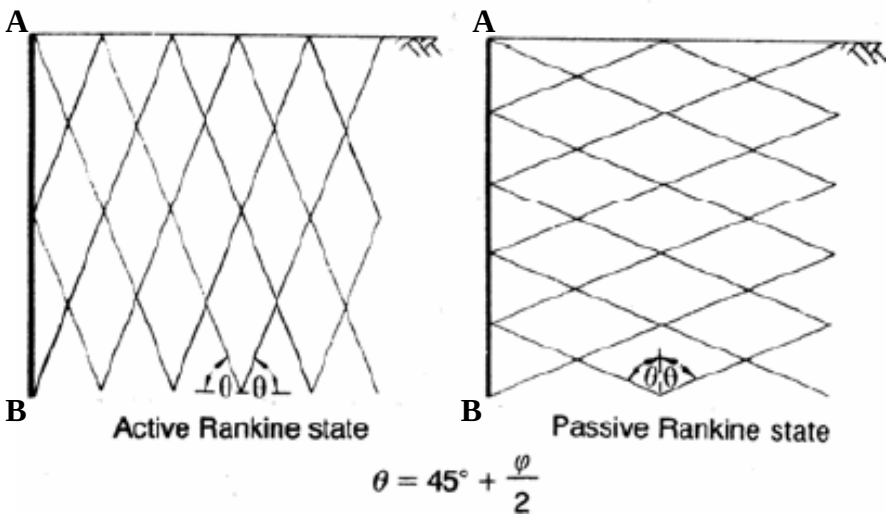

Figure 5 – Slip lines for Active and Passive States (Craig 2004)

the shear stress acts together with gravity to oppose the horizontal stress from the inward movement of the wall (Lambe, 1969). Where there are two sets of shear lines (failure planes) inclined at an angle of $(45° + \phi/2)$ to the *vertical* (Craig, 2004).

Therefore, the two different pressure cases include:

- active pressure; and
- passive pressure.

Craig (2004) refers to these two pressures as limit pressures; this will be discussed in more detail within section 2.2.1 and section 2.2.2.

2.2.1 *Active earth pressure*

Cohesionless Soils, $c = 0$

A retaining wall can undergo several types of movements which can possibly lead to failure due to active pressure; these types of movements are detailed in Figure 6.

2.2.2
2.2.3
2.2.4
2.2.5
2.2.6
2.2.7
2.2.8
2.2.9

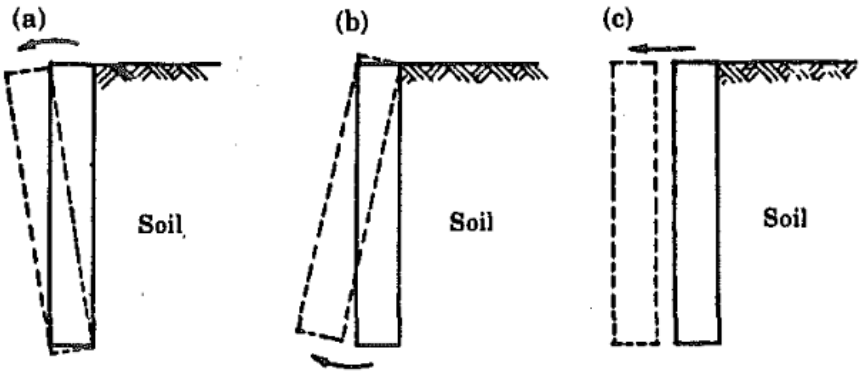

(a) Rotational About Toe (b) Rotational About Top
(c) Translational

Active Case

Figure 6 – Rotational, Translational Retaining Wall Active Case (Sherif, et al., 1984)

If the wall is allowed to move away from the backfill, such to represent an active case, then the overall lateral principle stress (σ_x) will decrease (Braja & Khaled, 2014). Therefore, active case represents a minimal value since the

soil can laterally expand as the wall moves outwards. When the soil expansion is large enough, then the minimum value of σ_x is achieved, leading to a state of plastic equilibrium (White, 2011). Since the horizontal stress (σ_x) is the cause of this development, then σ_x must be the minor principle stress, σ_3 (Craig, 2004). Therefore the major principle stress (σ_1) is the vertical stress, σ_z.

The relationship between the major and minor principle stresses when the soil reaches a plastic equilibrium state can be determined through the Mohr circle.

Now, if the wall undergoes a rotational movement about the toe, detailed in Figure 6a, the horizontal stress at any depth would not alter, $\sigma_h' = K_o\sigma_o'$. Figure 7 details the stress condition in the soil represented by the Mohr's circle 'state of rest'. However, for an active case the horizontal principle stress detailed in Eq. (2.5) would decrease (i.e. $\sigma_h' < K_o\sigma_o'$). This state of stress is represented by the Mohr's circle 'active Rankine state'.

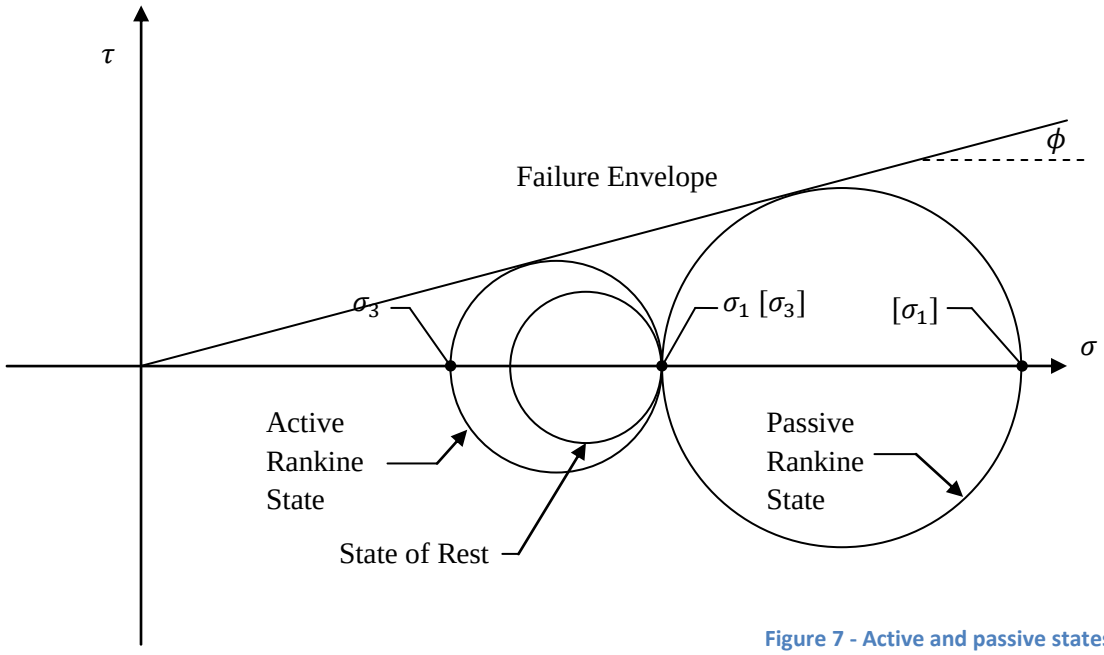

Figure 7 - Active and passive states

$$\sigma_3 = \sigma_1\left(\frac{1-\sin\phi}{1+\sin\phi}\right) - 2c\sqrt{\frac{1-\sin\phi}{1+\sin\phi}} \qquad \text{Eq. 2.5}$$

Where;

σ_1 = vertical effective overburden pressure = γz (Braja & Khaled, 2014);

$\sigma_3 =$ horizontal principle stress $=$ active pressure (p_a); and

If the active earth pressure coefficient is defined as $K_a = \frac{1-\sin\phi}{1+\sin\phi}$, then equation 2.5 is rewritten:

$$p_a = \gamma z K_a - 2c\sqrt{K_a} \qquad \text{Eq. 2.6}$$

Active Rankine state occurs when the horizontal stress is equal to the active pressure.

Where;

$$K_a = \frac{\sigma'_a}{\sigma'_o} = \left(\frac{1-\sin\phi}{1+\sin\phi}\right) = \tan^2\left(45 - \frac{\phi'}{2}\right) \qquad \text{Eq. 2.7}$$

Values of Rankine's active pressure coefficients (Eq. 2.7) for various values of ϕ' are detailed in Appendix D.

Inclined Backfill

In a case where the backfill contained behind a frictionless retaining wall is a granular type soil ($c' = 0$) and the angle is inclined to the horizontal at which the soil rises (α), then the active earth pressure coefficient, K_a can be determined:

$$K_a = cos\alpha \times \left[\frac{cos\alpha - \sqrt{(cos^2\alpha - cos^2\phi')}}{cos\alpha + \sqrt{(cos^2\alpha - cos^2\phi')}}\right] \qquad \text{Eq. 2.8}$$

Where;

$\phi' =$ angle of friction of soil.

This data from Eq. 2.8 for various values of ϕ' and α has been represented and detailed in Appendix E.

From this collection of data the Rankine active pressure at any depth can be determined:

$$\sigma'_a = \gamma z K_a \qquad \text{Eq. 2.9}$$

And;

The total force per unit length of wall:

$$P_a = \frac{1}{2}\gamma K_a (H - z_o)^2 \qquad \text{Eq. 2.10}$$

Cohesive Soils

For a frictionless retaining wall with cohesive soil backfill, at any depth the active soil pressure against the wall can be determined:

$$\sigma_a' = \gamma z K_a - 2\sqrt{K_a}c'$$

It is detailed in Figure 8a the variation of $\gamma z K_a$ with depth, and detailed in Figure 8b the variation of $2\sqrt{K_a}c'$ with depth.

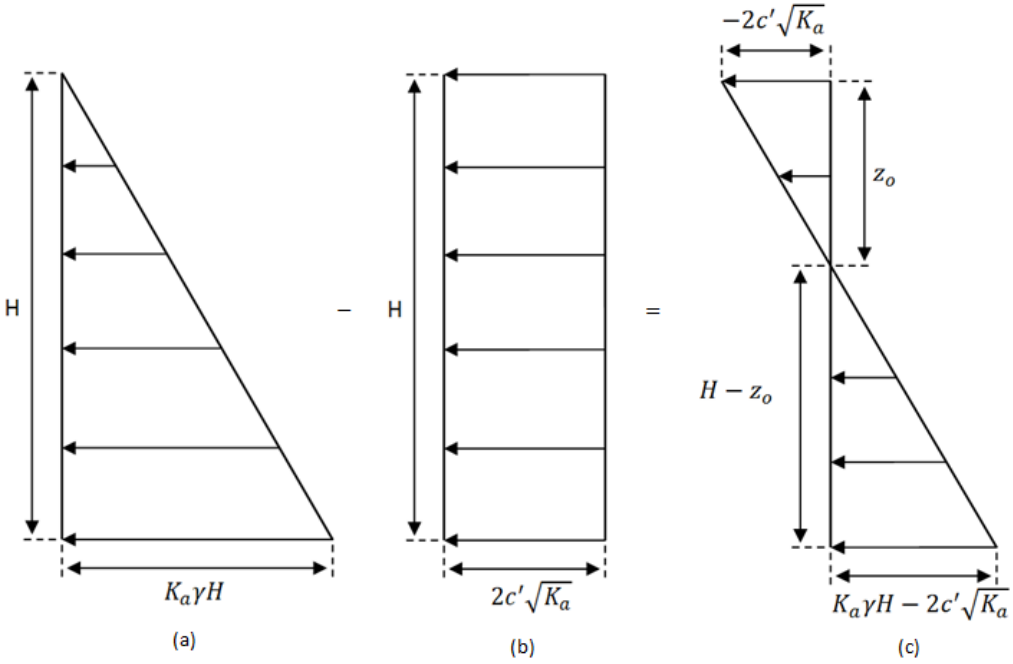

Figure 8 - Earth pressure distribution, cohesive backfill (Braja, 2014)

Therefore, overtime, tensile cracks will develop at the soil-wall interface up to a total depth z_o (Braja & Khaled, 2014). The area of the total pressure diagram in Figure 8c can be used to calculate the total active force per unit length of wall. For calculation of the total active force with a horizontal cohesive backfill,

$$P_a = 0.5 K_a \gamma H_2^2 - 2\sqrt{K_a}c' \qquad \text{Eq. 2.11}$$

It was detailed by Braja that for active earth pressures for clayey soils is equated differently to that of soft soils. The formula denoted below can be compared to that of Eq. 2.13.

$$P_a = \frac{1}{2}\gamma(H - z_o)^2 \frac{1}{N_\phi} - 2c' \frac{H}{\sqrt{N_\phi}} \qquad \text{Eq. 2.12}$$

Where,

$N_\phi = \tan^2\left(45 + \frac{\phi}{2}\right)$; and

$c' =$ cohesion of soil

For soft soils, $N_\phi = 1$. Therefore:

$$P_a = \frac{1}{2}\gamma(H - z_o)^2 - 2c'H \qquad \text{Eq. 2.13}$$

Inclined Backfill

For a cohesive backfill, the active pressure at any depth is determined:

$$\sigma'_a = \gamma z K'_a \cos\alpha \qquad \text{Eq. 2.14}$$

2.2.2 *Passive earth pressure*

Cohesionless Soils, $c = 0$

A retaining wall can undergo several types of movements which can possibly lead to failure due to passive pressure, they are:

- rotational about the toe;
- rotational about the top; and
- translational as a rigid body.

These types of movements are detailed in Figure 9.

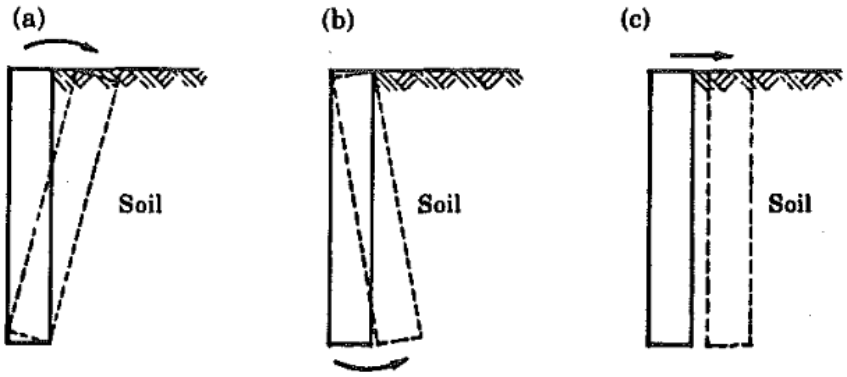

(a) Rotational About Toe (b) Rotational About Top
(c) Translational

Passive Case

Figure 9 – Rotational, Translational Retaining Wall Passive Case (Sherif, et al., 1984)

If the wall is allowed to move towards the backfill, such to represent a passive case, then the overall lateral principle stress will increase due to compression (Braja & Khaled, 2014). Therefore, passive case represents a maximum value since the soil is laterally compacted as the wall moves inwards. When this maximum value is achieved the limiting compressive strength of the soil is reached (White, 2011).

The relationship between the major and minor principle stresses when the soil reaches a plastic equilibrium state can be determined through the Mohr circle detailed in Figure 7.

Now, if the wall undergoes a rotational movement about the toe, detailed in Figure 9a, the horizontal stress at any depth would not alter, $\sigma_h{}' = K_o\sigma_o{}'$. Figure 9 details the stress condition in the soil represented by the Mohr's circle 'state of rest'. However, for a passive case the horizontal principle stress detailed in Eq. (2.5) would increase (i.e. $\sigma_h' > K_o\sigma_o'$). In this situation the wall will create a state where the soil element will be represented by the Mohr's circle 'passive Rankine state'. Failure of the soil will occur at this point in time where the Mohr's circle touches the failure envelope (Braja & Khaled, 2014). This horizontal principle stress can be determined through the following:

$$\sigma_p' = \sigma_o' \tan^2\left(45 + \frac{\phi}{2}\right) + 2c' \tan\left(45 + \frac{\phi}{2}\right) \qquad \text{Eq. 2.15}$$

Where;

$$\frac{\sigma_p'}{\sigma_o'} = \text{ratio of effective stresses} = \mathrm{K_p} = \tan^2\left(45 + \frac{\phi'}{2}\right) \qquad \text{Eq. 2.16}$$

Therefore, from equation 2.15:

$\sigma_p' =$ horizontal principle stress $=$ passive pressure (p_p);

$$p_p' = K_p\gamma z + 2c'\sqrt{K_p} \qquad \text{Eq. 2.17}$$

The passive force per unit length of wall can be determined:

$$P_p = \frac{1}{2}\gamma H^2 K_p \qquad \text{Eq. 2.18}$$

Rankine's passive earth pressure coefficient has been determined in Appendix D for various values of ϕ'.

Inclined Backfill

The Rankine passive pressure at any depth containing a granular backfill ($c' = 0$) can be determined similar to that of equation 2.15, 2.17 and 2.18.

That is;

Rankine passive pressure:

$$\sigma_p' = \gamma z K_p \qquad \text{Eq. 2.19}$$

And;

The total passive force per unit length of wall:

$$P_p = \frac{1}{2}\gamma K_p (H - z_o)^2 \qquad \text{Eq. 2.20}$$

The resultant force $P_p$is inclined at an angle of α to the horizontal and intersects the wall at a distance of H/3 from the bottom of the wall.

Where;

$$K_p = cos\alpha \times \left[\frac{cos\alpha + \sqrt{(cos^2\alpha - cos^2\phi')}}{cos\alpha - \sqrt{(cos^2\alpha - cos^2\phi')}}\right] \qquad \text{Eq. 2.21}$$

Rankine's passive earth pressure coefficient has been determined in Appendix E for various values of α and ϕ'.

Cohesive Soils

At any point, the horizontal effective pressure at any depth, is calculated through the Rankine earth pressure, and is given as:

$$\sigma_P' = \sigma_o' K_P + 2c'\sqrt{K_P} \qquad \text{Eq. 2.22}$$

The force per unit length of the wall is determined:

$$P_P = \frac{1}{2}\gamma H^2 K_P + 2c' H\sqrt{K_P} \qquad \text{Eq. 2.23}$$

Inclined

It was detailed my Braja that for passive earth pressures for cohesive materials such as clayey soils is equated differently to that of non-cohesive materials. The formula denoted below can be compared to that of Eq. 2.23.

$$P_p = \gamma(H - z_o)N_\phi + 2c'\sqrt{N_\phi} \qquad \text{Eq. 2.24}$$

2.3 Coulomb Earth Pressure Theory

Rankine's earth pressure theory involves the assumption that the retaining wall is frictionless. Coulombs method for calculating earth pressure is similar; however friction is taken into consideration. This theory also involves the consideration of the stability of the wedge of soil between the retaining wall and a trial failure plane (Craig, 2004). The forces per unit length of the wall acting on the wedge are determined by calculating the equilibrium of forces acting on the wedge. This calculation is made when the wedge is at the point of sliding up or down the failure plane. The forces include:

- weight of the wedge, W;
- active/passive force, P_a or P_p; and
- resultant force, R, of the normal and shear forces on the failure plane BC

In both active and passive cases the shape of the failure plane is curved near the bottom of the wall due to wall friction, this is detailed in Figure 10. However, in the Coulomb theory the failure plane is assumed to be plane active and passive case.

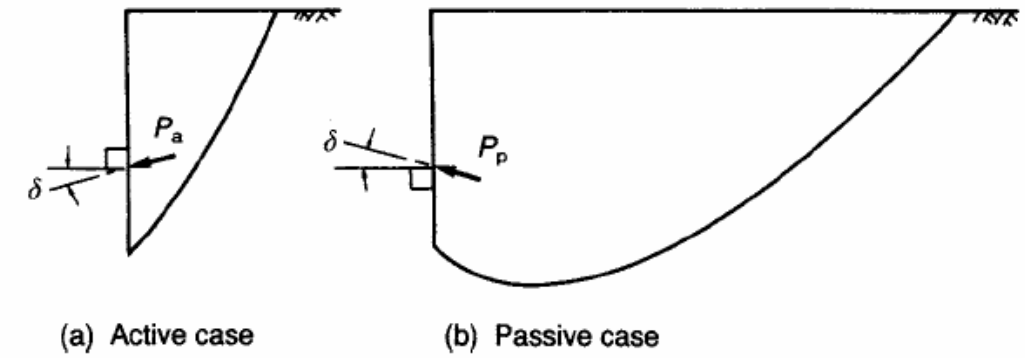

Figure 10 - Curvature due to wall friction (Craig, 2004)

2.3.1 *Active earth pressure*

Figure 11 details a failure wedge ABC, with active forces on the wedge between the wall surface and the failure plane BC. Soil type contains cohesion parameter *c* equal to zero. For the failure condition, the soil wedge acting under its own weight (W) is in equilibrium. The reaction force (P) between the wall and soil and the reaction on the failure plane (R). Since the wedge moves down the failure plane BC, then the reaction force P is declined at an angle δ to the normal. At failure, the reaction force R along the failure plane is declined at an angle of ϕ to the normal. These three forces are then connected head-to-tail (triangle of forces) to determine the magnitude of P. This is detailed in Figure 11.

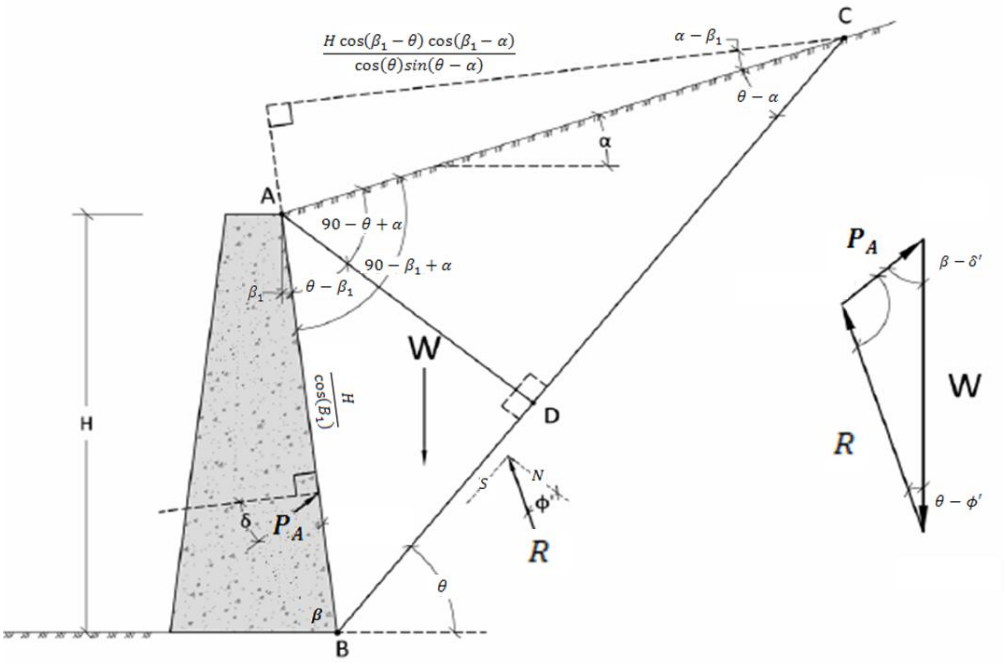

Figure 11 - Coulombs active theory (Valsson, 2011)

In this procedure, multiple cases of failure planes will need to be selected to determine the maximum value of P, which would be defined as the maximum active thrust on the retaining wall (Craig, 2004). However, an alternative method in calculating P would include expressing P in terms of W and the angles θ, and differentiating with respect to θ. That is, $\partial P/\partial\theta = 0$:

$$P_a = \frac{1}{2}K_a\gamma H^2 \qquad \text{Eq. 2.25}$$

Where;

$$K_a = \frac{sin^2(\beta + \phi')}{sin^2\beta sin(\beta - \delta')\left[1 + \sqrt{\left(\frac{sin(\phi' + \delta')sin(\phi' - \alpha)}{sin(\beta - \delta') \times sin(\alpha + \beta)}\right)}\right]^2} \quad \text{Eq. 2.26}$$

The calculated maximum active thrust is assumed to act at a total distance of H/3 above the base of the retaining wall. Coulomb's active earth pressure coefficient has been determined in Appendix G for various values of ϕ' and Appendix I for various values of α and ϕ'.

Now;

Coulombs theory can be associated with soil cohesion c greater than zero. A value is then selected for the wall parameter, c_w. From Figure 12, tension cracks are assumed to extend to a total depth z_0, there the new failure plane extends from the heel of the wall (B) to the bottom of the tension zone (C). The forces acting on the wedge at failure include:

- the weight of the wedge (W);
- the reaction force (P) between the wall and soil declined at an angle δ to the normal;
- the reaction on the failure place (R) declined at an angle of ϕ to the normal;
- The force due to the constant component of shearing resistance on the wall $C_w = c_w \times EB$. Where EB is the vertical distance from the base of the wall to the bottom of the tension zone;
- The force on the failure plane due to the constant component of shear strength ($C = c \times BC$).

All five forces have known directions together with known magnitudes $W, C_w and\ C$ and therefore the value of P can be determined through a triangle of forces, this is detailed in Figure 12. The value of P must be calculated through multiple instances where the maximum P is determined.

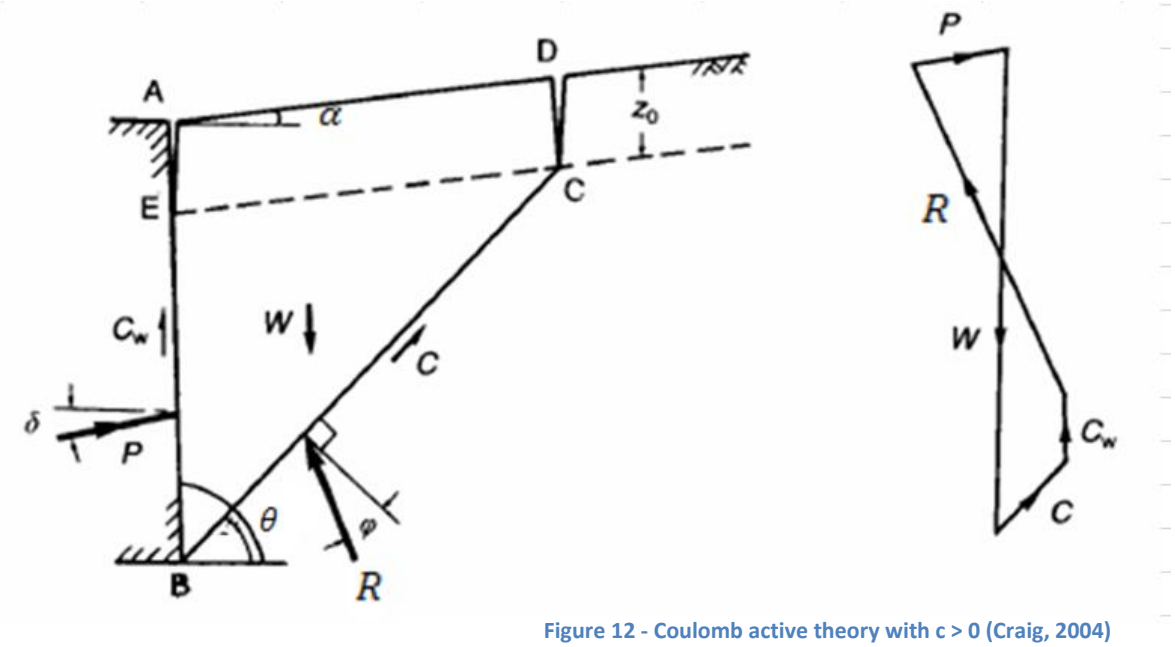

Figure 12 - Coulomb active theory with c > 0 (Craig, 2004)

An alternative method in calculating P would include expressing P in terms of horizontal and vertical forces, and differentiating with respect to θ. That is, $\partial P/\partial\theta = 0$:

$$P_a = \frac{1}{2}\gamma(H^2 - z_0^2) - 2c_u(h - z_0)\sqrt{1 + \frac{c_w}{c_u}}$$

A second coefficient K_{ac} is calculated for drained and undrained:

undrained conditions:

$$K_{ac} = 2\sqrt{1 + \frac{c_w}{c_u}}$$

drained conditions:

$$K_{ac} = 2\sqrt{K_a\left[1 + \frac{c_w}{c'}\right]}$$

In general, active pressure at depth z:

$$p_a = K_a\gamma z - K_{ac}c \qquad \text{Eq. 2.27}$$

Where;

$$K_{ac} = 2\sqrt{K_a\left[1 + \frac{c_w}{c}\right]} \qquad \text{Eq. 2.28}$$

The depth of a dry tension crack ($p_a = 0$) is:

$$z_0 = \frac{2c\sqrt{1 + \frac{c_w}{c}}}{\gamma\sqrt{K_a}} \qquad \text{Eq. 2.29}$$

The depth of a water filled crack (z_{0w}) is given from the condition:

$$p_a = \gamma_w z_{0w}$$

2.3.2 *Passive earth pressure*

Figure 13 details the Coulombs passive case; the reaction force P is inclined at an angle δ to the normal. At failure, the reaction force R along the failure plane is inclined at an angle of ϕ to the normal. The overall passive resistance is equal to the minimum value of P, this is given by:

$$P_p = \frac{1}{2}K_p\gamma H^2 \qquad \text{Eq. 2.30}$$

Where;

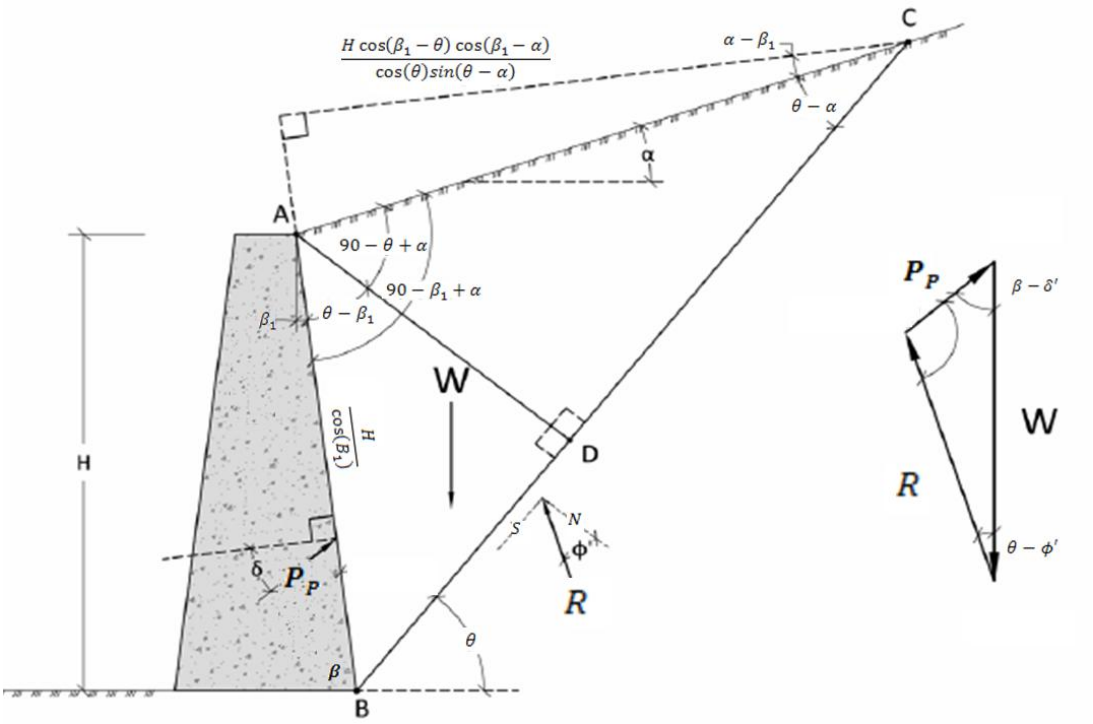

Figure 13 - Coulombs passive case (Valsson, 2011)

$$K_p = \frac{sin^2(\beta - \phi')}{sin^2\beta \times sin(\beta + \delta') \left[1 - \sqrt{\left(\frac{sin(\phi' + \delta') \times sin(\phi' + \alpha)}{sin(\beta + \delta') \times sin(\alpha + \beta)}\right)}\right]^2} \quad \text{Eq. 2.31}$$

The calculated maximum passive thrust is assumed to act at a total distance of H/3 above the base of the retaining wall. Coulomb's passive earth pressure coefficient has been determined in Appendix H for various values of ϕ' Appendix J for various values of α and ϕ'.

In summary Rankine's theory considers the back of the wall frictionless, while coulomb considers friction between both wall and soil. As a result, when friction angle is equal to zero ($\delta = 0$) Coulombs formulas are equated equally to that of Rankine's. Equation 2.8 and 2.21 were used to determine Rankine values detailed in Table 1, while equations 2.26 and 2.31 were used to determine Coulomb values detailed in Table 2. A more detailed outline of Rankine's coefficients can be found in appendix D, while Coulombs coefficients are further detailed in appendix G and H.

Table 1 - Rankine coefficients

RANKINE		
ϕ' (deg)	K_a	K_p
24	0.4217	2.3712
25	0.4059	2.4639
26	0.3905	2.5611
27	0.3755	2.6629
28	0.3610	2.7698
29	0.3470	2.8821
30	0.3333	3.0000
31	0.3201	3.1240
32	0.3073	3.2546
33	0.2948	3.3921
34	0.2827	3.5371
35	0.2710	3.6902
36	0.2596	3.8518
37	0.2486	4.0228
38	0.2379	4.2037
39	0.2275	4.3955
40	0.2174	4.5989

Table 2 - Coulomb coefficients

COULOMB, $\delta' = 0$		
ϕ' (deg)	K_a	K_p
24	0.4217	2.3712
25	0.4059	2.4639
26	0.3905	2.5611
27	0.3755	2.6629
28	0.3610	2.7698
29	0.3470	2.8821
30	0.3333	3.0000
31	0.3201	3.1240
32	0.3073	3.2546
33	0.2948	3.3921
34	0.2827	3.5371
35	0.2710	3.6902
36	0.2596	3.8518
37	0.2486	4.0228
38	0.2379	4.2037
39	0.2275	4.3955
40	0.2174	4.5989

In reality designers will find Rankine's approach to calculating soil pressure a simplified method over Coulombs approach. Rankine's results gives a lower value than the true value due to a more efficient distribution of stress could possibly exist, this is known as a lower bound solution. In contrast, Coulombs method is more practical for a real life scenario, as this involves friction. Briaud (2013) details that Coulombs solution is a limit equilibrium solution which is greater than the true solution; this is known as an upper bound solution. In this context, Coulombs passive earth pressure coefficient calculates out to be a very large result, possible too large. It was recommended by Craig (2004) that an alternative method be used when determining Coulombs passive earth pressure coefficient.

Therefore, if an upper bound is conservative than Coulombs approach would be advisable. If a lower bound is conservative then Rankine's approach would be advisable.

3. LIMIT ANALYSIS

Limit analysis is a method of approximating limit pressures that provide a lower and upper bound to the true limit load. They are widely used to analyse the stability of geotechnical structures. The upper bound theorem states that collapse must occur if the rate of work due to external forces of the kinematic system in equilibrium equals or exceeds the rate of dissipated internal energy for all kinematically acceptable velocity fields (Vrecl & Trauner, 2010). The lower bound theorem states that collapse will *not* occur if external loads are in equilibrium with an internal stress field without violating the yield criterion anywhere in the soil mass (Di Santolo, et al., 2012). When both upper and lower bound solution are equal, then the solution is found (HKU,2013), an illustration is detailed in Figure 14.

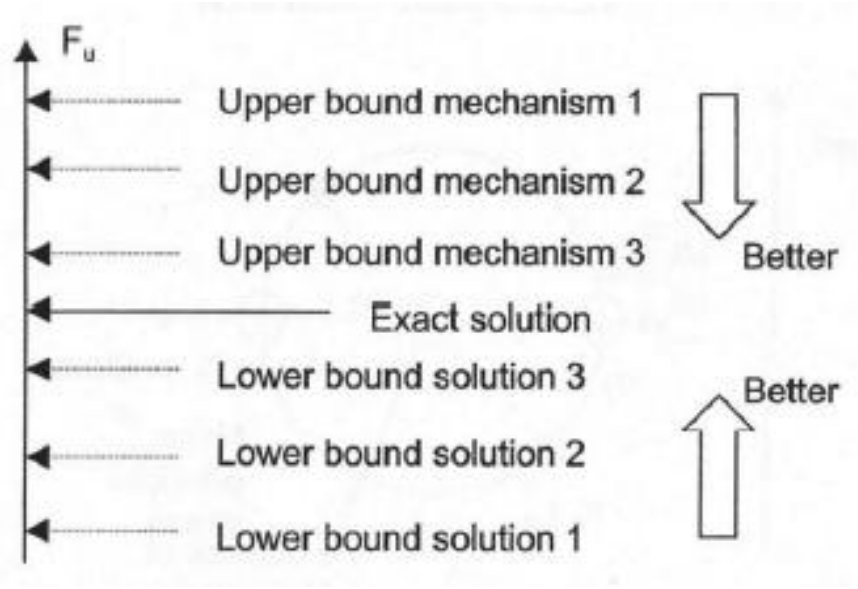

Figure 14 - upper and lower bound (HKU, 2013)

Scott Clayton
0061010140

3.1 Two-Dimensional Stress

Plane stress is a state of stress where two faces of an element (cubic) are free of stress. Figure 15 depicts a soil element with shear and normal stresses acting.

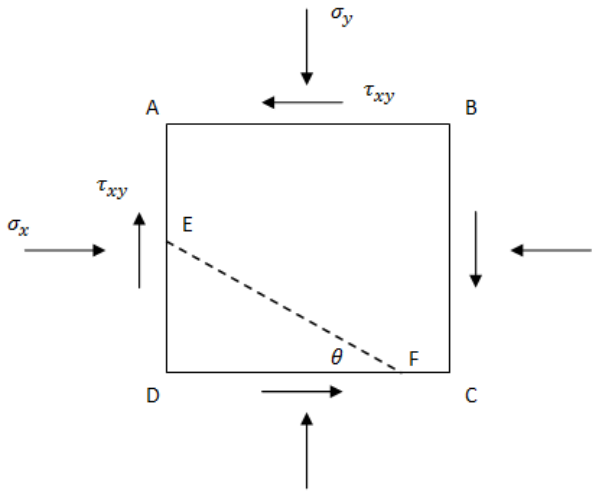

Figure 15 - Shear and normal stresses acting on element

The conditions for equilibrium of a triangular element detailed in Figure 16 with faces perpendicular to the $x, y, and\ n$ axes are

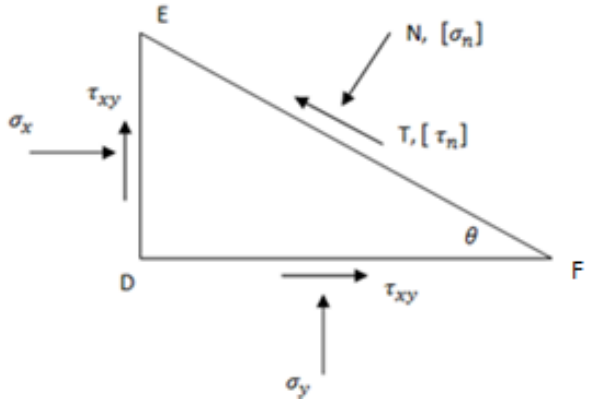

Figure 16 - Free body diagram CED

It should be noted that the following equations are summarised and for a more detailed outline of equations preformed, refer to Appendix B.

Resolve forces in direction of σ_n

$$\sigma_n = \tau_{xy} \sin 2\theta + \frac{\sigma_y + \sigma_x}{2} + \frac{\sigma_y - \sigma_x}{2} \cos 2\theta \qquad \text{Eq. 3.1}$$

Resolve forces in direction of τ_n

$$\tau_n = \frac{1}{2}(\sigma_y - \sigma_x)\sin 2\theta - \tau_{xy}\cos 2\theta \qquad \text{Eq. 3.2}$$

The directions of planes on which $\tau_n = 0$ can be found by substituting $\tau_n = 0$ in equation 3.2, we get

$$\tan 2\theta = \frac{2\tau_{xy}}{(\sigma_y - \sigma_x)} \qquad \text{Eq. 3.3}$$

Equation 3.3 will give two sets of orthogonal planes. This means that there are two planes at right angle to each other on which the shear stress is zero. As a result, since the shear stress is equal to zero on these planes, then these are the planes on which the principal stresses act.

The principal stresses on these planes can be evaluated by substituting equation 3.3 into 3.1, which yields

$$\therefore \sigma_n = \frac{\sigma_y + \sigma_x}{2} \pm \sqrt{\left(\frac{\sigma_y - \sigma_x}{2}\right)^2 + \tau_{xy}^2}$$

Two variables of σ_n are obtained, the major (larger value, σ_1) and the minor (smaller value, σ_3) of the two principal stresses, this is detailed in Figure 16.

The *Major* Principal Stress

$$\sigma_n = \sigma_1 = \frac{\sigma_y + \sigma_x}{2} + \sqrt{\left(\frac{\sigma_y - \sigma_x}{2}\right)^2 + \tau_{xy}^2}$$

The *Minor* Principal Stress

$$\sigma_n = \sigma_3 = \frac{\sigma_y + \sigma_x}{2} - \sqrt{\left(\frac{\sigma_y - \sigma_x}{2}\right)^2 + \tau_{xy}^2}$$

From Figure 17, the points R and M represents the stress conditions on planes DA and DC. A line RM will intersect the normal stress axis at the center, O. Where OR is the radius of the Mohr cirlce and is equal to:

$$\sqrt{\left(\frac{\sigma_y-\sigma_x}{2}\right)^2+\tau_{xy}^2}$$

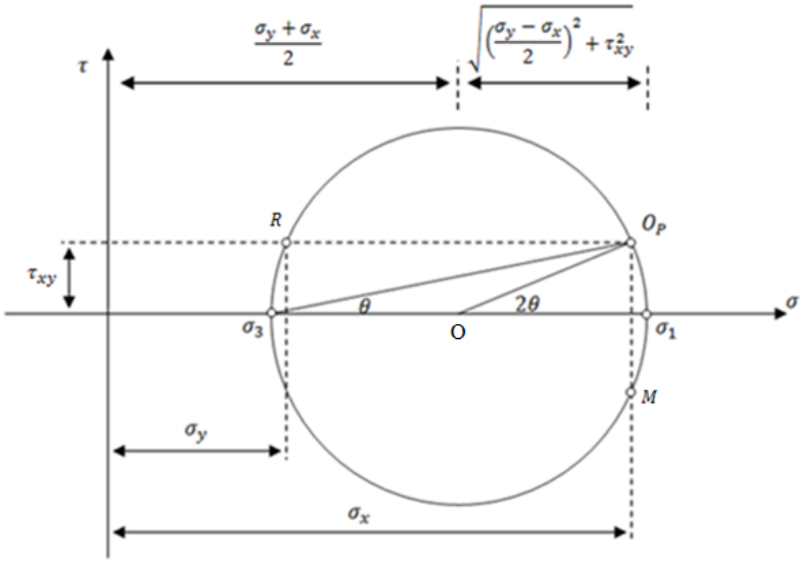

Figure 17 - two dimensional stress state (Davis & Selvadurai, 2005)

3.2 Lower Bound

The Lower Bound (LB) solution is identified by calculating the stress under which the soil is in equilibrium. The higher the lower bound solution, the closer it becomes to the exact solution (HKU, 2013).

There are three essential steps for LBs, the first includes the assumption of safe distribution of stress, which must be in equilibrium. The second is the stresses must be less than or equal to the stresses which will cause failure. The last is the use of Mohr circles at different regions to determine the collapse load. It is worthwhile to note that the LB method provides pessimistic answers (Liu, 2010). The advantage of the lower bound solution allows the evaluation of the thrust magnitude, inclination and the point of action (Di Santolo, et al., 2012).

In order to calculate the lower bound solution the stress distribution (equilibrium with the external loads) must not exceed the failure stresses (Di Santolo, et al.,

2012). With an inclined backfill angle of 20° to the horizontal, a statically admissible stress field which must satisfy all stress boundaries conditions is:

$$\sigma = \gamma H(\cos^2 \alpha - K_h \sin \alpha \cos \alpha)$$

$$\tau = \gamma H(\sin \alpha \cos \alpha - K_h \cos^2 \alpha)$$

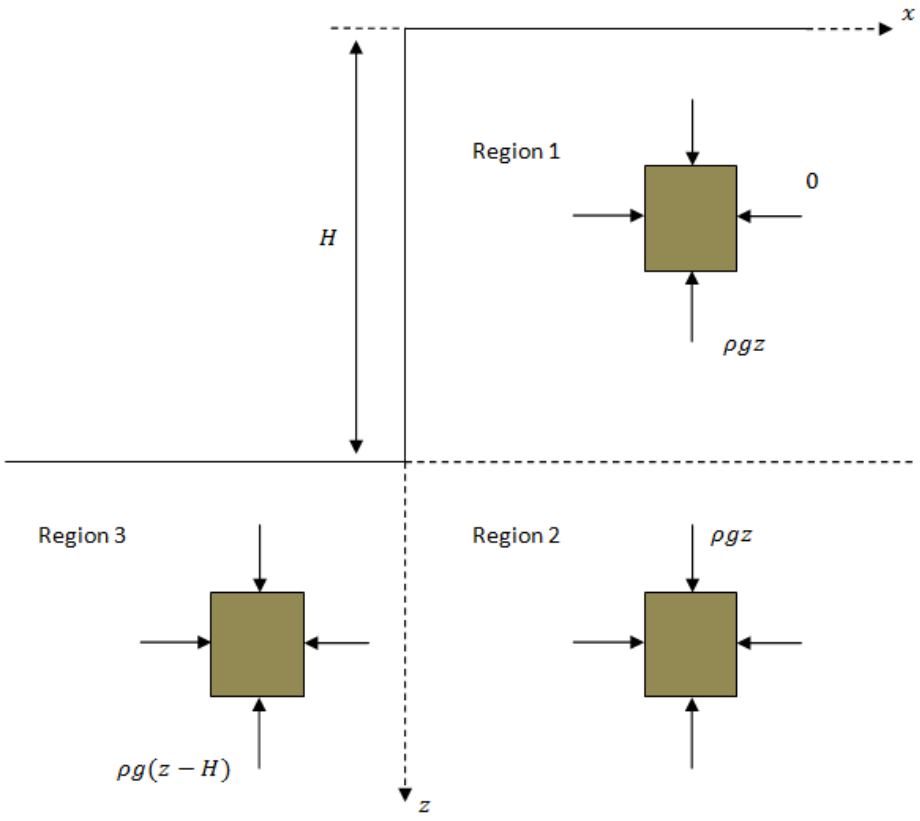

Figure 18 - Discontinuous stress field for vertical cut

Region 1

The stresses identified in region 1 include:

$$\sigma_{xx} = 0, \quad \sigma_{zz} = \rho g z$$

Since the coordinate origin is located at the top of the cut these stresses will satisfy equilibrium as well as the traction free boundaries, traction free boundary simply means the surface is free from any external stresses. The Mohr circle for region 1 is detailed in Figure 19.

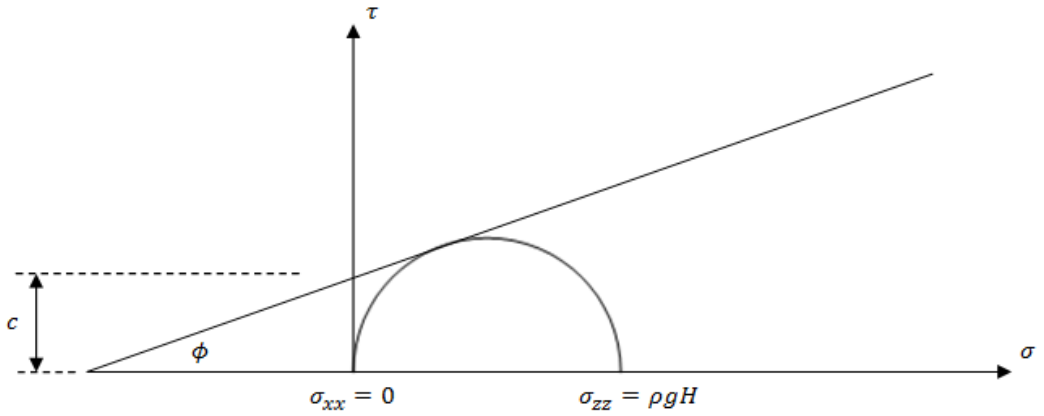

Figure 19 - Mohr diagram for region 1

Region 2

The stress located in the z-component must be continuous across the dashed line, therefore will be given $\sigma_{zz} = \rho g z$. The stress in the x-component is unidentified at current state.

Region 3

Stress in the x-component from region 2 must remain continuous across the dashed line, and to satisfy the zero traction boundary condition on the surface, therefore $\sigma_{zz} = \rho g(z - H)$ (Davis & Selvadurai, 2005). Note for the LB theorem, the stresses everywhere cannot exceed yield point.

Now refer back to Figure 16, the Mohr circle will achieve its greatest diameter when $z = H$. Therefore, the maximum possible height will occur when the Mohr circle touches the yield envelope. Hence, the critical height is given by

$$\rho g H_L = \frac{2c \cos \phi}{1 - \sin \phi} \qquad \text{Eq. 3.4}$$

Where;

$H_L =$ critical height determined from the lower bound theorem.

Let's refer back to the horizontal stress, σ_{xx}, now in order for the LB theorem to work we must find a stress field that will satisfy equilibrium throughout, while also nowhere exceeding the yield point. This can be achieved by letting;

$$\sigma_{xx} = \rho g(z - H)$$

in both regions 2 and 3.

An isotropic stress field will be created in region 3, while a Mohr circle for region 2 no greater than that detailed in Figure 19.

Eq. 3.4 represents an equation which can be rearranged, hence let $\cos\phi = \sqrt{1-\sin^2\phi} = \sqrt{(1-\sin\phi)(1+\sin\phi)}$

Therefore,

$$H_L = \frac{2c\sqrt{(1-\sin\phi)(1+\sin\phi)}}{(1-\sin\phi)\rho g}$$

Now, let

$$N = \frac{1+\sin\phi}{1-\sin\phi}$$

Hence, the lower bound critical height is

$$H_L = \frac{2c}{\rho g}\sqrt{N}$$

3.3 Upper Bound

The Upper Bound (UB) solution is identified by calculating the stress that causes the soil to fail. The lower the upper bound solution, the closer it becomes to the exact solution (HKU, 2013).

There are two essential steps for UBs, the first includes the determination of dissipation along interface of velocity jumps using velocity diagrams, a hodograph has been detailed in Figure 20. The second is the use of energy balance to determine the collapse load. It is worthwhile to note that the UB method provides optimistic answers (Liu, 2010).

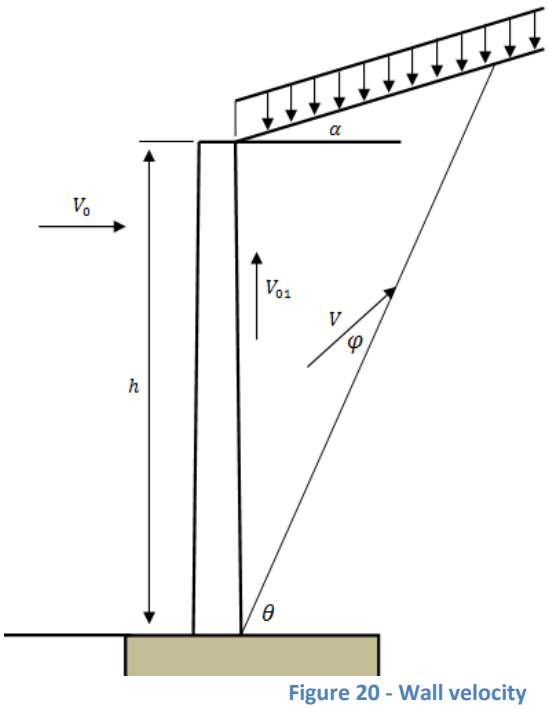

Figure 20 - Wall velocity

There are two cases which will be considered throughout the calculations; they include the passive and active cases.

3.3.1 *Passive case*

In the passive case, the wall moves to the right and the failure wedge moves up and to the right. The force triangle from the hodograph has been constructed and detailed in Figure 21. The wall velocity relative to the stationary mass is V_0. The other velocities include:

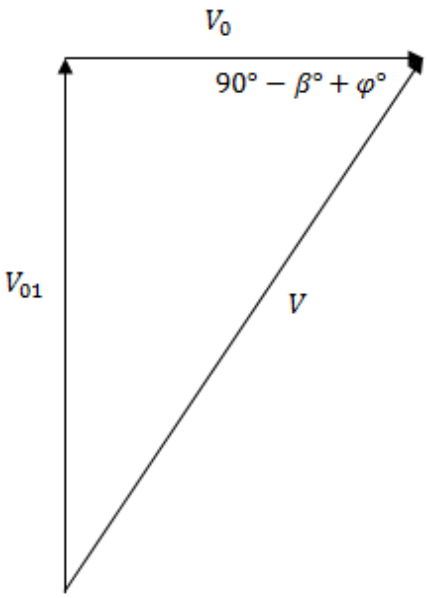

Figure 21 - Passive force triangle

$$V = V_0 \csc(\beta - \phi)$$

$$V_{01} = V_0 \cot(\beta - \phi)$$

From Figure 20, length (L) of the slip line is determined from the simple sine rule.

$$\frac{L}{\sin(90 + \alpha)} = \frac{H}{\sin[180 - (90 + \alpha) - (\beta)]}$$

$$\frac{L}{\sin(90 + 20)} = \frac{H}{\sin[180 - (90 + 20) - (\beta)]}$$

$$\frac{L}{\sin 110} = \frac{H}{\sin(70 - \beta)}$$

$$L = \frac{H \sin 110}{\sin(70 - \beta)}$$

The weight of the failure wedge is:

$$W = \frac{\rho g H^2}{2} \tan(\beta)$$

$$= \frac{26.5 \times 9.81 \times 2.2^2}{2} \times \tan(\beta)$$

$$W = 629.11 \tan \beta$$

Thus, the rate of dissipation is:

$$D = cLV\cos\phi + P_P V_{01}\sin\delta$$

$$D = c\frac{H\sin 110}{\sin(70-\beta)} \times V_0 \csc(\beta-\phi)\cos\phi + P_P V_0 \cot(\beta-\phi)\sin\delta \qquad \text{Eq. 3.5}$$

And, the power of the external forces is:

$$R = P_P V_0 \cos\delta - WV_0 \cot(\beta-\phi)$$

$$R = P_P V_0 \cos\delta - \frac{\rho g H^2}{2}\tan(\beta)\, V_0 \times \cot(\beta-\phi) \qquad \text{Eq. 3.6}$$

Where, P_P represents the passive thrust on the wall.

Now, in order to calculate a dimensionless form for the passive thrust, we must equate both 3.5 and 3.6.

$$c\frac{H\sin 110}{\sin(70-\beta)} \times V_0 \csc(\beta-\phi)\cos\phi + P_P V_0 \cot(\beta-\phi)\sin\delta$$
$$= P_P V_0 \cos\delta - \frac{\rho g H^2}{2}\tan(\beta)\, V_0 \times \cot(\beta-\phi)$$

$$P_P V_0(\cos\delta - \cot(\beta-\phi)\sin\delta)$$
$$= \frac{\rho g H^2}{2}\tan(\beta)\, V_0 \times \cot(\beta-\phi)$$
$$+ c\frac{H\sin 110}{\sin(70-\beta)} V_0 \csc(\beta-\phi)\cos\phi$$

$$\therefore \frac{P_P V_0}{cH} = \frac{\frac{\rho g H}{2c}\tan(\beta)\, V_0 \times \cot(\beta-\phi) + \frac{\sin 110}{\sin(70-\beta)} V_0 \csc(\beta-\phi)\cos\phi}{(\cos\delta - \cot(\beta-\varphi)\sin\delta)}$$

$$\frac{P_P}{cH} = \frac{\frac{\rho g H}{2c}\tan(\beta)\cot(\beta-\phi) + \frac{\sin 110}{\sin(70-\beta)} \times \csc(\beta-\phi)\cos\phi}{(\cos\delta - \cot(\beta-\phi)\sin\delta)}$$

To Simplify multiply both the denominator and numerator of the RHS by $\sin(\beta-\phi)$ (assuming $\beta \neq 0$)

$$P = \frac{\tan(\beta)\cos(\beta-\phi) + \frac{\sin 110}{\sin(70-\beta)}\cos\phi}{\sin(\beta-\phi)\cos\delta - \cos(\beta-\phi)\sin\delta}$$

Furthermore

$$P = \frac{\tan(\beta)\cos(\beta-\phi) + \dfrac{\sin 110}{\sin(70-\beta)}\cos\phi}{\sin(\beta-\phi-\delta)}$$

Or

$$P = \frac{\sin(\beta)\cos(\beta-\phi)}{\cos(\beta)\sin(\beta-\phi-\delta)} + \frac{\sin(110)\cos\phi}{\sin(70-\beta)\sin(\beta-\phi-\delta)}$$

Now, let

$$P_1 = \frac{\sin(\beta)\cos(\beta-\phi)}{\cos(\beta)\sin(\beta-\phi-\delta)} \qquad \textit{AND} \qquad P_2 = \frac{\sin(110)\cos\phi}{\sin(70-\beta)\sin(\beta-\phi-\delta)}$$

Now, to minimise $P_P$we must adjust β and hence find the upper bound for the passive state. When we do this it is found that β (critical value) is dependent of δ.

Hence,

$$\frac{\partial}{\partial\beta}\sin(\beta)\cos(\beta-\phi) = \cos(\beta)\cos(\beta-\phi) - \sin(\beta)\sin(\beta-\phi)$$

$$= \cos(\beta+(\beta-\phi))$$

$$= \cos(2\beta-\phi)$$

$$\frac{\partial}{\partial\beta}\cos(\beta)\sin(\beta-\phi-\delta)$$

$$= \cos(\beta)\cos(\beta-\phi-\delta) - \sin(\beta)\sin(\beta-\phi-\delta)$$

$$= \cos(\beta+(\beta-\phi-\delta))$$

$$= \cos(2\beta-\phi-\delta)$$

$$\frac{\partial}{\partial\beta}\sin(110)\cos\phi = 0$$

$$\frac{\partial}{\partial\beta}\sin(70-\beta)\sin(\beta-\phi-\delta)$$
$$= \cos(70-\beta)\sin(\beta-\phi-\delta)$$
$$+ \sin(70-\beta)\cos(\beta-\phi-\delta)$$
$$= \sin((70-\beta)+(\beta-\phi-\delta))$$
$$= \sin(70-\phi-\delta)$$

Thus, using quotient rule

$$\frac{\partial P_1}{\partial\beta} = \frac{\cos(2\beta-\phi)\cos(\beta)\sin(\beta-\phi-\delta) - \sin(\beta)\cos(\beta-\phi)\cos(2\beta-\phi-\delta)}{\cos^2(\beta)\sin^2(\beta-\phi-\delta)}$$

And

$$\frac{\partial P_2}{\partial\beta} = -\frac{\sin(70-\phi-\delta)\sin(110)\cos\phi}{\sin^2(70-\beta)\sin^2(\beta-\phi-\delta)}$$

Now, setting $\frac{\partial P}{\partial\beta} = 0$ results in $\frac{\partial P_1}{\partial\beta} = -\frac{\partial P_2}{\partial\beta}$ (assuming $\sin(\beta-\phi-\delta) \neq 0$)

$$[\cos(2\beta-\phi)\cos(\beta)\sin(\beta-\phi-\delta)$$
$$- \sin(\beta)\cos(\beta-\phi)\cos(2\beta-\phi-\delta)]\sin^2(70-\beta)$$
$$= \cos^2(\beta)\,[\sin(70-\phi-\delta)\sin(110)\cos\phi] \qquad (\mathbf{1})$$

in which $\beta \neq 70$ and $\beta \neq 90$

Furthermore

$$\cos(2\beta-\phi)\sin(\beta-\phi-\delta) = \frac{1}{2}[\sin(3\beta-2\phi-\delta) - \sin(\beta+\delta)]$$

And

$$\cos(2\beta-\phi-\delta)\cos(\beta-\phi) = \frac{1}{2}[\cos(\beta-\delta) + \cos(3\beta-2\phi-\delta)]$$

The LHS of (1) simplifies to

$$\frac{\sin^2(70-\beta)}{2}\big[[\sin(3\beta-2\phi-\delta) - \sin(\beta+\delta)]\cos(\beta)$$
$$- [\cos(\beta-\delta) + \cos(3\beta-2\phi-\delta)]\sin(\beta)\big]$$

$$\frac{\sin^2(70-\beta)}{2}[\sin(3\beta-2\phi-\delta)\cos(\beta)-\sin(\beta+\delta)\cos(\beta)-\cos(\beta-\delta)\sin(\beta)$$
$$-\cos(3\beta-2\phi-\delta)\sin(\beta)]$$

But

$$\sin(3\beta-2\phi-\delta)\cos(\beta)=\frac{1}{2}[\sin(4\beta-2\phi-\delta)+\sin(2\beta-2\phi-\delta)]$$

And

$$\cos(3\beta-2\phi-\delta)\sin(\beta)=\frac{1}{2}[\sin(4\beta-2\phi-\delta)-\sin(2\beta-2\phi-\delta)]$$

And

$$\sin(\beta+\delta)\cos(\beta)=\frac{1}{2}[\sin(2\beta+\delta)+\sin(\delta)]$$

And

$$\cos(\beta-\delta)\sin(\beta)=\frac{1}{2}[\sin(2\beta-\delta)+\sin(\delta)]$$

Therefore

$$\frac{\sin^2(70-\beta)}{2}[0.5\sin(4\beta-2\phi-\delta)+0.5\sin(2\beta-2\phi-\delta)-0.5\sin(2\beta+\delta)$$
$$-0.5\sin(\delta)-0.5\sin(2\beta-\delta)-0.5\sin(\delta)-0.5\sin(4\beta-2\phi-\delta)$$
$$+0.5\sin(2\beta-2\phi-\delta)]$$

$$\frac{\sin^2(70-\beta)}{2}[\sin(2\beta-2\phi-\delta)-\sin(\delta)-0.5\sin(2\beta+\delta)-0.5\sin(2\beta-\delta)]$$

But

$$\sin(2\beta+\delta)=\sin 2\beta\cos\delta+\cos 2\beta\sin\delta$$

And

$$\sin(2\beta-\delta)=\sin 2\beta\cos\delta-\cos 2\beta\sin\delta$$

$$\frac{\sin^2(70-\beta)}{2}[\sin(2\beta-2\phi-\delta)-\sin(\delta)-0.5\sin 2\beta\cos\delta-0.5\cos 2\beta\sin\delta$$
$$-0.5\sin 2\beta\cos\delta+0.5\cos 2\beta\sin\delta]$$

$$\frac{\sin^2(70-\beta)}{2}[\sin(2\beta-2\phi-\delta)-\sin(\delta)-\sin 2\beta\cos\delta]$$

But

$$\sin^2(70-\beta)=\frac{1-\cos(140-2\beta)}{2}$$

Then

$$[1-\cos(140-2\beta)][\sin(2\beta-2\phi-\delta)-\sin(\delta)-\sin 2\beta\cos\delta]$$

$$\begin{aligned}[\sin(2\beta-2\phi-\delta)&-\sin(2\beta-2\phi-\delta)\cos(140-2\beta)-\sin(\delta)\\&+\sin(\delta)\cos(140-2\beta)-\sin 2\beta\cos\delta\\&+\sin 2\beta\cos\delta\cos(140-2\beta)]\end{aligned}$$

But

$$\begin{aligned}&\sin(2\beta-2\phi-\delta)\cos(140-2\beta)\\&\quad=\frac{1}{2}[\sin(140-2\phi-\delta)+\sin(4\beta-2\phi-\delta-140)]\end{aligned}$$

And

$$\sin(2\beta)\cos(140-2\beta)=\frac{1}{2}[\sin(140)+\sin(4\beta-140)]$$

Then

$$\begin{aligned}[\sin(2\beta-2\phi-\delta)&-0.5\sin(140-2\phi-\delta)-0.5\sin(4\beta-2\phi-\delta-140)\\&-\sin(\delta)+\sin(\delta)\cos(140-2\beta)-\sin 2\beta\cos\delta+0.5\sin(140)\\&+0.5\sin(4\beta-140)\cos\delta]\end{aligned}$$

$$\begin{aligned}[\sin(2\beta-2\phi-\delta)&-0.5\sin(4\beta-2\phi-\delta-140)+\sin(\delta)\cos(140-2\beta)\\&-\sin 2\beta\cos\delta+0.5\sin(4\beta-140)\cos\delta-\sin(\delta)+0.5\sin(140)\\&-0.5\sin(140-2\phi-\delta)]\end{aligned}$$

But

$$\cos(140-2\beta)=\cos 140\cos 2\beta+\sin 140\sin 2\beta$$

And

$$\sin(4\beta - 140) = \sin 4\beta \cos 140 - \cos 4\beta \sin 140$$

Then

$$\begin{aligned}[\sin(2\beta - 2\phi - \delta) - 0.5\sin(4\beta - 2\phi - \delta - 140) + \sin(\delta)\cos 140\cos 2\beta \\ + \sin 140 \sin 2\beta \sin(\delta) - \sin 2\beta \cos\delta + 0.5\cos\delta \sin 4\beta \cos 140 \\ - 0.5\cos\delta \cos 4\beta \sin 140 - \sin(\delta) + 0.5\sin(140) \\ - 0.5\sin(140 - 2\phi - \delta)]\end{aligned}$$

For a blasted rock backfill with $\phi = 30°$ and $\delta = 20°$,

$$\begin{aligned}\sin(2\beta - 80) - 0.5\sin(4\beta - 220) - 0.262\cos 2\beta + 0.220\sin 2\beta - 0.940\sin 2\beta \\ - 0.360\sin 4\beta - 0.302\cos 4\beta - 0.342 + 0.321 - 0.347\end{aligned}$$

$$\begin{aligned}\sin(2\beta - 80) - 0.5\sin(4\beta - 220) - 0.262\cos 2\beta - 0.720\sin 2\beta - 0.360\sin 4\beta \\ - 0.302\cos 4\beta - 0.368\end{aligned}$$

But

$$\sin(2\beta - 80) = \sin 2\beta \cos 80 - \cos 2\beta \sin 80$$

And

$$\sin(4\beta - 220) = \sin 4\beta \cos 220 - \cos 4\beta \sin 220$$

$$\begin{aligned}\sin 2\beta \cos 80 - \cos 2\beta \sin 80 - 0.5\sin 4\beta \cos 220 + 0.5\cos 4\beta \sin 220 \\ - 0.262\cos 2\beta - 0.720\sin 2\beta - 0.360\sin 4\beta - 0.302\cos 4\beta \\ - 0.368\end{aligned}$$

$$-0.546\sin 2\beta - 1.247\cos 2\beta - 0.080\sin 4\beta - 0.717\cos 4\beta - 0.368$$

But

$$\sin 4\beta = 2\sin 2\beta \cos 2\beta$$

And

$$\sin 2\beta = 2\sin\beta\cos\beta$$

And

$$\cos 2\beta = 1 - 2\sin^2\beta$$

And

$$\cos 4\beta = 1 - 2\sin^2 2\beta$$

Then

$$-1.092\sin\beta\cos\beta - 1.247 + 2.494\sin^2\beta - 0.160\sin 2\beta\cos 2\beta - 0.717 + 1.434\sin^2 2\beta - 0.368$$

But

$$\sin 2\beta\cos 2\beta = (2\sin\beta\cos\beta)(1 - 2\sin^2\beta) = 2\sin\beta\cos\beta - 4\sin\beta\cos\beta\sin^2\beta$$

Then

$$-1.412\sin\beta\cos\beta + 2.494\sin^2\beta + 0.64\sin\beta\cos\beta\sin^2\beta + 1.434\sin^2 2\beta - 2.332$$

But

$$\sin^2\beta = 1 - \cos^2\beta$$

And

$$\sin^2 2\beta = 1 - \cos^2 2\beta$$

Then

$$-0.772\sin\beta\cos\beta - 2.494\cos^2\beta - 0.64\sin\beta\cos\beta\cos^2\beta - 1.434\cos^2 2\beta + 1.596$$

$$-0.772\sin\beta\cos\beta - \cos^2\beta\,(2.494 + 0.64\sin\beta\cos\beta) - 1.434\cos^2 2\beta + 1.596$$

Now, let's consider the RHS

$$\cos^2(\beta)\,[\sin(70 - \phi - \delta)\sin(110)\cos\phi]$$

$$0.278\cos^2(\beta)$$

Let the $RHS = LHS$

$$-0.772\sin\beta\cos\beta - \cos^2\beta\,(2.494 + 0.64\sin\beta\cos\beta) - 1.434\cos^2 2\beta + 1.596 = 0.278\cos^2(\beta)$$

$$-\frac{0.772\sin\beta\cos\beta}{\cos^2(\beta)} - 2.216 - 0.64\sin\beta\cos\beta - 1.434\frac{\cos^2 2\beta}{\cos^2(\beta)} + \frac{1.596}{\cos^2(\beta)} = 0$$

Now, through the use of iterations, the value for β is 63.2, for a cohesionless soil, $c = 0$, with $\phi = 30°$ and $\delta = 20°$, then the passive upper bound estimates to:

$$\frac{P_P}{cH} = \frac{\frac{\rho g H}{2c}\tan(\beta)\cot(\beta-\phi) + \frac{\sin 110}{\sin(70-\beta)} \times \csc(\beta-\phi)\cos\phi}{(\cos\delta - \cot(\beta-\phi)\sin\delta)}$$

$$\frac{P_P}{cH} = \frac{\frac{\rho g H}{2c}\tan(63.2)\cot(63.2-30) + \frac{\sin 110}{\sin(70-63.2)} \times \csc(63.2-30) \times \cos 30}{(\cos 20 - \cot(63.2-30)\sin 20)}$$

$$\frac{P_P}{cH} = \frac{3.04\frac{\rho g H}{2c} + 12.55}{0.42} = 30.01$$

3.3.2 *Active case*

In the active case, the wall moves to the left and the failure wedge moves down and to the left. The force triangle from the hodograph has been constructed and detailed in Figure 22. The relative velocities include:

$$V = V_0\csc(\beta+\varphi)$$

$$V_{01} = V_0\cot(\beta+\varphi)$$

From Figure 20, length (L) of the slip line is determined from the simple sine rule.

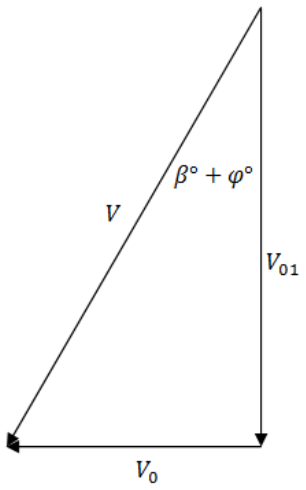

Figure 22 - Active force triangle

$$\frac{L}{\sin(90+\alpha)} = \frac{H}{\sin[180-(90+\alpha)-(\beta)]}$$

$$\frac{L}{\sin(90+20)} = \frac{H}{\sin[180-(90+20)-(\beta)]}$$

$$\frac{L}{\sin 110} = \frac{H}{\sin(70-\beta)}$$

$$L = \frac{H \sin 110}{\sin(70-\beta)}$$

The weight of the failure wedge is:

$$W = \frac{\rho g H^2}{2}\tan(\beta)$$

$$= \frac{26.5 \times 9.81 \times 2.2^2}{2} \times \tan(\beta)$$

$$W = 629.11 \tan\beta$$

Thus, the rate of dissipation is:

$$D = cLV\cos\phi + P_P V_{01}\sin\delta$$

$$D = c\frac{H \sin 110}{\sin(70-\beta)} \times V_0 \csc(\beta+\varphi)\cos\phi - P_A V_0 \cot(\beta+\varphi)\sin\delta \qquad \text{Eq. 3.7}$$

And, the power of the external forces is:

$$R = -P_A V_0 \cos\delta + W V_0 \cot(\beta+\phi)$$

$$R = -P_A V_0 \cos\delta + \frac{\rho g H^2}{2}\tan(\beta)\, V_0 \times \cot(\beta+\phi) \qquad \text{Eq. 3.8}$$

Where, P_P represents the passive thrust on the wall.

Now, in order to calculate a dimensionless form for the passive thrust, we must equate both 3.7 and 3.8.

$$c\frac{H \sin 110}{\sin(70-\beta)} \times V_0 \csc(\beta+\varphi)\cos\phi - P_A V_0 \cot(\beta+\varphi)\sin\delta$$

$$= -P_A V_0 \cos\delta + \frac{\rho g H^2}{2}\tan(\beta)\, V_0 \times \cot(\beta+\phi)$$

$$P_A V_0(\cos\delta - \sin\delta\cot(\beta+\varphi))$$
$$= \frac{\rho g H^2}{2}\tan(\beta)\,V_0 \times \cot(\beta+\phi)$$
$$- c\frac{H\sin 110}{\sin(70-\beta)}V_0\csc(\beta+\varphi)\cos\phi$$

$$\therefore \frac{P_A V_0}{cH}$$
$$= \frac{\frac{\rho g H}{2c}\tan(\beta)\,V_0 \times \cot(\beta+\phi) - \frac{\sin 110}{\sin(70-\beta)} \times V_0\csc(\beta+\varphi)\cos\phi}{(\cos\delta - \sin\delta\cot(\beta+\varphi))}$$

$$\frac{P_A}{cH} = \frac{\frac{\rho g H}{2c}\tan(\beta)\cot(\beta+\phi) - \frac{\sin 110}{\sin(70-\beta)} \times \csc(\beta+\varphi)\cos\phi}{(\cos\delta - \sin\delta\cot(\beta+\varphi))}$$

To Simplify multiply both the denominator and numerator of the RHS by $\sin(\beta+\phi)$ (assuming $\beta \neq 0$)

$$P = \frac{\tan(\beta)\cos(\beta+\phi) - \frac{\sin 110}{\sin(70-\beta)}\cos\phi}{\sin(\beta+\phi)\cos\delta - \cos(\beta+\phi)\sin\delta}$$

Furthermore

$$P = \frac{\tan(\beta)\cos(\beta+\phi) - \frac{\sin 110}{\sin(70-\beta)}\cos\phi}{\sin(\beta+\phi-\delta)}$$

Or

$$P = \frac{\sin(\beta)\cos(\beta+\phi)}{\cos(\beta)\sin(\beta+\phi-\delta)} - \frac{\sin(110)\cos\phi}{\sin(70-\beta)\sin(\beta+\phi-\delta)}$$

Now, let

$$P_1 = \frac{\sin(\beta)\cos(\beta+\phi)}{\cos(\beta)\sin(\beta+\phi-\delta)} \qquad \textit{AND} \qquad P_2 = \frac{\sin(110)\cos\phi}{\sin(70-\beta)\sin(\beta+\phi-\delta)}$$

Now, to minimise P_P we must adjust β and hence find the upper bound for the passive state. When we do this it is found that β (critical value) is dependent of δ.

Hence,

$$\frac{\partial}{\partial\beta}\sin(\beta)\cos(\beta+\phi) = \cos(\beta)\cos(\beta+\phi) - \sin(\beta)\sin(\beta+\phi)$$

$$= \cos(\beta + (\beta+\phi))$$

$$= \cos(2\beta+\phi)$$

$$\frac{\partial}{\partial\beta}\cos(\beta)\sin(\beta+\phi-\delta)$$

$$= \cos(\beta)\cos(\beta+\phi-\delta) - \sin(\beta)\sin(\beta+\phi-\delta)$$

$$= \cos(\beta + (\beta+\phi-\delta))$$

$$= \cos(2\beta+\phi-\delta)$$

$$\frac{\partial}{\partial\beta}\sin(110)\cos\phi = 0$$

$$\frac{\partial}{\partial\beta}\sin(70-\beta)\sin(\beta+\phi-\delta)$$

$$= \cos(70-\beta)\sin(\beta+\phi-\delta)$$
$$+ \sin(70-\beta)\cos(\beta+\phi-\delta)$$

$$= \sin((70-\beta) + (\beta+\phi-\delta))$$

$$= \sin(70+\phi-\delta)$$

Thus, using quotient rule

$$\frac{\partial P_1}{\partial\beta}$$

$$= \frac{\cos(2\beta+\phi)\cos(\beta)\sin(\beta+\phi-\delta) - \sin(\beta)\cos(\beta+\phi)\cos(2\beta+\phi-\delta)}{\cos^2(\beta)\sin^2(\beta+\phi-\delta)}$$

$$\frac{\partial P_2}{\partial\beta} = -\frac{\sin(70+\phi-\delta)\sin(110)\cos\phi}{\sin^2(70-\beta)\sin^2(\beta+\phi-\delta)}$$

Now, setting $\frac{\partial P}{\partial\beta} = 0$ results in $\frac{\partial P_1}{\partial\beta} = -\frac{\partial P_2}{\partial\beta}$ (assuming $\sin(\beta+\phi-\delta) \neq 0$)

$$[\cos(2\beta+\phi)\cos(\beta)\sin(\beta+\phi-\delta) - \sin(\beta)\cos(\beta+\phi)\cos(2\beta+\phi-\delta)]\sin^2(70-\beta) = \cos^2(\beta)[\sin(70+\phi - \delta)\sin(110)\cos\phi] \quad (\mathbf{1})$$

in which $\beta \neq 70$ and $\beta \neq 90$

Furthermore

$$\cos(2\beta+\phi)\sin(\beta+\phi-\delta) = \frac{1}{2}[\sin(3\beta+2\phi-\delta) - \sin(\beta+\delta)]$$

And

$$\cos(2\beta+\phi-\delta)\cos(\beta+\phi) = \frac{1}{2}[\cos(\beta-\delta) + \cos(3\beta+2\phi-\delta)]$$

The LHS of (1) simplifies to

$$\frac{\sin^2(70-\beta)}{2}\big[[\sin(3\beta+2\phi-\delta) - \sin(\beta+\delta)]\cos(\beta) - [\cos(\beta-\delta) + \cos(3\beta+2\phi-\delta)]\sin(\beta)\big]$$

$$\frac{\sin^2(70-\beta)}{2}[\sin(3\beta+2\phi-\delta)\cos(\beta) - \sin(\beta+\delta)\cos(\beta) - \cos(\beta-\delta)\sin(\beta) - \cos(3\beta+2\phi-\delta)\sin(\beta)]$$

But

$$\sin(3\beta+2\phi-\delta)\cos(\beta) = \frac{1}{2}[\sin(4\beta+2\phi-\delta) + \sin(2\beta+2\phi-\delta)]$$

And

$$\cos(3\beta+2\phi-\delta)\sin(\beta) = \frac{1}{2}[\sin(4\beta+2\phi-\delta) - \sin(2\beta+2\phi-\delta)]$$

And

$$\sin(\beta+\delta)\cos(\beta) = \frac{1}{2}[\sin(2\beta+\delta) + \sin(\delta)]$$

And

$$\cos(\beta - \delta)\sin(\beta) = \frac{1}{2}[\sin(2\beta - \delta) + \sin(\delta)]$$

Therefore

$$\frac{\sin^2(70-\beta)}{2}[0.5\sin(4\beta + 2\phi - \delta) + 0.5\sin(2\beta + 2\phi - \delta) - 0.5\sin(2\beta + \delta) - 0.5\sin(\delta) - 0.5\sin(2\beta - \delta) - 0.5\sin(\delta) - 0.5\sin(4\beta + 2\phi - \delta) + 0.5\sin(2\beta + 2\phi - \delta)]$$

$$\frac{\sin^2(70-\beta)}{2}[\sin(2\beta + 2\phi - \delta) - \sin(\delta) - 0.5\sin(2\beta + \delta) - 0.5\sin(2\beta - \delta)]$$

But

$$\sin(2\beta + \delta) = \sin 2\beta \cos\delta + \cos 2\beta \sin\delta$$

And

$$\sin(2\beta - \delta) = \sin 2\beta \cos\delta - \cos 2\beta \sin\delta$$

$$\frac{\sin^2(70-\beta)}{2}[\sin(2\beta + 2\phi - \delta) - \sin(\delta) - 0.5\sin 2\beta\cos\delta - 0.5\cos 2\beta\sin\delta - 0.5\sin 2\beta\cos\delta + 0.5\cos 2\beta\sin\delta]$$

$$\frac{\sin^2(70-\beta)}{2}[\sin(2\beta + 2\phi - \delta) - \sin(\delta) - \sin 2\beta\cos\delta]$$

But

$$\sin^2(70-\beta) = \frac{1 - \cos(140 - 2\beta)}{2}$$

Then

$$[1 - \cos(140 - 2\beta)][\sin(2\beta + 2\phi - \delta) - \sin(\delta) - \sin 2\beta\cos\delta]$$

$$[\sin(2\beta + 2\phi - \delta) - \sin(2\beta + 2\phi - \delta)\cos(140 - 2\beta) - \sin(\delta) + \sin(\delta)\cos(140 - 2\beta) - \sin 2\beta\cos\delta + \sin 2\beta\cos\delta\cos(140 - 2\beta)]$$

But

$$\sin(2\beta + 2\phi - \delta)\cos(140 - 2\beta) = \frac{1}{2}[\sin(140 + 2\phi - \delta) + \sin(4\beta + 2\phi - \delta - 140)]$$

And

$$\sin(2\beta)\cos(140 - 2\beta) = \frac{1}{2}[\sin(140) + \sin(4\beta - 140)]$$

Then

$$\begin{aligned}[\sin(2\beta + 2\phi - \delta) - 0.5\sin(140 + 2\phi - \delta) - 0.5\sin(4\beta + 2\phi - \delta - 140) \\ - \sin(\delta) + \sin(\delta)\cos(140 - 2\beta) - \sin 2\beta\cos\delta + 0.5\sin(140) \\ + 0.5\sin(4\beta - 140)\cos\delta]\end{aligned}$$

$$\begin{aligned}[\sin(2\beta + 2\phi - \delta) - 0.5\sin(4\beta + 2\phi - \delta - 140) + \sin(\delta)\cos(140 - 2\beta) \\ - \sin 2\beta\cos\delta + 0.5\sin(4\beta - 140)\cos\delta - \sin(\delta) + 0.5\sin(140) \\ - 0.5\sin(140 + 2\phi - \delta)]\end{aligned}$$

But

$$\cos(140 - 2\beta) = \cos 140\cos 2\beta + \sin 140\sin 2\beta$$

And

$$\sin(4\beta - 140) = \sin 4\beta\cos 140 - \cos 4\beta\sin 140$$

Then

$$\begin{aligned}[\sin(2\beta + 2\phi - \delta) - 0.5\sin(4\beta + 2\phi - \delta - 140) + \sin(\delta)\cos 140\cos 2\beta \\ + \sin 140\sin 2\beta\sin(\delta) - \sin 2\beta\cos\delta + 0.5\cos\delta\sin 4\beta\cos 140 \\ - 0.5\cos\delta\cos 4\beta\sin 140 - \sin(\delta) + 0.5\sin(140) \\ - 0.5\sin(140 + 2\phi - \delta)]\end{aligned}$$

Since $\phi = 30°$ and $\delta = 20°$,

$$\begin{aligned}\sin(2\beta + 40) - 0.5\sin(4\beta - 100) - 0.262\cos 2\beta + 0.220\sin 2\beta - 0.940\sin 2\beta \\ - 0.360\sin 4\beta - 0.302\cos 4\beta - 0.342 + 0.321\end{aligned}$$

$$\sin(2\beta + 40) - 0.5\sin(4\beta - 100) - 0.262\cos 2\beta - 0.720\sin 2\beta - 0.360\sin 4\beta - 0.302\cos 4\beta - 0.021$$

But

$$\sin(2\beta + 40) = \sin 2\beta \cos 40 + \cos 2\beta \sin 40$$

And

$$\sin(4\beta - 100) = \sin 4\beta \cos 100 - \cos 4\beta \sin 100$$

Then

$$\sin 2\beta \cos 40 + \cos 2\beta \sin 40 - 0.5\sin 4\beta \cos 100 + 0.5\cos 4\beta \sin 100 - 0.720\sin 2\beta - 0.360\sin 4\beta - 0.302\cos 4\beta - 0.021$$

$$0.046\sin 2\beta + 0.643\cos 2\beta - 0.447\sin 4\beta + 0.190\cos 4\beta - 0.021$$

But

$$\sin 4\beta = 2\sin 2\beta \cos 2\beta$$

And

$$\sin 2\beta = 2\sin\beta \cos\beta$$

And

$$\cos 2\beta = 1 - 2\sin^2\beta$$

And

$$\cos 4\beta = 1 - 2\sin^2 2\beta$$

Then

$$0.092\sin\beta \cos\beta + 0.643 - 1.286\sin^2\beta - 0.894\sin 2\beta \cos 2\beta + 0.190 - 0.38\sin^2 2\beta - 0.021$$

$$0.092\sin\beta \cos\beta - 1.286\sin^2\beta - 0.894\sin 2\beta \cos 2\beta - 0.38\sin^2 2\beta + 0.812$$

But

$$\sin 2\beta \cos 2\beta = (2\sin\beta\cos\beta)(1 - 2\sin^2\beta) = 2\sin\beta\cos\beta - 4\sin\beta\cos\beta\sin^2\beta$$

Then

$$0.092\sin\beta\cos\beta - 1.286\sin^2\beta - 1.788\sin\beta\cos\beta + 3.576\sin\beta\cos\beta\sin^2\beta - 0.38\sin^2 2\beta + 0.812$$

But

$$\sin^2\beta = 1 - \cos^2\beta$$

And

$$\sin^2 2\beta = 1 - \cos^2 2\beta$$

Then

$$-1.696\sin\beta\cos\beta - 1.286 + 1.286\cos^2\beta + 3.576\sin\beta\cos\beta - 3.576\sin\beta\cos\beta\cos^2\beta - 0.38 + 0.38\cos^2 2\beta + 0.812$$

$$1.88\sin\beta\cos\beta + \cos^2\beta\,(1.286 - 3.576\sin\beta\cos\beta) + 0.38\cos^2 2\beta - 0.854$$

Now, let's consider the RHS

$$\cos^2(\beta)\,[\sin(70 + \phi - \delta)\sin(110)\cos\phi]$$

$$0.801\cos^2(\beta)$$

Let the $RHS = LHS$

$$1.88\sin\beta\cos\beta + \cos^2\beta\,(1.286 - 3.576\sin\beta\cos\beta) + 0.38\cos^2 2\beta - 0.854$$

$$= 0.801\cos^2(\beta)$$

$$\frac{1.88\sin\beta\cos\beta}{\cos^2(\beta)} + 0.485 - 3.576\sin\beta\cos\beta + 0.38\frac{\cos^2 2\beta}{\cos^2(\beta)} - \frac{0.85}{\cos^2(\beta)} = 0$$

Now, through the use of iterations, the value for β is 55, for a cohesionless soil, $c = 0$, with $\phi = 30°$ and $\delta = 20°$, then the active upper bound estimates to:

$$\frac{P_A}{cH} = \frac{\frac{\rho g H}{2c}\tan(\beta)\cot(\beta+\phi) - \frac{\sin 110}{\sin(70-\beta)} \times \csc(\beta+\varphi)\cos\phi}{(\cos\delta - \sin\delta\cot(\beta+\varphi))}$$

$$\frac{P_A}{cH} = \frac{\tan(55)\cot(55+30) - \frac{\sin 110}{\sin(70-55)}\csc(55+30)\cos 30}{(\cos 20 - \sin 20\cot(55+30))}$$

$$\frac{P_A}{cH} = \frac{3.06\frac{\rho g H}{2c} - 3.16}{0.91} = -3.47$$

Scott Clayton
0061010140

4. ANALYSE OF CANTILEVER WALL

4.1 Properties

Bruner (1983) mentions the design of the stem height in cantilever retaining walls is a function of the difference in required elevation on each side of the stem, and additionally, the depth of cover on the toe side of the stem. Bruner (1983) also elaborates that the design of the footing width is a function of the height of the stem and its stability requirements. The geometrical data is detailed in Figure 24.

Therefore, a stability analysis is undertaken in order to determine the minimum required heel width of a cantilever retaining wall. This minimum width is determined by checking the Ultimate Limit State (ULS), which involves:

- Failure of the Ground (GEO) – This involves the bearing failure of the foundation and the sliding resistance on the base.

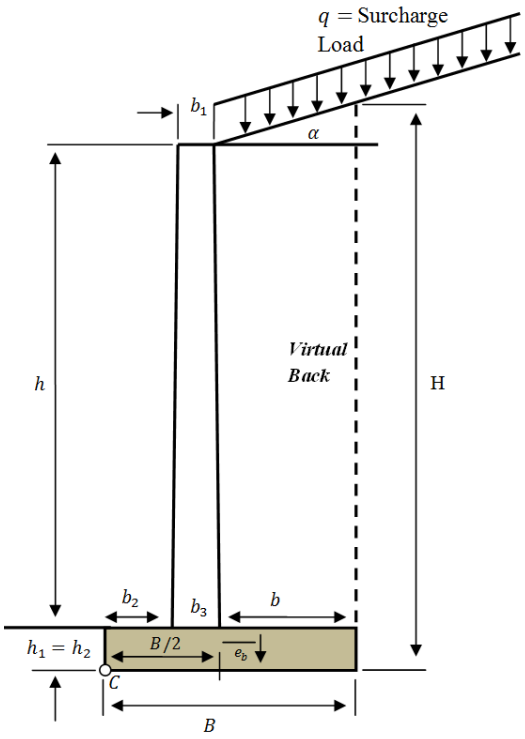

Figure 23 - Dimensions for given wall

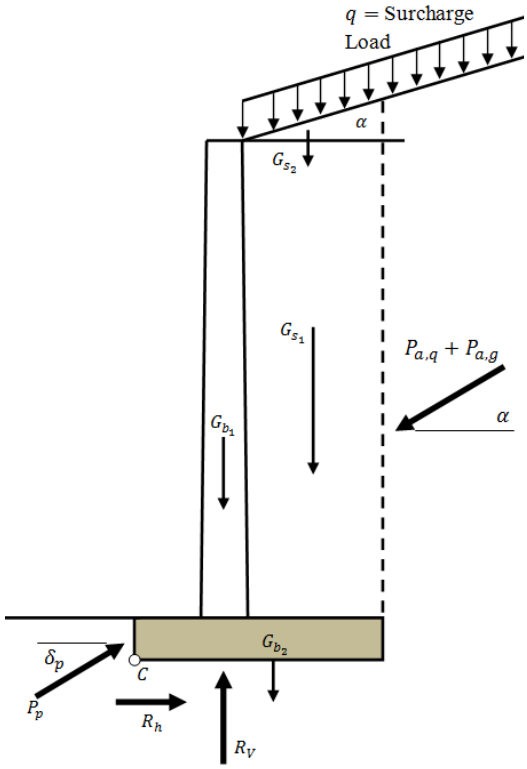

Figure 24 - Actions

For GEO ULS the failure will occur in the ground, hence the wall movements will be large enough to mobilise the active earth pressures along the virtual back of the wall (Frank, et al., 2004). This pressure is inclined at an angle equal to that of the sloped backfill; this is detailed in Figure 23. It must be noted that the active earth pressure located on the virtual back implies that the width of the heel (b) is large enough to allow the development of a conjugate Coulomb type failure surface located above the heel within the soil mass. This failure surface is inclined at an angle of $(45 + \varphi_k'/2)$. Therefore, the width of the heel should not be much smaller, hence a minimum value of:

$$b = b_{min} = h\tan(45 - \phi'/2) \qquad \text{Eq. 4.1}$$

4.2 Backfill Soil

Course grained, granular soils are known for their high permeability and are therefore the preferred backfill soils. The large void spaces allow quick dissipation of the excess pore water pressure, which brings about a drained condition and reduces the stresses imposed on the retaining wall. However, the outcome will principally depend on cost and availability of such materials. The drained condition only occurs when the water dissipates through the soil, therefore *only* the soil particles support the loads. Alternatively, the undrained condition only occurs when the water is retained within the soil, therefore the loads are supported by both soil particles and water (White, 2011). Drained or undrained condition primarily depends on the soil type, geological formation, distribution of grain size, artificial drainage systems (installed in backfill), and rate of loading (Budhu, 2007).

The use of fine grained backfill such as clayey materials is not recommended, as clays are known to shrink and swell depending on seasonal variations in moisture content. If these soils are used as backfill it may lead to increased pressure acting against the wall. Therefore, when compared to cohesionless materials, long term settlement problems are significantly greater (Brand, 1982). If cohesive materials are used within backfills, then attention must be paid to the provision of drainage systems in order to prevent accumulation of water pressure.

4.3 Stability Check

The Factor of Safety (FoS) has a large influence on the design of a retaining wall. For instance, the international building code (2006) requires a global FoS of 1.5 against overturning and lateral sliding of retaining walls (GuhaRay, et al., 2013).

Various definitions of FoS are used in geotechnical engineering. There are three commonly used FoS listed below:

- factor on material strength;
- factor on load; and
- factor defined as ratio of resisting forces to disturbing forces.

As mentioned in paragraph 4.1, a limit state is a state when a structure no longer satisfies the relevant design criteria. For any given design, stability is provided and the design is far from its ultimate limit state. Therefore to undertake an ULS analysis it is required to drive the system till collapse.

In order to drive a system to ULS which correspond to the three FoS definitions list above, include:

- reducing the soil strength;
- increasing an existing load; and
- place an additional load in the system.

Whenever soil is excavated there is a chance that movement of soil will cause collapse (covered in paragraph 2.2.1 and 2.2.2), this may either be influenced by:

- *sliding* forward (translational, 2.2.1c.);
- *bearing capacity* failure;
- *overturn* about its toe (2.2.1a.);
- rotation around a failure plane which encompasses the structure; and
- slipping down a inclined slope.

If the soil which is being excavated contains moderate amounts of water either by the intrusion of surface water or by the water table. Then the danger of collapse is greatly increased through increase in pore water pressure.

4.3.1 *Tension at Base*

The eccentricity, e, of the resultant force which acts on the base slab is calculated as

$$e = \frac{B_{min}}{2} + \frac{M_o}{R_V} \qquad \text{Eq. 4.2}$$

Where;

B_{min} = width of the base slab;

$\sum M_O$ = sum of the moments of forces overturning about the toe.

$\sum R_V$ = sum of all the vertical forces acting on the wall.

Eccentricity should be less then $B/6$ in order for there to be no tension soil pressure developed at the base. If this condition is satisfied then criterion for overturning is automatically satisfied.

However, if $e > B/6$ then tension soil pressure will be present at the heel of the base slab, and redistribution of soil pressure takes place to keep it compressive throughout (Braja, 2014).

4.3.2 *Check for Overturning*

The FoS against overturning of a wall about its toe is expressed;

$$F_o = \frac{\sum M_R}{\sum M_O} \qquad \text{Eq. 4.3}$$

Where;

$\sum M_R$ = sum of the moments of forces resisting overturning;

A global FoS required against overturning is no less than 2.

4.3.3 *Check for Bearing Capacity Failure*

The FoS for bearing of the retaining wall along the base is expressed as

$$F_b = \frac{q_u}{P_{max}} \qquad \text{Eq. 4.4}$$

Where, the maximum pressure acting at the base slab of the wall is expressed as

$$P_{max} = \frac{\sum R_V}{B_{min}}\left(1 + \frac{6e}{B_{min}}\right)$$

and;

The ultimate bearing capacity q_u is expressed as

$$q_u = c_f N_c \lambda_{cs} \lambda_{cd} \lambda_{ci} + q N_q \lambda_{qs} \lambda_{qd} \lambda_{qi} + \frac{1}{2} \gamma_f B' N_y \lambda_{ys} \lambda_{yd} \lambda_{yi}$$

Where:

$\lambda_{cs}\lambda_{qs}\lambda_{ys}$ are considered shape factors, which are used to determine the bearing capacity of a rectangular footing (Braja & Khaled, 2014).

$\lambda_{cd}\lambda_{qd}\lambda_{yd}$ are considered depth factors, which account for the shearing resistance developed along the failure surface in soil located above the footing (Braja & Khaled, 2014).

$\lambda_{ci}\lambda_{qi}\lambda_{yi}$ are considered inclination factors, which are used to determine the bearing capacity of a footing, where the load application is inclined at a certain angle to the vertical (Braja & Khaled, 2014).

Table 3 – Bearing capacity factors (Braja, 2014)

ϕ	N_c	N_q	N_γ
0	5.14	1.00	0.00
5	6.49	1.57	0.45
10	8.35	2.47	1.22
15	10.98	3.94	2.65
20	14.83	6.40	5.39
25	20.72	10.66	10.88
30	30.14	18.40	22.40
35	46.12	33.30	48.03
40	75.31	64.20	109.41
45	133.88	134.88	271.76
50	266.89	319.07	762.89

From table 4, for blasted rock with $\phi = 30$ the bearing capacity factors are $N_c = 30.14, N_q = 18.40,$ and $N_y = 22.40$

A global FoS required against bearing failure is no less than 3.

4.3.4 *Check for Sliding along Base*

The FoS for sliding of the retaining wall along the base is expressed as

$$F_s = \frac{R_V \tan \delta}{R_H} \qquad \text{Eq. 4.5}$$

Where;

$R_H =$ sum of all the horizontal forces acting on the wall.

A global FoS required against sliding is no less than 1.5.

4.3.5 *Applied Forces*

Determining the total active and passive horizontal forces acting on a cantilever retaining wall will result in determining whether the structure is safe against sliding. Horizontal active forces acting on the virtual back (P_{ah}) and the horizontal resistance (P_{ph}) has been identified in Figure 23. It is recognised in this situation that P_{ph} should be treated as a favourable force as to appose P_{ah} (Frank, et al., 2004).

Horizontal active force, P_{ah};

$= (P_{ah,q} + P_{ah,g}) \cos \alpha$

Where;

$P_{ah,q} = K_{ah} q H$

$P_{ah,g} = 0.5 K_{ah} \gamma H^2$

Resistance force, P_{ph};

$= (G_b + G_s + P_{av} - P_{pv}) \tan \alpha$

Where;

$\boldsymbol{G_b} = G_{b_1} + G_{b_2}$

$G_{b_1} = 0.5(b_1 + b_3) h \gamma_b$

$$G_{b_2} = (b_2 + b_3 + b)h_2\gamma_b$$

$$\boldsymbol{G_s} = G_{s_1} + G_{s_2}$$

$$G_{s_1} = bh\gamma$$

$$G_{s_2} = 0.5b^2\gamma \tan\alpha$$

$$\boldsymbol{P_{av}} = P_{av,q} + P_{av,g}$$

$$P_{av,q} = P_{ah,q} \tan\alpha$$

$$P_{av,g} = P_{ah,g} \tan\alpha$$

$$\boldsymbol{P_{pv}} = P_{ph} \tan\delta_p$$

4.4 Scenario: Blasted Rock Backfill AND Blasted Rock Foundation

Table 4 - Wall properties

Wall Properties		
Total Wall Height (m)	H_1	2.5
Virtual Wall Height (m)	H_2	2.962
Wall Stem Height (m)	h	2.2
Wall Stem Thickness: top (m)	b_1	0.50
Wall Stem Thickness: bottom (m)	b_3	0.70
Width of toe (m)	b_2	0.95
Width of heel (m)	b	1.270
Toe embedment depth (m)	h_1	0.30
Wall Toe Height (m)	h_2	0.30
Slope Anlge (Degrees)	$\boldsymbol{\alpha}$	20
Wall Base Width (m)	B_{min}	2.92
Poisson's Ratio	v_b	0.2
Young's Modulus ($\times 10^3$ MPa)	E_b	25
Total Unit Weight (kN/m^3)	y_b	23.5

A surcharge load, $q = 10\ kPa$

For ***Active*** Forces applied on the virtual wall:

$$P_{ah} = (P_{ah,q} + P_{ah,g})\cos\alpha = (K_{ah}qH_2 + 0.5K_{ah}\gamma_s H_2^2)\cos\alpha$$

From Appendix G, with variable given in Appendix B and Table 4:

α (deg)	ϕ (deg)	$\delta' = \frac{2}{3}\phi'$	K_a	$\delta' = \frac{\phi'}{2}$	K_a
20	30	20.0000	0.4142	15.000	0.4150

Between wall friction angle $\delta' = \frac{2}{3}\phi'$ *and* $\delta' = \frac{\phi'}{2}$

$K_a = 0.5(0.4142 + 0.4150) = 0.4146$

From Equation 4.1:

$$b = 2.20 \times \tan\left(45 - \frac{30}{2}\right) = 1.27\ m$$

Where, virtual back, H_2*:*

$= h_2 + h + b\tan\alpha = 0.300 + 2.200 + [1.270] \times \tan(20)$

$H_2 = 2.962\ m$

$\therefore P_{ah} = (0.4146 \times 10 \times 2.962 + 0.5 \times 0.4146 \times 26.5 \times 2.962^2)\cos(20°)$

$= (12.280 + 48.196)\cos 20$

$$\boldsymbol{P_{ah} = 56.83\ kPa}$$

$P_{av} = P_{av,q} + P_{av,g} = P_{ah,q}\tan\alpha + P_{ah,g}\tan\alpha$

$= 12.280 \times \tan 20 + 48.196 \times \tan 20$

$= 4.470 + 17.542$

$$\boldsymbol{P_{av} = 22.01\ kPa}$$

For ***Passive*** Forces:

From Appendix H, with variable given in Appendix B and Table 4:

α (deg)	ϕ (deg)	$\delta' = \frac{2}{3}\phi'$	K_p	$\delta' = \frac{\phi'}{2}$	K_p
20	30	20.0000	6.1054	15.000	4.9765

Between wall friction angle $\delta' = \frac{2}{3}\phi'$ *and* $\delta' = \frac{\phi'}{2}$

$K_a = 0.5(6.1054 + 4.9765) = 5.541$

From Eq. 3.18 or 3.25, $c' = 0$*:*

$P_{ph} = 0.5K_{ph}\gamma_s h_1^2$

$= 0.5 \times 5.541 \times 26.5 \times 0.30^2$

$$\boldsymbol{P_{ph} = 6.61\ kPa}$$

$P_{pv} = P_{ph} \tan \delta_p$

$= 6.61 \times \tan 20$

$$\boldsymbol{P_{pv} = 2.41\ kPa}$$

Now, $\sum F_V$;

$R_v = G_b + G_s + P_{a,v} - P_{p,v}$

$G_b = G_{b_1} + G_{b_2} = 0.5(b_1 + b_3)h\gamma_b + (b_2 + b_3 + b)h_2\gamma_b$

$= 0.5(0.50 + 0.70) \times 2.2 \times 23.5 + (0.95 + 0.70 + 1.27) \times 0.3 \times 23.5$

$= 31.02 + 20.586$

$G_b = 51.606\ kN$

$G_s = G_{s_1} + G_{s_2} = bh\gamma_s + 0.5b^2\gamma_s \tan \alpha$

$= 1.27 \times 2.2 \times 26.5 + 0.5 \times 1.27^2 \times 26.5 \times \tan 20$

$= 74.041 + 7.778$

$G_s = 81.819\ kN$

$\therefore R_v = 51.606 + 81.819 + 22.01 - 2.41$

$$\therefore \boldsymbol{R_v = 153.03\ kN}$$

Now, $\sum F_H$;

$R_h = P_{ah} - P_{ph}$

$= 56.83 - 6.61$

$$\therefore \boldsymbol{R_h = 50.22\ kN}$$

Calculating eccentricity, through the overturning moment, M_o;

$M_o = \sum F_H Y_o - \sum F_V X_o$

$$+\circlearrowleft \sum F_H Y_o = P_{ah,q}(H_2/2) + P_{ah,g}(H_2/3) - P_{ph}(h_1/3)$$

$$= 12.280 \times \left(\frac{2.962}{2}\right) + 48.196 \times \left(\frac{2.962}{3}\right) - 6.61 \times \left(\frac{0.30}{3}\right)$$

$$= 18.187 + 47.586 - 0.661$$

$$= 65.112\ kN/m$$

$$+\circlearrowleft \sum F_V X_o = P_{av,q}(b_2 + b_3 + b) + P_{av,g}(b_2 + b_3 + b) + G_{b1}\left(b_2 + \frac{b_3}{2}\right) +$$

$$G_{b2}\frac{(b_2 + b_3 + b)}{2} + G_{s1}\left(b_2 + b_3 + \frac{b}{2}\right) + G_{s2}\left(b_2 + b_3 + \frac{2b}{3}\right)$$

$$= 4.470 \times (0.95 + 0.70 + 1.27) + 17.542 \times (0.95 + 0.70 + 1.27) +$$

$$31.02 \times \left(0.95 + \frac{0.70}{2}\right) + 20.586 \times \left(\frac{0.95 + 0.70 + 1.27}{2}\right) +$$

$$74.041 \times \left(0.95 + 0.70 + \frac{1.27}{2}\right) + 7.778 \times \left(0.95 + 0.70 + \frac{2 \times 1.27}{3}\right)$$

$$= 13.052 + 51.223 + 40.326 + 30.056 + 169.184 + 19.419$$

$$= 323.260\ kN/m$$

$$\therefore \boldsymbol{M_o = 65.112 - 323.260 = -258.15\ kN/m}$$

The eccentricity *e* of the resultant force which acts on the base slab can be determined from Eq. 5.2. If eccentricity is less than or equal to $B/6$ then there will be no tensile pressure developing at the base. If this is the case than the criterion for overturning is satisfied. However, if eccentricity is greater than $B/6$ then tension will be present at the heel of the base slab, and the soil pressure will have redistributed to keep it compressive throughout (Braja, 2014).

Where;

$B_{min} = b_2 + b_3 + b$

$= 0.95 + 0.70 + 1.270$

$B_{min} = 2.92\ m$

$$\therefore e_b = -\left[\frac{2.92}{2} + \frac{(-258.15)}{154.27}\right]$$

$\therefore \boldsymbol{e_b = 0.21}$

Where, $e_b < B/6$

$\therefore OK$, no tension at base

Effective foundation width, B';

$= B_{min} - 2 \times |e_b|$

$= 2.92 - 2 \times 0.21$

$B' = 2.50\ m$

The idea behind the effective width is detailed in Figure 25.

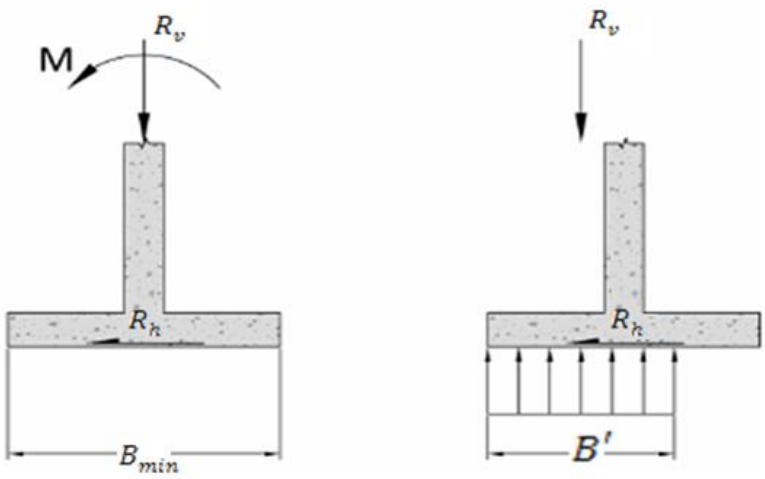

Figure 25 - Effective width (Braja, 2014)

The maximum allowable pressure exerted onto the base slab is given by P_{max};

$$= \frac{\sum R_v}{B_{min}}\left(1 + \frac{6e}{B_{min}}\right)$$

$$= \frac{154.27}{2.92}\left(1 + \frac{6 \times 0.21}{2.92}\right)$$

$$= 52.832 \times 1.432$$

$$= 75.66\ kN/m$$

Now, to determine the factor of safety of the chosen the foundation:

The ultimate *bearing capacity* is given by:

$$q_u = c_f N_c \lambda_{cd} \lambda_{ci} + q N_q \lambda_{qd} \lambda_{qi} + \frac{1}{2} \gamma_f B' N_y \lambda_{yd} \lambda_{yi}$$

The bearing capacity factors were determined in paragraph 4.2.3

Depth Factors

$$\frac{h_1}{B} = \frac{0.3}{2.92} = 0.10$$

If the value of $h_1/B_{min} \leq 1$, then:

$$\lambda_{cd} = 1 + 0.4 \frac{h_1}{B_{min}}$$

$$= 1.04$$

$$\lambda_{qd} = 1 + 2 \tan \phi' (1 - \sin \phi')^2 \frac{h_1}{B_{min}}$$

$$= 1.03$$

$$\lambda_{yd} = 1$$

However, if the value of $h_1/\mathrm{B_{min}} > 1$, then:

$$\lambda_{\mathrm{cd}} = 1 + 0.4 \tan^{-1} \left(\frac{h_1}{\mathrm{B_{min}}} \right)$$

$$\lambda_{\mathrm{qd}} = 1 + 2 \tan \phi' (1 - \sin \phi')^2 \tan^{-1} \left(\frac{h_1}{\mathrm{B_{min}}} \right)$$

$$\lambda_{\mathrm{yd}} = 1$$

Inclination Factors

$$\lambda_{ci} = \lambda_{qi} = \left(1 - \frac{\psi}{90} \right)^2$$

Where

$$\psi = \tan^{-1} \left(\frac{P_a \cos \alpha}{R_v} \right)$$

$$= \tan^{-1}\left(\frac{60.49\cos 20}{153.05}\right)$$

$$\psi = 20.37$$

$$\lambda_{ci} = \lambda_{qi} = \left(1 - \frac{\psi}{90}\right)^2$$

$$\lambda_{ci} = \lambda_{qi} = 0.60$$

$$\lambda_{yi} = \left(1 - \frac{20.37}{30}\right)^2$$

$$\lambda_{yi} = 0.10$$

Since $c_f' = 0$, blasted rock foundation

$$q = \gamma_f h_1$$

$$= 7.95\ kN/m^2$$

$$q_u = 0 \times 30.14 \times 1.04 \times 0.60 + 7.95 \times 18.40 \times 1.03 \times 0.60 + \frac{1}{2} \times 26.5 \times 2.50 \times 22.40 \times 1 \times 0.1$$

$$= 164.60\ kN/m^2$$

Therefore, from Eq. 5.4 the Factor of safety against bearing capacity failure is:

$$F_b = \frac{q_u}{P_{max}} = \frac{164.60}{75.66} = 2.18 > 2.00$$

Therefore, OK.

Now, the FoS of sliding failure can be determined with Eq.5.5:

$$F_s = \frac{R_V\ tan\ \delta}{R_H}$$

$$= \frac{154.27 \times \tan 20}{50.22}$$

$$= 1.12 < 1.50$$

Therefore, *NOT* OK.

Now, the FoS of overturning failure for the chosen strip footing:

$$F_o = \frac{\sum M_R}{\sum M_o}$$

$$= \frac{(P_{av} \times B_{min}) + \left(G_{b1} \times \left[B_{min} - b - \frac{b_3}{2}\right]\right) + \left(G_{b2} \times \frac{B_{min}}{2}\right) + \left(G_s \times \left[B_{min} - \frac{b}{2}\right]\right)}{P_{ah} \times \frac{H_2}{3}}$$

$$= \frac{(22.01 \times 2.92) + \left(31.02 \times \left[2.92 - 1.270 - \frac{0.70}{2}\right]\right) + \left(20.586 \times \frac{2.92}{2}\right) + \left(81.819 \times \left[2.92 - \frac{1.27}{2}\right]\right)}{56.83 \times \frac{2.962}{3}}$$

$$= \frac{64.269 + 40.326 + 30.056 + 186.956}{56.110}$$

$$= \frac{321.607}{56.110}$$

$$= 5.73 > 2$$

Therefore, OK.

Table 5 – Factor of Safety for bearing, sliding, and overturning

Case	H_1 (m)	B_{min} (m)	R_V (kN)	P_{ah} (kPa)	e_b (m)	B' (m)	P_{max} (kPa)	FoS Bearing	FoS Sliding	FoS Overturning	Backfill material	Foundation material
1	2.5	2.92	153.03	56.83	0.21	2.50	75.66	3.96	1.12	5.73	Bl. Rock	Bl. Rock
2	5.0	4.25	532.16	205.65	-0.07	4.12	113.71	3.62	1.03	3.77	Bl. Rock	Bl. Rock
3	7.5	5.58	1135.94	446.34	-0.36	4.85	124.64	4.78	1.01	3.14	Bl. Rock	Bl. Rock
4	10.0	6.90	1965.64	778.93	-0.66	5.58	121.26	6.45	0.99	2.83	Bl. Rock	Bl. Rock
5	2.5	2.72	81.58	11.26	0.74	1.25	78.74	6.83	0.15	16.37	Sand	Bl. Rock
6	5.0	3.84	300.73	22.59	0.30	3.26	114.23	5.98	0.52	16.60	Sand	Bl. Rock
7	7.5	4.97	615.19	33.92	0.28	4.40	166.23	6.25	1.06	18.56	Sand	Bl. Rock
8	10.0	6.09	1060.08	98.62	0.13	5.83	196.18	6.69	3.67	9.94	Sand	Bl. Rock
9	2.5	2.80	120.98	43.88	0.14	2.52	59.06	5.75	0.55	5.52	Gravel	Bl. Rock
10	5.0	3.99	393.92	153.72	-0.17	3.65	73.59	5.80	0.50	3.51	Gravel	Bl. Rock
11	7.5	5.19	821.17	329.43	-0.49	4.21	68.66	9.00	0.48	2.88	Gravel	Bl. Rock
12	10.0	6.39	1402.72	571.03	-0.81	4.76	51.76	15.68	0.47	2.57	Gravel	Bl. Rock
13	2.5	3.05	63.43	11.73	2.47	1.88	121.66	4.35	0.04	20.21	Clay/Cl. Silt	Bl. Rock
14	5.0	4.52	334.59	23.55	0.92	2.67	164.98	3.75	0.19	22.58	Clay/Cl. Silt	Bl. Rock
15	7.5	5.98	759.72	35.36	0.69	4.61	214.66	4.32	0.43	26.54	Clay/Cl. Silt	Bl. Rock
16	10.0	7.45	1338.83	47.18	0.60	6.24	267.23	4.62	0.77	30.88	Clay/Cl. Silt	Bl. Rock
17	2.5	2.92	154.27	56.83	0.21	2.50	75.66	6.55	1.12	5.73	Bl. Rock	Gravel
18	5.0	4.25	532.16	205.65	-0.07	4.12	113.71	7.46	1.03	3.77	Bl. Rock	Gravel
19	7.5	5.58	1135.94	446.34	-0.36	4.85	124.64	8.67	1.01	3.14	Bl. Rock	Gravel
20	10.0	6.90	1965.64	778.93	-0.66	5.58	121.26	11.16	0.99	2.83	Bl. Rock	Gravel
21	2.5	2.72	81.58	11.26	0.74	1.25	78.74	9.85	0.15	16.37	Sand	Gravel
22	5.0	3.84	300.73	22.59	0.30	3.26	114.23	17.79	0.52	16.60	Sand	Gravel
23	7.5	4.97	615.19	33.92	0.28	4.40	166.23	18.10	1.06	18.56	Sand	Gravel
24	10.0	6.09	1060.08	98.62	0.13	5.83	196.18	18.37	3.67	9.94	Sand	Gravel
25	2.5	2.80	120.98	43.88	0.14	2.52	59.06	9.25	0.55	5.52	Gravel	Gravel

26	5.0	3.99	393.92	153.72	-0.17	3.65	73.59	10.75	0.50	3.51	Gravel	Gravel
27	7.5	5.19	821.17	329.43	-0.49	4.21	68.66	15.22	0.48	2.88	Gravel	Gravel
28	10.0	6.39	1402.72	571.03	-0.81	4.76	51.76	25.26	0.47	2.57	Gravel	Gravel
29	2.5	3.05	63.43	11.73	2.47	1.89	121.66	6.61	0.04	20.21	Clay/Cl. Silt	Gravel
30	5.0	4.52	334.59	23.55	0.92	2.67	164.98	10.67	0.19	22.58	Clay/Cl. Silt	Gravel
31	7.5	5.98	759.72	35.36	0.69	4.61	214.66	14.03	0.43	26.54	Clay/Cl. Silt	Gravel
32	10.0	7.45	1338.83	47.18	0.60	6.24	267.23	15.55	0.77	30.88	Clay/Cl. Silt	Gravel
33	2.5	2.92	154.27	56.83	0.21	2.50	75.66	35.24	1.47	5.73	Bl. Rock	Sand
34	5.0	4.25	532.16	205.65	-0.07	4.12	113.71	32.96	1.17	3.77	Bl. Rock	Sand
35	7.5	5.58	1135.94	446.34	-0.36	4.85	124.64	35.77	1.09	3.14	Bl. Rock	Sand
36	10.0	6.90	1965.64	778.93	-0.66	5.58	121.26	42.67	1.05	2.83	Bl. Rock	Sand
37	2.5	2.72	81.58	11.26	0.74	1.25	78.74	27.82	0.33	16.37	Sand	Sand
38	5.0	3.84	300.73	22.59	0.30	3.26	114.23	18.35	0.76	16.60	Sand	Sand
39	7.5	4.97	615.19	33.92	0.28	4.40	166.23	16.89	1.36	18.56	Sand	Sand
40	10.0	6.09	1060.08	98.62	0.13	5.83	196.18	15.98	2.10	20.95	Sand	Sand
41	2.5	2.80	120.98	43.88	0.14	2.52	59.06	28.14	0.98	5.52	Gravel	Sand
42	5.0	3.99	393.92	153.72	-0.17	3.65	73.59	39.31	0.67	3.51	Gravel	Sand
43	7.5	5.19	821.17	329.43	-0.49	4.21	68.66	50.35	0.58	2.88	Gravel	Sand
44	10.0	6.39	1402.72	571.03	-0.81	4.76	51.76	77.59	0.54	2.57	Gravel	Sand
45	2.5	3.05	63.43	11.73	2.47	1.89	121.66	17.97	0.13	20.21	Clay/Cl. Silt	Sand
46	5.0	4.52	334.59	23.55	0.92	2.67	164.98	13.60	0.48	22.58	Clay/Cl. Silt	Sand
47	7.5	5.98	759.72	35.36	0.69	4.61	214.66	13.12	1.01	26.54	Clay/Cl. Silt	Sand
48	10.0	7.45	1338.83	47.18	0.60	6.24	267.23	12.60	1.73	30.88	Clay/Cl. Silt	Sand
49	2.5	2.92	154.27	56.83	0.21	2.50	75.66	27.23	2.86	5.73	Bl. Rock	Clay/Cl. Silt
50	5.0	4.25	532.16	205.65	-0.07	4.12	113.71	17.85	1.71	3.77	Bl. Rock	Clay/Cl. Silt
51	7.5	5.58	1135.94	446.34	-0.36	4.85	124.64	17.20	1.42	3.14	Bl. Rock	Clay/Cl. Silt
52	10.0	6.90	1965.64	778.93	-0.66	5.58	121.26	18.64	1.28	2.83	Bl. Rock	Clay/Cl. Silt
53	2.5	2.72	81.58	11.26	0.74	1.25	78.74	25.46	1.03	16.37	Sand	Clay/Cl. Silt
54	5.0	3.84	300.73	22.59	0.30	3.26	114.23	17.76	1.72	16.60	Sand	Clay/Cl. Silt

55	7.5	4.97	615.19	33.92	0.28	4.40	166.23	14.06	2.55	18.56	Sand	Clay/Cl. Silt
56	10.0	6.09	1060.08	98.62	0.13	5.83	196.18	11.82	3.51	20.95	Sand	Clay/Cl. Silt
57	2.5	2.80	120.98	43.88	0.14	2.52	59.06	25.29	2.70	5.52	Gravel	Clay/Cl. Silt
58	5.0	3.99	393.92	153.72	-0.17	3.65	73.59	19.67	1.35	3.51	Gravel	Clay/Cl. Silt
59	7.5	5.19	821.17	329.43	-0.49	4.21	68.66	22.07	0.99	2.88	Gravel	Clay/Cl. Silt
60	10.0	6.39	1402.72	571.03	-0.81	4.76	51.76	30.75	0.83	2.57	Gravel	Clay/Cl. Silt
61	2.5	3.05	63.43	11.73	2.47	1.89	121.66	15.37	0.36	20.21	Clay/Cl. Silt	Clay/Cl. Silt
62	5.0	4.52	334.59	23.55	0.92	2.67	164.98	13.59	0.82	22.58	Clay/Cl. Silt	Clay/Cl. Silt
63	7.5	5.98	759.72	35.36	0.69	4.61	214.66	11.39	1.47	26.54	Clay/Cl. Silt	Clay/Cl. Silt
64	10.0	7.45	1338.83	47.18	0.60	6.24	267.23	9.77	2.31	30.88	Clay/Cl. Silt	Clay/Cl. Silt

The results from Table 5 details that the FoS for bearing is largest when founded on soils with low soil friction angles, and maximum total footing width, B_{min}. However, B_{min} is greatest when the friction angle is also at its minimum, and the height of the stem is at its maximum, this relates back to Eq. 4.1. This meets expectations, as the bearing capacity is also connected to the friction angle through the capacity factors $N_c, N_q,$ and N_y from Table 3. Figure 26 to Figure 29 shows a direct relation between bearing and height of the retaining wall, while detailing different relations for various foundations.

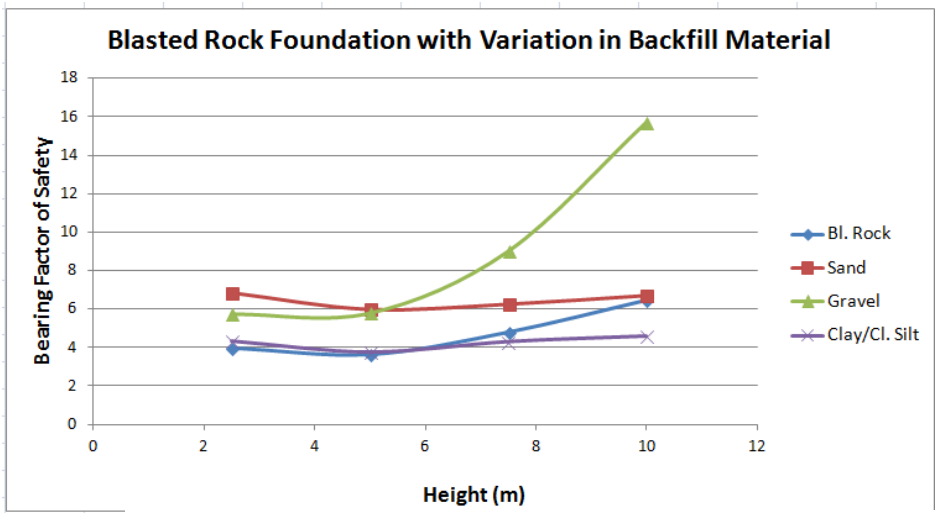

Figure 26 - Bearing FoS rock foundation

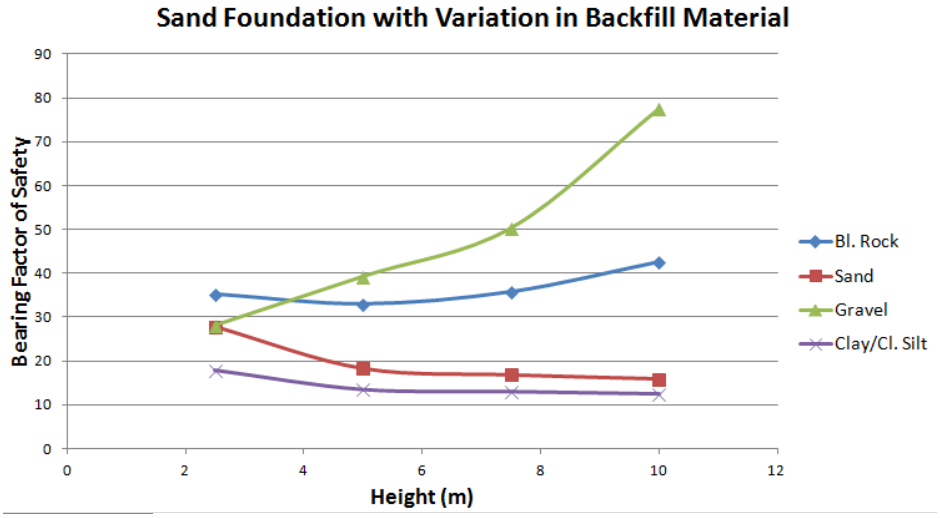

Figure 27 - Bearing FoS sand foundation

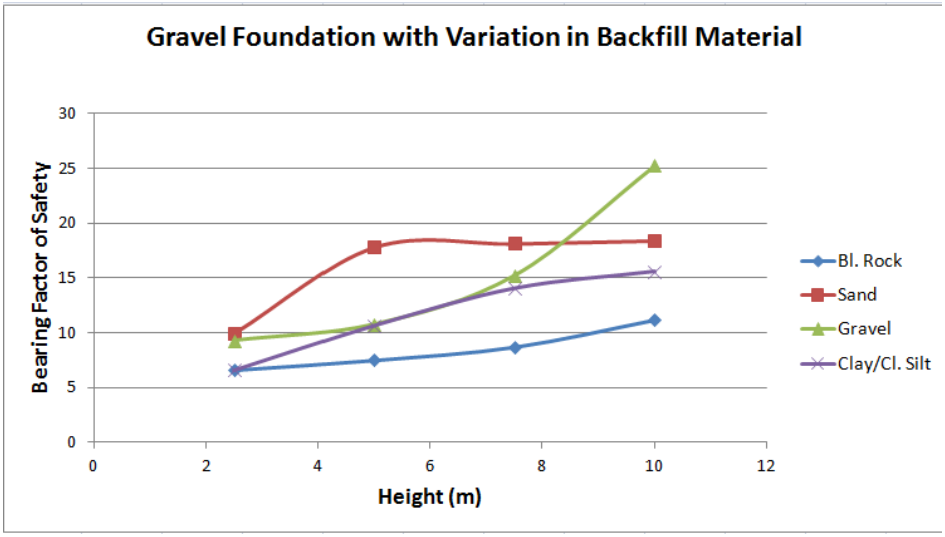

Figure 28 - Bearing FoS gravel foundation

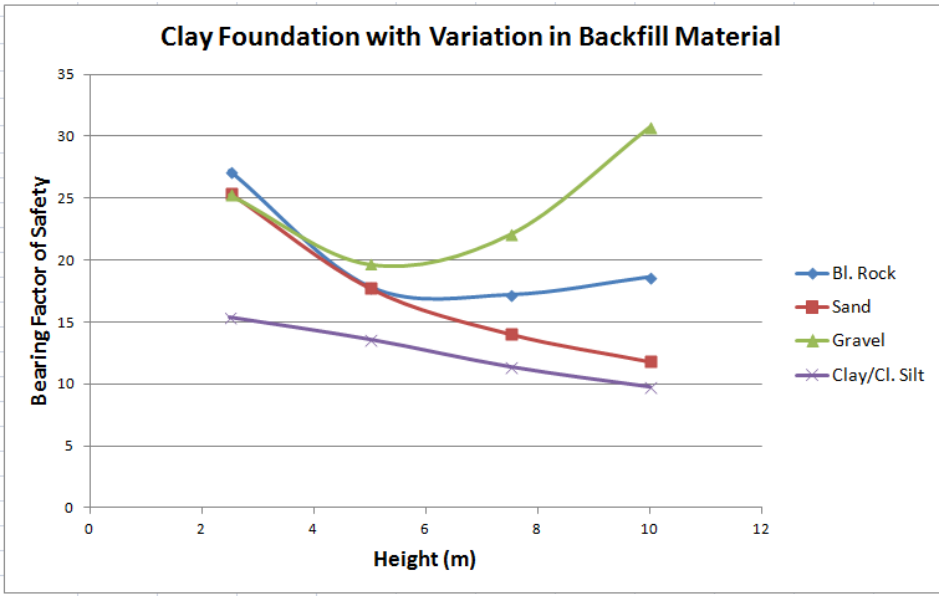

Figure 29 - Bearing FoS Clay/Cl. Silt foundation

From Figure 26 to Figure 29 it is clear that the soils with high friction angle (i.e. gravel and sand) influence the factor of safety against bearing, and as mention earlier a high friction angle also has a direct impact on the capacity factors. Throughout Figure 26 to Figure 29 a trough is generally represented at the 5 metre location for the given backfills, the reason for this is primarily due to eccentricity, where a very low eccentricity was accounted for at this point.

From Figure 30 to Figure 34 it is clear that the soils lack the ability to prevent sliding, in many cases this can be improved through the use of stability enhancements. These enhancements may include nails and grout, or the possibility of freezing could be introduced for a long term scenario. These stability enhancements will be covered in more depth later within the report. One other method to increase sliding resistance is to introduce a sloped footing; however this method of design is not universal. However, effectiveness is increased when coefficient of friction of concrete against soil is reasonably low (Elman and Terry, 1987).

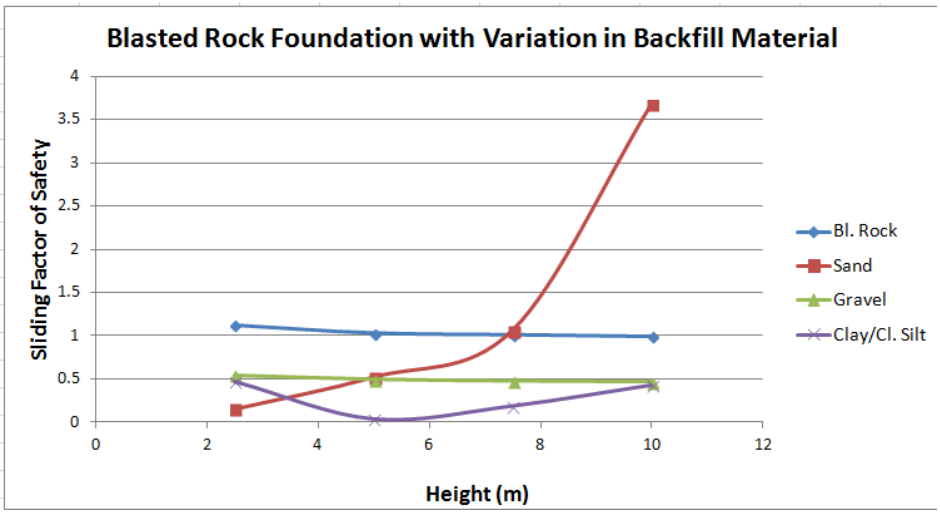

Figure 30 - Sliding FoS Blasted Rock foundation

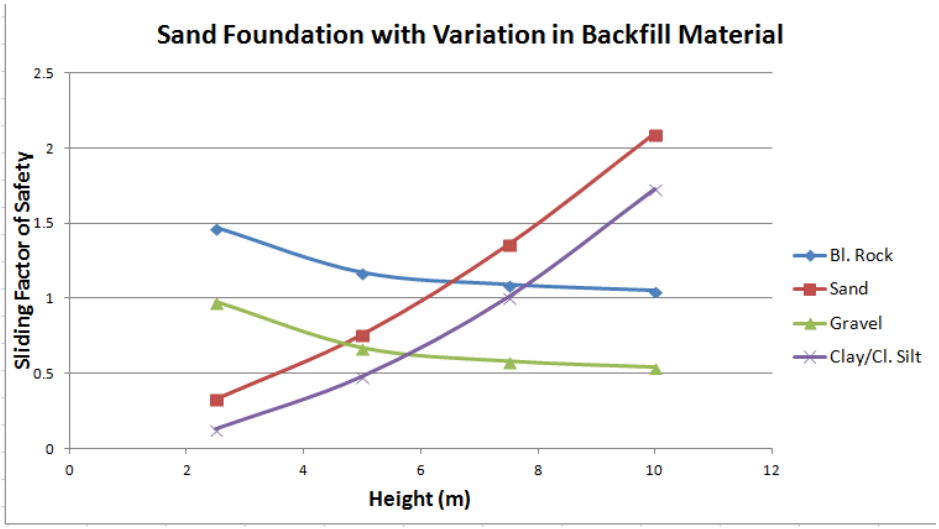

Figure 31 - Sliding FoS Sand foundation

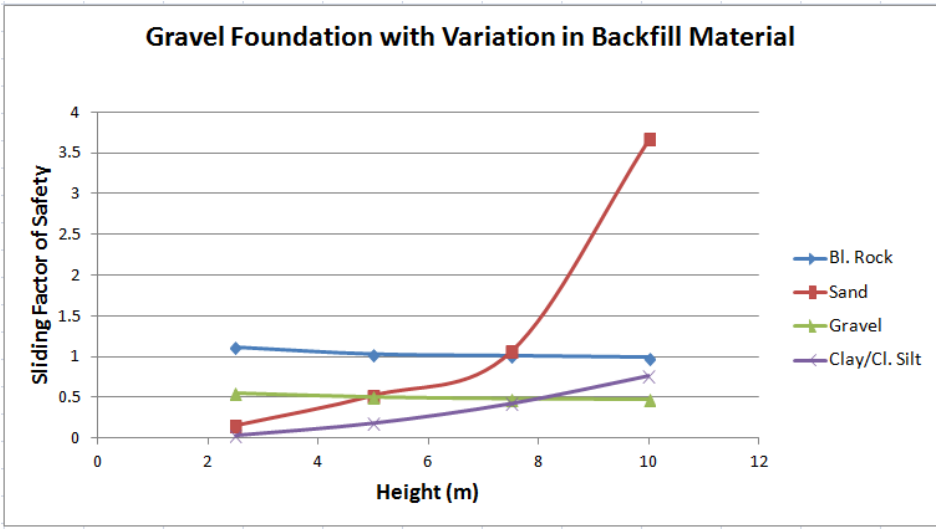

Figure 32 - Sliding FoS Gravel foundation

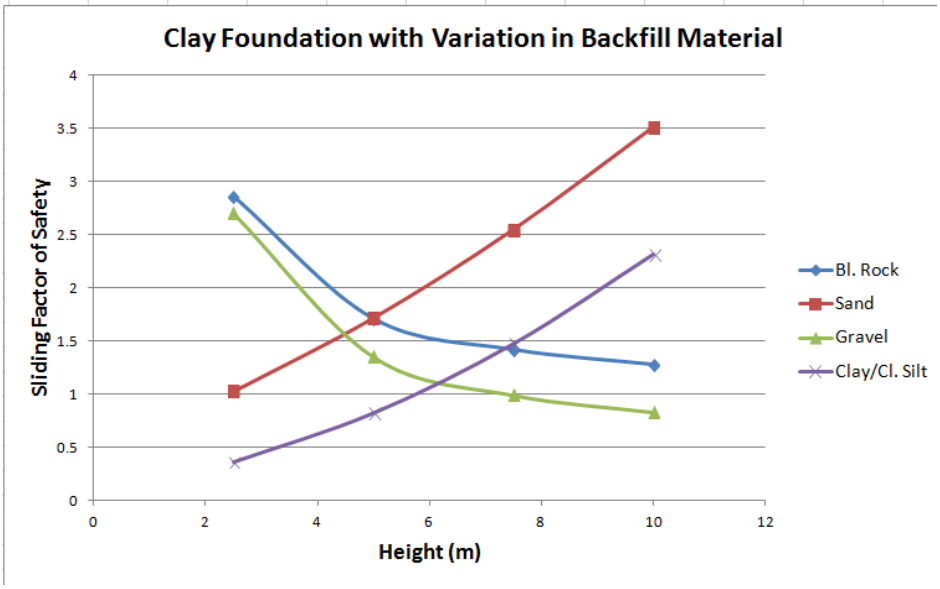

Figure 33 - Sliding FoS Clay/Cl. Silt foundation

From Figure 34 to Figure 37 it is clear that the soils resisting moments are greater than the overturning moments. It's noticed that cohesive materials have a considerably larger overturning factor of safety; this is due to a dramatic reduction in lateral thrust due to their shear strength parameters.

Overturning about the toe is one other safety factor which was the last consideration in the calculations; this is primarily based on the resisting moments being greater than the forces overturning about the toe, while keeping in mind what was covered in paragraph 4.3.2, that is, a global FoS required against overturning is no less than 2. If further increase is required for overturning, then the enlargement of the footing width should be undertaken. The footing is a predominant link to increasing/decreasing the resisting moments of the cantilever structure and therefore the FoS against overturning.

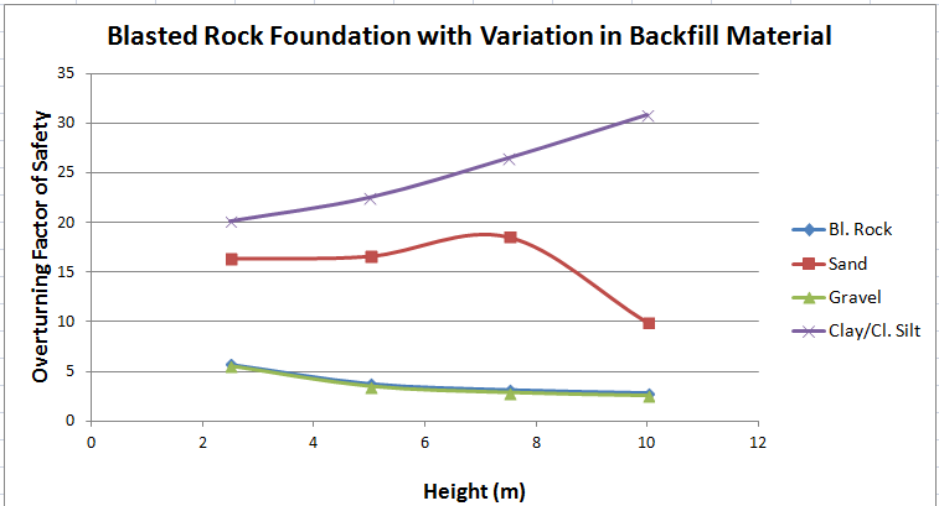

Figure 34 - Overturning FoS for blasted rock foundation

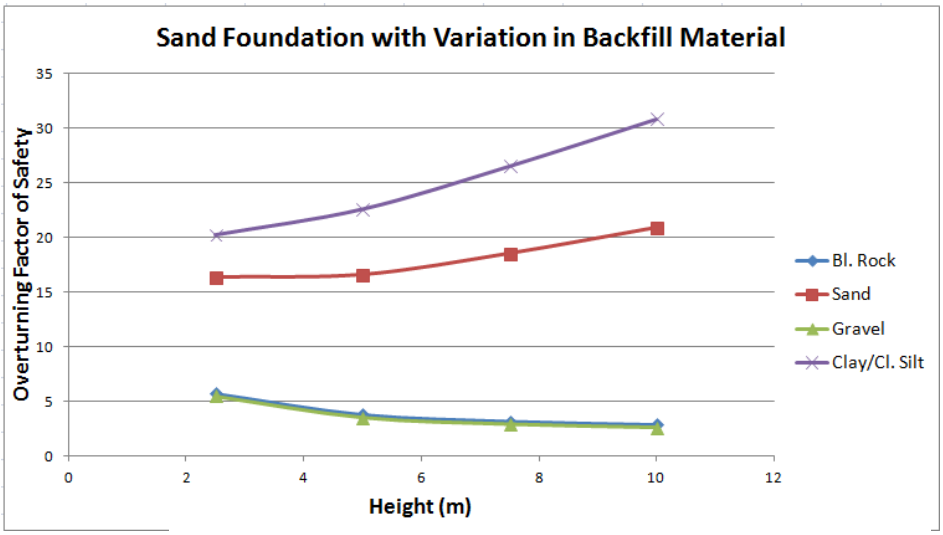

Figure 35 - Overturning FoS for sand foundation

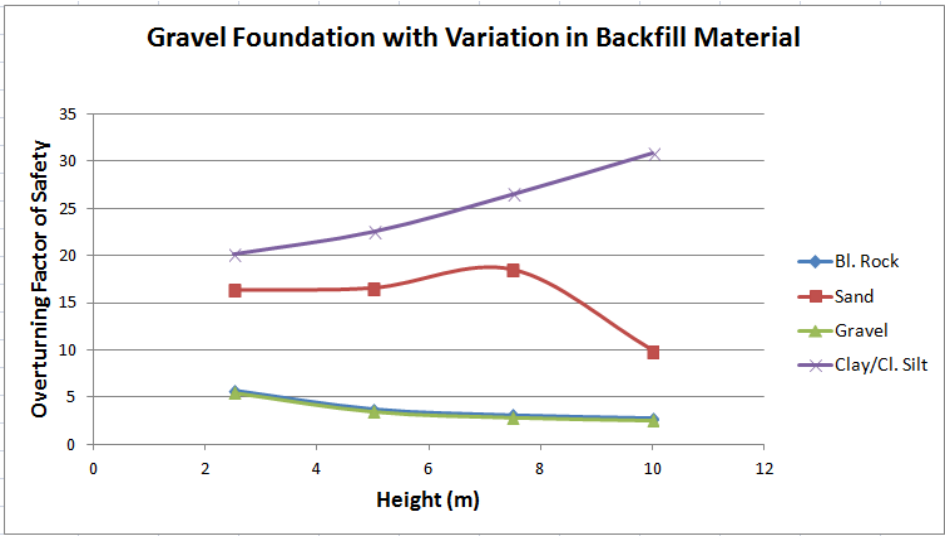

Figure 36 - Overturning FoS for gravel foundation

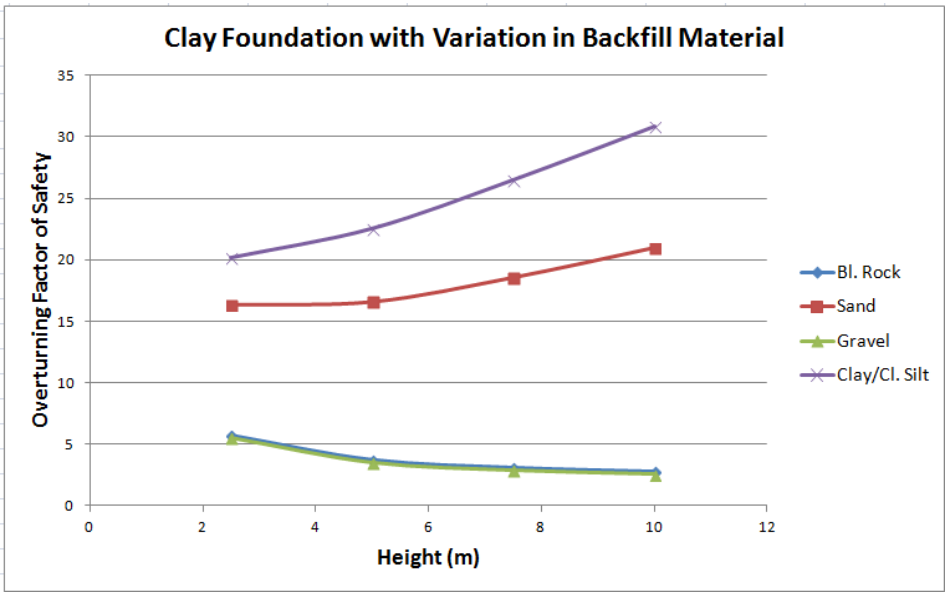

Figure 37 - Overturning FoS for clay/cl silt foundation

5. APPROACHES TO IMPROVE STABILITY

To enhance the stability of backfill for those cases which failed in the above cases indentified in paragraph 4.2.6.

5.1. Nails

Soil nailing is a reinforcing technique used for stabilising both granular and cohesive soils as well as heterogeneous deposits (Sengupta & Giri, 2011), through the introduction of a serious of thin elements called nails (Palmeira, at al., 1995). Steel bars or metal tubes are the predominant materials used for nails, as they tend to resist tensile forces, shear stresses and bending moments. The nails are simply driven in the ground as driven nails or placed in drilled holes then grouted along its length to unify it with the ground, known as grouted nails (Mittle & Biswas, 2006). Figure 24 details an overview of soil nailing for a vertical cut.

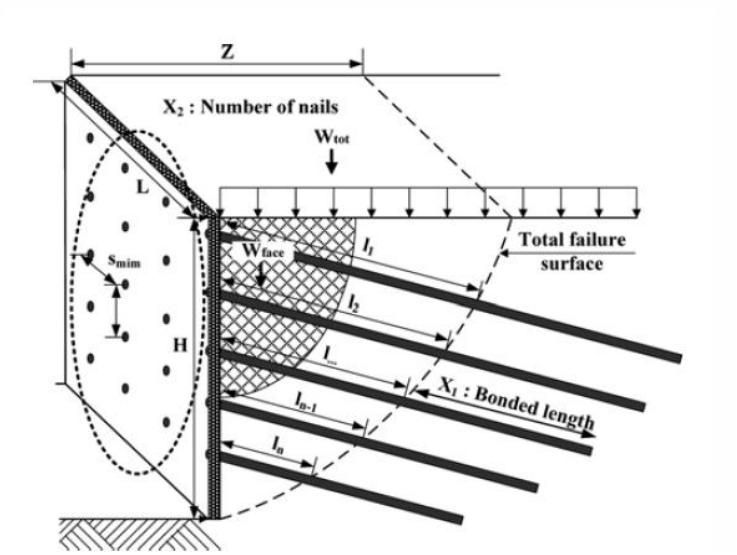

Figure 38 - soil nailing overview

However, there are disadvantages to steel products, main being the susceptibility to oxidation when exposed to chlorides, further accelerated near aggressive environments such as coastal regions. In these cases, Glass Fiber Reinforced Plastic (GFRP) bars are an option for reinforcement; these bars have corrosive resistance, electromagnetic transparency, and compelling physical and mechanical properties (Kemp & Blowes, 2011), other advantages of GFRP include:

- tensile strength is twice that of normal structural steel;
- the weight is quarter that of steel with equivalent strength;
- no interference with sensitive electronic equipment or instruments; and
- no thermal bridge within structure.

In 2004, a major study by ISIS Canada was undertaken to determine any negative side effects which the concrete would present in relation to the GFRP, this exposure was left for 5 to 8 years. Two examination processes were used to determine this, they are:

- Scanning Electron Microscopy (SEM) – used to examine the individual glass fibres and the glass fibre/matrix interface; and
- Energy Dispersive X-ray (EDX) – was sued to detect potential chemical changes in the glass fibres and matrix due to the alkali content from the concrete solution.

The result from both SEM and EDX detailed no degradation of the GFRP in the concrete structure. The EDX also detailed no alkali ingress in the GFRP from the concrete solution. The original state of GFRP was also unaltered and therefore intact (Kemp & Blowes, 2011).

5.2. Freezing

This technique is used to arrest soil and water movements through the use of freeze pipes. When the temperature around these pipes reaches zero degrees, the water within the pores begin to freeze. With cohesionless soils the groundwater in the pores freezes rapidly. However, with cohesive materials such as clays, the groundwater is molecularly bonded, so temperature as low as -25 degrees may be required. Figure 25 details the process by which a row of shafts are drilled vertically into the ground. Coolant, which is chilled to below freezing (detailed in blue arrows) is pumped in the freezing pipes. The

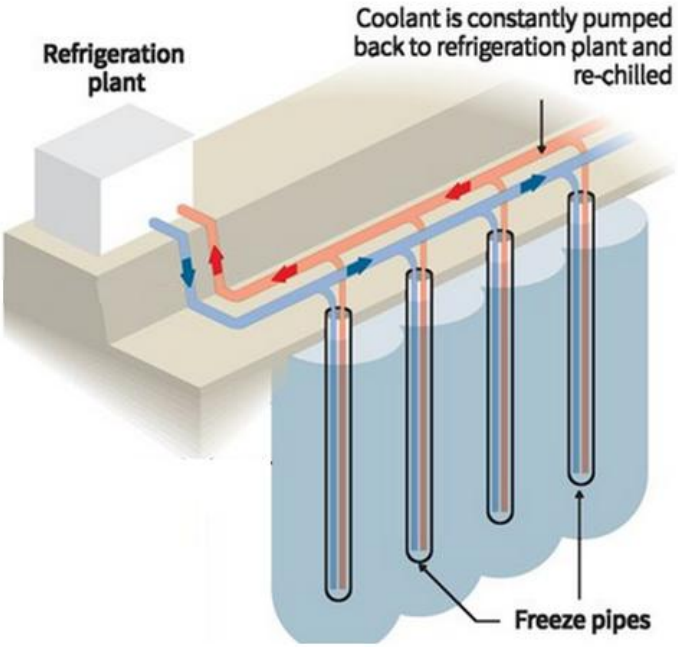

Figure 39 - Ground freezing (Kiger, 2013)

groundwater around these pipes freezes; effectively creating a frozen wall of soil in a 6 to 8 week period.

This process is minimally invasive that requires limited physical penetration into the ground, unlike other excavation support techniques which requires displacement. This technique propagates thermally; hence, the soils are relatively left undisturbed throughout its installation and operating process. The main conditions for use of ground freezing primarily include:

- Grounds where penetration by jet grouting, drilling, clamshell excavation or other possible cut off tools is limited;
- Filled grounds and grounds containing obstructions; and
- Disturbed grounds due to unstable conditions or water inflow.

This process also presents negligible change in the groundwater regime outside the confined area following thawing (MoreTrench, 2014). In case of a contamination, this technique will eliminate all movement and further spread, while also providing earth support for the excavation of the contaminated soil.

5.2.1 *Brine Freezing*

This technique is often used in large, long term project schedules where freeze formation periods are measured in weeks and months. Brine is the most common cooling agent, where it is chilled to a temperature between $-15℃$ and $-25℃$ (MoreTrench, 2014). The process takes form of that detailed in Figure 25, where the chilled brine is pumped down the freeze pipes and out, drawing heat from the surrounding soils. The brine returns back to the refrigeration unit which it is then chilled and recirculated.

5.2.2 *Liquid Nitrogen Freezing*

This technique is often used in emergency situations, as it acts more quickly than brine. It can also be utilised on small projects where temporary freezing is required. However, the use of liquid nitrogen is more costly per day compared to that of circulating chilled brine.

6. OPTUMG2

OptumG2 is a 2D finite element program used to investigate geotechnical stability and deformation analysis. The software is capable of various types of analyses, these include:

- strength reduction;
- elastoplastic analysis;
- limit analysis;
- seepage analysis;
- staged construction; and
- initial stress analysis.

All computed results (i.e. stress, strain, displacement, etc.) visually display their results in a colour distribution on the background mesh; examples are displayed in Appendix K. This deformation process can be accessed via a movie for more effective visualisation. The typical applications which this software can represent other than retaining systems include excavation, tunnelling, foundations, long wall mining etc.

6.1 Strength reduction

The use of strength reduction analysis is to identify a set of reduced material parameters that will lead to the development of collapse. This resulting reduction factor is taken as the strength based factor of safety. Therefore, a factor greater than 1.00 details a stable system, while a factor less than 1.00 details an unstable system and addition strength is required to prevent collapse. Hence, it's recognised that this analysis determines the strength necessary to prevent collapse given certain loads.

Figure 26 details a scenario where a 7.5 metre wall is retaining gravel backfill on a blasted rock foundation. The material is detailed in Appendix C, with a rigid wall of unit weight 23.5 kN/m^3.

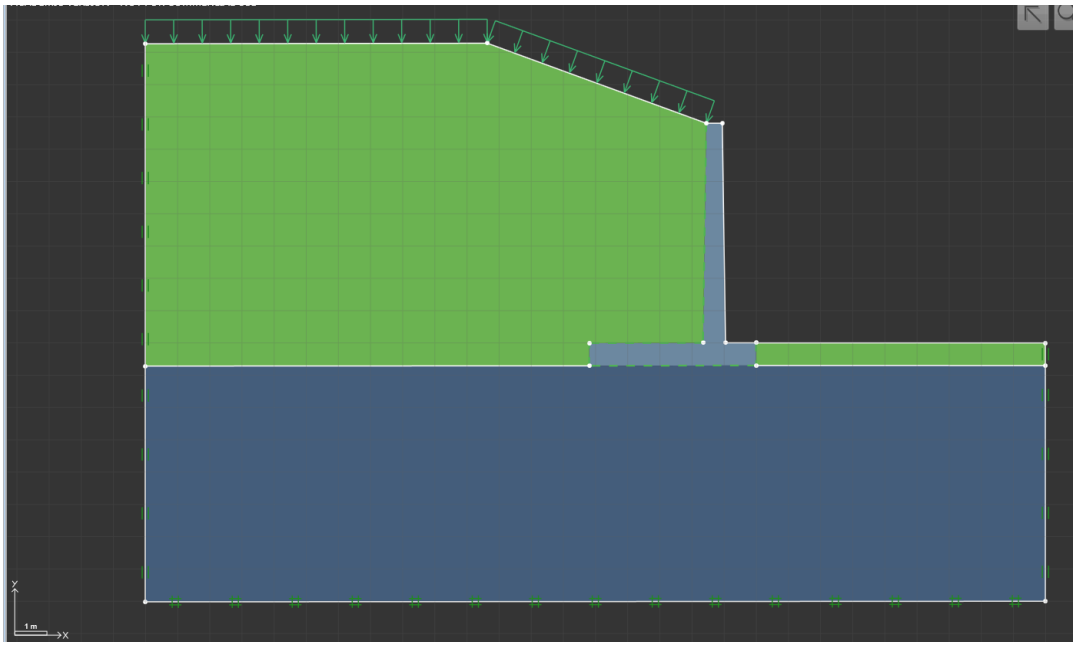

Figure 40 - 7.5 metre stem wall

For this example, Table 4 details the lower and upper bound calculations for a fixed number of elements, without the use of mesh adaptivity. It should be noted that without the use of subdivisions, mesh adaptivity will be of little utility; this is so a reasonable initial solution is available. It can be seen that the increase in elements details a more accurate result; furthermore, the use of subdivisions enhances the accuracy again. However, when using between 1000 to 4000 elements it is detailed in Table 4 that there is a significant gap difference between both lower and upper bound values. Therefore, without the use of subdivisions it is recommended that 4000 elements or greater should be used.

Table 6 – Strength reduction factor with and without subdivisions

	No Subdivision		
No. Elements	Lower Bound	Upper Bound	Mean $\pm$ Error
1 000	0.161	1.283	0.722 ± 0.561
2 000	0.118	1.266	0.692 ± 0.574
4 000	1.173	1.242	1.208 ± 0.035
8 000	1.180	1.227	1.204 ± 0.024
16 000	1.180	1.221	1.201 ± 0.021

	Subdivision		
No. Elements	Lower Bound	Upper Bound	Mean ± Error
1 000	1.160	1.285	1.223 ± 0.063
2 000	1.164	1.254	1.209 ± 0.045
4 000	1.180	1.238	1.209 ± 0.029
8 000	1.180	1.227	1.204 ± 0.024
16 000	1.180	1.221	1.201 ± 0.021

On close examination of each element run, in-between 1000 to 2000, it's identified that only a single layer of elements run across the width of the wall at any one time (detailed in Figure 27 and 28). When the number of elements

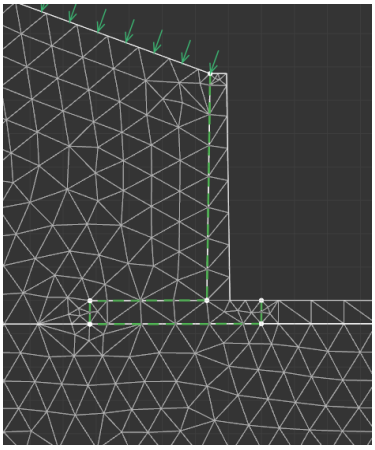

Figure 41 - 1000 elements

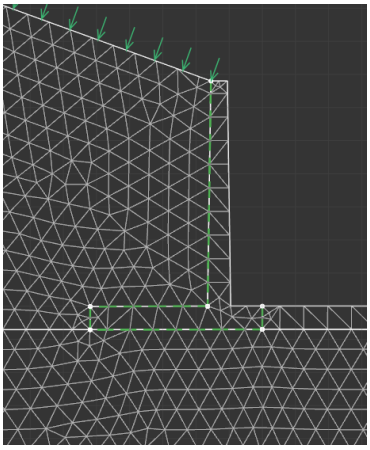

Figure 42 - 2000 elements

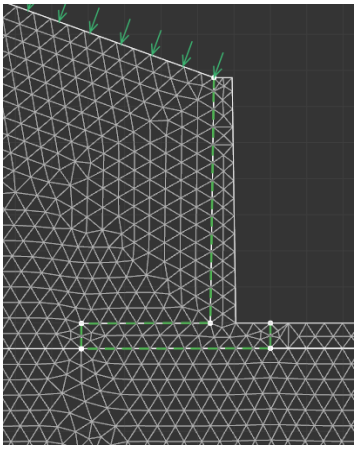

Figure 43 - 4000 elements

reaches 4000 or greater, two layers of elements is present; this is detailed in Figure 29. This is the reason why the results improve dramatically from 4000 and greater.

However, when subdivisions are present a double layer of elements run across the width of the wall at any one time (Figure 31, 32 and 33), irrelevant of element numbers. This is one method to drastically improve results from 1000 elements or greater. These values are detailed on the right side of Table 4, while an overview is detailed in Figure 30.

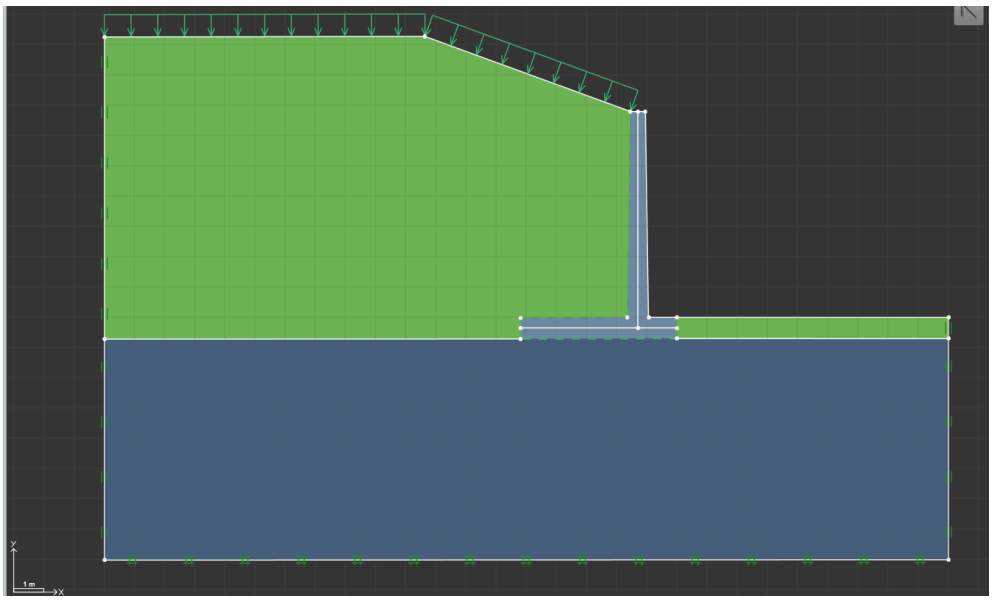

Figure 44 - Subdivided 7.5 metre stem wall

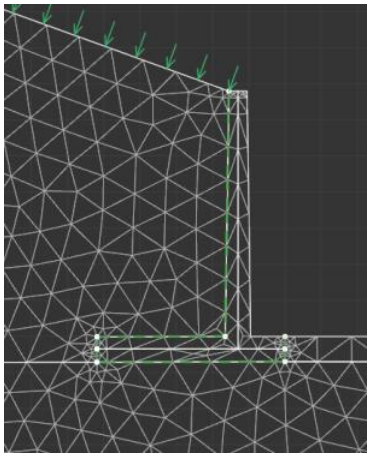

Figure 45 - 1000 elements with subdivision

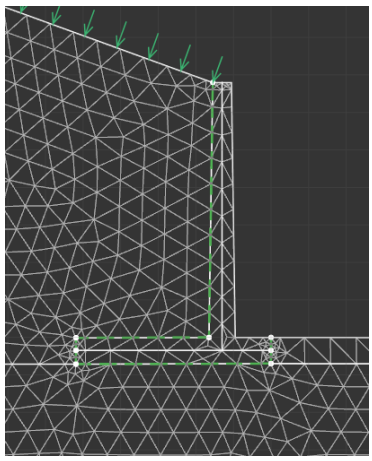

Figure 46 - 2000 elements with subdivision

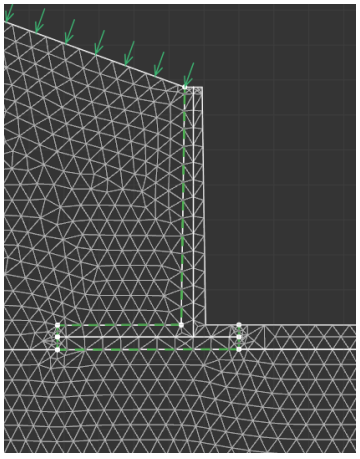

Figure 47 - 4000 elements with subdivision

Now, one additional method to further enhance the given calculation is by utilising mesh adaptivity with subdivisions. The previous calculation on subdivisions have been taken from Table 4 and relocated in Table 5, however, now mesh adaptivity has been undertaken in order to compare.

Table 7 – Strength reduction factor with and without mesh adaptivity

	Subdivision *without* Mesh Adaptivity		
No. Elements	Lower Bound	Upper Bound	Mean ± Error
1 000	1.160	1.285	1.223 ± 0.063
2 000	1.164	1.254	1.209 ± 0.045
4 000	1.180	1.238	1.209 ± 0.029
8 000	1.180	1.227	1.204 ± 0.024
16 000	1.180	1.221	1.201 ± 0.021

	Subdivision *with* Mesh Adaptivity		
No. Elements	Lower Bound	Upper Bound	Mean ± Error
1 000	1.180	1.227	1.204 ± 0.024
2 000	1.182	1.214	1.198 ± 0.016
4 000	1.188	1.208	1.198 ± 0.010
8 000	1.191	1.203	1.197 ± 0.006
16 000	1.192	1.200	1.196 ± 0.004

It can be seen with the utility of mesh adaptivity, that 1000 elements is equivalent to 8000 elements without. Therefore, in my follow calculations subdivisions will be used with the addition of mesh adaptivity, with a total of 1000 elements, ensuring accurate results.

6.2 Lower and Upper Bound Calculations

The following calculations illustrate the Strength based Factor of Safety (SFoS) for each case, where SFoS lower than 1.00 illustrates an unstable case and SFoS higher than 1.00 illustrate a stable case.

Table 8 – Strength based Factor of Safety

Case	H_1 (m)	Lower Bound	Upper Bound	Mean (FoS_s)	Error ($\pm$)	Backfill Material	Foundation Material
1	2.5	0.437	0.478	0.458	0.021	Bl. Rock	Bl. Rock
2	5.0	1.086	1.120	1.103	0.017	Bl. Rock	Bl. Rock
3	7.5	1.070	1.105	1.088	0.018	Bl. Rock	Bl. Rock
4	10.0	1.058	1.101	1.080	0.022	Bl. Rock	Bl. Rock
5	2.5	2.560	2.616	2.588	0.028	Sand	Bl. Rock
6	5.0	1.970	2.055	2.013	0.043	Sand	Bl. Rock
7	7.5	1.744	1.777	1.761	0.017	Sand	Bl. Rock
8	10.0	1.590	1.662	1.626	0.036	Sand	Bl. Rock
9	2.5	1.325	1.371	1.348	0.023	Gravel	Bl. Rock
10	5.0	1.203	1.252	1.228	0.025	Gravel	Bl. Rock
11	7.5	1.180	1.227	1.204	0.024	Gravel	Bl. Rock
12	10.0	1.144	1.195	1.170	0.026	Gravel	Bl. Rock
13	2.5	4.296	4.438	4.367	0.071	Clay/Cl. Silt	Bl. Rock
14	5.0	3.207	3.314	3.261	0.054	Clay/Cl. Silt	Bl. Rock
15	7.5	2.676	2.775	2.723	0.050	Clay/Cl. Silt	Bl. Rock
16	10.0	2.374	2.449	2.412	0.038	Clay/Cl. Silt	Bl. Rock
17	2.5	0.437	0.481	0.459	0.022	Bl. Rock	Gravel
18	5.0	1.086	1.120	1.103	0.017	Bl. Rock	Gravel
19	7.5	1.076	1.109	1.093	0.017	Bl. Rock	Gravel
20	10.0	1.064	1.100	1.082	0.018	Bl. Rock	Gravel
21	2.5	2.680	2.737	2.709	0.029	Sand	Gravel
22	5.0	2.076	2.155	2.116	0.040	Sand	Gravel
23	7.5	1.832	1.859	1.846	0.014	Sand	Gravel
24	10.0	1.669	1.736	1.703	0.034	Sand	Gravel
25	2.5	1.327	1.362	1.345	0.018	Gravel	Gravel
26	5.0	1.204	1.252	1.228	0.024	Gravel	Gravel
27	7.5	1.190	1.227	1.209	0.019	Gravel	Gravel
28	10.0	1.174	1.210	1.192	0.018	Gravel	Gravel
29	2.5	4.377	4.535	4.456	0.079	Clay/Cl. Silt	Gravel
30	5.0	3.323	3.397	3.360	0.037	Clay/Cl. Silt	Gravel
31	7.5	2.790	2.875	2.833	0.043	Clay/Cl. Silt	Gravel
32	10.0	2.482	2.573	2.528	0.046	Clay/Cl. Silt	Gravel
33	2.5	0.439	0.487	0.463	0.024	Bl. Rock	Sand
34	5.0	1.086	1.127	1.107	0.021	Bl. Rock	Sand
35	7.5	1.077	1.111	1.092	0.020	Bl. Rock	Sand
36	10.0	1.071	1.106	1.089	0.018	Bl. Rock	Sand
37	2.5	3.268	3.357	3.313	0.045	Sand	Sand
38	5.0	2.276	2.343	2.310	0.034	Sand	Sand
39	7.5	1.946	1.965	1.956	0.010	Sand	Sand
40	10.0	1.771	1.824	1.800	0.027	Sand	Sand
41	2.5	1.327	1.383	1.355	0.028	Gravel	Sand
42	5.0	1.212	1.258	1.235	0.023	Gravel	Sand
43	7.5	1.182	1.230	1.206	0.024	Gravel	Sand
44	10.0	1.174	1.214	1.194	0.020	Gravel	Sand

45	2.5	5.581	5.685	5.628	0.057	Clay/Cl. Silt	Sand
46	5.0	3.941	4.036	3.989	0.048	Clay/Cl. Silt	Sand
47	7.5	3.238	3.349	3.294	0.056	Clay/Cl. Silt	Sand
48	10.0	2.824	2.933	2.879	0.055	Clay/Cl. Silt	Sand
49	2.5	0.439	0.490	0.465	0.026	Bl. Rock	Clay/Cl. Silt
50	5.0	1.078	1.128	1.103	0.025	Bl. Rock	Clay/Cl. Silt
51	7.5	1.070	1.115	1.093	0.023	Bl. Rock	Clay/Cl. Silt
52	10.0	1.064	1.111	1.088	0.024	Bl. Rock	Clay/Cl. Silt
53	2.5	3.270	3.407	3.339	0.069	Sand	Clay/Cl. Silt
54	5.0	2.276	2.369	2.323	0.047	Sand	Clay/Cl. Silt
55	7.5	1.946	1.978	1.962	0.016	Sand	Clay/Cl. Silt
56	10.0	1.771	1.848	1.810	0.039	Sand	Clay/Cl. Silt
57	2.5	1.327	1.386	1.357	0.030	Gravel	Clay/Cl. Silt
58	5.0	1.213	1.263	1.238	0.025	Gravel	Clay/Cl. Silt
59	7.5	1.190	1.238	1.214	0.024	Gravel	Clay/Cl. Silt
60	10.0	1.174	1.220	1.197	0.023	Gravel	Clay/Cl. Silt
61	2.5	8.332	8.442	8.387	0.055	Clay/Cl. Silt	Clay/Cl. Silt
62	5.0	5.044	5.151	5.098	0.054	Clay/Cl. Silt	Clay/Cl. Silt
63	7.5	3.872	3.978	3.925	0.053	Clay/Cl. Silt	Clay/Cl. Silt
64	10.0	3.204	3.290	3.247	0.043	Clay/Cl. Silt	Clay/Cl. Silt

It is detailed in Table 8 the upper and lower bound values, where each case was simulated using OptumG2; 64 cases with different wall and soil variables have been represented in detail. The failure modes are detailed in Appendix K for each separate simulated case.

Since the material is reduced till failure occurs it's important to extend the boundaries of the model so not to affect the development of the failure mechanism. This is achieved by increasing the models environment, i.e. backfill, foundation. Hereafter, reducing the strength of the materials will both decrease the bearing capacity of the foundation and increases the earth pressures from the backfill.

Calculations have been undertaken in paragraph 3.2 and 3.3 to mathematically determine the lower and upper bounds of a particular soil scenario. It should be noted that not all upper and lower bound values have been calculated for this section, and should be considered as future works. However, an outline and accurate assumption can be gathered from what has been provided, detailing that the hand calculations appear to overestimate the cohesionless materials. Figure 48 to Figure 51 were produced from OptumG2, where cohesionless materials are either on the verge of failure or yielded failure under initial conditions.

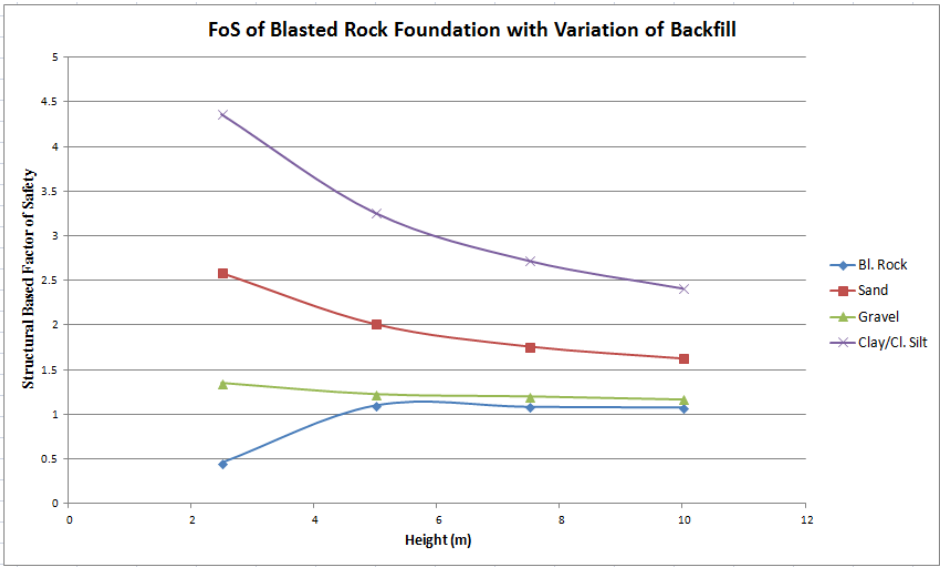

Figure 48 – Blasted rock foundation using OptumG2

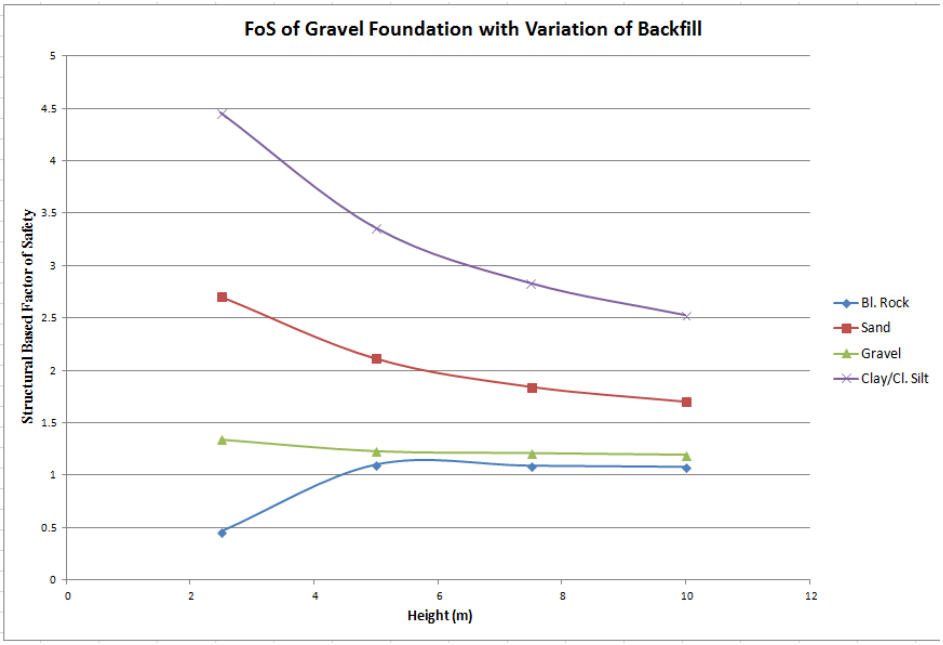

Figure 49 - gravel foundation using OptumG2

Scott Clayton
0061010140

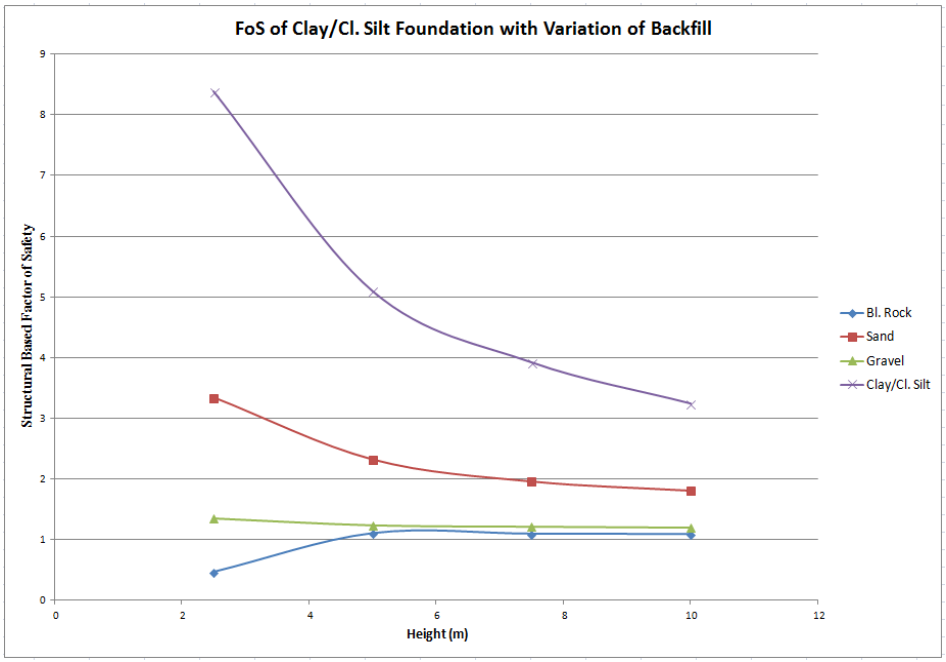

Figure 50 – Clay/Cl silt foundation using OptumG2

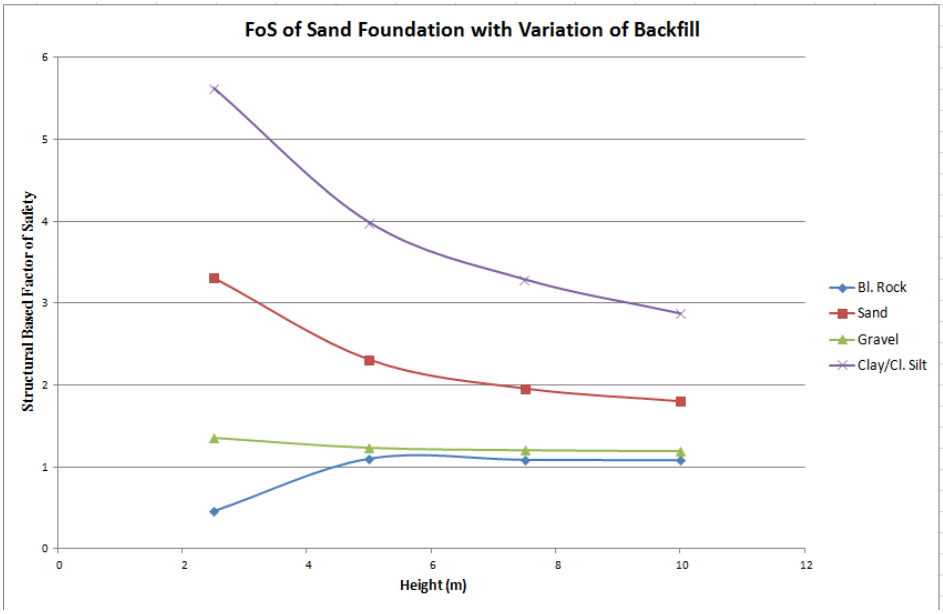

Figure 51 – Sand foundation using OptumG2

6.3 Elastoplastic Analysis

This analysis details the total displacement of the model over a long term period. Figure 52 to Figure 55 details a visual description of the failure mode; however, this is all it provides. The internal failures are not portrayed within the failure wedge; however, the more red a zone appears the larger the displacement in that zone.

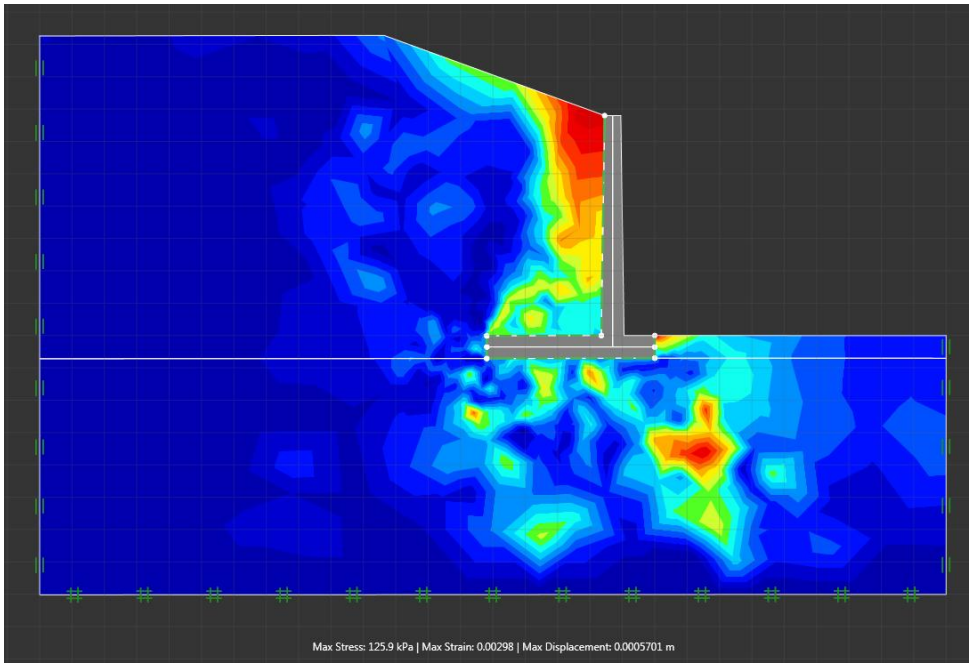

Figure 52 - Total displacement

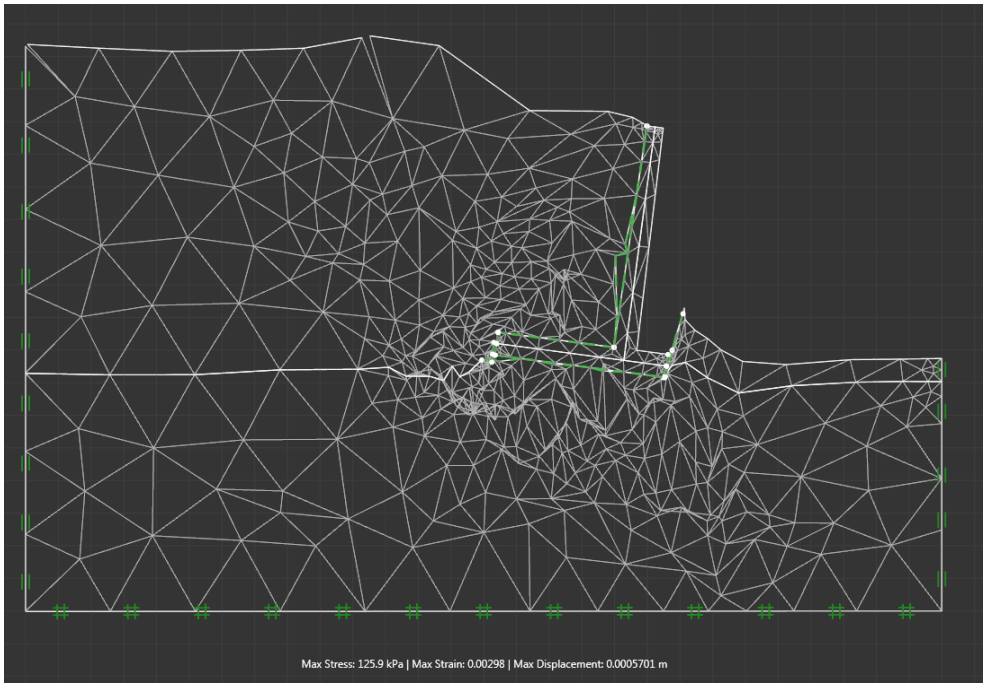

Figure 53 - Long term displacement with the use of internal mesh

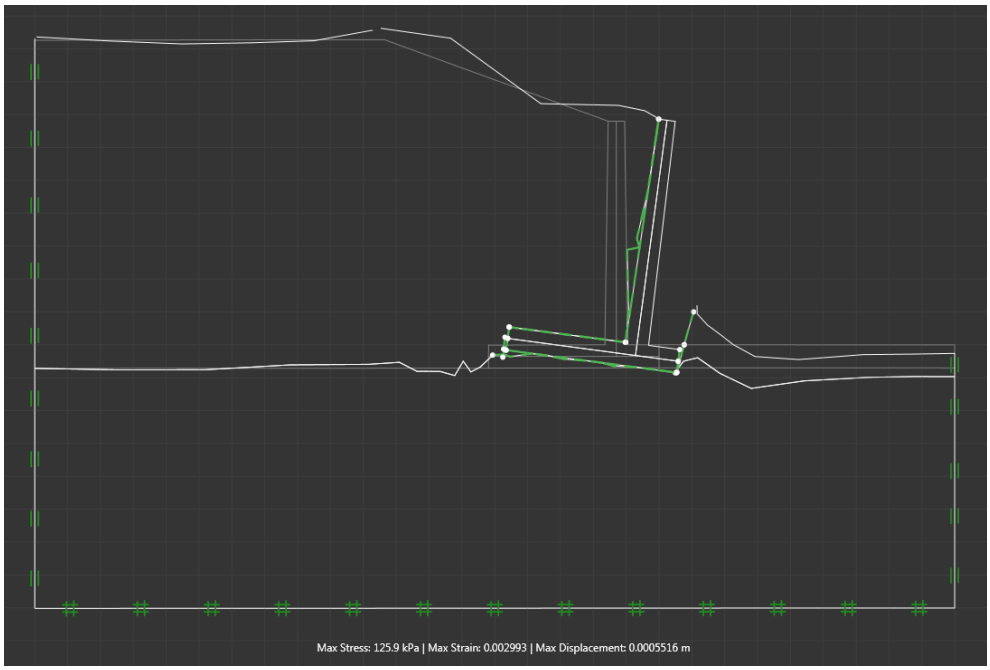

Figure 54 - Long term displacement without the use of internal mesh

The calculation time for Figure 52 to Figure 54 was 19 seconds, while Figure 55 took just under 7 minutes. Figure 55 details a finer mesh and hence, a more accurate result; however, it's in no way a more effective outcome. As a result, it may be true that by increasing the element number we would effectively decrease the discretization error of the problem, but if the goal is to better visualise the failure mechanism then a lower element number will be more than effective.

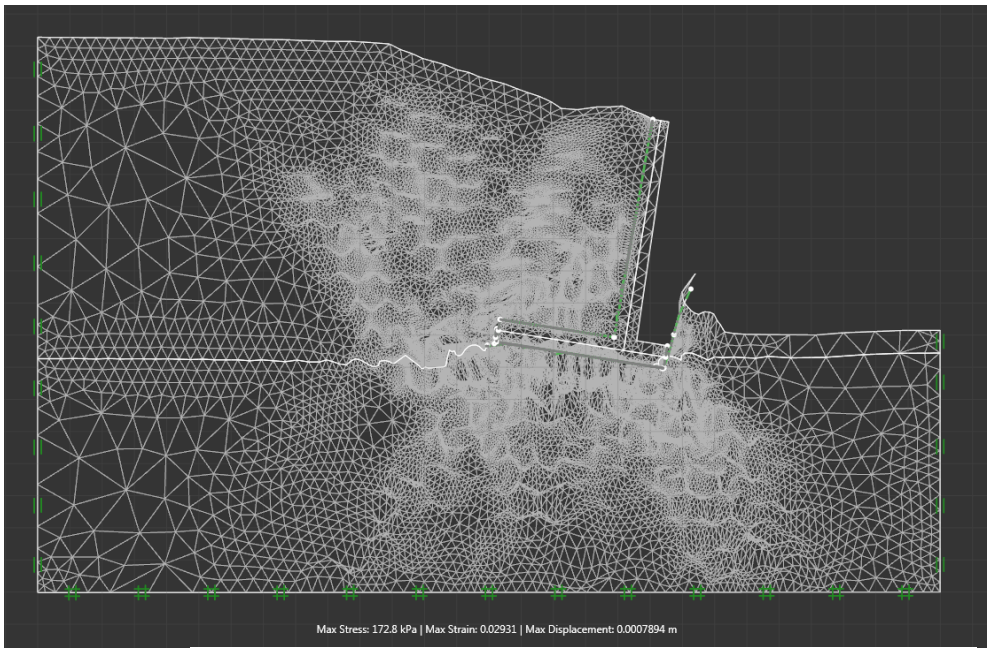

Figure 55 - Long term displacement with 100 000 elements

7. CONCLUSION

In this study of earth pressures, it's been concluded that shear strength parameters (cohesion and friction angle) of the soil are significant parameters affecting lateral pressures. As a result, an increase in the shear strength parameter results in a significant decrease in the total lateral thrust. Also, as expected, when wall friction angle is equal to zero both Coulomb's and Rankine's methods delivered identical values of active and passive earth pressure coefficients.

The significants of my findings determined which height retaining wall could and could not efficiently support a backfill and foundation material through the consideration of bearing, sliding and overturning. This was evaluated through both hand calculation and numerical simulations.

Throughout my hand calculation I've determined the most and least effective retaining structure in terms of bearing, sliding and overturning FoSs for inclined backfills. The footing width has been identified is a major consideration when determining bearing and overturning. The FoS for these two failure modes was found to decrease when founded on soils with low soil friction angles, and maximum footing width. For bearing this met my expectations, as the bearing capacity is also connected to the friction angle through the capacity factors $N_c, N_q,$ and N_y from Table 3.

It has been mathematically proven that overturning will be prevented if the resisting moments are greater than the forces overturning about the toe. It has also been identified that the footing is a predominant link to increasing or decreasing the resisting moments of the cantilever structure and therefore the FoS against overturning.

Cases which were derived from the hand calculation where modelled in OptumG2. The soil strength parameters for each soil type for both backfill and foundation were placed into the software without any extra safety factors. The software reduced these parameters until failure to calculate end results. My hand calculations were compared to that calculated from the software detailed in Table 7 seems to overestimate the earth pressures for cohesionless backfill materials. According to

OptumG2 simulations, some of the results presented under initial conditions, for cohesionless materials have either failed or are on the verge of failure.

There is a significant amount of information which could be analysed for further investigations. The use of rigid walls which was used in this report for the analysis of the 64 cases could be substituted for a flexible wall and possibly study into the effects of stiffness of this wall. An approach in the analysis of sloped footings could be studied to determine whether it has a direct increase to the resistance of sliding, and to continue the investigation on the hand calculations of all the upper and lower bounds values.

8. REFERENCES

Braja, D. M., 2014. *Geotechnical Engineering Handbook.* 1st ed. s.l.:J. Ross Publishing, lnc.

Braja, D. M. & Khaled, S., 2014. *Principles of Geotechnical Engineering.* eight ed. Stamford: Christopher M. Shortt.

Brand, E. W., 1982. *Guide to retaining wall design.* 1st ed. Hong Kong: Engineering Developement Department.

Briaud, J. L., 2013. *Geotechnical Engineering: Unsaturated and Saturated Soils.* 2nd ed. New Jersy: John Wiley & Sons.

Bruner, R. F., 1983. *Cantilever Retaining Wall Design,* Texas: Graduate College of Texas A&M University.

Budhu, M., 2007. *Soil Mechanics and Foundations.* 2nd ed. s.l.:John Wiley & Son Publishing.

Craig, R. F., 2004. *Craig's Soil Mechanics.* 7th ed. New York: Spon Press.

Davis, R. O. & Selvadurai, A. P., 2005. *Plasticity and Geomechanics.* 1st ed. Cambridge: Cambridge University Press.

Denson, J., 2013. *CSE Landscape Architect.* [Online]
Available at: http://www.cselandscapearchitect.com/2013/04/15/three-reasons-why-retaining-walls-fail/
[Accessed 12 May 2014].

Di Santolo, S. A., Evangelista, A. & Aversa, S., 2012. *Upper and lower bound solution for dynamic active earth pressure on cantilever walls,* Italy: 15 WCEE, Lisbon.

Donkada, S. & Menon, D., 2012. *Optimal Design of Reinforced Concrete Retaining Walls.* [Online]
Available at:
http://www.google.com.au/url?sa=t&rct=j&q=&esrc=s&source=web&cd=1&ved=0CCcQFjAA&url=http%3A%2F%2Fwww.sefindia.org%2Fforum%2Fdownload.php%3Fid%3D7582%26sid%3D630f3a10384aefe98aabaf9fc6ee2c0c&ei=vn4zU_eSDcbnrAelk4G4Bw&usg=AFQjCNHRzl0rUQEOrfmAH4C5kF1S7_aSSg&
[Accessed 27 March 2014].

Elman, M. T. & Terry, C. F., 1987. Retaining walls with sloped base. *Journal of Geotechnical Engineering,* 115(5), p. 746.

Frank, R. et al., 2004. *Designers' Guide to EN 1997-1 Eurocode 7: Geotechnical design - General rules.* 1st ed. Great Britain: Thomas Telford.

GuhaRay, A., Ghosh, S. & Baidya, D. K., 2013. Risk factor based design of cantilever retaining walls. *Geotechnical and Geological Engineering,* 32(1), pp. 179-189.

HandBook016, 2010. *Geotechnical Engineering in road construction.* Sydney: Standards Australia International Ltd.

Hanna, A. & Al-Romhein, R., 2008. At-Rest Earth Pressure of Overconsolidated Cohesionless Soil. *Journal of Geotechnical and Geoenvironmental Engineering,* 134(3), pp. 408-412.

HKU, 2013. *Soil Mechanics: Part B,* China: HKU.

Jaky, J., 1994. The Coefficient of Earth Pressure at Rest. *Journal of the Society of Hungarian Architects and Engineers,* Volume 7, pp. 355-358.

Kemp, M. & Blowes, D., 2011. *Concrete reinforcement and glass fibre reinforced polymer,* Brisbane: Queensland Roads.

Kiger, P. J., 2013. *Can an Ice Wall Stop Radioactive Water Leaks from Fukushima.* [Online]
Available at: http://news.nationalgeographic.com/news/energy/2013/08/130819-japan-ice-wall-for-fukushima-radioactive-leaks/
[Accessed 7 10 2014].

Lambe, T. W., 1969. *Soil Mechanics.* 1st ed. New York: John Wiley & Sons.

Liu, M., 2010. *Shallow Foundations,* Sydney: University of Sydney.

Mittle, S. & Biswas, A. K., 2006. River bank erosion control by soil nailing. *Geotechnical and Geological Engineering,* 24(6), pp. 1821-1833.

MoreTrench, 2014. *Ground Freezing.* [Online]
Available at: http://www.moretrench.com/cmsAdmin/uploads/GroundFreezing-LowRes.pdf
[Accessed 7 10 2014].

Palmeira, E. M., Zirlis, A. C. & Ortigau, J. R., 1995. Experience with soil nailing in Brazil: 1970-1994. *ICE - Geotecnical Engineering,* 113(2), pp. 93-106.

Sengupta, A. & Giri, D., 2011. Dynamic analysis of soil-nailed slope. *Proceedings of the Institution of Civil Engineers,* 164(4), pp. 225-234.

Sherif, M. A., Fang, Y. S. & Sherif, R. I., 1984. K_a and K_o Behind Rotating and Non-Yielding Walls. *Journal of Geotechnical Engineering,* Volume 110, pp. 41-56.

Shroff, A. V. & Shah, D. L., 2003. *Soil Mechanics and Geotechnical Engineering.* 1 ed. India: Balkema, A.A..

UMR, 2014. *Cantilever Walls.* [Online]
Available at:
http://web.mst.edu/~rogersda/umrcourses/ge441/online_lectures/retention_structures/GE441-Lecture6-4.pdf
[Accessed 28 March 2014].

Valsson, S. M., 2011. *Earth pressures against and stability of retaining structures,* Reykjavik: University of Iceland.

Vrecl, H. K. & Trauner, L., 2010. Upper-bound approach for analysis of cantilever retaining walls. *Canadian Geotechnical Journal,* 47(9), pp. 999-1010.

White, M., 2011. *Retaining Walls,* British Columbia: University of British Columbia.

9. APPENDIX A – Project Specification

University of Southern Queensland

FACULTY OF ENGINEERING AND SURVEYING

ENG4111 RESEARCH PROJECT
PROJECT SPECIFICATION

FOR: **Scott Edward CLAYTON**

TOPIC: Lateral Earth Pressure Problems involved with Cantilever Retaining Structures and Stability of those Structures.

SUPERVISOR: Kazem Ghabraie

ENROLMENT: ENG4111 – S1, 2014

ENG4112 – S2, 2014

PROJECT AIM: To determine mathematically and graphically the lateral earth pressures influenced by surrounding earth on a cantilever retaining wall.

PROGRAMME:

1. Research the background of Rankine and Coulomb, and evaluating any possible link between the two theories.
2. Identify any possible scenarios where Rankine's theory would and would not work.
3. Identify any possible scenarios where Coulomb theory would and would not work.
4. Identify which material would be optimum for backfill (incline) and foundations, whether it is blasted rock, clay, gravel or silty clay.
5. Using suitable numerical methods to determine the lateral earth pressures, stress lines, failure modes, etc. influenced on cantilever retaining walls.

If time permits:

6. Determine methods for increasing stability of a retaining wall due to pressures

AGREED: _____ (Student) _____ (Supervisor)

Date: / / 2014 Date: / / 2014

Examiner/Co-examiner: _____

10. APPENDIX B – Acting Forces

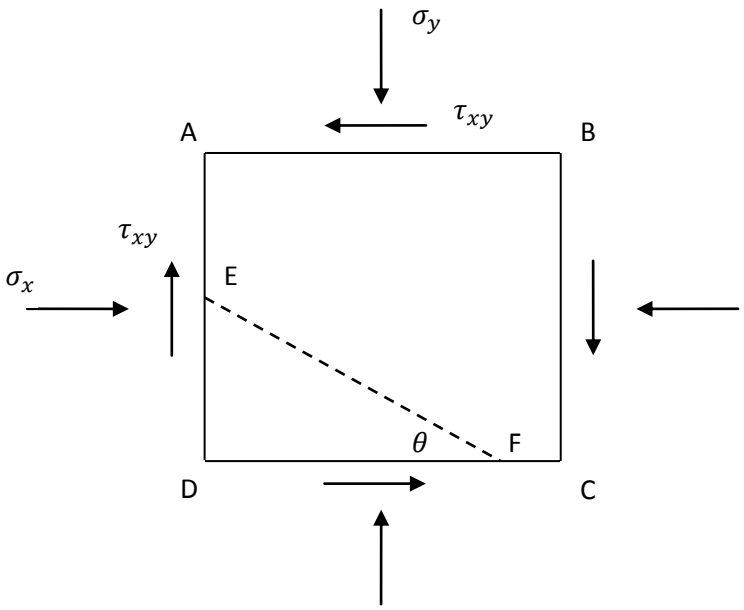

Noting that $-\tau_{xy} = \tau_{yx}$,

Force Diagrams detailed below allow for calculations of forces acting on edges DE and DF

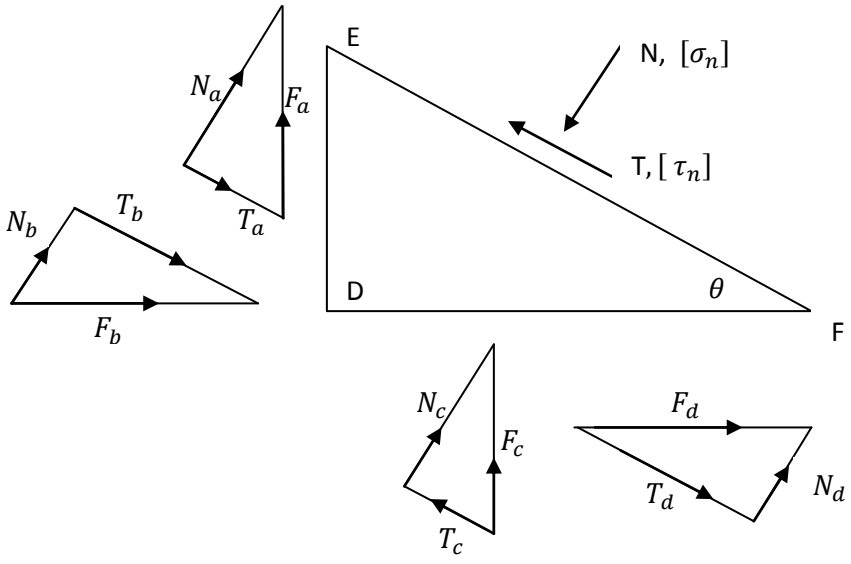

Therefore,

$$F_a = \tan\theta \times \tau_{xy} \qquad N_a = F_a \cos\theta \qquad T_a = F_a \sin\theta$$
$$F_b = \tan\theta \times \sigma_x \qquad N_b = F_b \sin\theta \qquad T_b = F_b \cos\theta$$
$$F_c = \sigma_y \qquad N_c = F_c \cos\theta \qquad T_c = F_c \sin\theta$$
$$F_d = \tau_{xy} \qquad N_d = F_d \sin\theta \qquad T_d = F_d \cos\theta$$

Now;

Resolve forces in direction of σ_n:

$$\frac{\sigma_n}{\cos\theta} = N_a + N_b + N_c + N_d$$

$$= \left[(\tan\theta \times \tau_{xy})\cos^2\theta\right] + \left[(\tan\theta \times \sigma_x)\sin\theta\cos\theta\right] + \left[(\sigma_y)\cos^2\theta\right] + \left[(\tau_{xy})\sin\theta\cos\theta\right]$$

$$= \left[\left(\frac{\sin\theta}{\cos\theta} \times \tau_{xy}\right)\cos^2\theta\right] + \left[\left(\frac{\sin\theta}{\cos\theta} \times \sigma_x\right)\sin\theta\cos\theta\right] + \left[(\sigma_y)\cos^2\theta\right] + \left[(\tau_{xy})\sin\theta\cos\theta\right]$$

$$= \left[\sin\theta \times \tau_{xy} \times \cos\theta\right] + \left[\sin^2\theta \times \sigma_x\right] + \left[\sigma_y \times \cos^2\theta\right] + \left[\tau_{xy} \times \sin\theta \times \cos\theta\right]$$

$$= \left[\tau_{xy}\sin\theta\cos\theta\right] + \left[\tau_{xy}\sin\theta\cos\theta\right] + \left[\sigma_x\sin^2\theta\right] + \left[\sigma_y\cos^2\theta\right]$$

$$\sigma_n = 2\left[\tau_{xy}\sin\theta\cos\theta\right] + \left[\sigma_x\sin^2\theta\right] + \left[\sigma_y\cos^2\theta\right]$$

However, Since

$$2(\sin\theta \times \cos\theta) = \sin 2\theta;$$

$$\sin^2\theta = \frac{1}{2}(1 - \cos 2\theta); \text{ and}$$

$$\cos^2\theta = \frac{1}{2}(1 + \cos 2\theta).$$

Then;

$$\sigma_n = \tau_{xy}\sin 2\theta + \frac{\sigma_x}{2}(1 - \cos 2\theta) + \frac{\sigma_y}{2}(1 + \cos 2\theta)$$

$$= \tau_{xy}\sin 2\theta + \frac{\sigma_x}{2} - \frac{\sigma_x\cos 2\theta}{2} + \frac{\sigma_y}{2} + \frac{\sigma_y\cos 2\theta}{2}$$

$$\therefore \sigma_n = \tau_{xy}\sin 2\theta + \frac{\sigma_y + \sigma_x}{2} + \frac{\sigma_y - \sigma_x}{2}\cos 2\theta \qquad \text{Eq. A.1}$$

Now, resolve the forces in the direction of τ_n:

$$\frac{\tau_n}{\cos\theta} = T_a + T_b - T_c + T_d$$

$$= \left[(\tan\theta \times \tau_{xy})\sin\theta \times \cos\theta\right] + \left[(\tan\theta \times \sigma_x)\cos^2\theta\right] - \left[(\sigma_y)\sin\theta \times \cos\theta\right] + \left[(\tau_{xy})\cos^2\theta\right]$$

$$= \left[\left(\frac{\sin\theta}{\cos\theta}\times \tau_{xy}\right)\sin\theta\times\cos\theta\right] + \left[\left(\frac{\sin\theta}{\cos\theta}\times \sigma_x\right)\cos^2\theta\right] - \left[(\sigma_y)\sin\theta\times\cos\theta\right] + \left[(\tau_{xy})\cos^2\theta\right]$$

$$= \left[(\sin\theta\times \tau_{xy})\sin\theta\right] + \left[(\sin\theta\times \sigma_x)\cos\theta\right] - \left[(\sigma_y)\sin\theta\times\cos\theta\right] + \left[(\tau_{xy})\cos^2\theta\right]$$

$$= \left[\tau_{xy}\sin^2\theta\right] + \left[\sigma_x\sin\theta\cos\theta\right] - \left[\sigma_y\sin\theta\cos\theta\right] + \left[\tau_{xy}\cos^2\theta\right]$$

$$= (\sigma_x - \sigma_y)\sin\theta\cos\theta + \left[\tau_{xy}\sin^2\theta\right] + \left[\tau_{xy}\cos^2\theta\right]$$

$$\tau_n = \frac{1}{2}(\sigma_x - \sigma_y)\sin 2\theta + \tau_{xy}\left[\sin^2\theta + \cos^2\theta\right]$$

However,

Since; $\cos^2\theta - \sin^2\theta = \cos 2\theta$

$$\tau_n = -\frac{1}{2}(\sigma_x - \sigma_y)\sin 2\theta + \tau_{xy}\left[-\sin^2\theta - \cos^2\theta\right]$$

$$\therefore \tau_n = \frac{1}{2}(\sigma_y - \sigma_x)\sin 2\theta - \tau_{xy}\cos 2\theta \qquad \text{Eq. A.2}$$

The directions of planes on which $\tau_n = 0$ can be found by substituting $\tau_n = 0$ in equation A.2, that is

$$0 = \frac{1}{2}(\sigma_y - \sigma_x)\sin 2\theta - \tau_{xy}\cos 2\theta$$

$$\frac{1}{2}(\sigma_y - \sigma_x)\sin 2\theta = \tau_{xy}\cos 2\theta$$

$$\frac{\sin 2\theta}{\cos 2\theta} = \frac{2\tau_{xy}}{(\sigma_y - \sigma_x)}$$

$$\tan 2\theta = \frac{2\tau_{xy}}{(\sigma_y - \sigma_x)} \qquad \text{Eq. A.3}$$

Equation A.3 will give two sets of orthogonal planes. This means that there are two planes at right angle to each other on which the shear stress is zero. As a result, since the shear stress is equal to zero on these planes, then these are the planes on which the principal stresses act.

The principal stresses on these planes can be evaluated by substituting equation A.3 into A.1, which yields

$$\sigma_n = \tau_{xy}\sin 2\theta + \frac{\sigma_y + \sigma_x}{2} + \frac{\sigma_y - \sigma_x}{2}\cos 2\theta$$

While noting from A.3*;*

$$\tan 2\theta = \frac{2\tau_{xy}}{(\sigma_y - \sigma_x)}$$

$$\frac{\sin 2\theta}{\cos 2\theta} = \frac{2\tau_{xy}}{(\sigma_y - \sigma_x)}$$

$$\sin 2\theta = \frac{2\tau_{xy}}{(\sigma_y - \sigma_x)} \cos 2\theta$$

$$\sin 2\theta = \frac{2\tau_{xy}}{\left[(\sigma_y - \sigma_x)^2 + 4\tau_{xy}^2\right]^{\frac{1}{2}}}$$

And;

$$\cos 2\theta = \frac{(\sigma_y - \sigma_x)}{2\tau_{xy}} \sin 2\theta$$

$$\cos 2\theta = \frac{(\sigma_y - \sigma_x)}{\left[(\sigma_y - \sigma_x)^2 + 4\tau_{xy}^2\right]^{\frac{1}{2}}}$$

Therefore;

$$\sigma_n = \tau_{xy} \times \frac{2\tau_{xy}}{\left[(\sigma_y - \sigma_x)^2 + 4\tau_{xy}^2\right]^{\frac{1}{2}}} + \frac{\sigma_y + \sigma_x}{2} + \left[\frac{\sigma_y - \sigma_x}{2} \times \frac{(\sigma_y - \sigma_x)}{\left[(\sigma_y - \sigma_x)^2 + 4\tau_{xy}^2\right]^{\frac{1}{2}}}\right]$$

$$= \frac{\sigma_y + \sigma_x}{2} + \frac{2\tau_{xy}^2}{\left[(\sigma_y - \sigma_x)^2 + 4\tau_{xy}^2\right]^{\frac{1}{2}}} + \frac{(\sigma_y - \sigma_x)^2}{2\left[(\sigma_y - \sigma_x)^2 + 4\tau_{xy}^2\right]^{\frac{1}{2}}}$$

$$= \frac{\sigma_y + \sigma_x}{2} + \frac{4\tau_{xy}^2}{2\left[(\sigma_y - \sigma_x)^2 + 4\tau_{xy}^2\right]^{\frac{1}{2}}} + \frac{(\sigma_y - \sigma_x)^2}{2\left[(\sigma_y - \sigma_x)^2 + 4\tau_{xy}^2\right]^{\frac{1}{2}}}$$

$$= \frac{\sigma_y + \sigma_x}{2} + \frac{(\sigma_y - \sigma_x)^2 + 4\tau_{xy}^2}{2\left[(\sigma_y - \sigma_x)^2 + 4\tau_{xy}^2\right]^{\frac{1}{2}}}$$

$$= \frac{\sigma_y + \sigma_x}{2} + \sqrt{\frac{(\sigma_y - \sigma_x)^4 + 16\tau_{xy}^4}{4\left[(\sigma_y - \sigma_x)^2 + 4\tau_{xy}^2\right]}}$$

$$= \frac{\sigma_y + \sigma_x}{2} + \sqrt{\frac{\left(\sigma_y - \sigma_x\right)^{2(2)} + 4(4)\tau_{xy}^{2(2)}}{4\left[\left(\sigma_y - \sigma_x\right)^2 + 4\tau_{xy}^2\right]}}$$

$$= \frac{\sigma_y + \sigma_x}{2} + \sqrt{\frac{\left(\sigma_y - \sigma_x\right)^2 + 4\tau_{xy}^2}{4}}$$

$$= \frac{\sigma_y + \sigma_x}{2} \pm \sqrt{\frac{\left(\sigma_y - \sigma_x\right)^2}{4} + \frac{4\tau_{xy}^2}{4}}$$

$$= \frac{\sigma_y + \sigma_x}{2} \pm \sqrt{\frac{\left(\sigma_y - \sigma_x\right)^2}{4} + \tau_{xy}^2}$$

$$\therefore \sigma_n = \frac{\sigma_y + \sigma_x}{2} \pm \sqrt{\left(\frac{\sigma_y - \sigma_x}{2}\right)^2 + \tau_{xy}^2}$$

Two variables of σ_n are obtained, the major (larger value) and the minor (smaller value) of the two principal stresses.

Hence;

The *Major* Principal Stress

$$\sigma_n = \sigma_1 = \frac{\sigma_y + \sigma_x}{2} + \sqrt{\left(\frac{\sigma_y - \sigma_x}{2}\right)^2 + \tau_{xy}^2}$$

The *Minor* Principal Stress

$$\sigma_n = \sigma_3 = \frac{\sigma_y + \sigma_x}{2} - \sqrt{\left(\frac{\sigma_y - \sigma_x}{2}\right)^2 + \tau_{xy}^2}$$

11. APPENDIX C – Soil Properties

Backfill Subsoil (Blasted Rock)		
Elastic Modulus MPa	E_b	90
Poisson's Ratio	v_b	0.33
Cohesion (kPa)	c	0
Total Unit Weight (kN/m^3)	y_b	26.5
Friction Angle	ϕ_b	30
Coefficient of Earth Pressure at rest	K_0	0.5
Backfill Soil (Gravel)		
Elastic Modulus MPa	E_b	100
Poisson's Ratio	v_b	0.25
Cohesion (kPa)	c	0
Total Unit Weight (kN/m^3)	y_b	19.62
Friction Angle	ϕ_b	35
Coefficient of Earth Pressure at rest	K_0	0.426
Backfill (Graded Sand)		
Elastic Modulus MPa	E_b	50
Poisson's Ratio	v_b	0.3
Cohesion (kPa)	c	20
Total Unit Weight (kN/m^3)	y_b	17.66
Friction Angle	ϕ_b	38
Coefficient of Earth Pressure at rest	K_0	0.5
Backfill (Clay/Cl. Silt)		
Elastic Modulus MPa	E_b	60
Poisson's Ratio	v_b	0.25
Cohesion (kPa)	c	100
Total Unit Weight (kN/m^3)	y_b	18.64
Friction Angle	ϕ_b	25
Coefficient of Earth Pressure at rest	K_0	0.426

Foundation Subsoil (Blasted Rock)		
Elastic Modulus MPa	E_f	100
Poisson's Ratio	v_f	0.33
Cohesion (kPa)	c	0
Total Unit Weight (kN/m^3)	y_f	26.5
Friction Angle	ϕ_f	30
Coefficient of Earth Pressure at rest	K_0	0.5
Foundation Soil (Gravel)		
Elastic Modulus MPa	E_f	160
Poisson's Ratio	v_f	0.25
Cohesion (kPa)	c	0
Total Unit Weight (kN/m^3)	y_f	19.62
Friction Angle	ϕ_f	35
Coefficient of Earth Pressure at rest	K_0	0.426
Foundation (Graded Sand)		
Elastic Modulus MPa	E_f	65
Poisson's Ratio	v_f	0.3
Cohesion (kPa)	c	20
Total Unit Weight (kN/m^3)	y_f	17.66
Friction Angle	ϕ_f	38
Coefficient of Earth Pressure at rest	K_0	0.5
Foundation (Clay/Cl. Silt)		
Elastic Modulus MPa	E_f	70
Poisson's Ratio	v_f	0.25
Cohesion (kPa)	c	100
Total Unit Weight (kN/m^3)	y_f	18.64
Friction Angle	ϕ_f	25
Coefficient of Earth Pressure at rest	K_0	0.426

12. APPENDIX D – Rankine Values of K_a and K_p for Horizontal backfill

$$K_a = \frac{\sigma'_a}{\sigma'_o} = \tan^2\left(45 - \frac{\phi'}{2}\right)$$

$$\mathrm{K_p} = \tan^2\left(45 + \frac{\phi'}{2}\right)$$

ϕ' (deg)	K_a
24	0.4217
25	0.4059
26	0.3905
27	0.3755
28	0.3610
29	0.3470
30	0.3333
31	0.3201
32	0.3073
33	0.2948
34	0.2827
35	0.2710
36	0.2596
37	0.2486
38	0.2379
39	0.2275
40	0.2174

ϕ' (deg)	K_p
24	2.3712
25	2.4639
26	2.5611
27	2.6629
28	2.7698
29	2.8821
30	3.0000
31	3.1240
32	3.2546
33	3.3921
34	3.5371
35	3.6902
36	3.8518
37	4.0228
38	4.2037
39	4.3955
40	4.5989

13. APPENDIX E – Rankine Active Values of $K_a, c' = 0$ for inclined backfill

$$K_a = cos\alpha \times \left[\frac{cos\alpha - \sqrt{(cos^2\alpha - cos^2\phi')}}{cos\alpha + \sqrt{(cos^2\alpha - cos^2\phi')}}\right]$$

α(deg)	ϕ' (deg)															
	25	26	27	28	29	30	31	32	33	34	35	36	37	38	39	40
0	0.4059	0.3905	0.3755	0.3610	0.3470	0.3333	0.3201	0.3073	0.2948	0.2827	0.2710	0.2596	0.2486	0.2379	0.2275	0.2174
1	0.4061	0.3907	0.3757	0.3612	0.3471	0.3335	0.3202	0.3074	0.2949	0.2828	0.2711	0.2597	0.2487	0.2380	0.2276	0.2175
2	0.4068	0.3913	0.3763	0.3618	0.3476	0.3339	0.3207	0.3078	0.2953	0.2832	0.2714	0.2600	0.2489	0.2382	0.2278	0.2177
3	0.4079	0.3924	0.3773	0.3627	0.3485	0.3347	0.3214	0.3084	0.2959	0.2837	0.2719	0.2605	0.2494	0.2386	0.2282	0.2181
4	0.4096	0.3939	0.3787	0.3639	0.3496	0.3358	0.3224	0.3094	0.2967	0.2845	0.2726	0.2611	0.2500	0.2392	0.2287	0.2186
5	0.4117	0.3959	0.3805	0.3656	0.3512	0.3372	0.3237	0.3105	0.2978	0.2855	0.2736	0.2620	0.2508	0.2399	0.2294	0.2192
6	0.4144	0.3983	0.3827	0.3676	0.3531	0.3389	0.3253	0.3120	0.2992	0.2868	0.2747	0.2631	0.2518	0.2409	0.2303	0.2200
7	0.4176	0.4012	0.3854	0.3701	0.3553	0.3410	0.3272	0.3138	0.3008	0.2883	0.2761	0.2644	0.2530	0.2420	0.2313	0.2209
8	0.4214	0.4047	0.3886	0.3730	0.3580	0.3435	0.3294	0.3159	0.3027	0.2900	0.2778	0.2659	0.2544	0.2432	0.2325	0.2220
9	0.4258	0.4087	0.3922	0.3764	0.3611	0.3463	0.3320	0.3182	0.3049	0.2921	0.2796	0.2676	0.2560	0.2447	0.2338	0.2233
10	0.4309	0.4134	0.3965	0.3802	0.3646	0.3495	0.3350	0.3210	0.3074	0.2944	0.2818	0.2696	0.2578	0.2464	0.2354	0.2247
11	0.4368	0.4186	0.4013	0.3846	0.3686	0.3532	0.3383	0.3241	0.3103	0.2970	0.2841	0.2718	0.2598	0.2482	0.2371	0.2263
12	0.4434	0.4247	0.4067	0.3896	0.3731	0.3573	0.3421	0.3275	0.3134	0.2999	0.2868	0.2742	0.2621	0.2503	0.2390	0.2281
13	0.4510	0.4315	0.4129	0.3952	0.3782	0.3620	0.3464	0.3314	0.3170	0.3031	0.2898	0.2770	0.2646	0.2527	0.2412	0.2301
14	0.4596	0.4392	0.4199	0.4015	0.3839	0.3671	0.3511	0.3357	0.3209	0.3068	0.2931	0.2800	0.2674	0.2552	0.2435	0.2322
15	0.4695	0.4480	0.4278	0.4086	0.3903	0.3729	0.3564	0.3405	0.3253	0.3108	0.2968	0.2834	0.2705	0.2581	0.2461	0.2346

16	0.4807	0.4580	0.4367	0.4165	0.3975	0.3794	0.3622	0.3458	0.3302	0.3152	0.3008	0.2871	0.2739	0.2612	0.2490	0.2373
17	0.4936	0.4694	0.4467	0.4255	0.4056	0.3867	0.3688	0.3518	0.3356	0.3201	0.3053	0.2911	0.2776	0.2646	0.2521	0.2401
18	0.5086	0.4824	0.4582	0.4357	0.4146	0.3948	0.3761	0.3584	0.3415	0.3255	0.3102	0.2956	0.2817	0.2683	0.2555	0.2433
19	0.5261	0.4975	0.4714	0.4473	0.4249	0.4039	0.3842	0.3657	0.3481	0.3315	0.3156	0.3006	0.2862	0.2724	0.2593	0.2467
20	0.5469	0.5152	0.4866	0.4605	0.4365	0.4142	0.3934	0.3739	0.3555	0.3381	0.3216	0.3060	0.2911	0.2769	0.2634	0.2504
21	0.5723	0.5361	0.5043	0.4758	0.4498	0.4259	0.4037	0.3830	0.3637	0.3455	0.3283	0.3120	0.2965	0.2818	0.2678	0.2545
22	0.6041	0.5616	0.5254	0.4936	0.4651	0.4392	0.4154	0.3934	0.3729	0.3537	0.3356	0.3186	0.3025	0.2872	0.2727	0.2590
23	0.6464	0.5936	0.5510	0.5147	0.4829	0.4545	0.4287	0.4050	0.3832	0.3628	0.3438	0.3259	0.3091	0.2932	0.2781	0.2638
24	0.7096	0.6362	0.5831	0.5404	0.5041	0.4724	0.4440	0.4183	0.3948	0.3731	0.3529	0.3341	0.3164	0.2997	0.2840	0.2692
25	0.9063	0.6999	0.6259	0.5727	0.5299	0.4936	0.4619	0.4336	0.4081	0.3847	0.3631	0.3431	0.3245	0.3070	0.2905	0.2750

14. APPENDIX F – Rankine Passive Values of $K_p, c' = 0$ for inclined backfill

$$K_p = cos\alpha \times \left[\frac{cos\alpha + \sqrt{(cos^2\alpha - cos^2\phi')}}{cos\alpha - \sqrt{(cos^2\alpha - cos^2\phi')}}\right]$$

α(deg)	ϕ' (deg)															
	25	26	27	28	29	30	31	32	33	34	35	36	37	38	39	40
0	2.4639	2.5611	2.6629	2.7698	2.8821	3.0000	3.1240	3.2546	3.3921	3.5371	3.6902	3.8518	4.0228	4.2037	4.3955	4.5989
1	2.4618	2.5589	2.6607	2.7676	2.8798	2.9977	3.1217	3.2522	3.3897	3.5347	3.6877	3.8493	4.0201	4.2010	4.3927	4.5960
2	2.4553	2.5524	2.6542	2.7610	2.8731	2.9909	3.1147	3.2451	3.3825	3.5273	3.6801	3.8415	4.0122	4.1929	4.3843	4.5874
3	2.4446	2.5416	2.6432	2.7499	2.8618	2.9795	3.1032	3.2333	3.3704	3.5150	3.6675	3.8286	3.9990	4.1793	4.3704	4.5730
4	2.4295	2.5264	2.6279	2.7344	2.8461	2.9635	3.0869	3.2168	3.3536	3.4978	3.6499	3.8106	3.9805	4.1603	4.3509	4.5530
5	2.4103	2.5070	2.6083	2.7145	2.8260	2.9431	3.0662	3.1957	3.3320	3.4757	3.6274	3.7875	3.9569	4.1360	4.3259	4.5272
6	2.3867	2.4833	2.5844	2.6903	2.8015	2.9182	3.0408	3.1699	3.3057	3.4489	3.5999	3.7594	3.9280	4.1064	4.2954	4.4959
7	2.3590	2.4553	2.5561	2.6618	2.7726	2.8888	3.0110	3.1395	3.2748	3.4173	3.5676	3.7263	3.8941	4.0716	4.2596	4.4590
8	2.3270	2.4231	2.5237	2.6290	2.7393	2.8551	2.9768	3.1046	3.2392	3.3810	3.5305	3.6883	3.8551	4.0316	4.2185	4.4167
9	2.2909	2.3868	2.4870	2.5919	2.7018	2.8171	2.9381	3.0653	3.1991	3.3401	3.4887	3.6455	3.8112	3.9865	4.1722	4.3690
10	2.2506	2.3463	2.4462	2.5507	2.6601	2.7748	2.8952	3.0216	3.1546	3.2946	3.4422	3.5980	3.7625	3.9365	4.1207	4.3161
11	2.2062	2.3017	2.4013	2.5054	2.6142	2.7283	2.8479	2.9736	3.1057	3.2447	3.3912	3.5457	3.7090	3.8816	4.0643	4.2579
12	2.1577	2.2530	2.3523	2.4559	2.5643	2.6777	2.7966	2.9213	3.0525	3.1904	3.3357	3.4890	3.6508	3.8219	4.0029	4.1948
13	2.1051	2.2002	2.2992	2.4025	2.5102	2.6230	2.7411	2.8649	2.9950	3.1318	3.2759	3.4278	3.5881	3.7575	3.9368	4.1268
14	2.0484	2.1434	2.2422	2.3450	2.4523	2.5643	2.6816	2.8045	2.9335	3.0691	3.2119	3.3623	3.5210	3.6887	3.8660	4.0540
15	1.9874	2.0826	2.1812	2.2836	2.3903	2.5017	2.6182	2.7401	2.8680	3.0024	3.1437	3.2926	3.4496	3.6154	3.7908	3.9766

16	1.9222	2.0176	2.1161	2.2183	2.3245	2.4353	2.5509	2.6718	2.7986	2.9316	3.0715	3.2188	3.3740	3.5379	3.7112	3.8947
17	1.8527	1.9484	2.0471	2.1491	2.2549	2.3650	2.4798	2.5998	2.7254	2.8571	2.9955	3.1411	3.2945	3.4564	3.6275	3.8086
18	1.7785	1.8750	1.9739	2.0759	2.1815	2.2910	2.4051	2.5240	2.6485	2.7788	2.9157	3.0596	3.2111	3.3709	3.5397	3.7183
19	1.6993	1.7970	1.8966	1.9988	2.1042	2.2133	2.3266	2.4447	2.5680	2.6970	2.8323	2.9744	3.1240	3.2816	3.4481	3.6241
20	1.6145	1.7141	1.8148	1.9176	2.0230	2.1318	2.2446	2.3618	2.4840	2.6116	2.7454	2.8857	3.0333	3.1888	3.3528	3.5262
21	1.5230	1.6257	1.7282	1.8320	1.9379	2.0466	2.1589	2.2754	2.3965	2.5229	2.6551	2.7936	2.9392	3.0924	3.2540	3.4247
22	1.4231	1.5308	1.6363	1.7417	1.8485	1.9575	2.0696	2.1855	2.3057	2.4308	2.5615	2.6983	2.8419	2.9928	3.1519	3.3198
23	1.3109	1.4274	1.5379	1.6462	1.7546	1.8643	1.9766	2.0920	2.2115	2.3355	2.4647	2.5998	2.7414	2.8901	3.0466	3.2117
24	1.1761	1.3118	1.4312	1.5443	1.6555	1.7667	1.8796	1.9950	2.1139	2.2370	2.3649	2.4983	2.6379	2.7844	2.9383	3.1006
25	0.9063	1.1736	1.3123	1.4343	1.5502	1.6641	1.7783	1.8942	2.0129	2.1352	2.2620	2.3938	2.5316	2.6758	2.8273	2.9867

15. APPENDIX G – Coulomb Active Values of $K_a, \beta = 90°$ for horizontal backfill ($\alpha = 0$),

$$K_a = \frac{sin^2(\beta + \phi')}{sin^2\beta \times sin(\beta - \delta') \left[1 + \sqrt{\left(\frac{sin(\phi' + \delta') \times sin(\phi' - \alpha)}{sin(\beta - \delta') \times sin(\alpha + \beta)}\right)}\right]^2}$$

ϕ' (deg)	δ' (deg)								
	0	5	10	15	20	25	30	25	40
24	0.4217	0.4013	0.3866	0.3765	0.3705	0.3679	0.3688	0.3731	0.3811
25	0.4059	0.3865	0.3726	0.3631	0.3574	0.3551	0.3560	0.3602	0.3679
26	0.3905	0.3722	0.3590	0.3501	0.3447	0.3425	0.3435	0.3477	0.3552
27	0.3755	0.3583	0.3459	0.3374	0.3323	0.3304	0.3314	0.3355	0.3429
28	0.3610	0.3448	0.3330	0.3251	0.3203	0.3186	0.3197	0.3237	0.3309
29	0.3470	0.3316	0.3206	0.3131	0.3087	0.3071	0.3083	0.3123	0.3192
30	0.3333	0.3189	0.3085	0.3014	0.2973	0.2959	0.2972	0.3011	0.3079
31	0.3201	0.3065	0.2967	0.2901	0.2863	0.2851	0.2864	0.2903	0.2969
32	0.3073	0.2945	0.2852	0.2791	0.2755	0.2745	0.2759	0.2797	0.2862
33	0.2948	0.2828	0.2741	0.2683	0.2651	0.2642	0.2656	0.2694	0.2758
34	0.2827	0.2714	0.2633	0.2579	0.2549	0.2542	0.2557	0.2594	0.2657
35	0.2710	0.2604	0.2528	0.2478	0.2450	0.2445	0.2460	0.2497	0.2558
36	0.2596	0.2497	0.2426	0.2379	0.2354	0.2350	0.2366	0.2402	0.2462
37	0.2486	0.2393	0.2326	0.2283	0.2260	0.2257	0.2274	0.2310	0.2369
38	0.2379	0.2292	0.2230	0.2190	0.2169	0.2167	0.2184	0.2220	0.2277
39	0.2275	0.2194	0.2136	0.2099	0.2080	0.2080	0.2097	0.2133	0.2189
40	0.2174	0.2098	0.2045	0.2011	0.1994	0.1995	0.2012	0.2047	0.2102

16. APPENDIX H – Coulomb Passive Values of $K_p, \beta = 90°$ for horizontal backfill ($\alpha = 0$),

$$K_p = \frac{sin^2(\beta - \phi')}{sin^2\beta \times sin(\beta + \delta') \left[1 - \sqrt{\left(\frac{sin(\phi' + \delta') \times sin(\phi' + \alpha)}{sin(\beta + \delta') \times sin(\alpha + \beta)}\right)}\right]^2}$$

ϕ' (deg)	δ' (deg)								
	0	5	10	15	20	25	30	25	40
24	2.3712	2.7189	3.1410	3.6698	4.3536	5.2698	6.5493	8.4316	11.3962
25	2.4639	2.8335	3.2852	3.8548	4.5967	5.5991	7.0133	9.1210	12.4991
26	2.5611	2.9541	3.4376	4.0515	4.8570	5.9547	7.5200	9.8851	13.7472
27	2.6629	3.0811	3.5989	4.2608	5.1360	6.3394	8.0748	10.7351	15.1669
28	2.7698	3.2149	3.7698	4.4839	5.4356	6.7566	8.6838	11.6841	16.7906
29	2.8821	3.3561	3.9510	4.7220	5.7580	7.2099	9.3545	12.7481	18.6588
30	3.0000	3.5052	4.1433	4.9765	6.1054	7.7036	10.0951	13.9459	20.8224
31	3.1240	3.6627	4.3477	5.2489	6.4804	8.2426	10.9159	15.3009	23.3462
32	3.2546	3.8293	4.5653	5.5409	6.8861	8.8327	11.8284	16.8414	26.3136
33	3.3921	4.0058	4.7971	5.8543	7.3259	9.4802	12.8470	18.6022	29.8334
34	3.5371	4.1928	5.0445	6.1915	7.8037	10.1930	13.9883	20.6271	34.0498
35	3.6902	4.3914	5.3088	6.5547	8.3239	10.9799	15.2726	22.9707	39.1569
36	3.8518	4.6023	5.5915	6.9468	8.8916	11.8514	16.7247	25.7028	45.4212
37	4.0228	4.8267	5.8946	7.3707	9.5128	12.8202	18.3747	28.9132	53.2159
38	4.2037	5.0658	6.2198	7.8301	10.1943	13.9008	20.2598	32.7188	63.0773
39	4.3955	5.3207	6.5695	8.3290	10.9441	15.1112	22.4264	37.2747	75.7974
40	4.5989	5.5930	6.9460	8.8720	11.7715	16.4727	24.9326	42.7896	92.5855

17. APPENDIX I – Coulomb Active Values of $K_a, \beta = 90°$ for inclined backfill

$$K_a = \frac{sin^2(\beta + \phi')}{sin^2\beta \times sin(\beta - \delta') \left[1 + \sqrt{\left(\frac{sin(\phi' + \delta') \times sin(\phi' - \alpha)}{sin(\beta - \delta') \times sin(\alpha + \beta)}\right)}\right]^2}$$

α (deg)	ϕ (deg)	$\delta' = \frac{2}{3}\phi'$	$K_a =$	$\delta' = \frac{\phi'}{2}$	$K_a =$
0	24	16.0000	0.3750	12.000	0.3821
	25	16.6667	0.3608	12.500	0.3674
	26	17.3333	0.3471	13.000	0.3532
	27	18.0000	0.3340	13.500	0.3395
	28	18.6667	0.3213	14.000	0.3264
	29	19.3333	0.3091	14.500	0.3137
	30	20.0000	0.2973	15.000	0.3014
	31	20.6667	0.2860	15.500	0.2896
	32	21.3333	0.2750	16.000	0.2782
	33	22.0000	0.2645	16.500	0.2671
	34	22.6667	0.2543	17.000	0.2564
	35	23.3333	0.2444	17.500	0.2461
	36	24.0000	0.2349	18.000	0.2361
	37	24.6667	0.2257	18.500	0.2265
	38	25.3333	0.2168	19.000	0.2172
	39	26.0000	0.2082	19.500	0.2081
	40	26.6667	0.1998	20.000	0.1994
5	24	16.0000	0.4032	12.000	0.4097
	25	16.6667	0.3872	12.500	0.3932
	26	17.3333	0.3719	13.000	0.3775
	27	18.0000	0.3572	13.500	0.3623
	28	18.6667	0.3431	14.000	0.3477
	29	19.3333	0.3295	14.500	0.3337
	30	20.0000	0.3165	15.000	0.3202
	31	20.6667	0.3039	15.500	0.3072
	32	21.3333	0.2919	16.000	0.2946
	33	22.0000	0.2803	16.500	0.2825
	34	22.6667	0.2691	17.000	0.2709
	35	23.3333	0.2583	17.500	0.2596
	36	24.0000	0.2479	18.000	0.2488
	37	24.6667	0.2379	18.500	0.2383
	38	25.3333	0.2282	19.000	0.2282
	39	26.0000	0.2188	19.500	0.2185
	40	26.6667	0.2098	20.000	0.2090
10	24	16.0000	0.4396	12.000	0.4453
	25	16.6667	0.4210	12.500	0.4263
	26	17.3333	0.4033	13.000	0.4082
	27	18.0000	0.3864	13.500	0.3909
	28	18.6667	0.3702	14.000	0.3743
	29	19.3333	0.3548	14.500	0.3584

	30	20.0000	0.3400	15.000	0.3432
	31	20.6667	0.3259	15.500	0.3286
	32	21.3333	0.3123	16.000	0.3145
	33	22.0000	0.2993	16.500	0.3011
	34	22.6667	0.2868	17.000	0.2881
	35	23.3333	0.2748	17.500	0.2757
	36	24.0000	0.2633	18.000	0.2637
	37	24.6667	0.2522	18.500	0.2522
	38	25.3333	0.2415	19.000	0.2412
	39	26.0000	0.2313	19.500	0.2305
	40	26.6667	0.2214	20.000	0.2202
15	24	16.0000	0.4915	12.000	0.4957
	25	16.6667	0.4682	12.500	0.4722
	26	17.3333	0.4464	13.000	0.4501
	27	18.0000	0.4259	13.500	0.4292
	28	18.6667	0.4065	14.000	0.4095
	29	19.3333	0.3881	14.500	0.3908
	30	20.0000	0.3707	15.000	0.3729
	31	20.6667	0.3541	15.500	0.3560
	32	21.3333	0.3384	16.000	0.3398
	33	22.0000	0.3234	16.500	0.3244
	34	22.6667	0.3091	17.000	0.3097
	35	23.3333	0.2954	17.500	0.2956
	36	24.0000	0.2823	18.000	0.2821
	37	24.6667	0.2698	18.500	0.2692
	38	25.3333	0.2578	19.000	0.2569
	39	26.0000	0.2463	19.500	0.2450
	40	26.6667	0.2353	20.000	0.2336
20	24	16.0000	0.5806	12.000	0.5816
	25	16.6667	0.5455	12.500	0.5467
	26	17.3333	0.5143	13.000	0.5156
	27	18.0000	0.4860	13.500	0.4874
	28	18.6667	0.4602	14.000	0.4614
	29	19.3333	0.4363	14.500	0.4374
	30	20.0000	0.4142	15.000	0.4150
	31	20.6667	0.3935	15.500	0.3941
	32	21.3333	0.3742	16.000	0.3744
	33	22.0000	0.3559	16.500	0.3559
	34	22.6667	0.3388	17.000	0.3384
	35	23.3333	0.3225	17.500	0.3218
	36	24.0000	0.3071	18.000	0.3061
	37	24.6667	0.2925	18.500	0.2911
	38	25.3333	0.2787	19.000	0.2769
	39	26.0000	0.2654	19.500	0.2633
	40	26.6667	0.2529	20.000	0.2504

18. APPENDIX J – Coulomb Passive Values of $K_p, \beta = 90°$ for inclined backfill

$$K_p = \frac{sin^2(\beta - \phi')}{sin^2\beta \times sin(\beta + \delta') \left[1 - \sqrt{\left(\frac{sin(\phi' + \delta') \times sin(\phi' + \alpha)}{sin(\beta + \delta') \times sin(\alpha + \beta)}\right)}\right]^2}$$

α (deg)	ϕ (deg)	$\delta' = \frac{2}{3}\phi'$	$K_a =$	$\delta' = \frac{\phi'}{2}$	$K_a =$
0	24	16.0000	3.7922	12.000	3.3374
	25	16.6667	4.0795	12.500	3.5524
	26	17.3333	4.3986	13.000	3.7870
	27	18.0000	4.7543	13.500	4.0436
	28	18.6667	5.1525	14.000	4.3251
	29	19.3333	5.6000	14.500	4.6348
	30	20.0000	6.1054	15.000	4.9765
	31	20.6667	6.6788	15.500	5.3547
	32	21.3333	7.3332	16.000	5.7748
	33	22.0000	8.0843	16.500	6.2432
	34	22.6667	8.9520	17.000	6.7674
	35	23.3333	9.9616	17.500	7.3567
	36	24.0000	11.1458	18.000	8.0221
	37	24.6667	12.5468	18.500	8.7774
	38	25.3333	14.2207	19.000	9.6392
	39	26.0000	16.2431	19.500	10.6285
	40	26.6667	18.7173	20.000	11.7715
5	24	16.0000	3.7922	12.000	3.3374
	25	16.6667	4.0795	12.500	3.5524
	26	17.3333	4.3986	13.000	3.7870
	27	18.0000	4.7543	13.500	4.0436
	28	18.6667	5.1525	14.000	4.3251
	29	19.3333	5.6000	14.500	4.6348
	30	20.0000	6.1054	15.000	4.9765
	31	20.6667	6.6788	15.500	5.3547
	32	21.3333	7.3332	16.000	5.7748
	33	22.0000	8.0843	16.500	6.2432
	34	22.6667	8.9520	17.000	6.7674
	35	23.3333	9.9616	17.500	7.3567
	36	24.0000	11.1458	18.000	8.0221
	37	24.6667	12.5468	18.500	8.7774
	38	25.3333	14.2207	19.000	9.6392
	39	26.0000	16.2431	19.500	10.6285
	40	26.6667	18.7173	20.000	11.7715
10	24	16.0000	3.7922	12.000	3.3374
	25	16.6667	4.0795	12.500	3.5524
	26	17.3333	4.3986	13.000	3.7870
	27	18.0000	4.7543	13.500	4.0436
	28	18.6667	5.1525	14.000	4.3251
	29	19.3333	5.6000	14.500	4.6348

	30	20.0000	6.1054	15.000	4.9765
	31	20.6667	6.6788	15.500	5.3547
	32	21.3333	7.3332	16.000	5.7748
	33	22.0000	8.0843	16.500	6.2432
	34	22.6667	8.9520	17.000	6.7674
	35	23.3333	9.9616	17.500	7.3567
	36	24.0000	11.1458	18.000	8.0221
	37	24.6667	12.5468	18.500	8.7774
	38	25.3333	14.2207	19.000	9.6392
	39	26.0000	16.2431	19.500	10.6285
	40	26.6667	18.7173	20.000	11.7715
15	24	16.0000	3.7922	12.000	3.3374
	25	16.6667	4.0795	12.500	3.5524
	26	17.3333	4.3986	13.000	3.7870
	27	18.0000	4.7543	13.500	4.0436
	28	18.6667	5.1525	14.000	4.3251
	29	19.3333	5.6000	14.500	4.6348
	30	20.0000	6.1054	15.000	4.9765
	31	20.6667	6.6788	15.500	5.3547
	32	21.3333	7.3332	16.000	5.7748
	33	22.0000	8.0843	16.500	6.2432
	34	22.6667	8.9520	17.000	6.7674
	35	23.3333	9.9616	17.500	7.3567
	36	24.0000	11.1458	18.000	8.0221
	37	24.6667	12.5468	18.500	8.7774
	38	25.3333	14.2207	19.000	9.6392
	39	26.0000	16.2431	19.500	10.6285
	40	26.6667	18.7173	20.000	11.7715
20	24	16.0000	3.7922	12.000	3.3374
	25	16.6667	4.0795	12.500	3.5524
	26	17.3333	4.3986	13.000	3.7870
	27	18.0000	4.7543	13.500	4.0436
	28	18.6667	5.1525	14.000	4.3251
	29	19.3333	5.6000	14.500	4.6348
	30	20.0000	6.1054	15.000	4.9765
	31	20.6667	6.6788	15.500	5.3547
	32	21.3333	7.3332	16.000	5.7748
	33	22.0000	8.0843	16.500	6.2432
	34	22.6667	8.9520	17.000	6.7674
	35	23.3333	9.9616	17.500	7.3567
	36	24.0000	11.1458	18.000	8.0221
	37	24.6667	12.5468	18.500	8.7774
	38	25.3333	14.2207	19.000	9.6392
	39	26.0000	16.2431	19.500	10.6285
	40	26.6667	18.7173	20.000	11.7715

19. APPENDIX K – Failure Modes with OptumG2

The numerical simulations was accomplished by what was described in paragraph 6.1, that is, a subdivided retaining structure, mesh adaptivity and 1000 elements. The following simulations represent a strength reduction analysis for each of the 64 cases. Both the lower and upper bounds have been displayed for each scenario.

Gravel Backfill

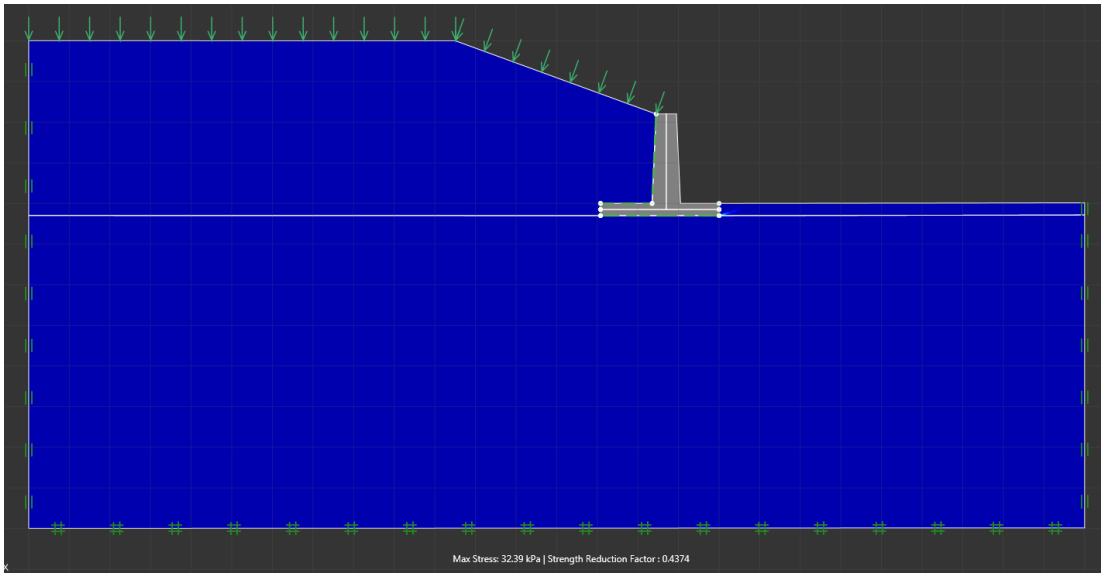

Figure 0.1 - Lower bound failure mode for case 1

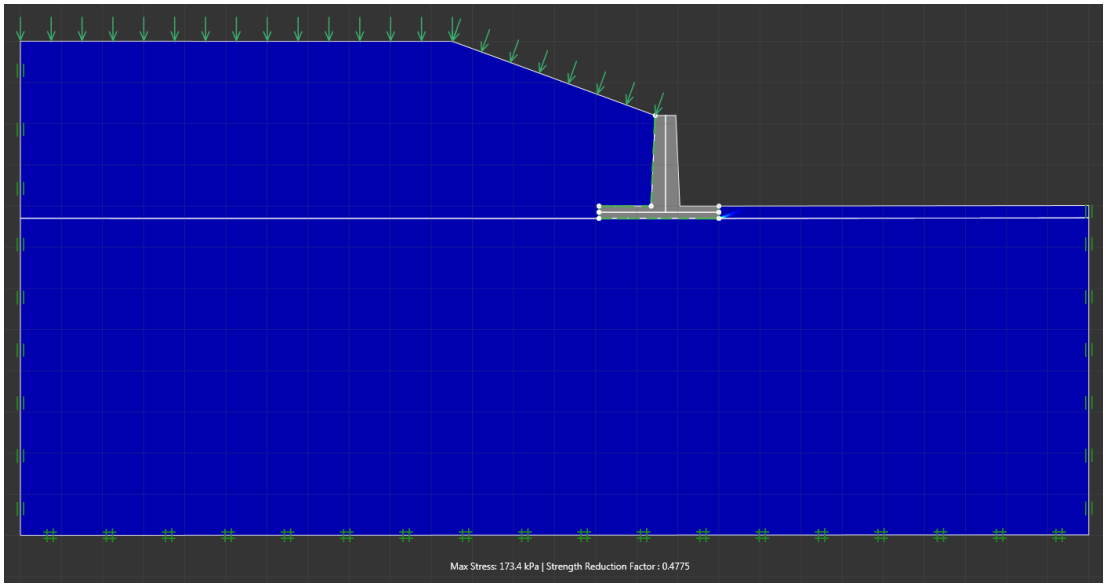

Figure 0.2 - Upper bound failure mode for case 1

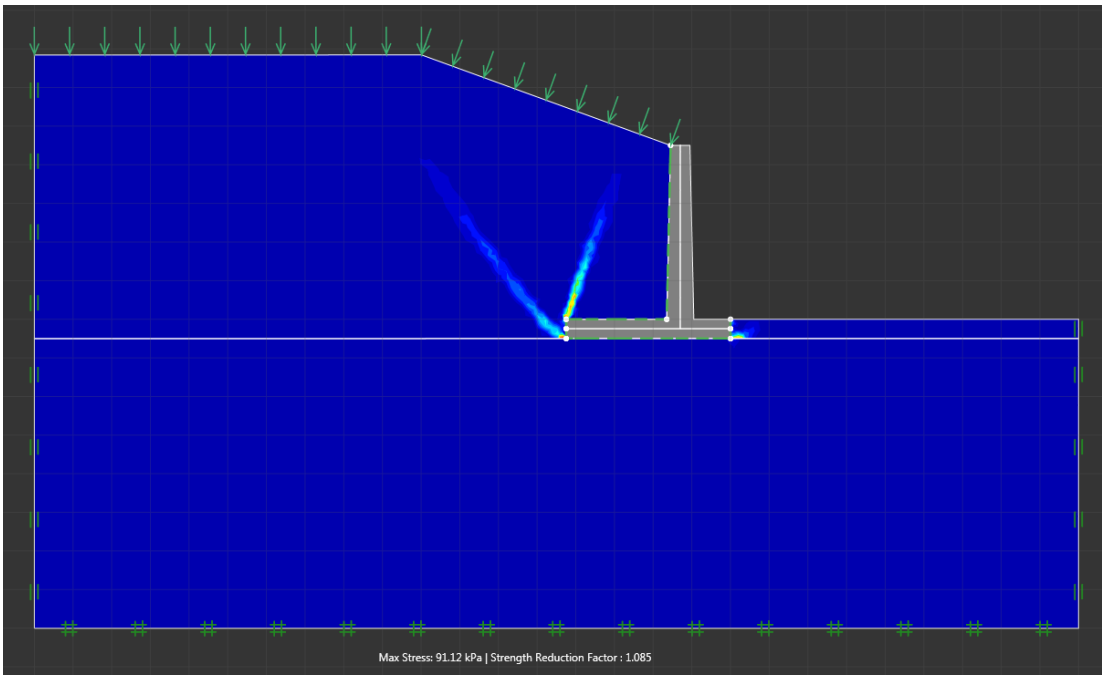

Figure 0.3 - Lower bound failure mode for case 2

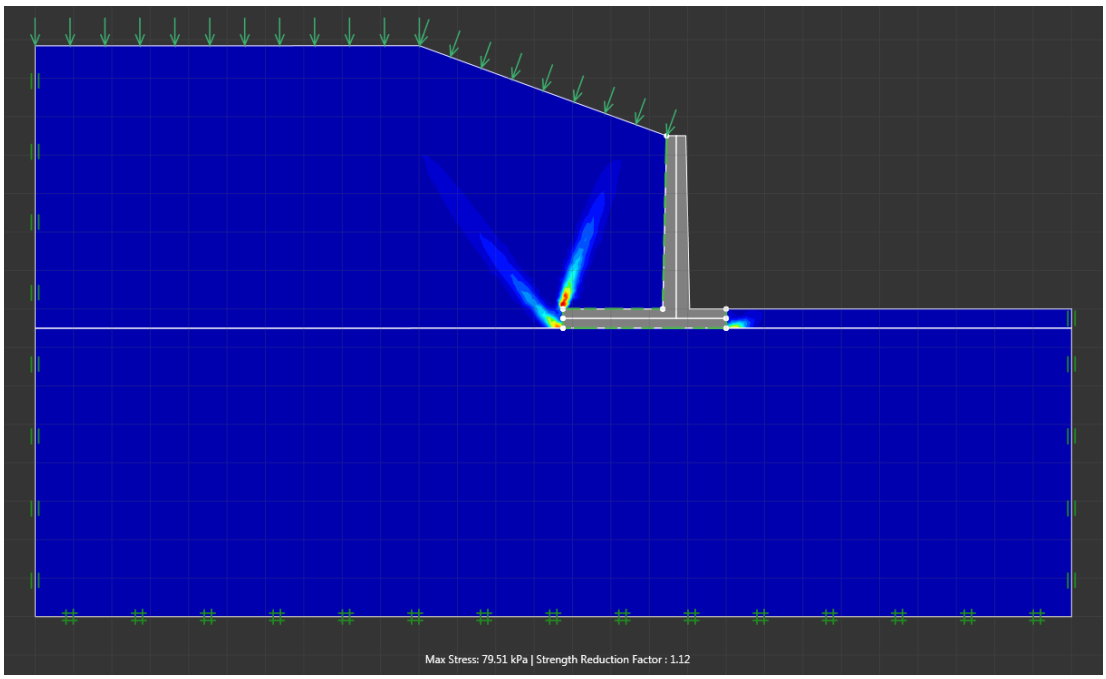

Figure 0.4 - Upper bound failure mode for case 2

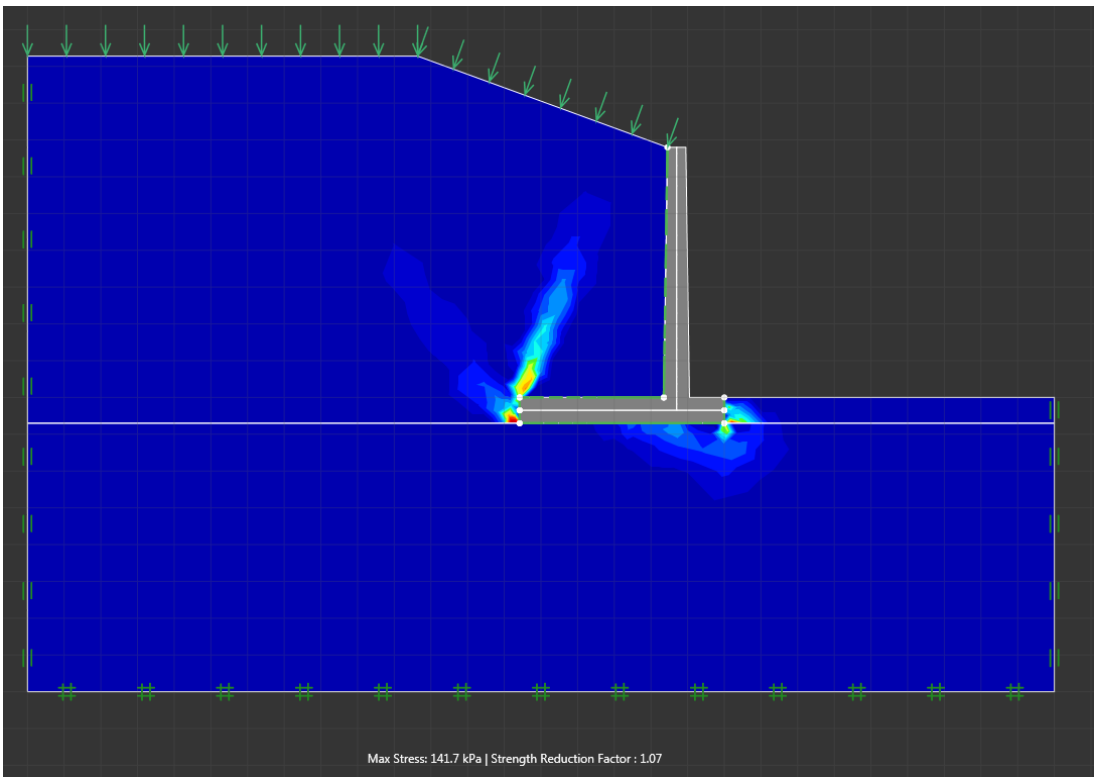

Figure 0.5 - Lower bound failure mode for case 3

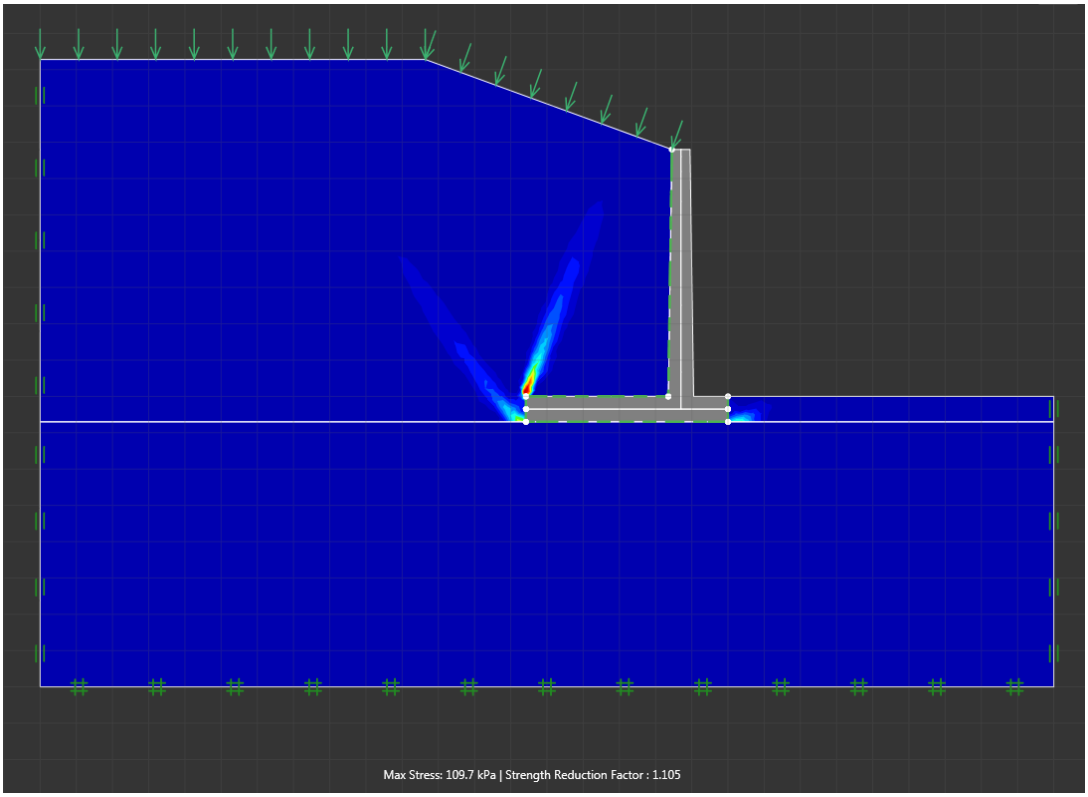

Figure 0.6 - Upper bound failure mode for case 3

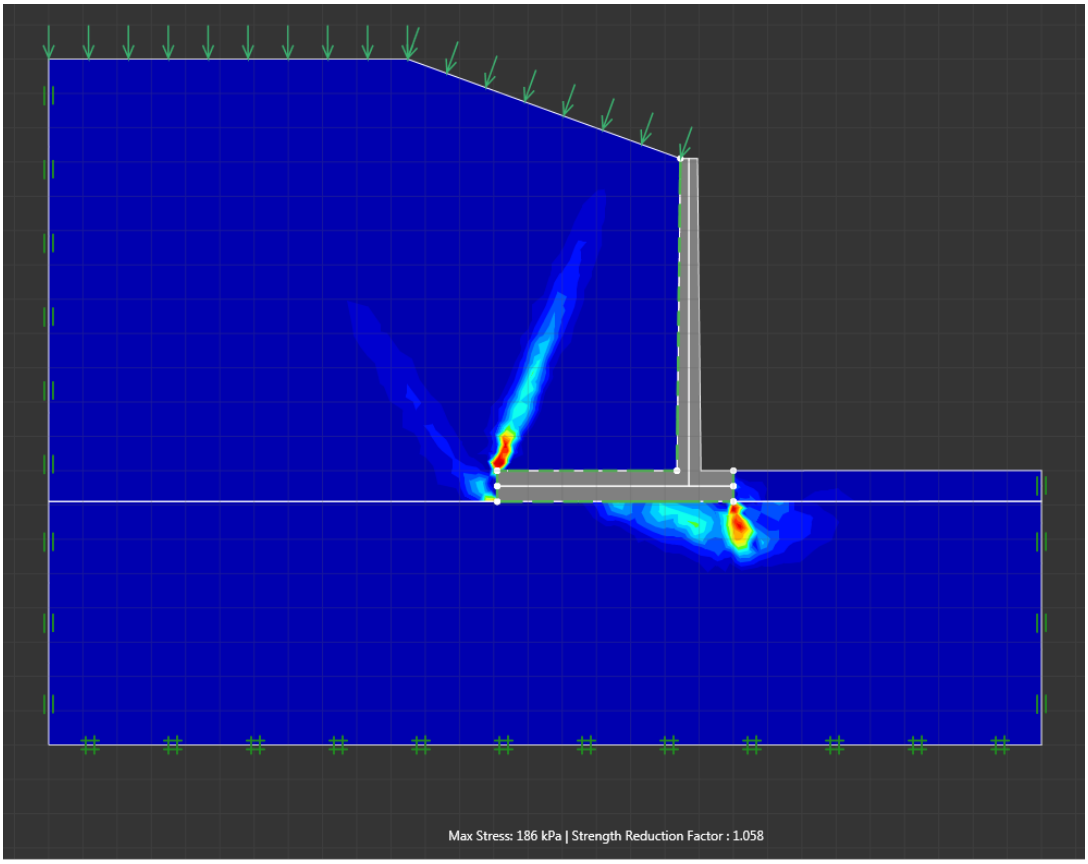

Figure 0.7 - Lower bound failure mode for case 4

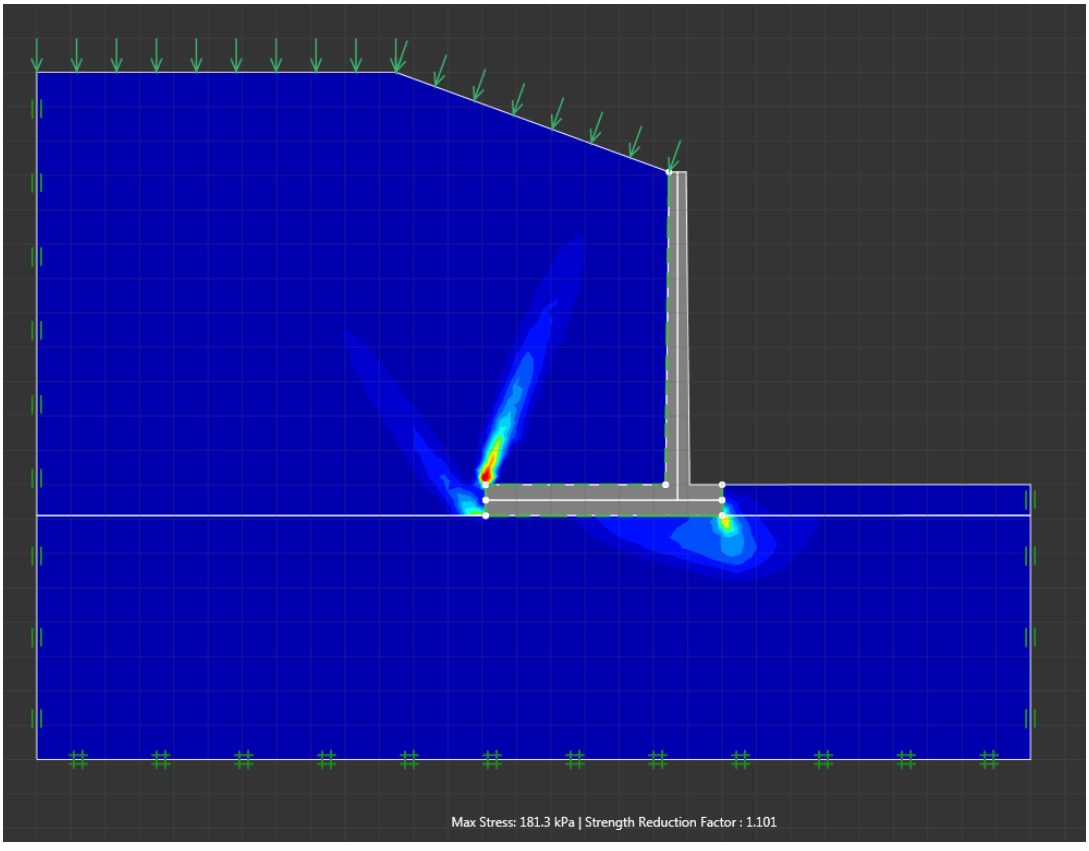

Figure 0.8 - Upper bound failure mode for case 4

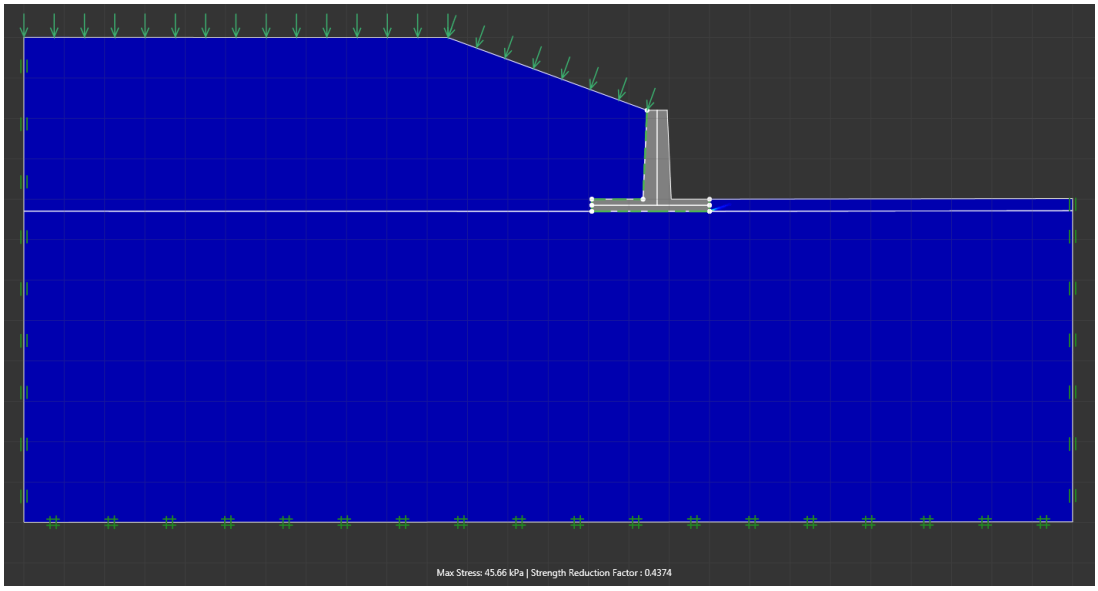

Figure 0.9 - Lower bound failure mode for case 5

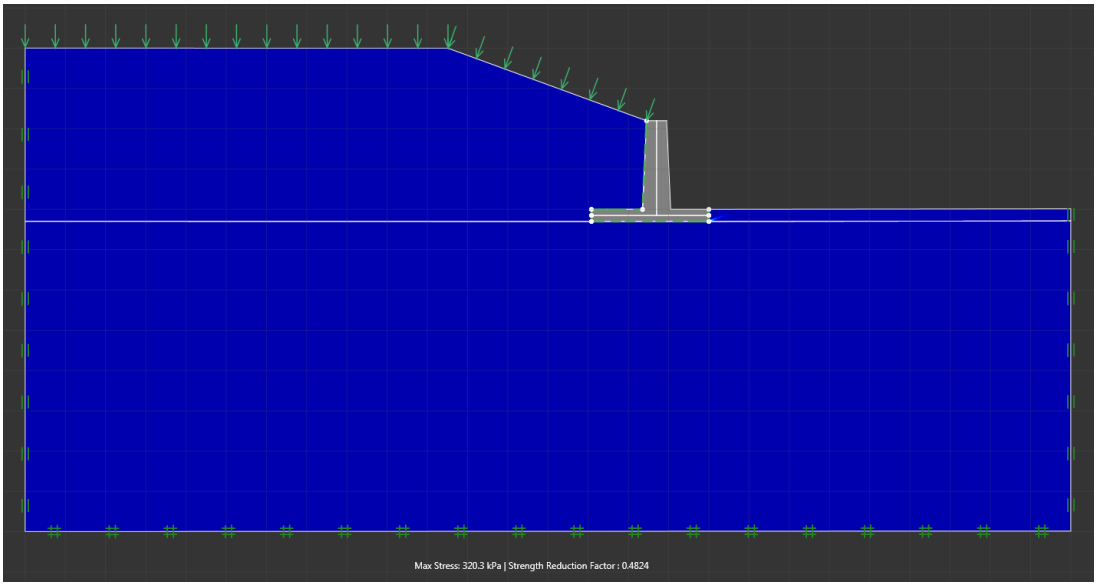

Figure 0.10 - Upper bound failure mode for case 5

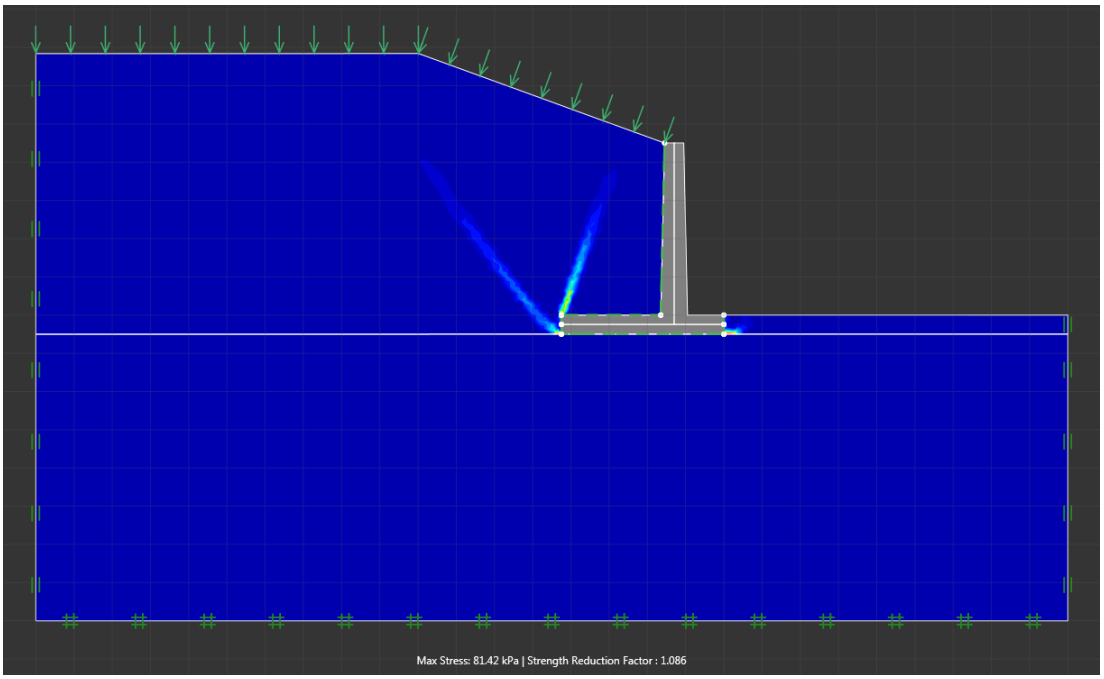

Figure 0.11 - Lower bound failure mode for case 6

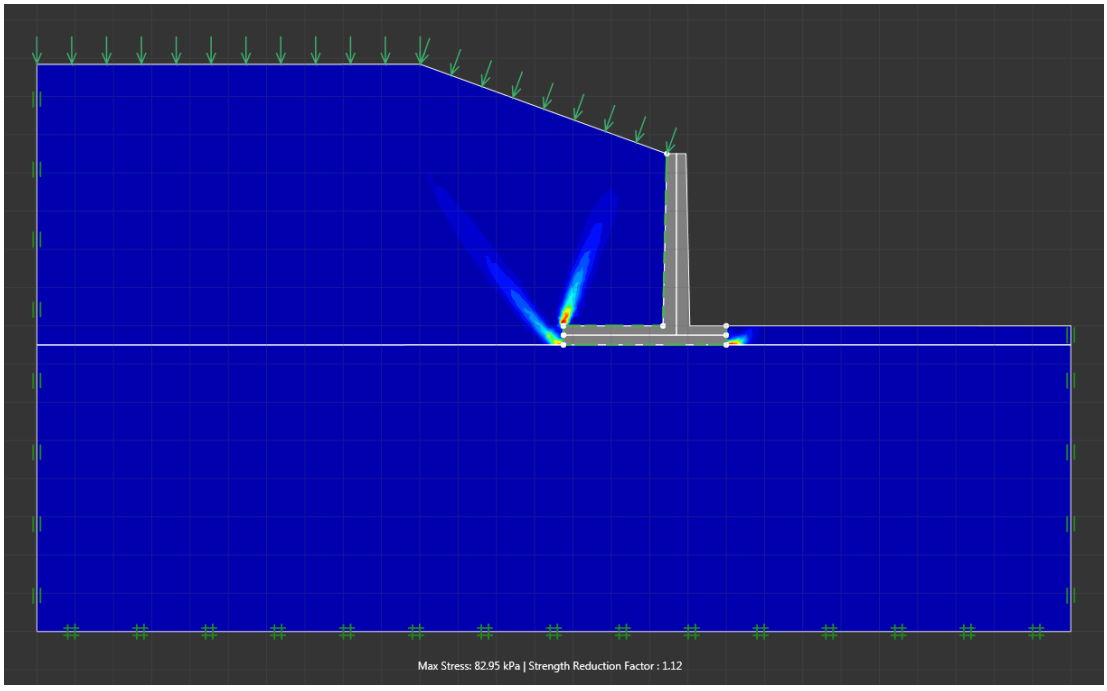

Figure 0.12 - Upper bound failure mode for case 6

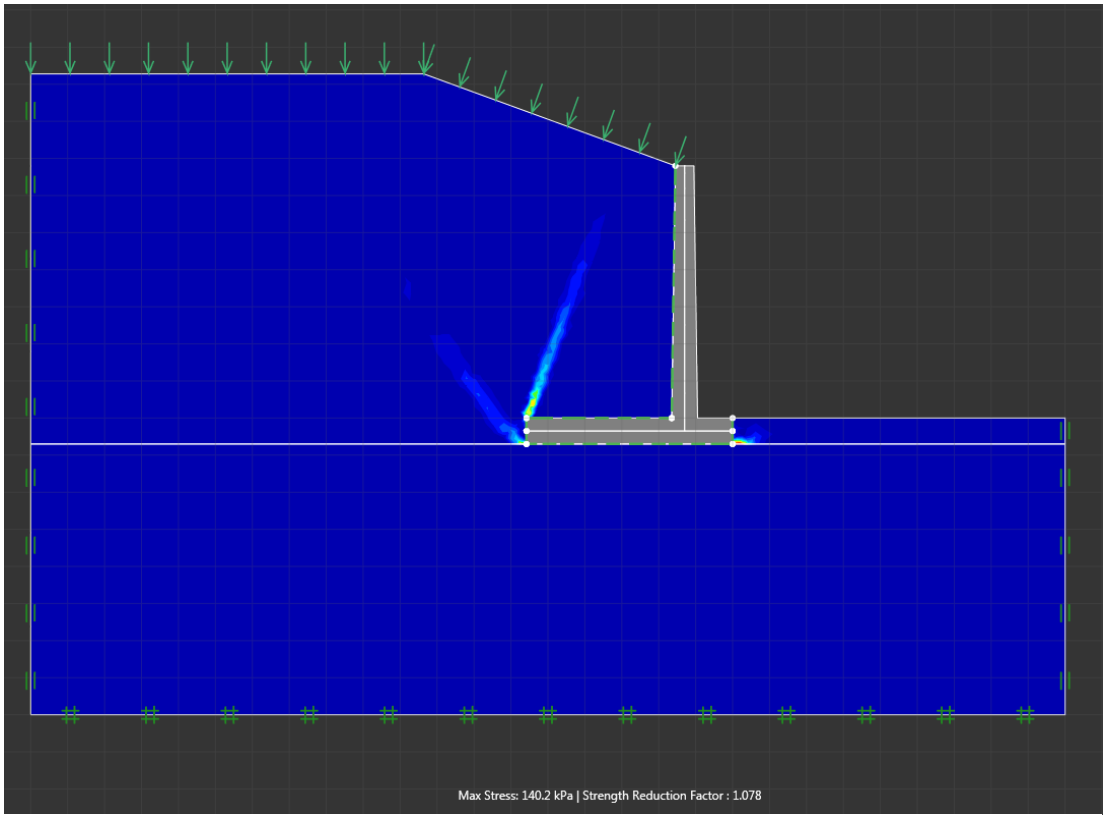

Figure 0.13 - Lower bound failure mode for case 7

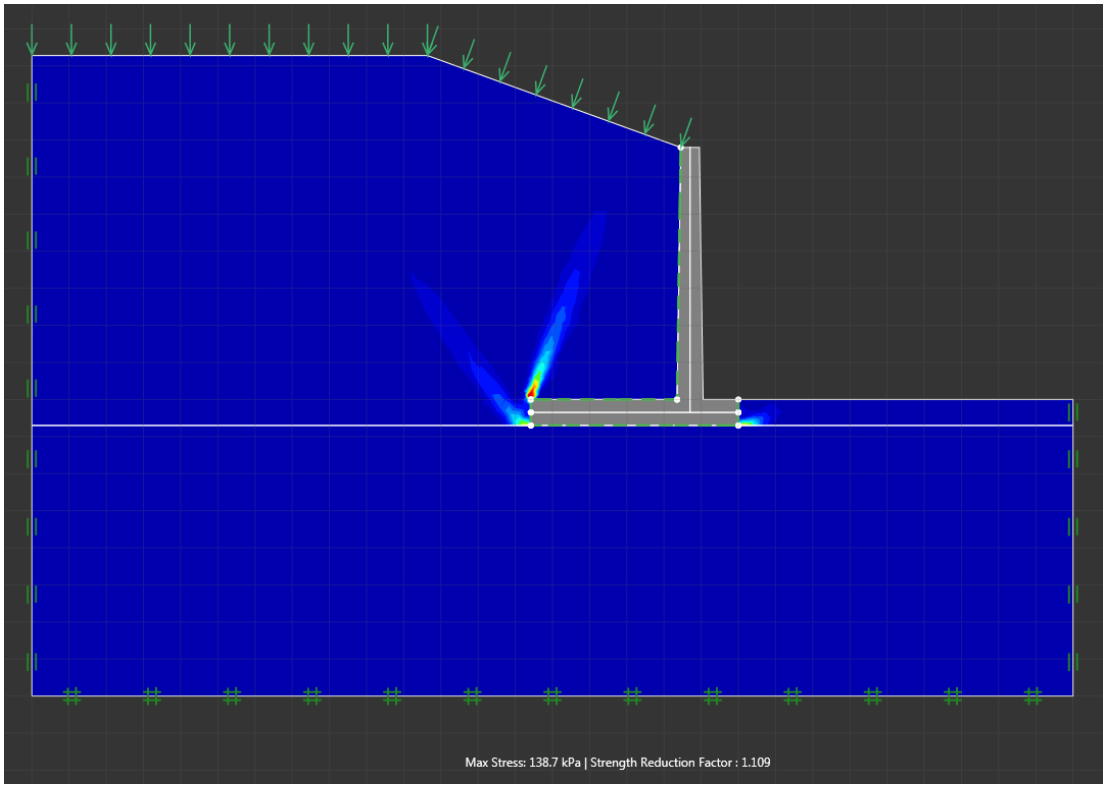

Figure 0.14 - Upper bound failure mode for case 7

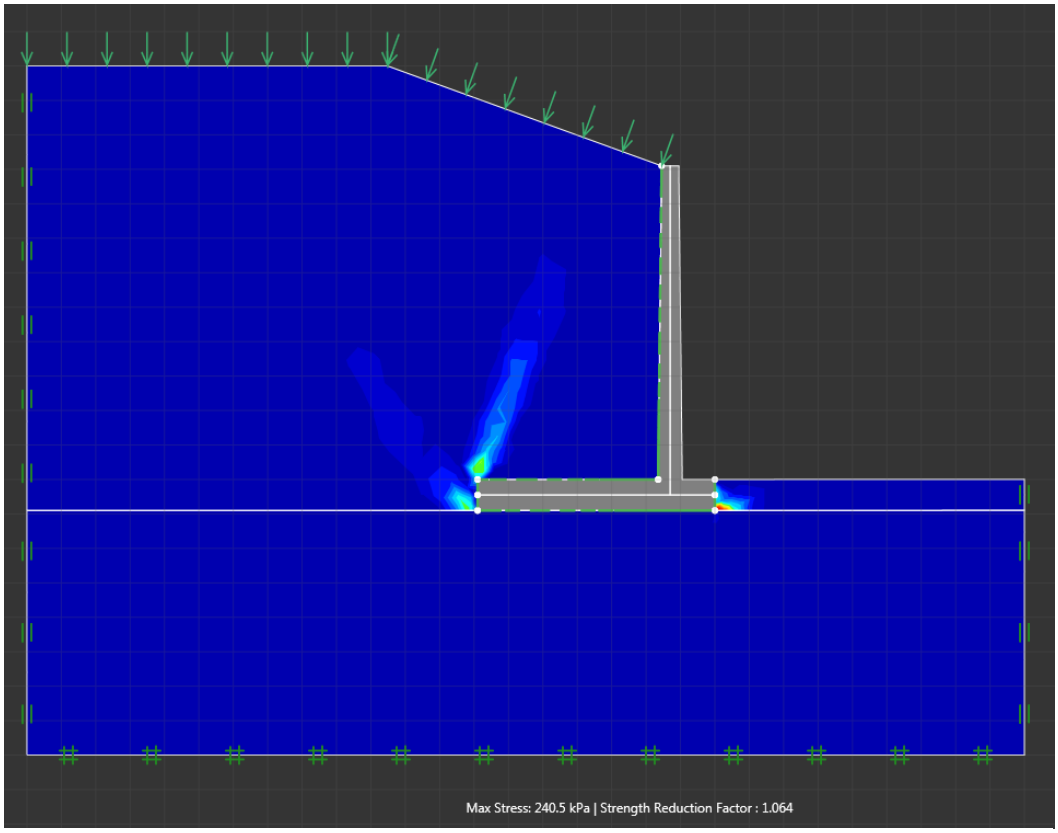

Figure 0.15 - Lower bound failure mode for case 8

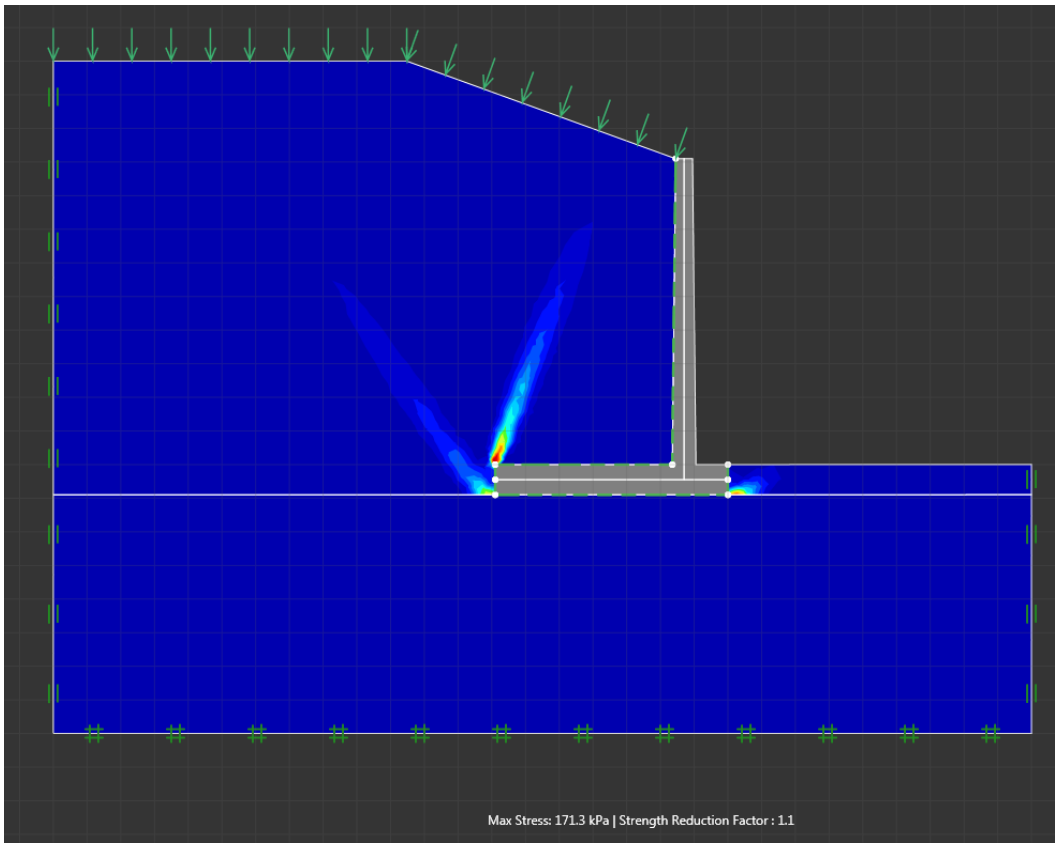

Figure 0.16 - Upper bound failure mode for case 8

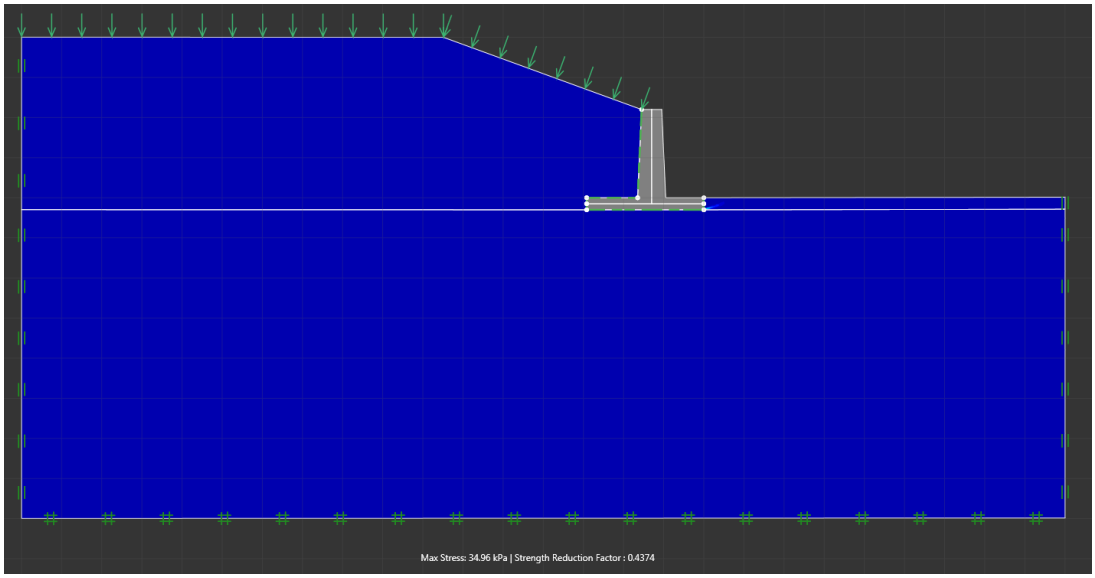

Figure 0.17 - Lower bound failure mode for case 9

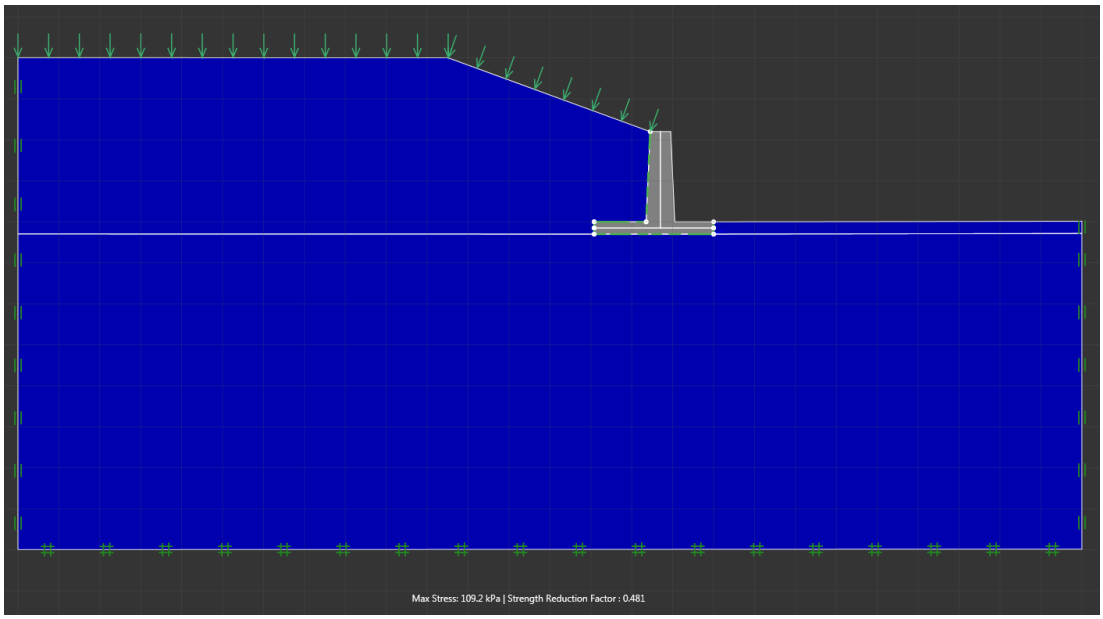

Figure 0.18 - Upper bound failure mode for case 9

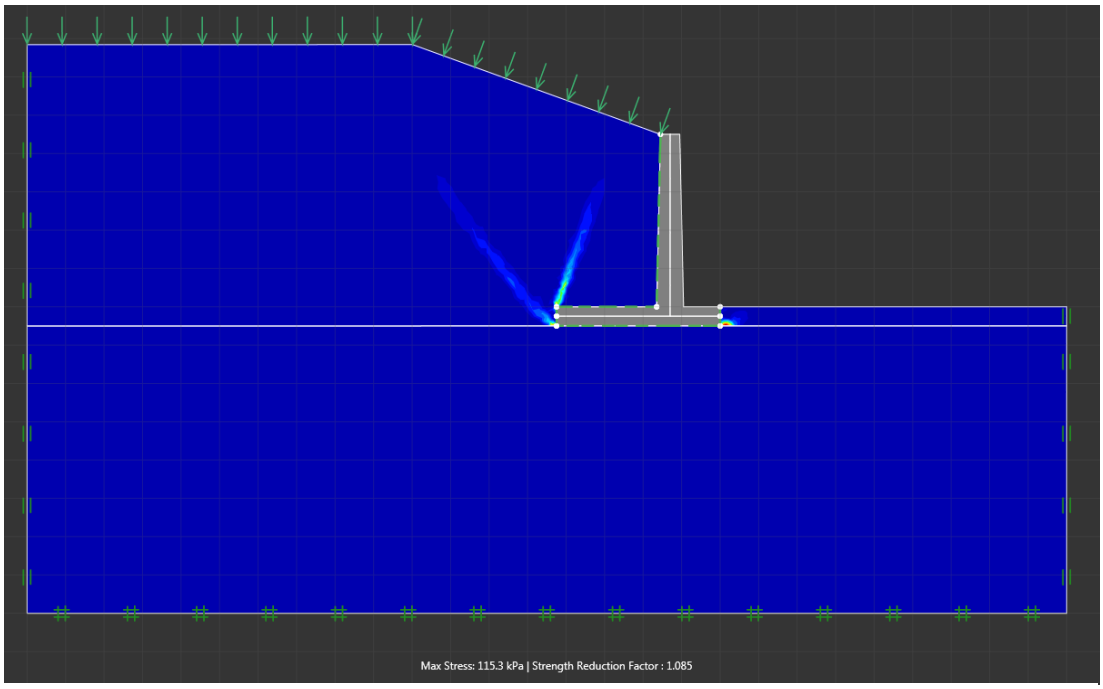

Figure 0.19 - Lower bound failure mode for case 10

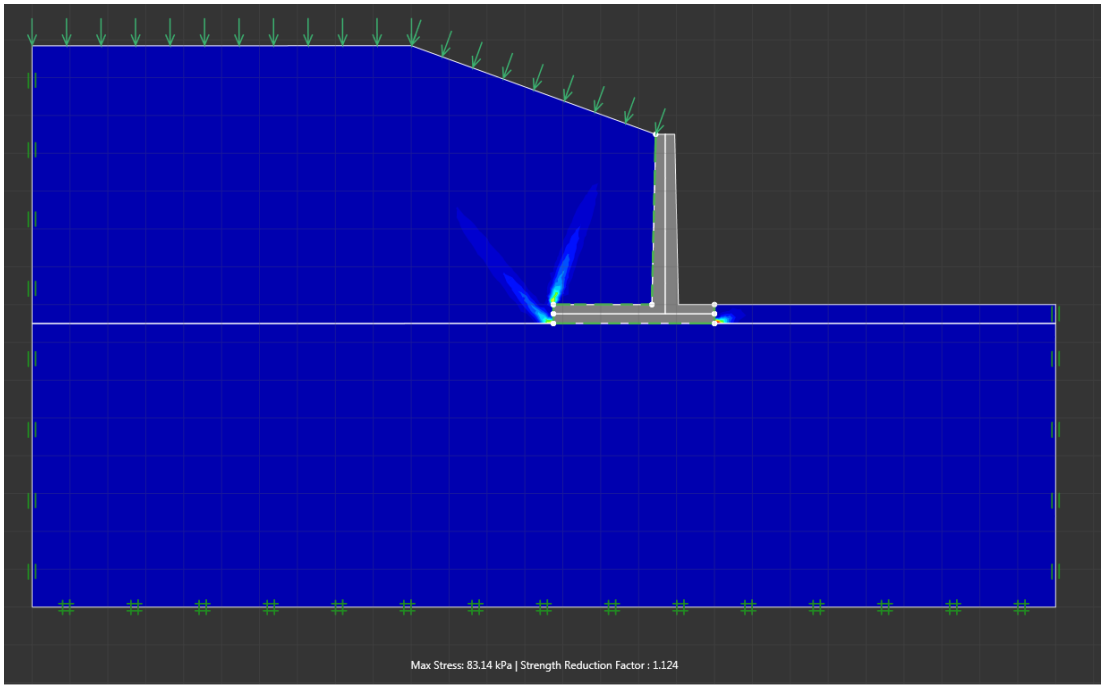

Figure 0.20 - Upper bound failure mode for case 10

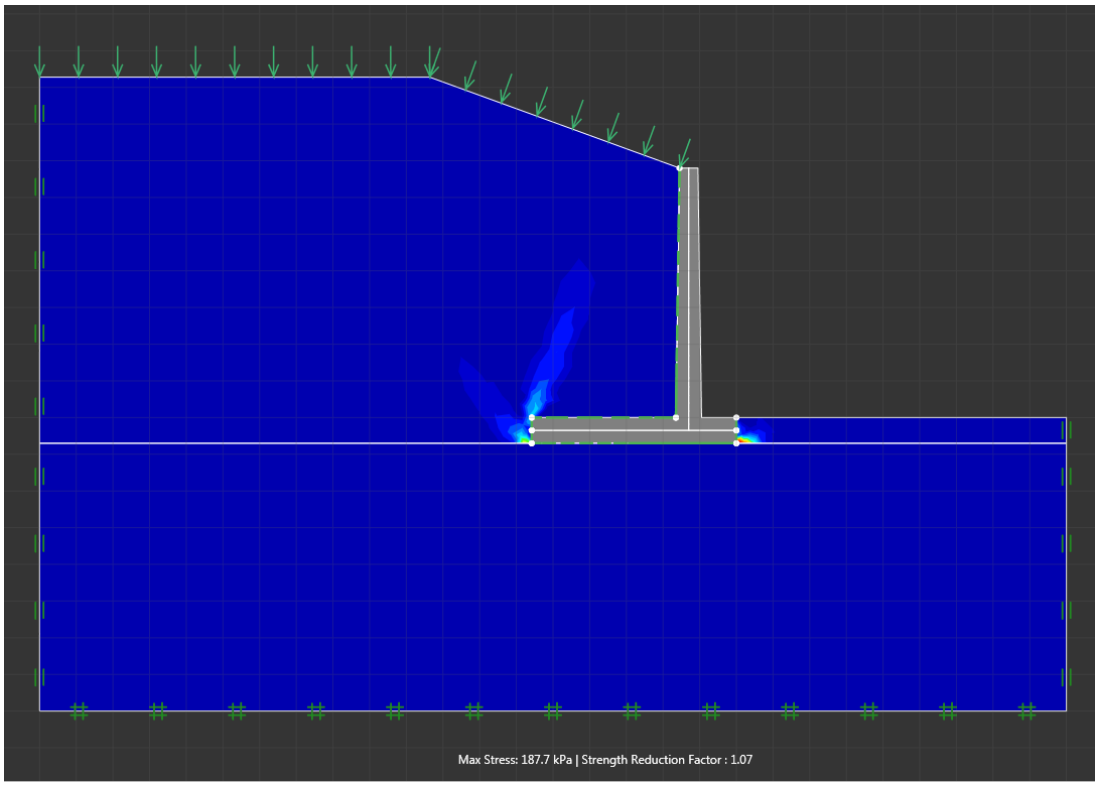

Figure 0.21 - Upper bound failure mode for case 11

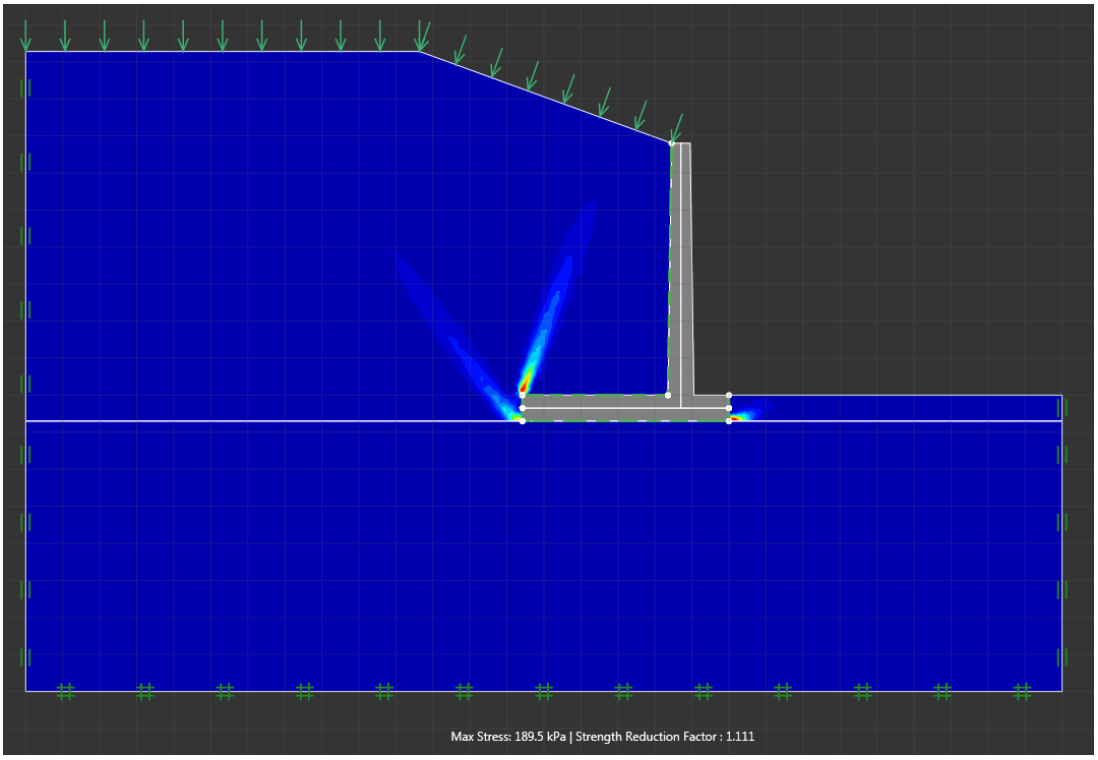

Figure 0.22 - Lower bound failure mode for case 11

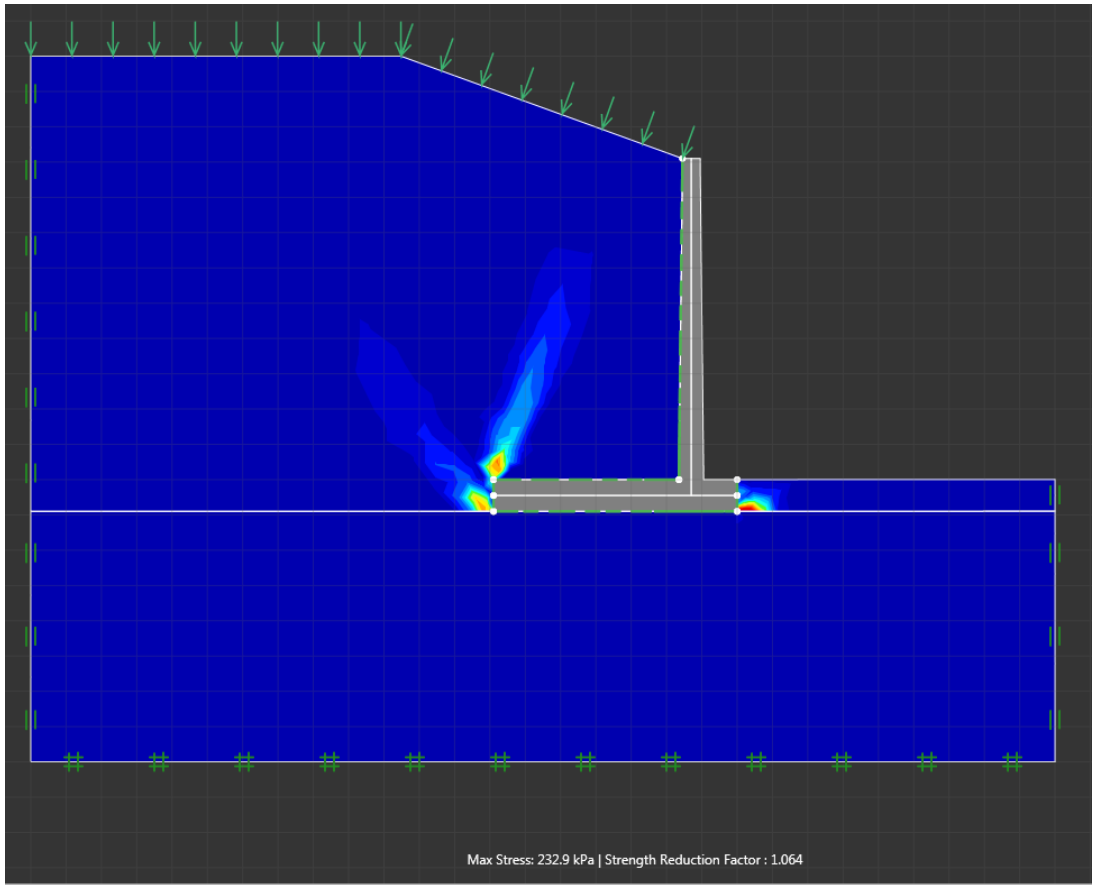

Figure 0.23 - Lower bound failure mode for case 12

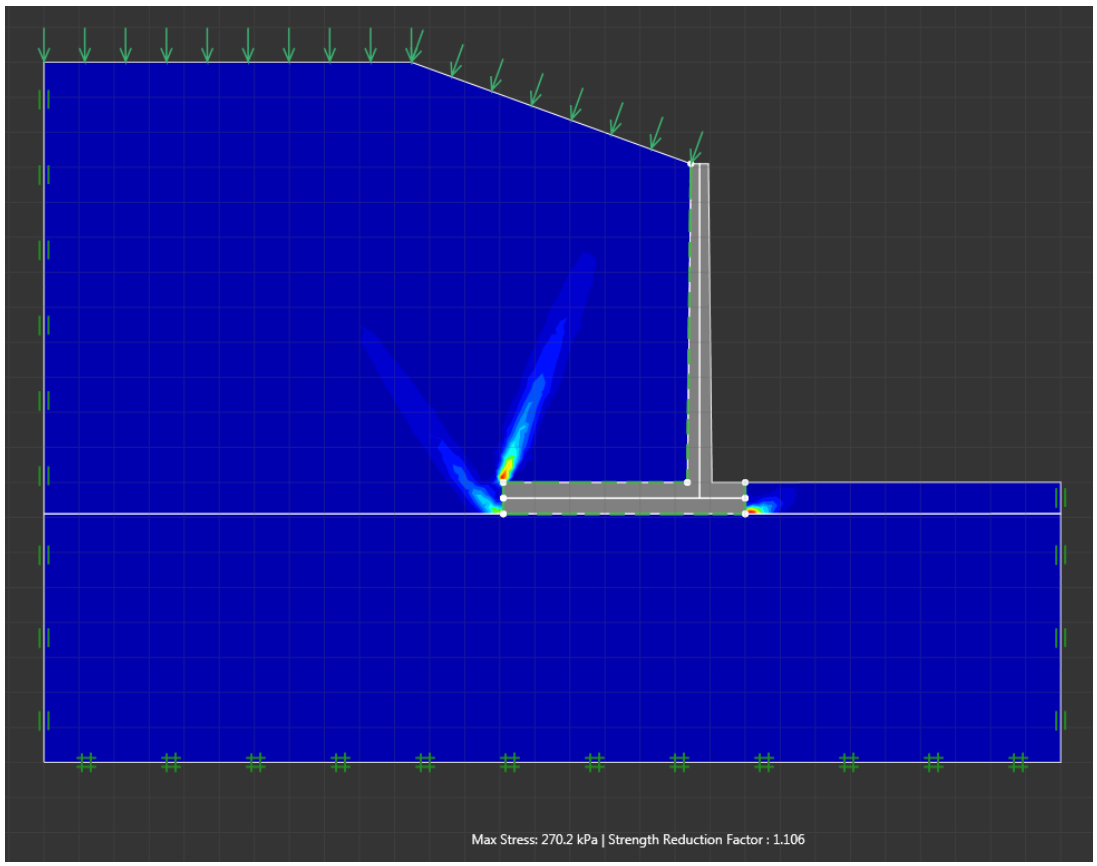

Figure 0.24 - Upper bound failure mode for case 12

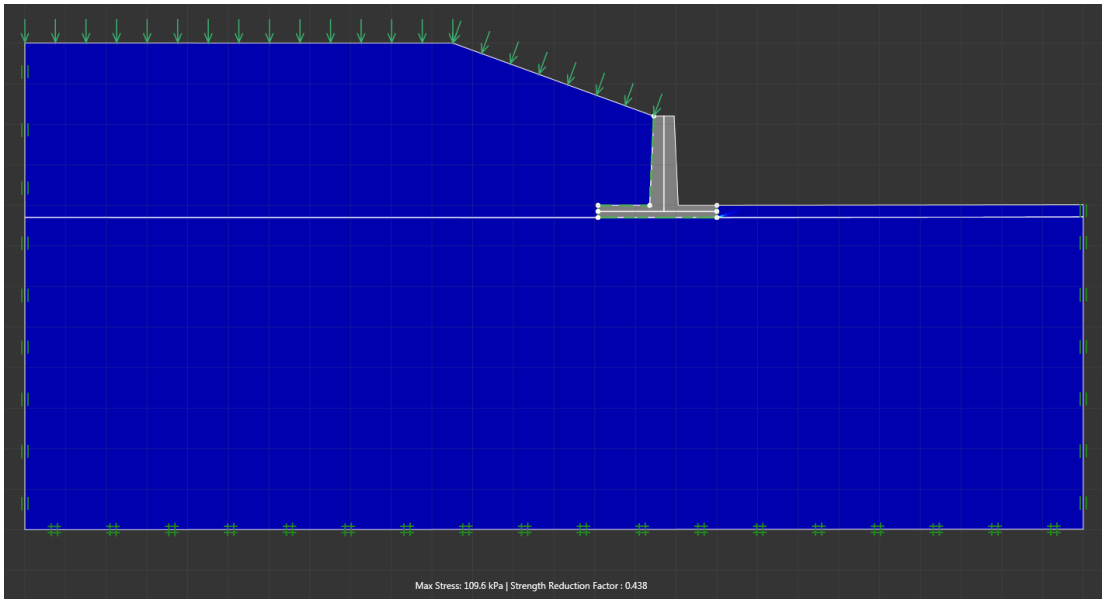

Figure 0.25 - Lower bound failure mode for case 13

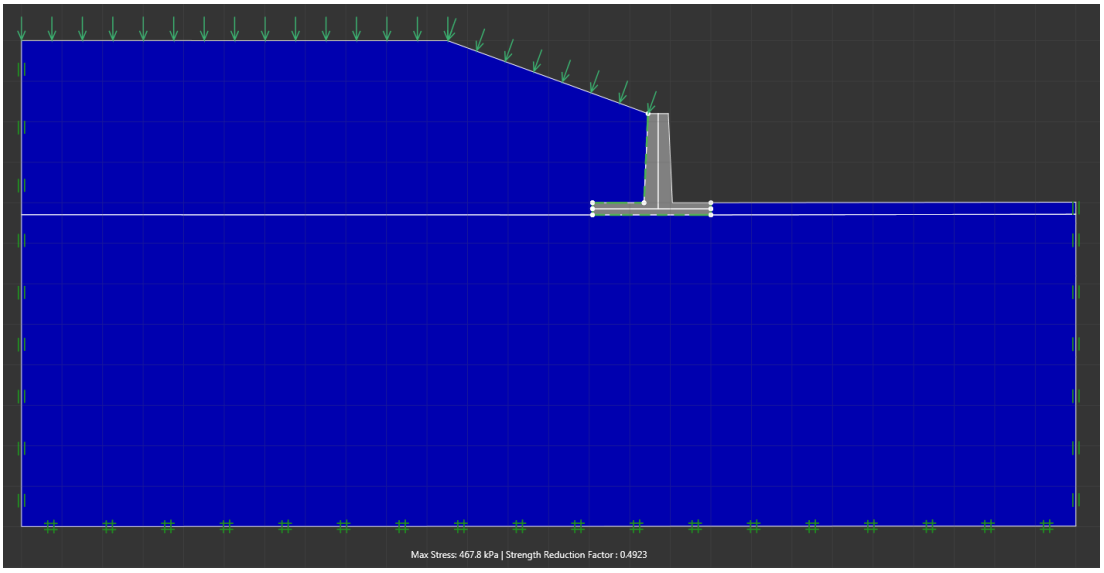

Figure 0.26 - Upper bound failure mode for case 13

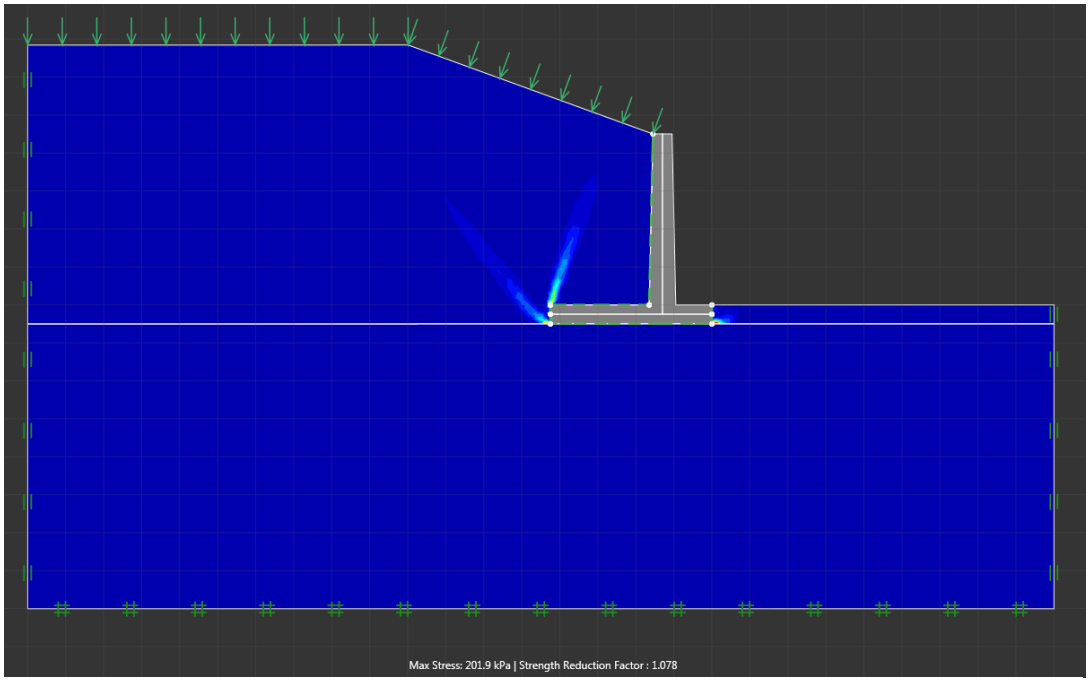

Figure 0.27 - Lower bound failure mode for case 14

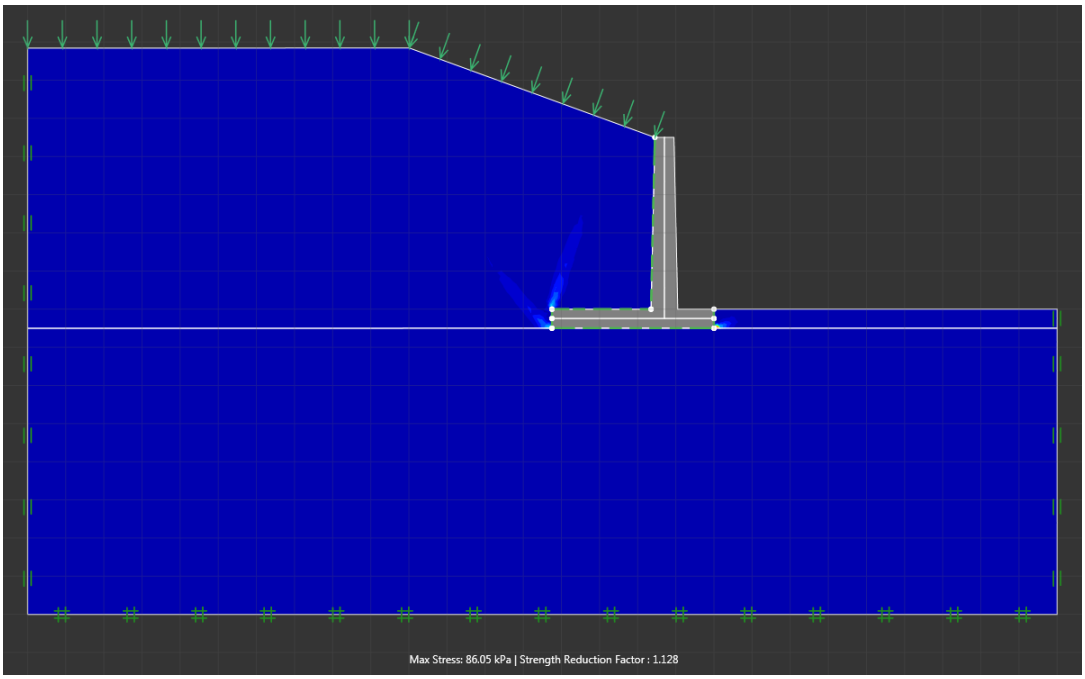

Figure 0.28 - Upper bound failure mode for case 14

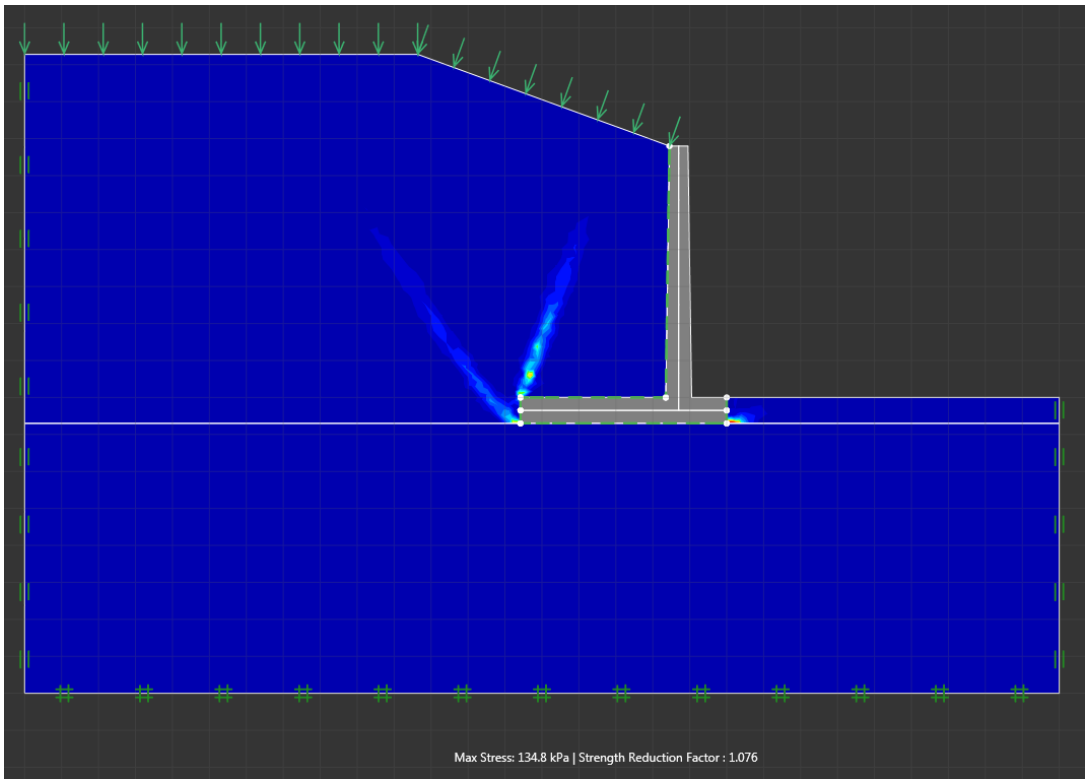

Figure 0.29 - Lower bound failure mode for case 15

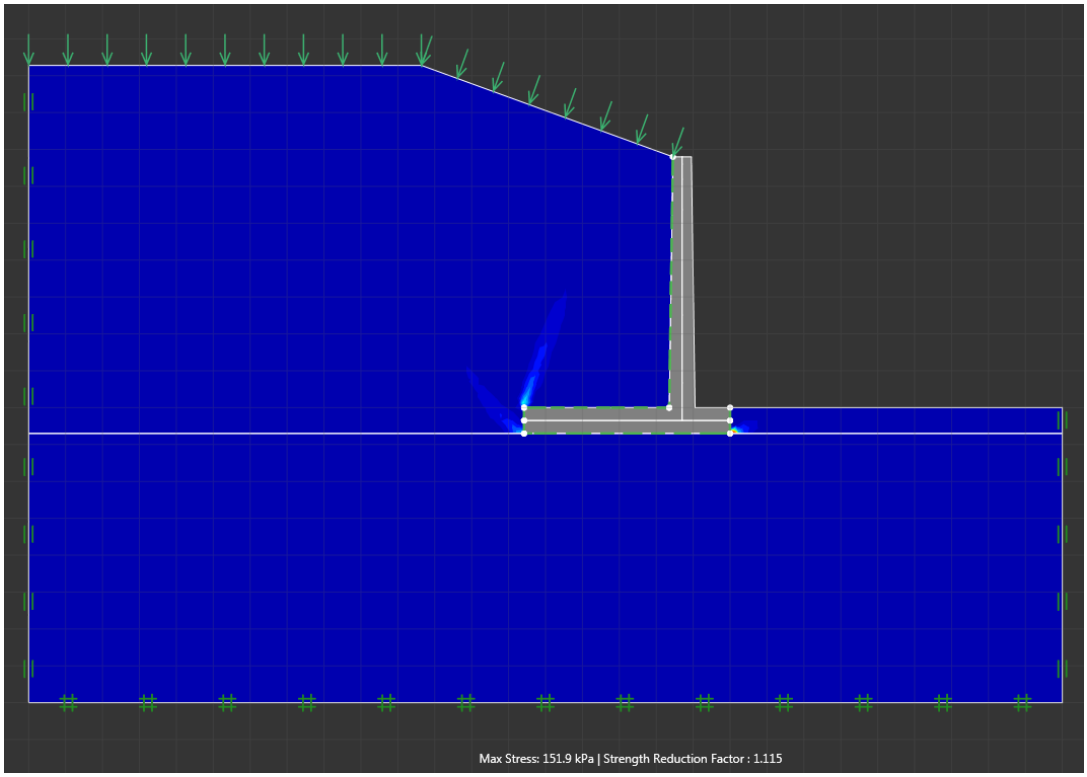

Figure 0.30 - Upper bound failure mode for case 15

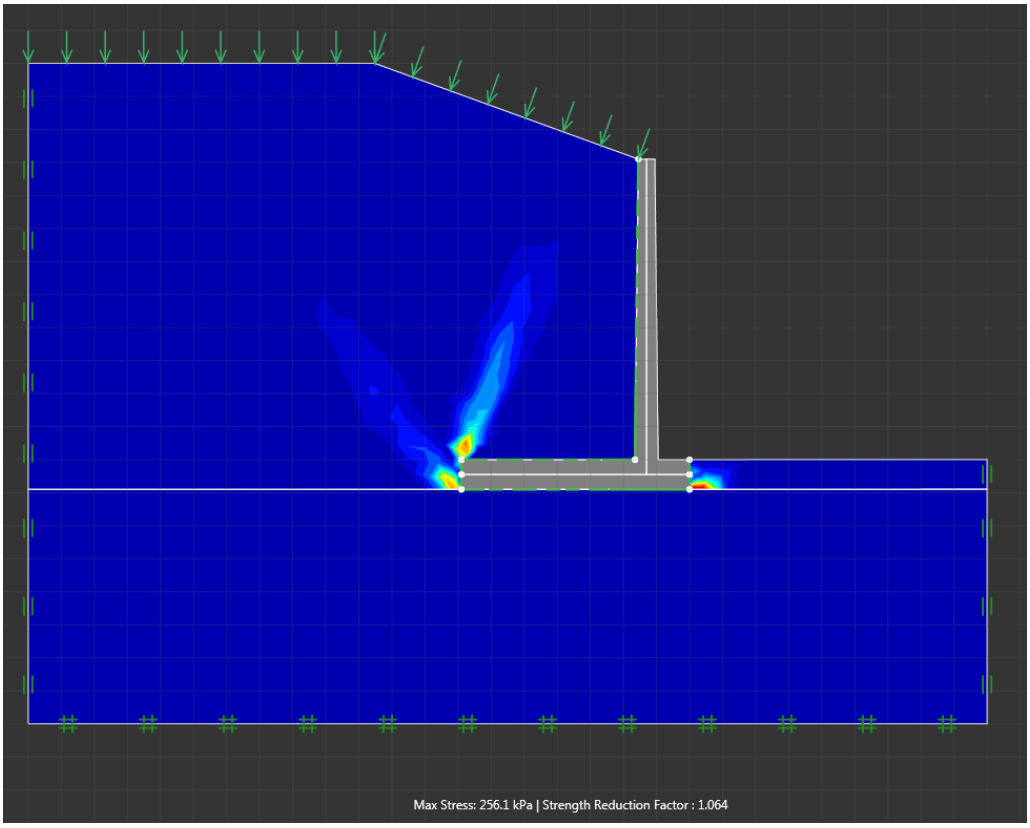

Figure 0.31 - Lower bound failure mode for case 16

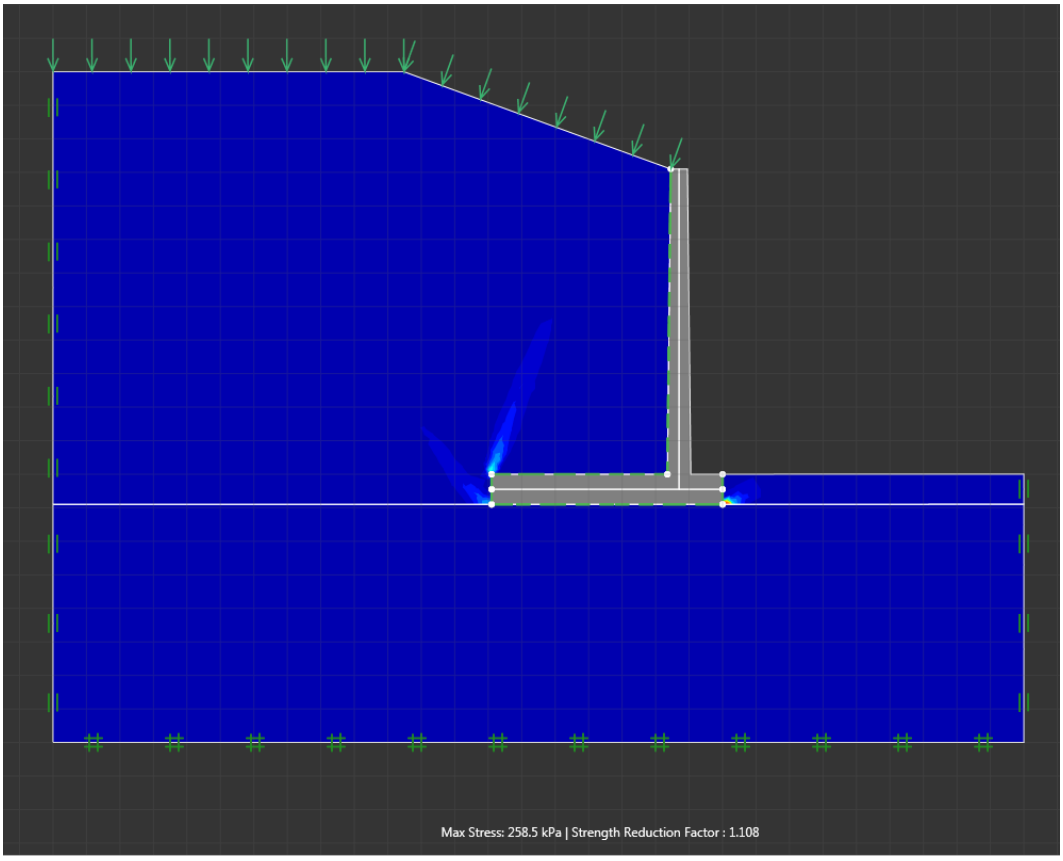

Figure 0.32 - Upper bound failure mode for case 16

Sand Backfill

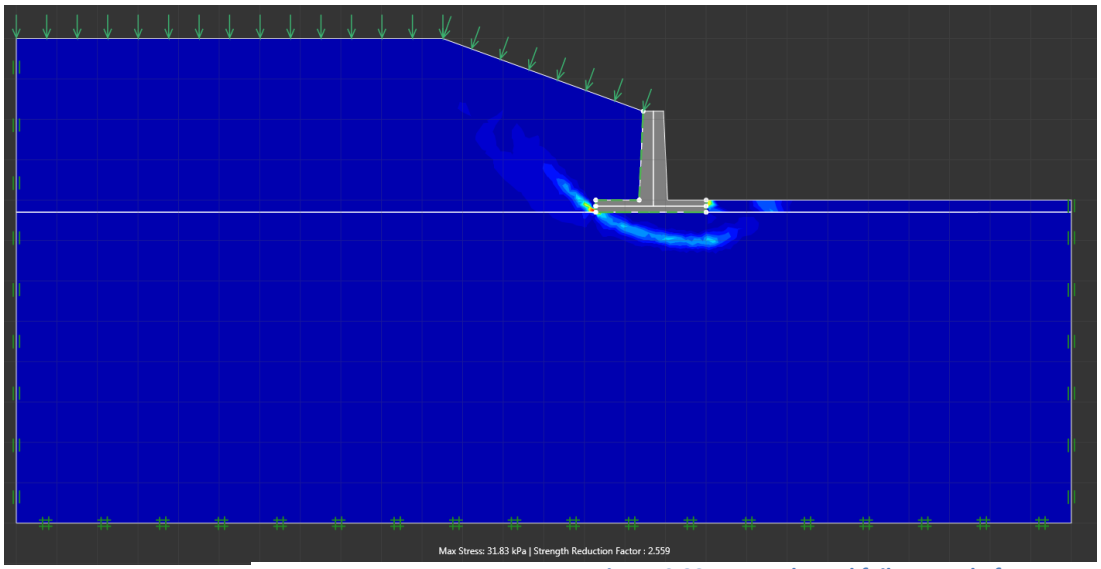

Figure 0.33 - Lower bound failure mode for case 17

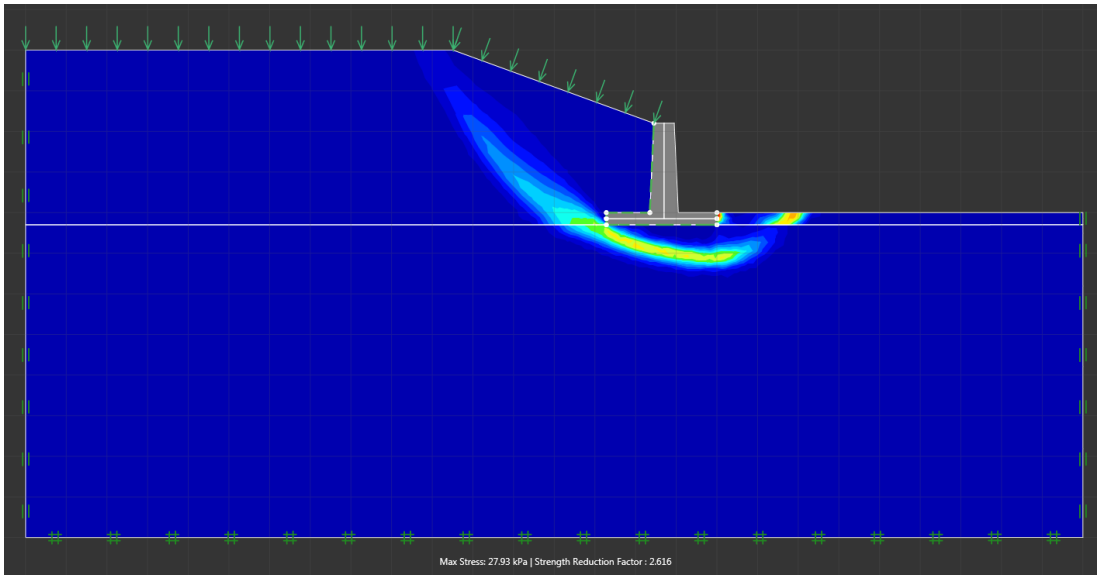

Figure 0.34 - Upper bound failure mode for case 17

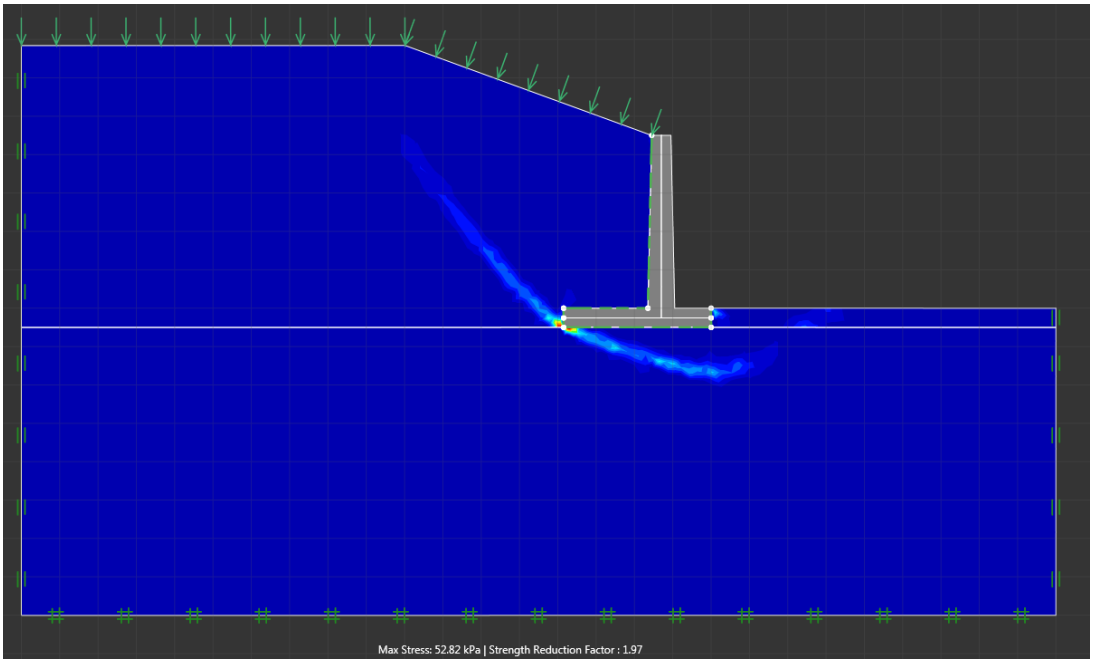

Figure 0.35 - Lower bound failure mode for case 18

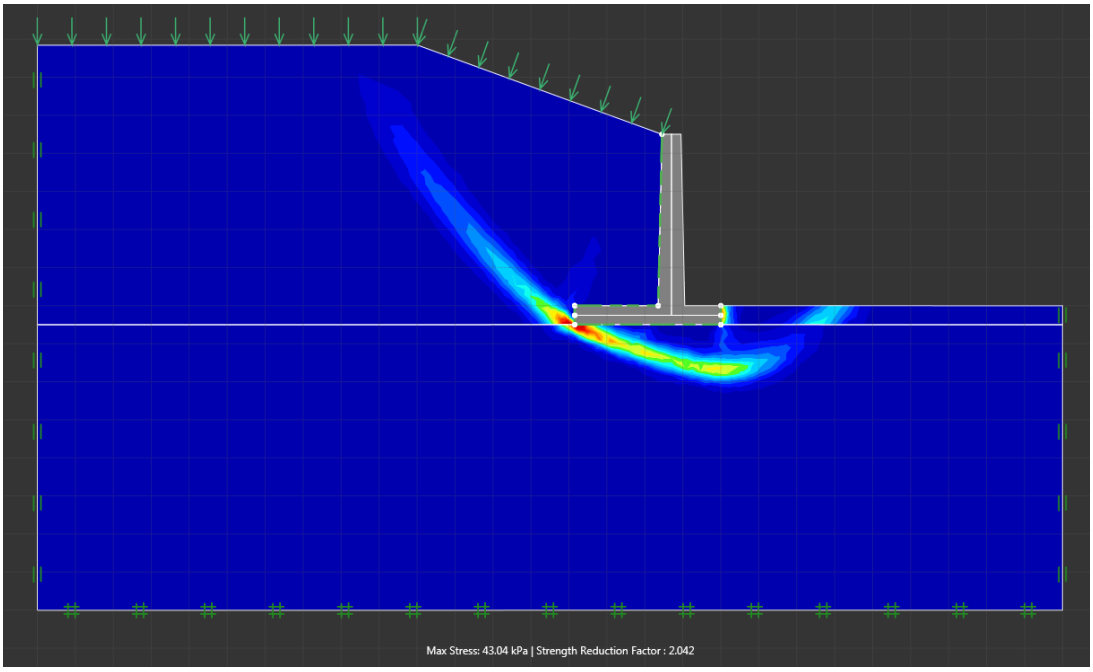

Figure 0.36 - Upper bound failure mode for case 18

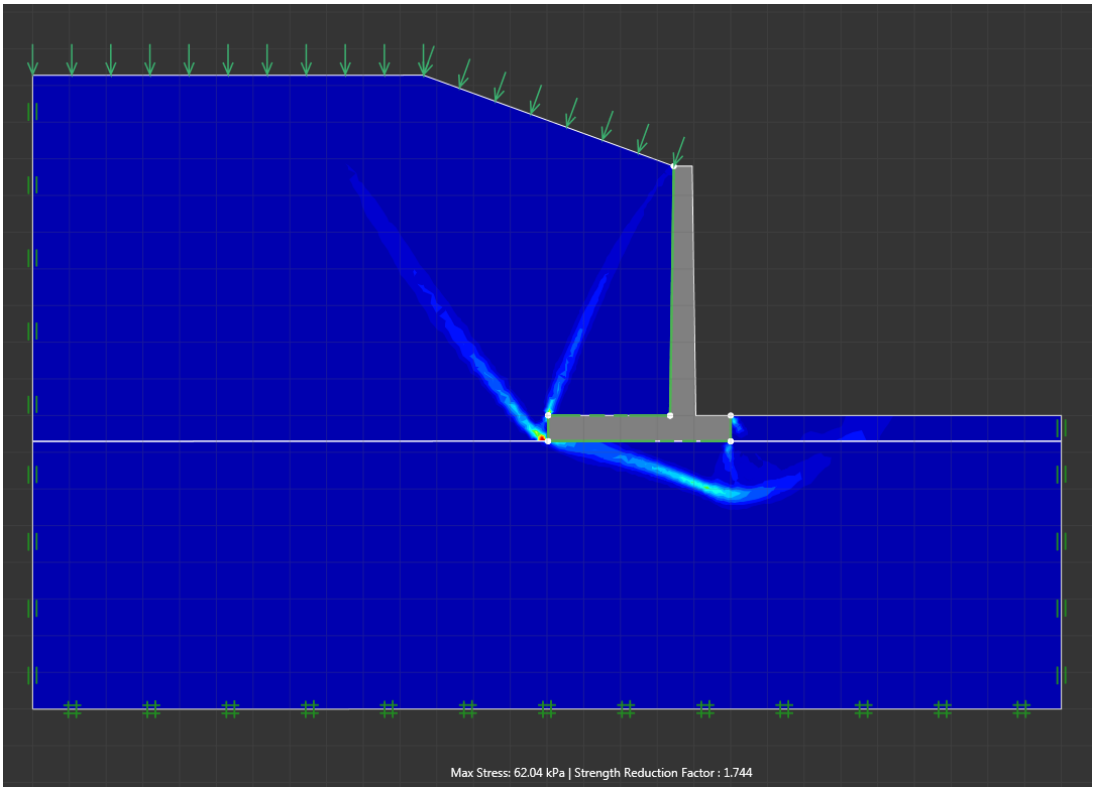

Figure 0.37 - Lower bound failure mode for case 19

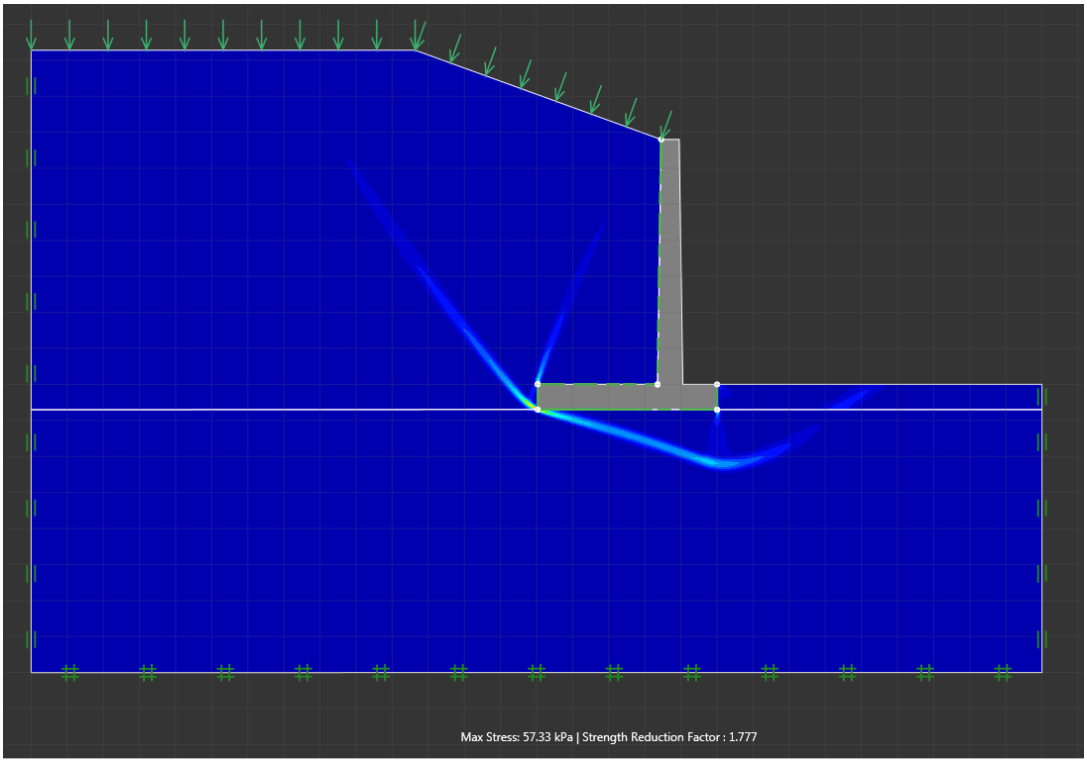

Figure 0.38 - Upper bound failure mode for case 19

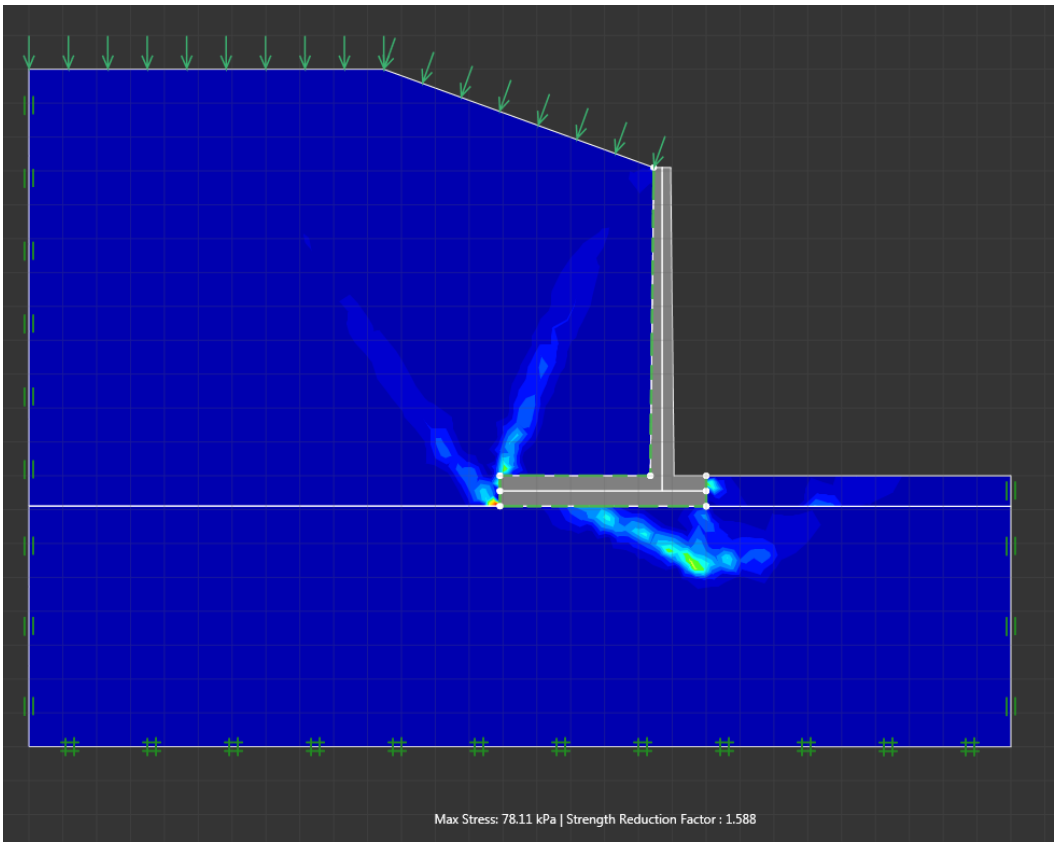

Figure 0.39 - Lower bound failure mode for case 20

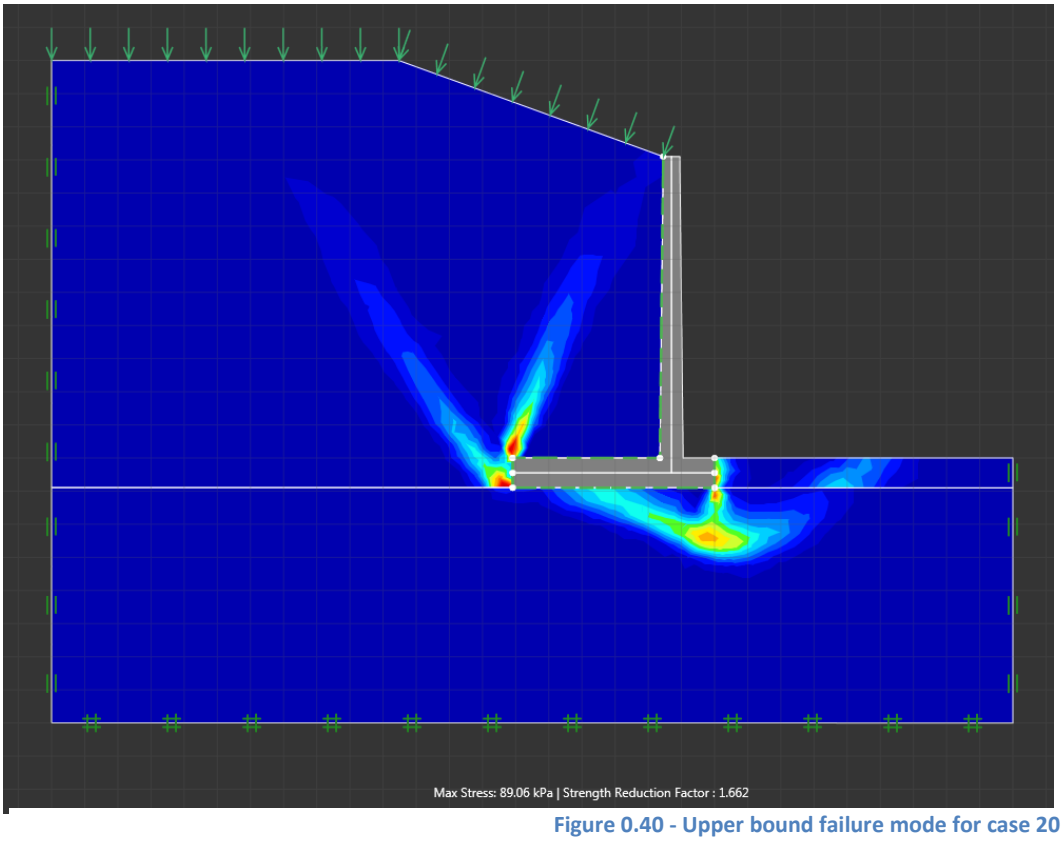

Figure 0.40 - Upper bound failure mode for case 20

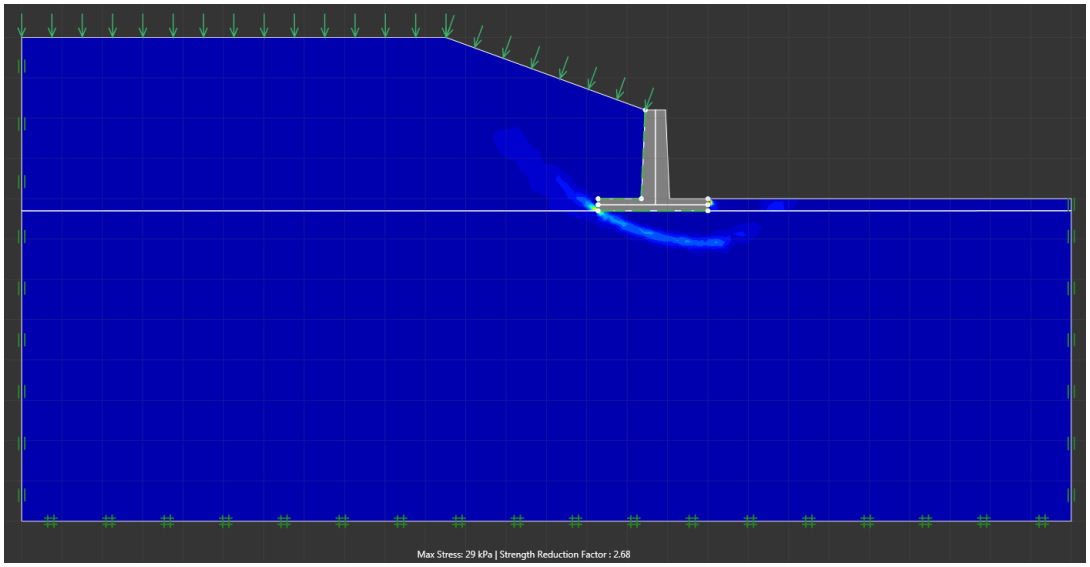

Figure 0.41 - Lower bound failure mode for case 21

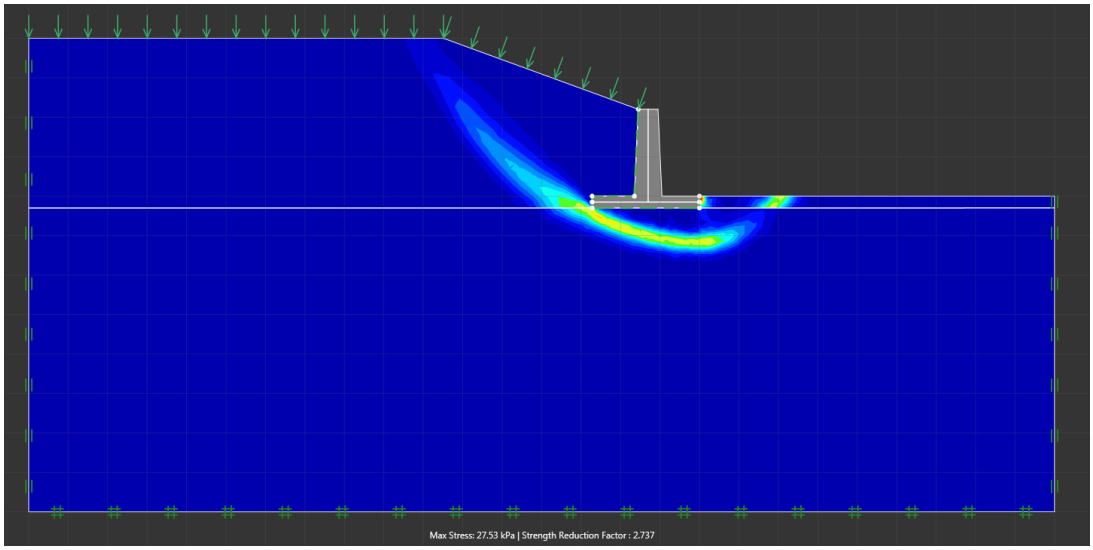

Figure 0.42 - Upper bound failure mode for case 21

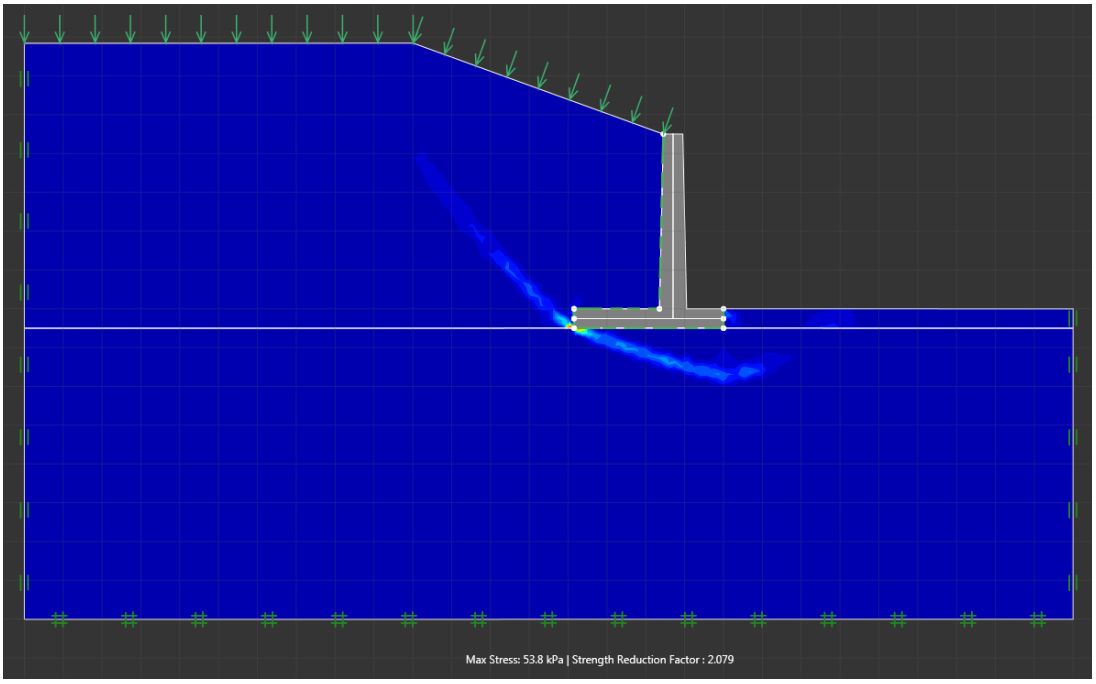

Figure 0.43 - Lower bound failure mode for case 22

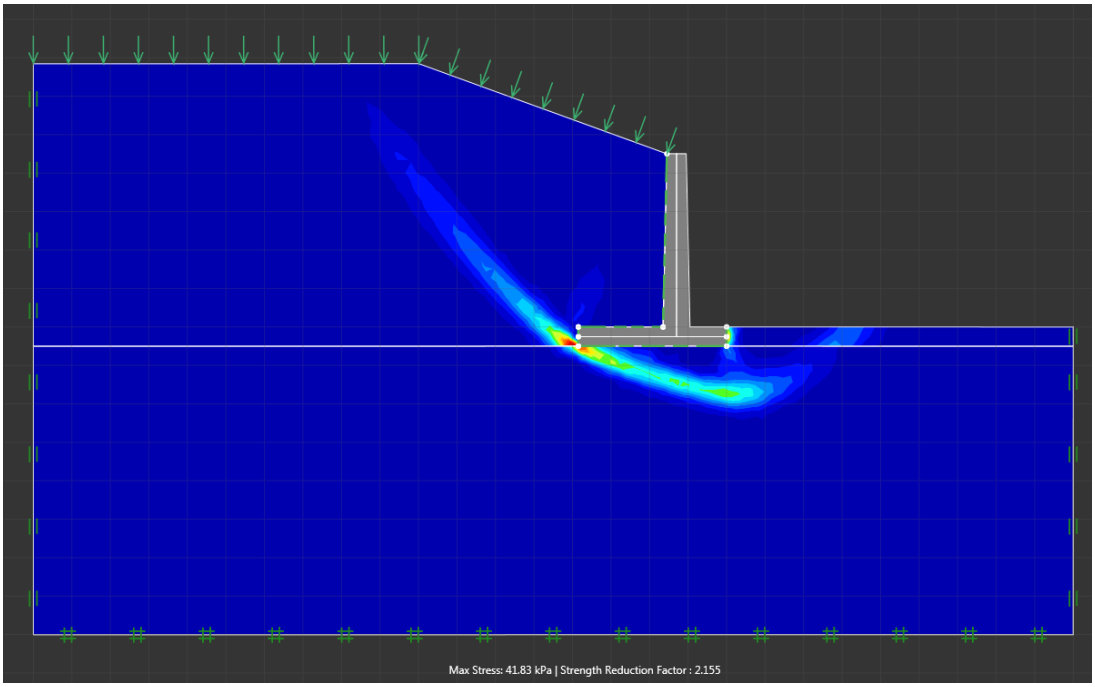

Figure 0.44 - Upper bound failure mode for case 22

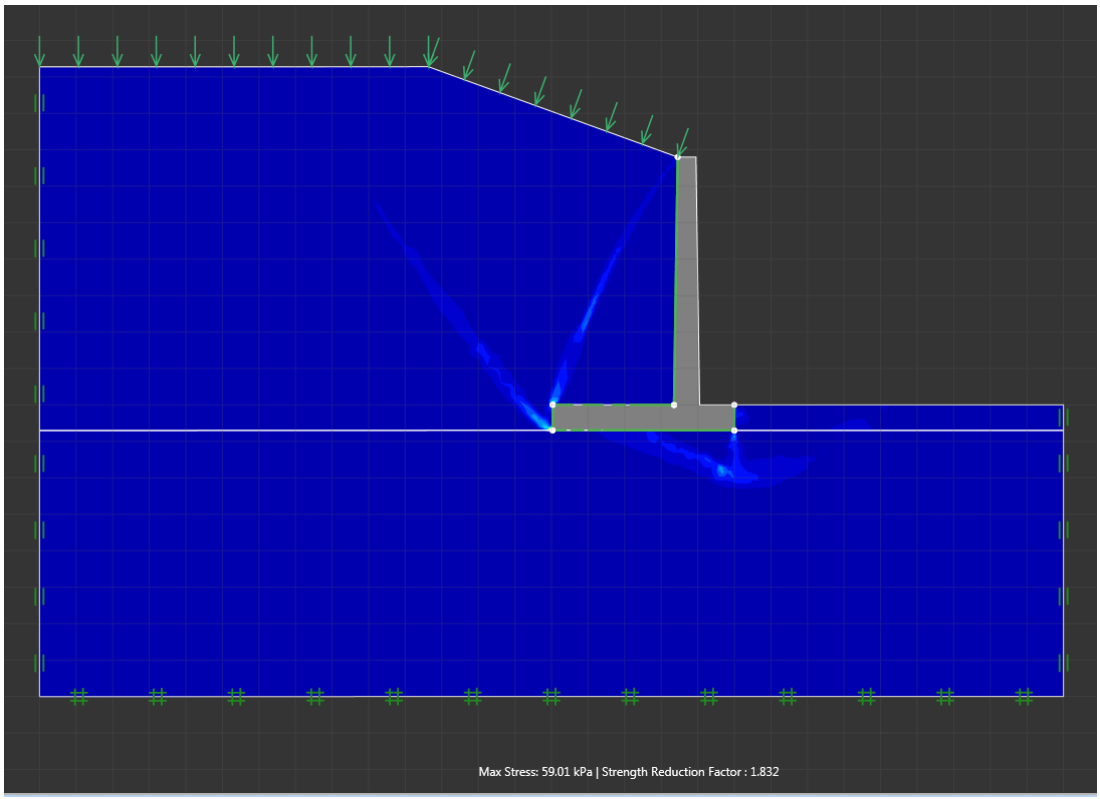

Figure 0.45 - Lower bound failure mode for case 23

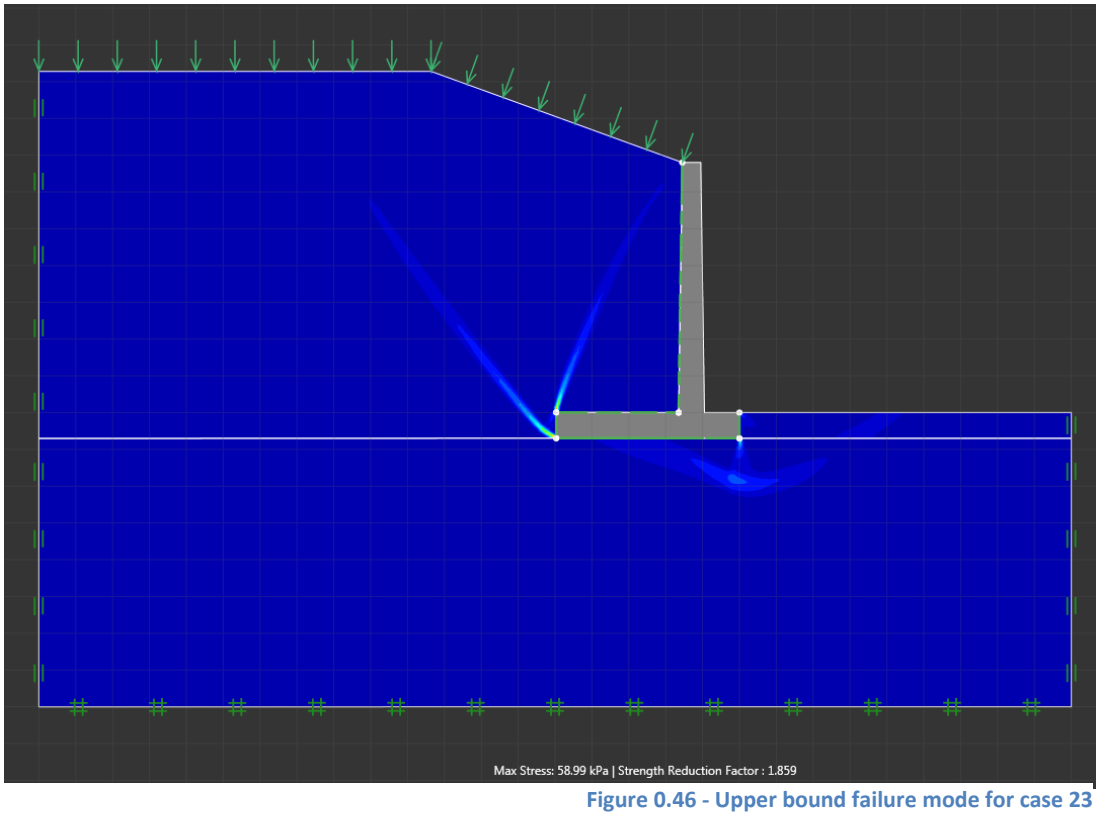

Figure 0.46 - Upper bound failure mode for case 23

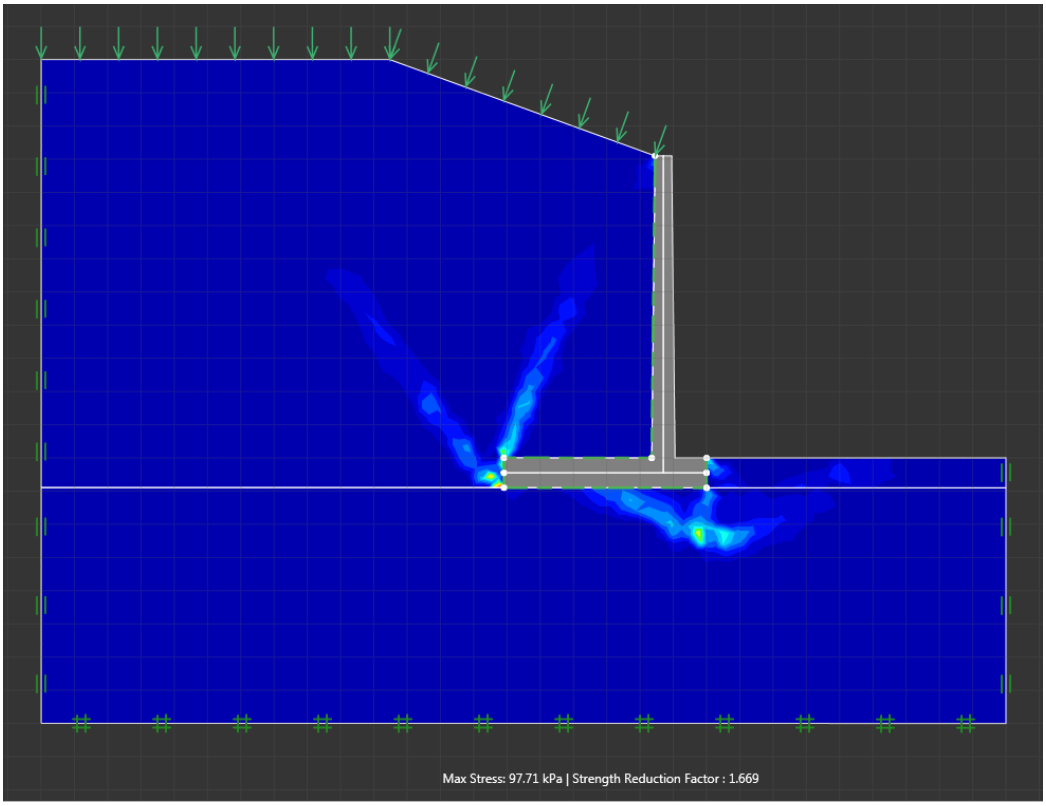

Figure 0.47 - Lower bound failure mode for case 24

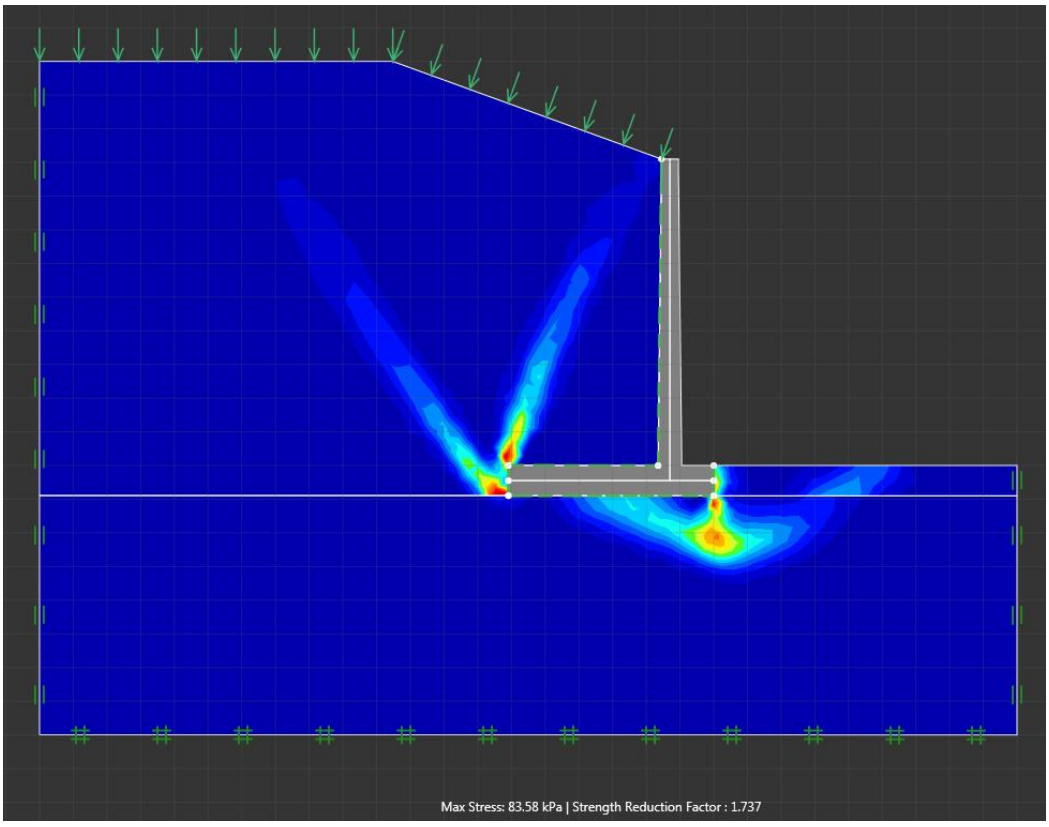

Figure 0.48 - Upper bound failure mode for case 24

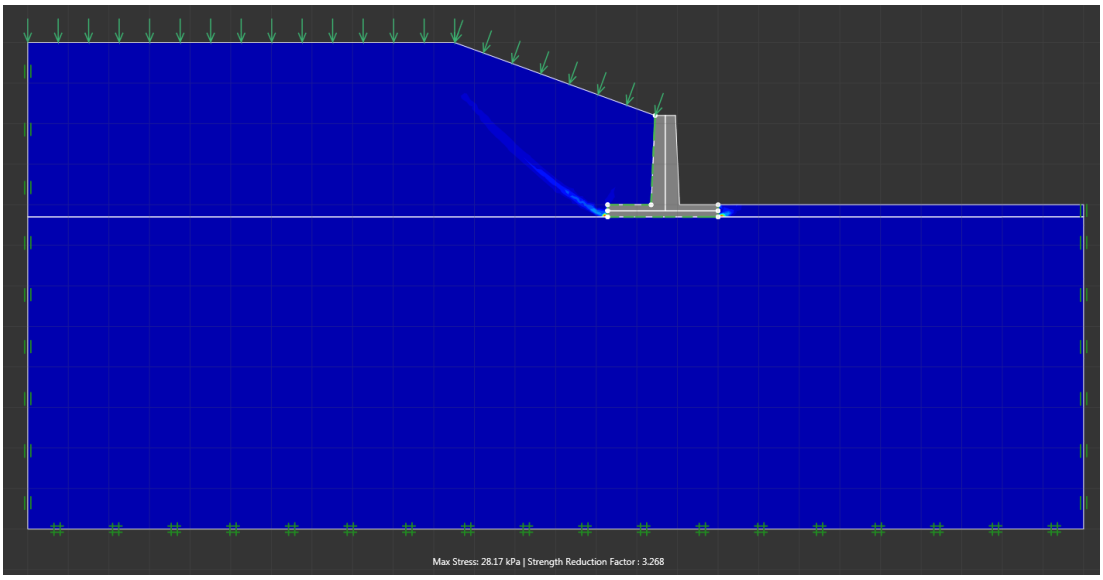

Figure 0.49 - Lower bound failure mode for case 25

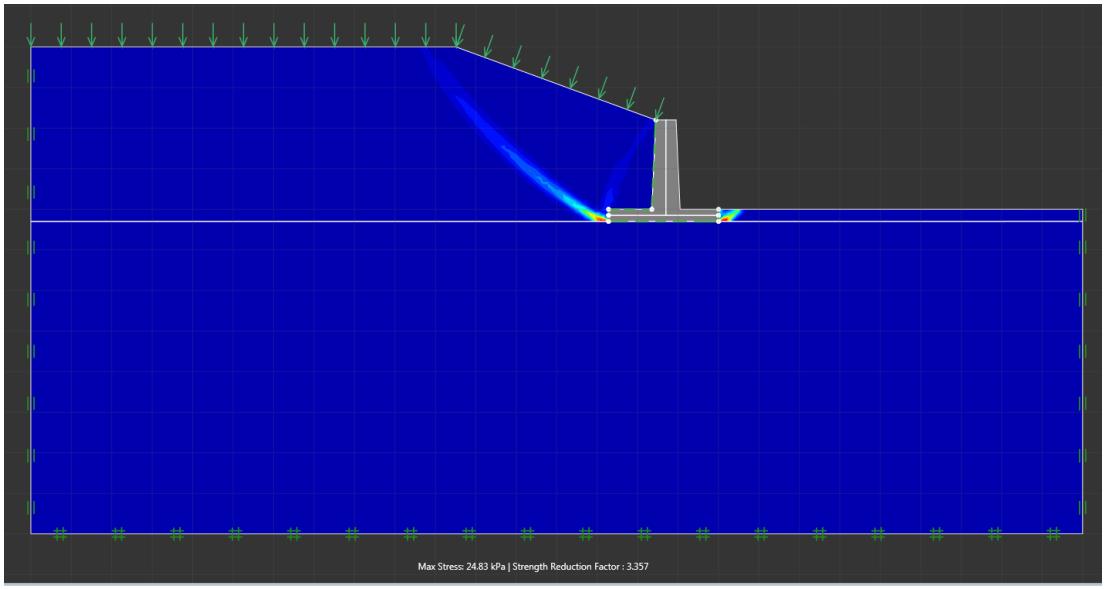

Figure 0.50 - Upper bound failure mode for case 25

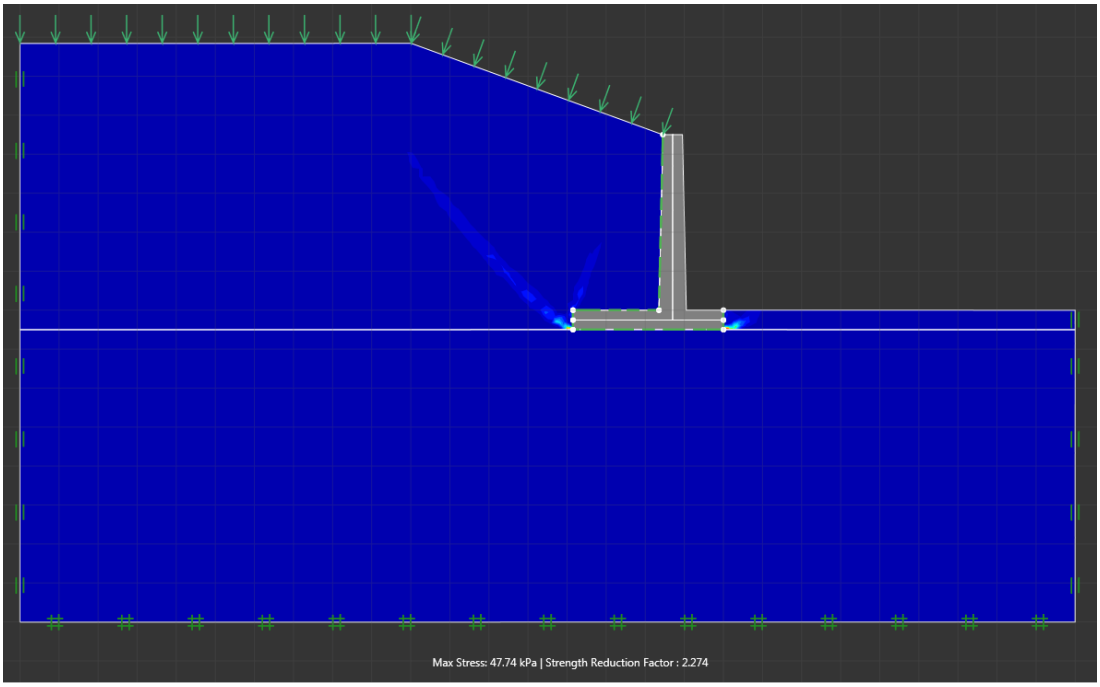

Figure 0.51 - Lower bound failure mode for case 26

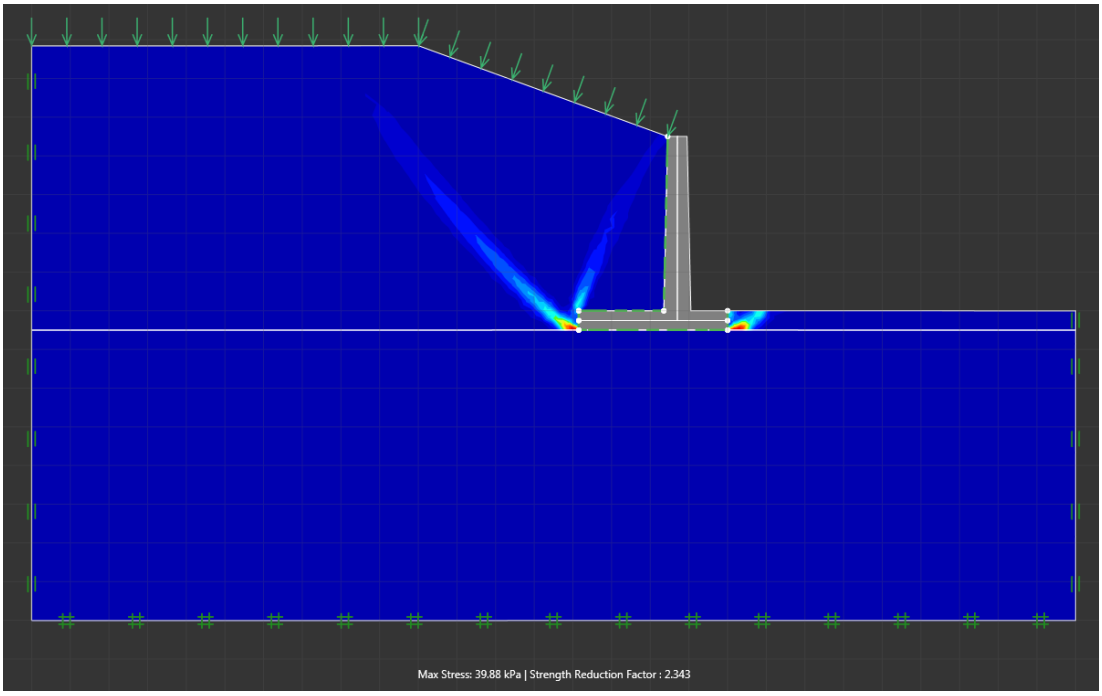

Figure 0.52 - Upper bound failure mode for case 26

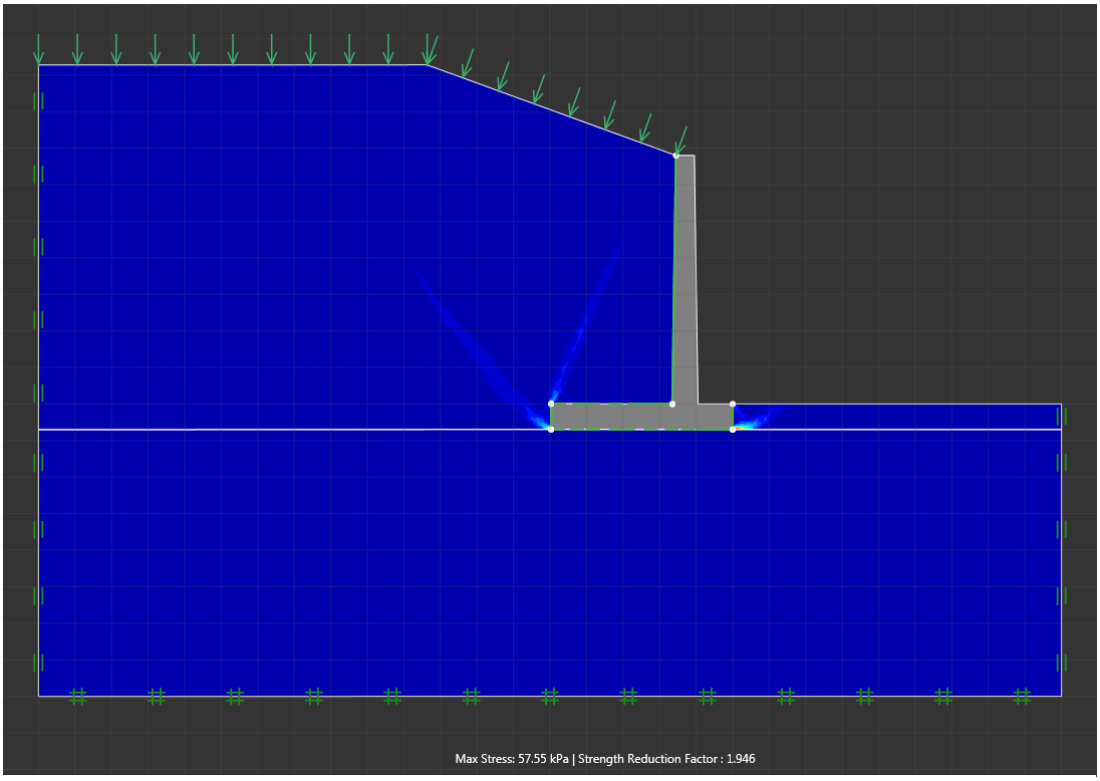

Figure 0.53 - Lower bound failure mode for case 27

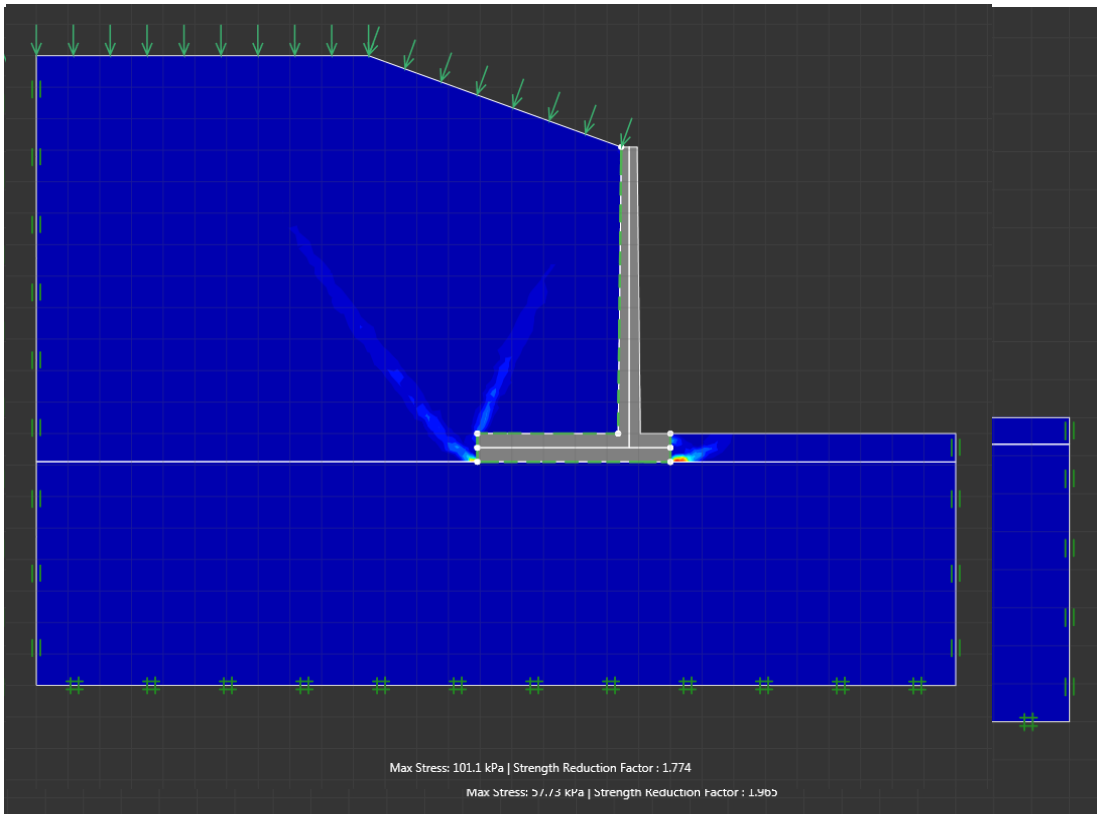

Figure 0.54 - Upper bound failure mode for case 27

Figure 0.55 - Lower bound failure mode for case 28

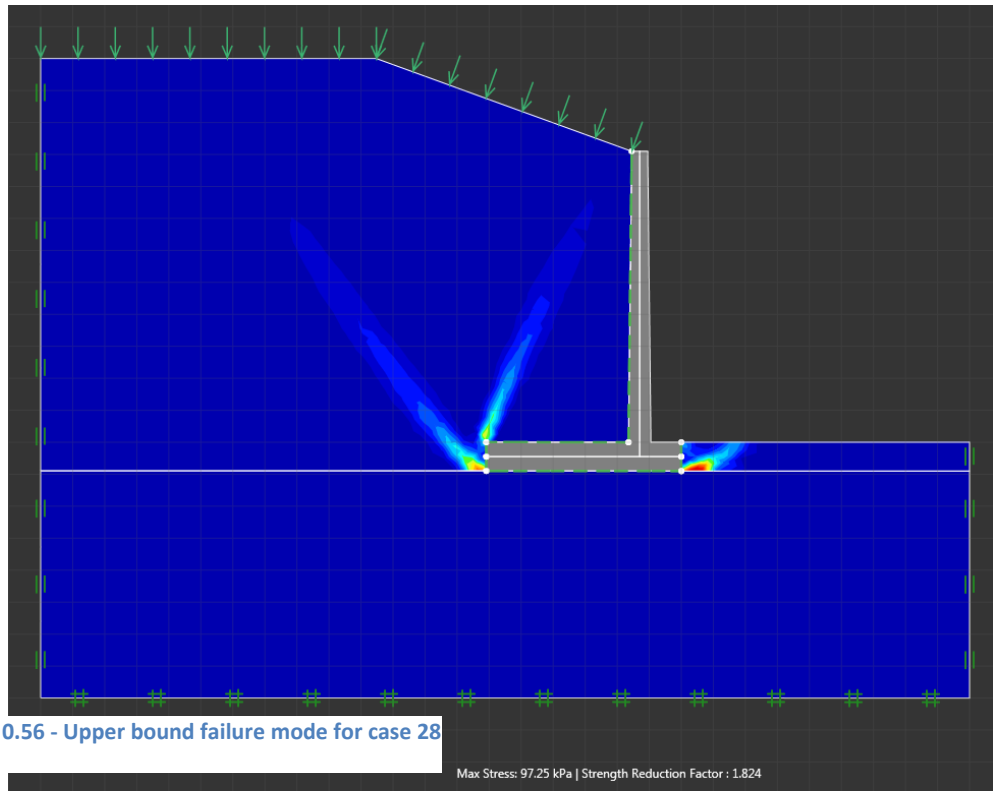

Figure 0.56 - Upper bound failure mode for case 28

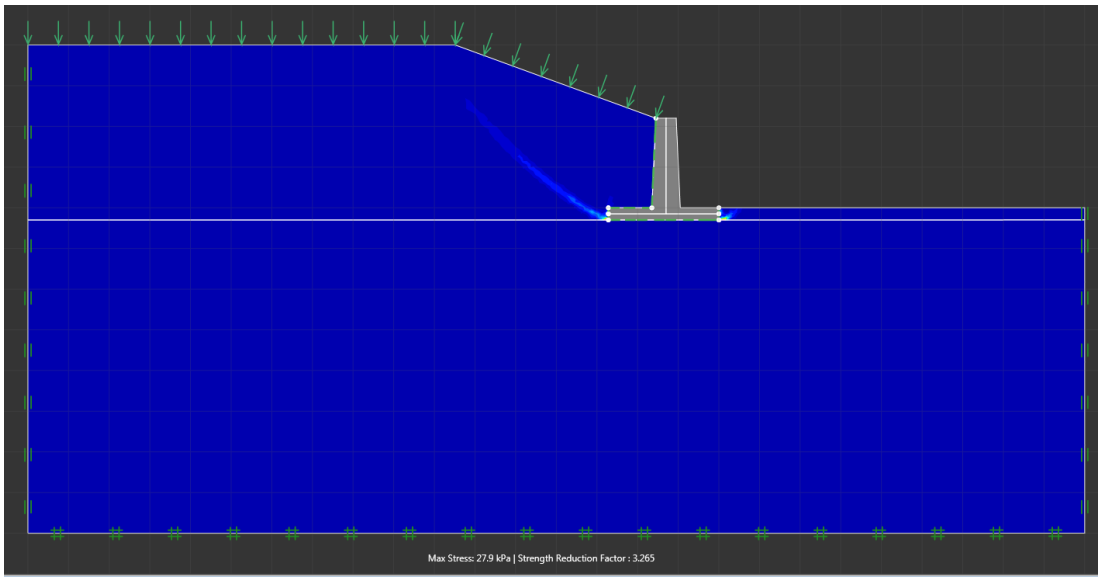

Figure 0.57 - Lower bound failure mode for case 29

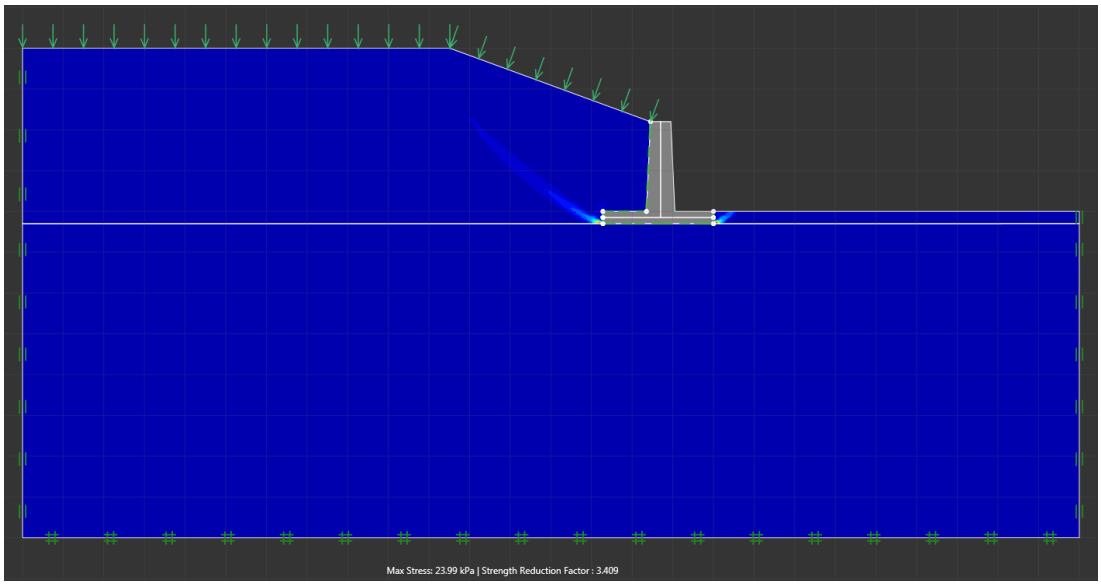

Figure 0.58 - Upper bound failure mode for case 29

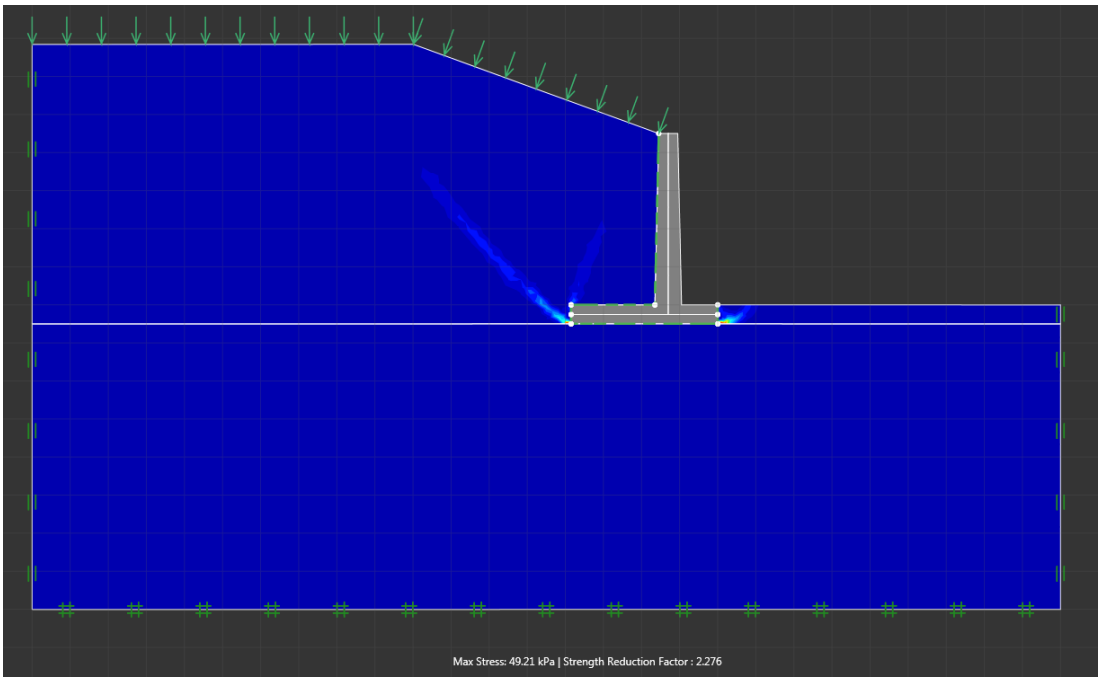

Figure 0.59 - Lower bound failure mode for case 30

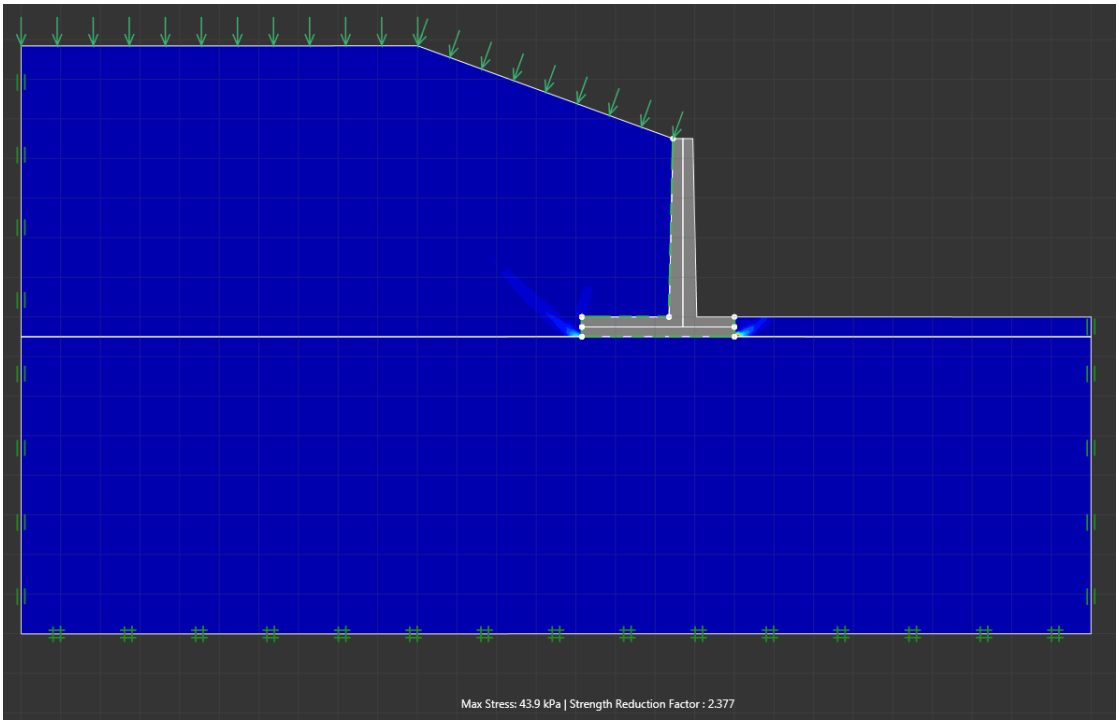

Figure 0.60 - Upper bound failure mode for case 30

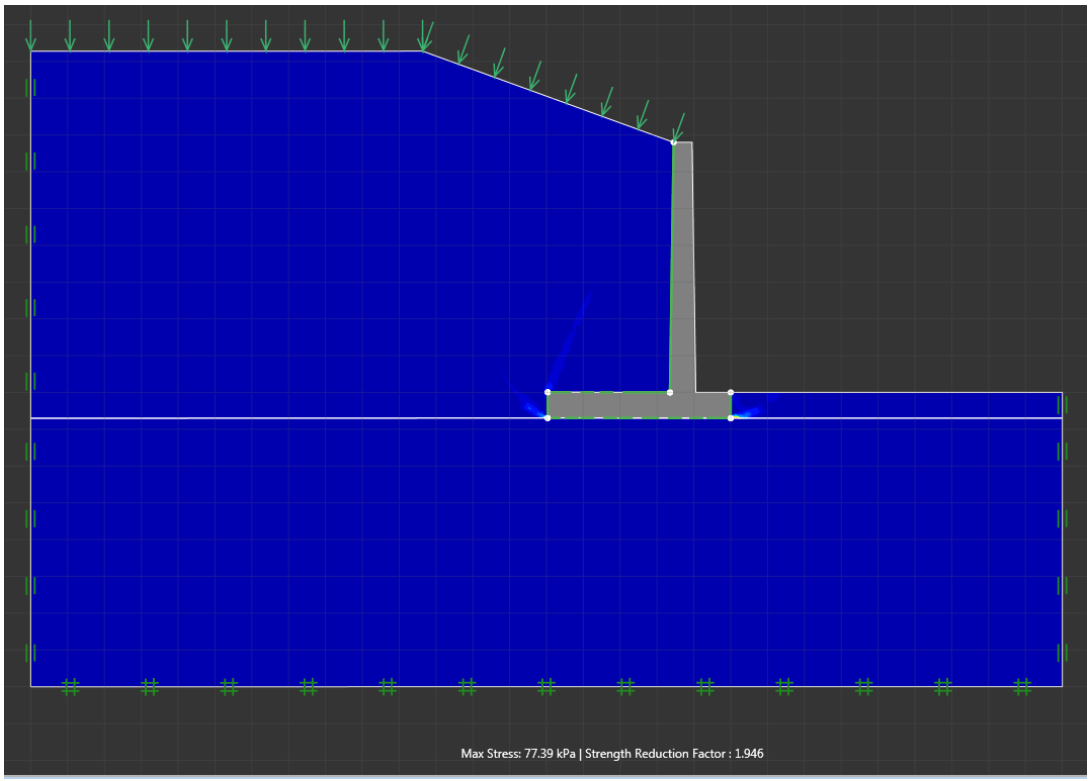

Figure 0.61 - Lower bound failure mode for case 31

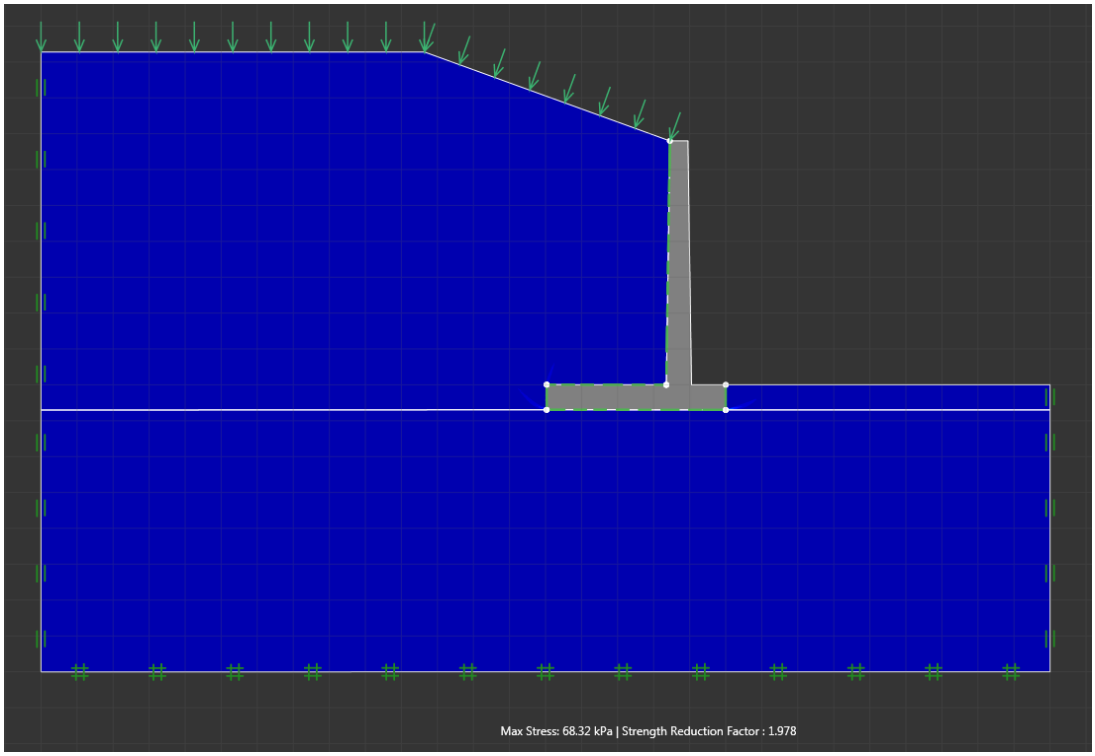

Figure 0.62 - Upper bound failure mode for case 31

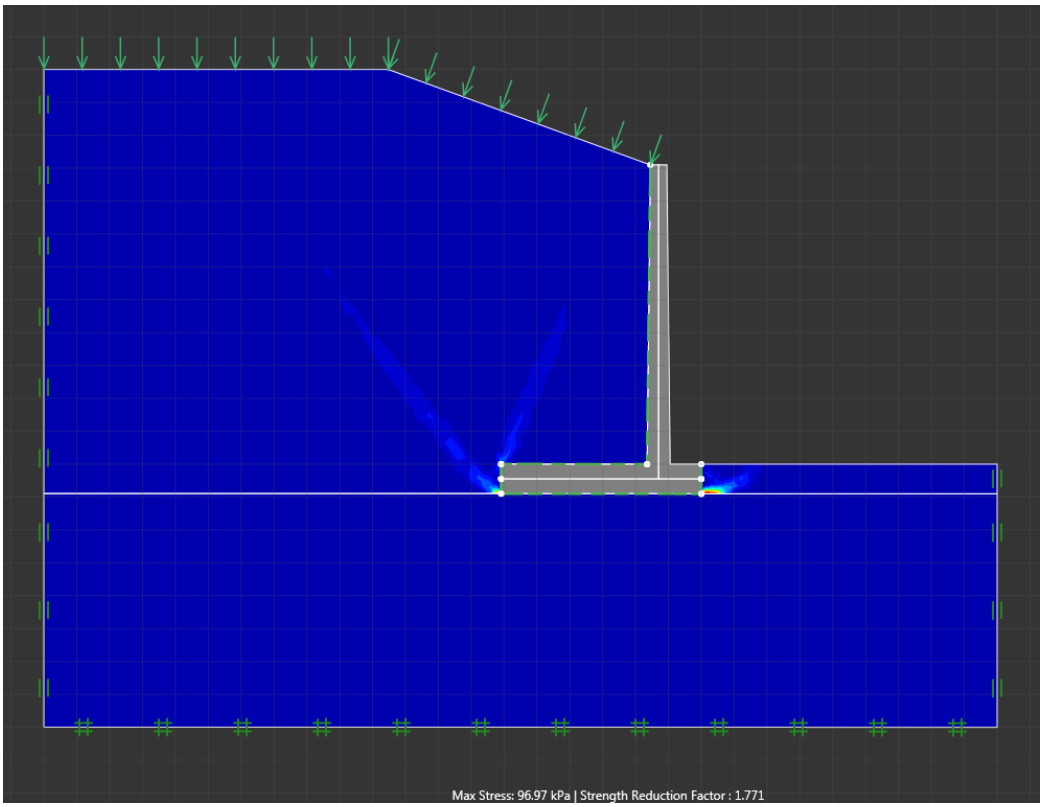

Figure 0.63 - Lower bound failure mode for case 32

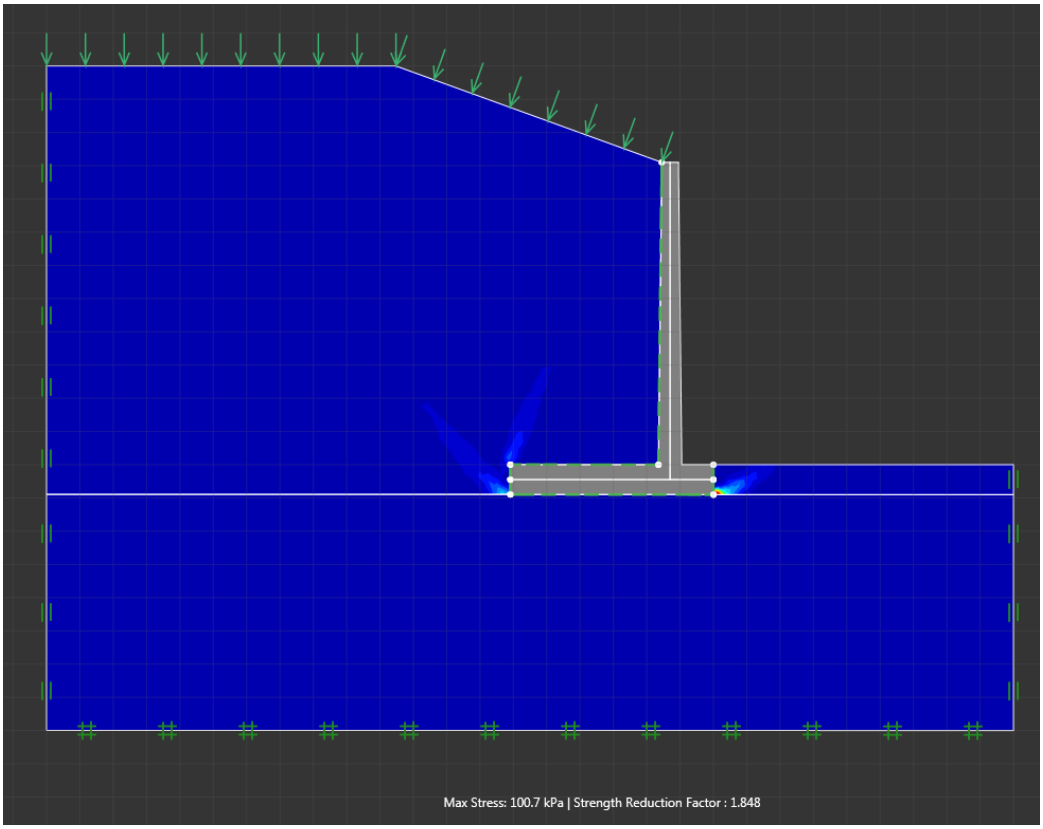

Figure 0.64 - Upper bound failure mode for case 32

Gravel Backfill

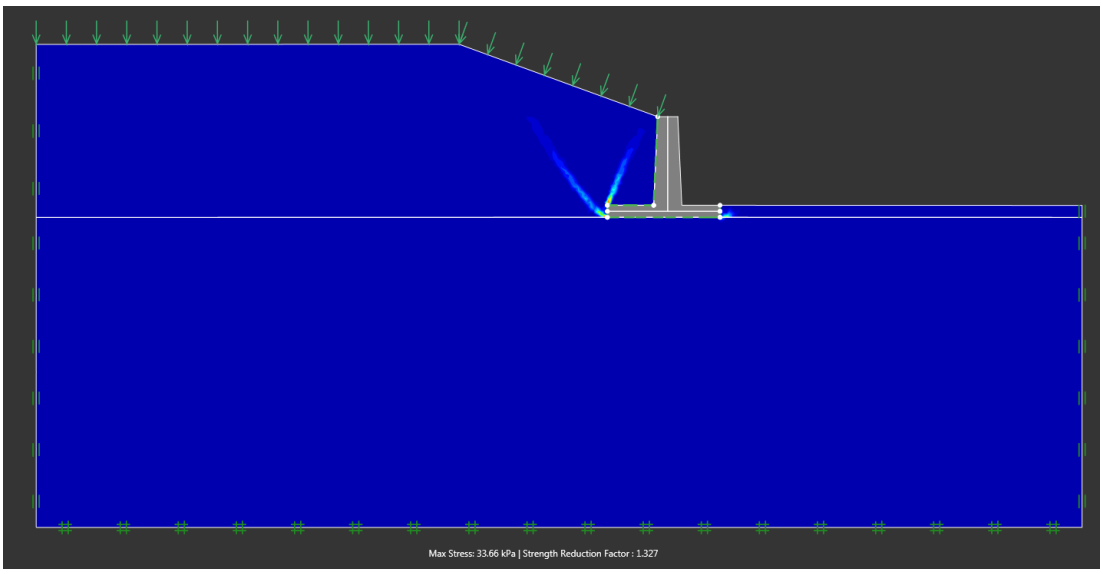

Figure 0.65 - Lower bound failure mode for case 33

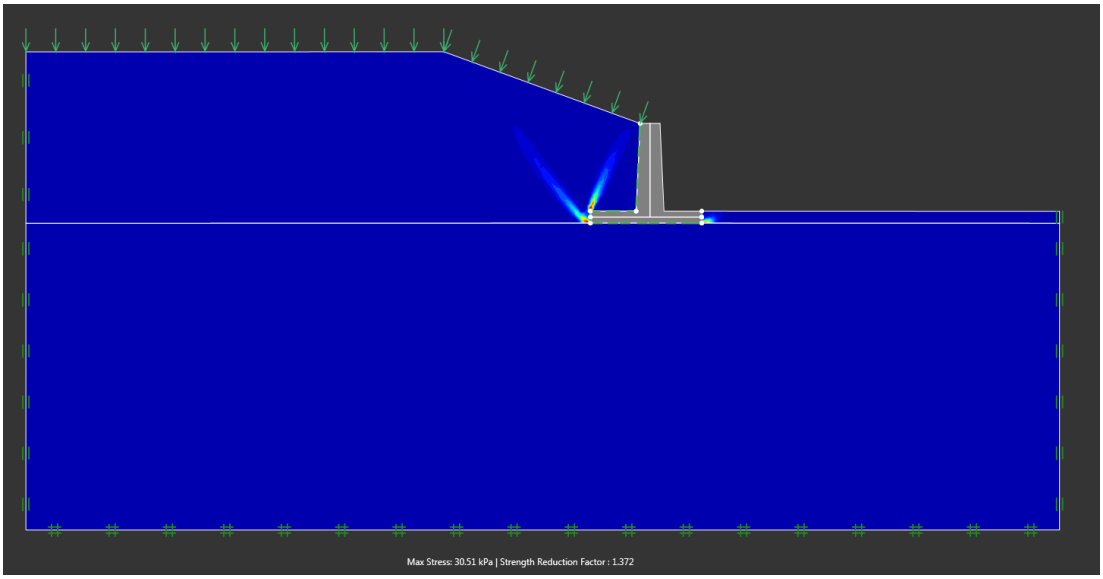

Figure 0.66 - Upper bound failure mode for case 33

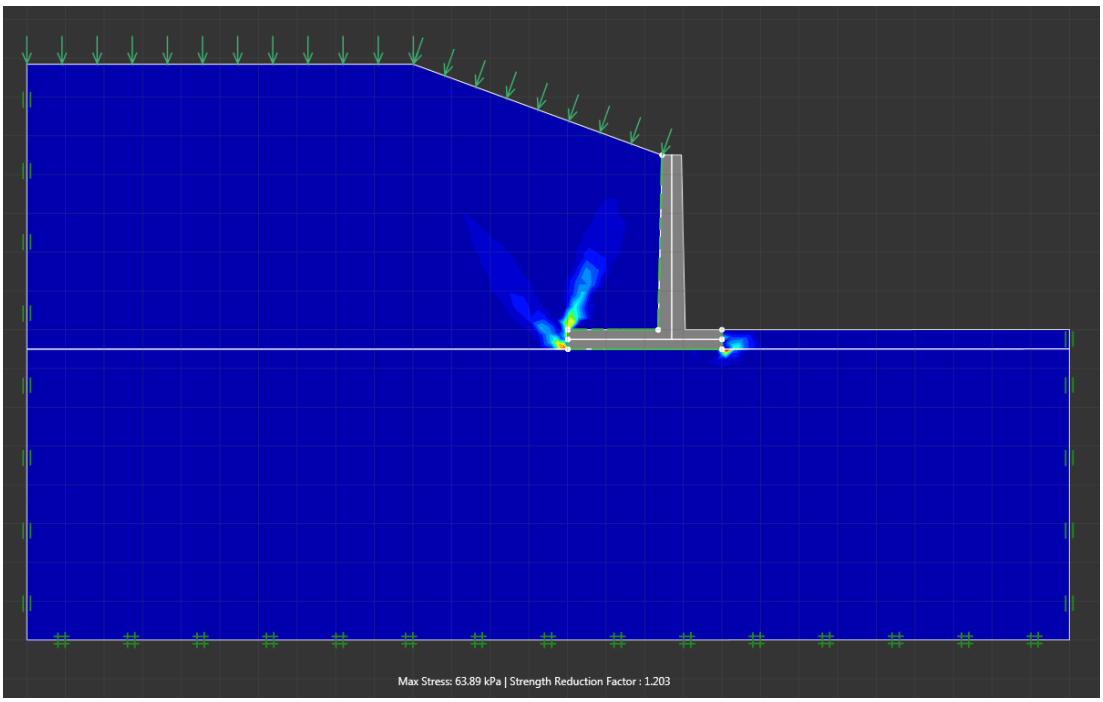

Figure 0.67 - Lower bound failure mode for case 34

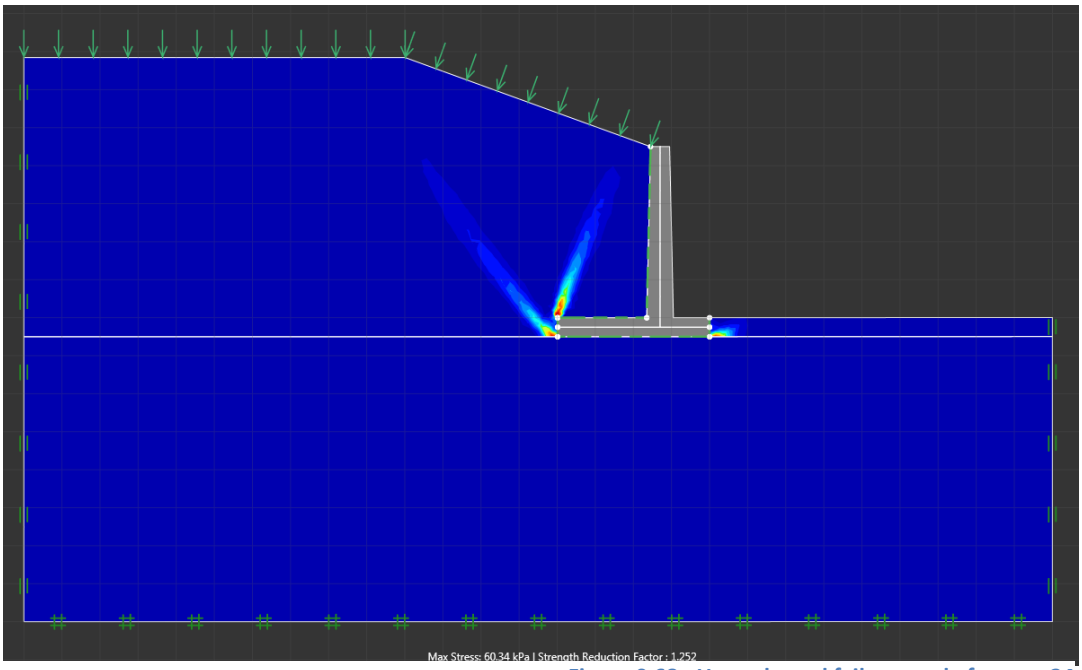

Figure 0.68 - Upper bound failure mode for case 34

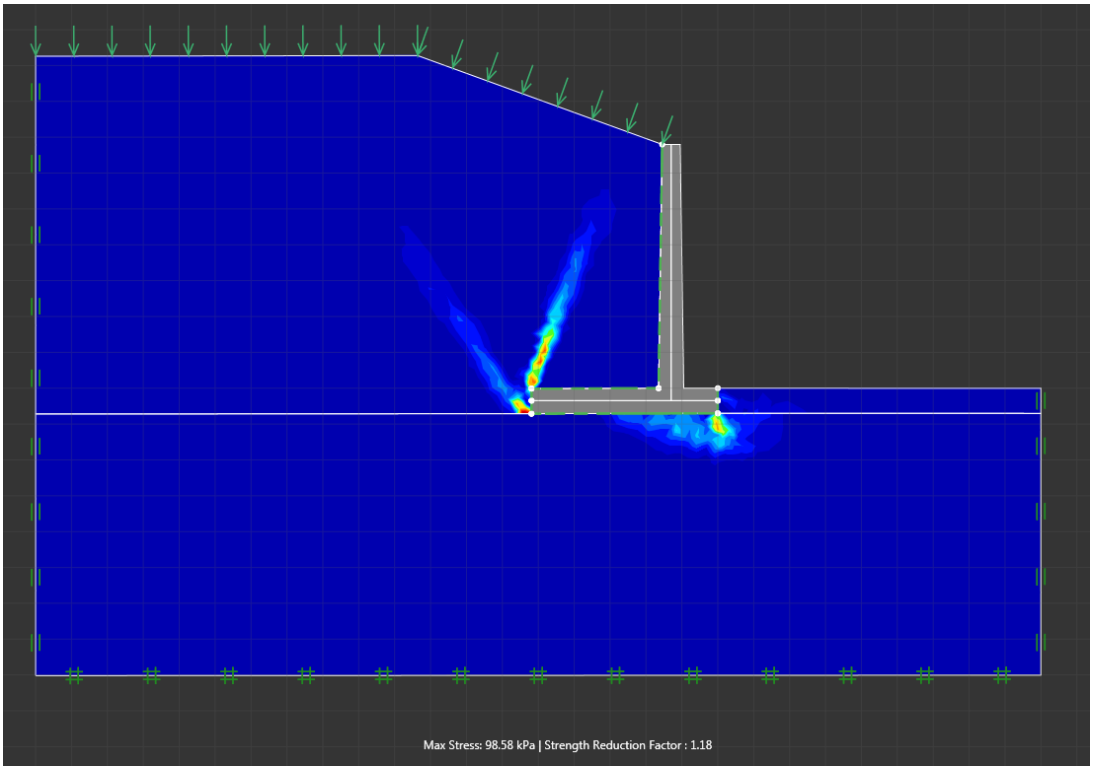

Figure 0.69 - Lower bound failure mode for case 35

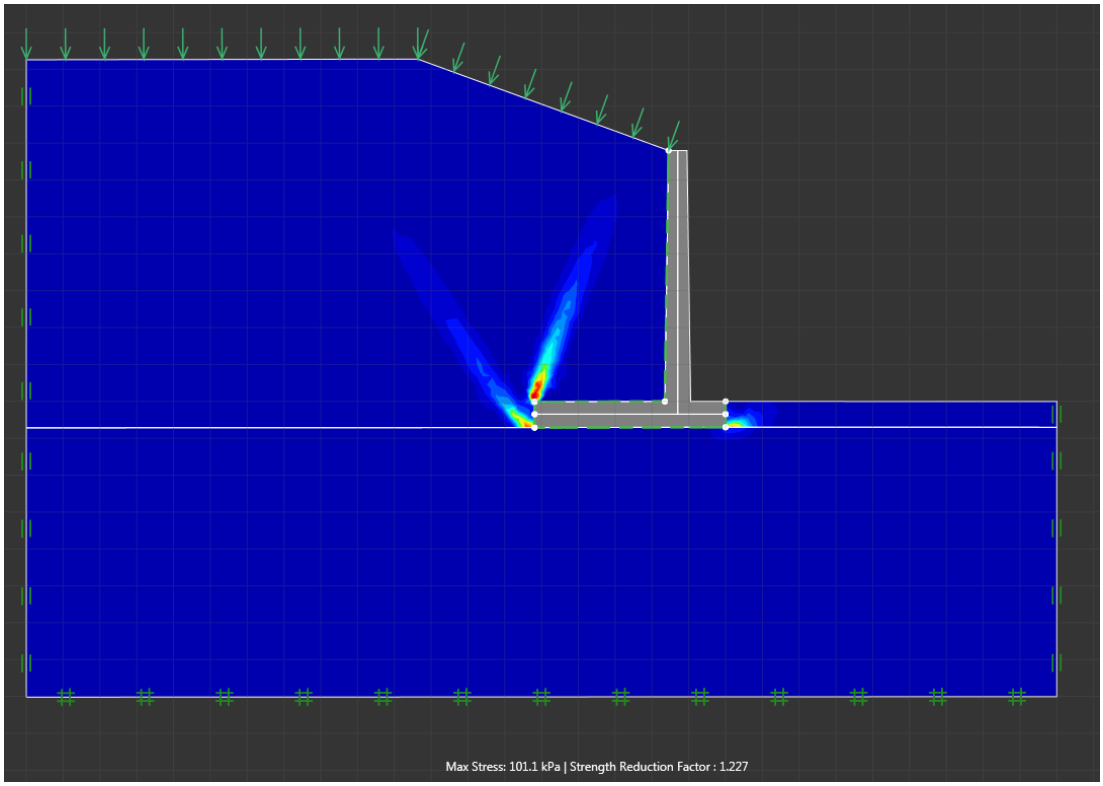

Figure 0.70 - Upper bound failure mode for case 35

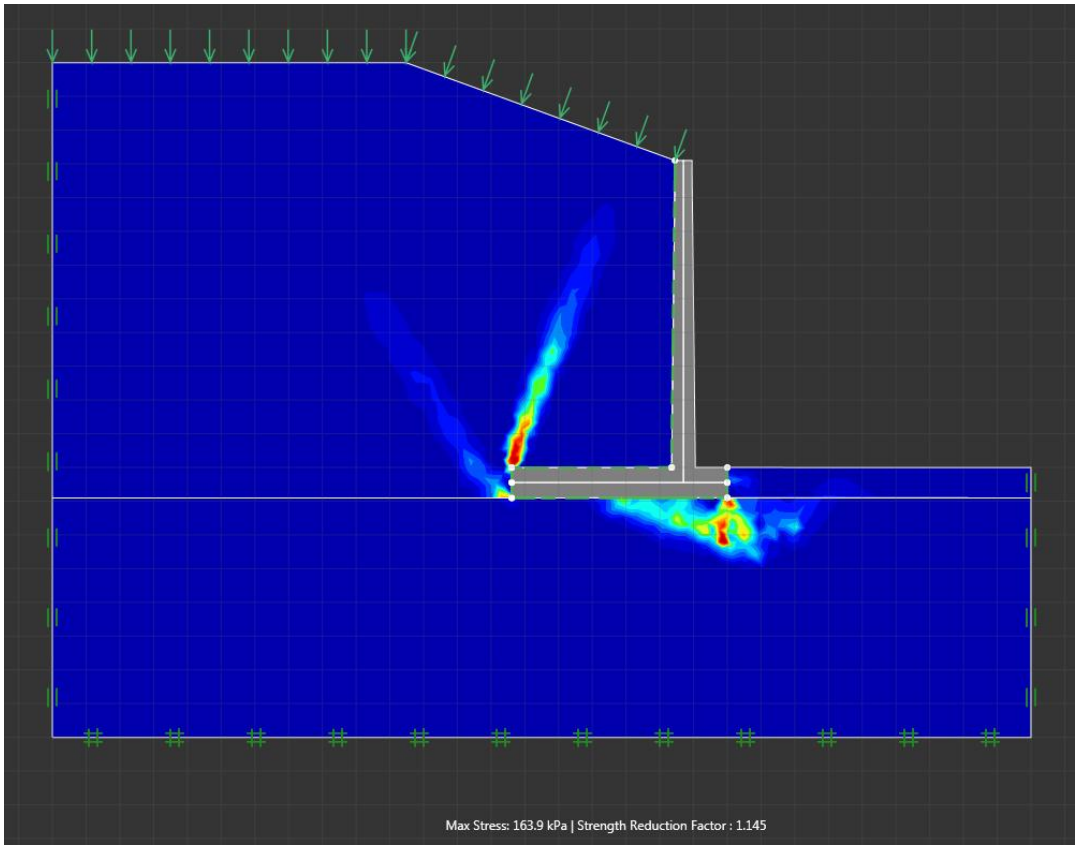

Figure 0.71 - Lower bound failure mode for case 36

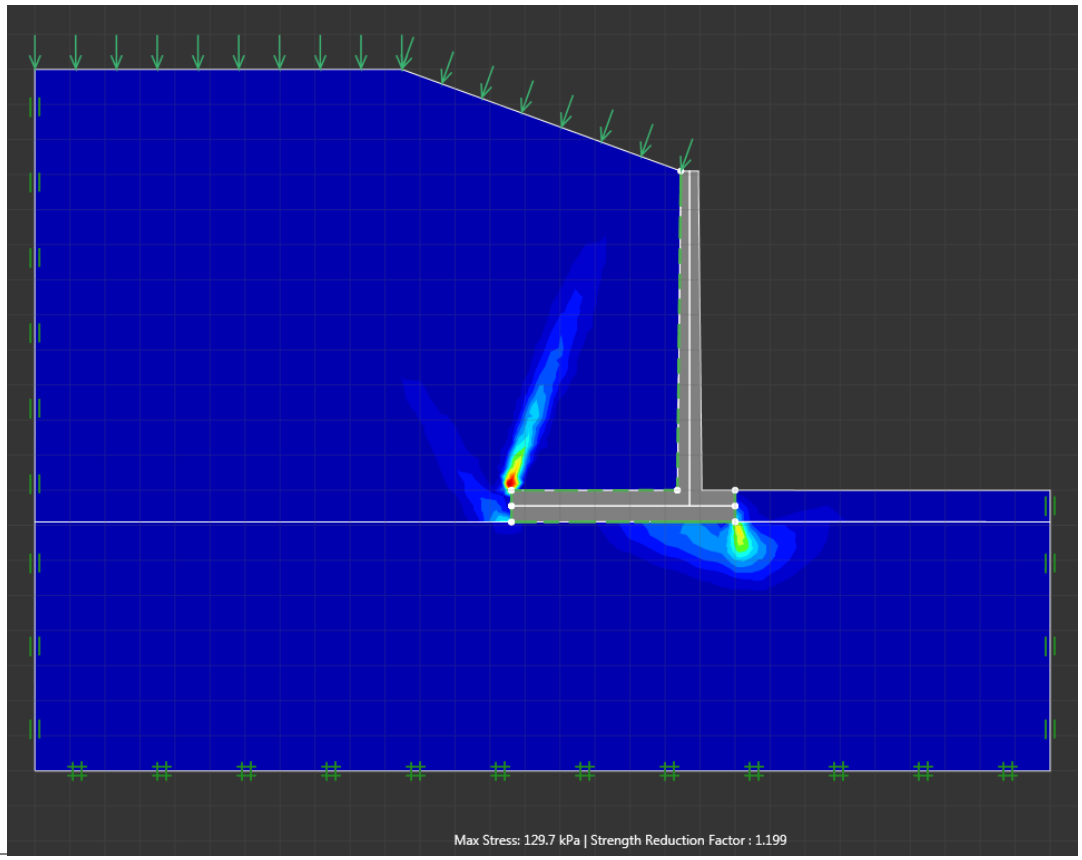

Figure 0.72 - Upper bound failure mode for case 36

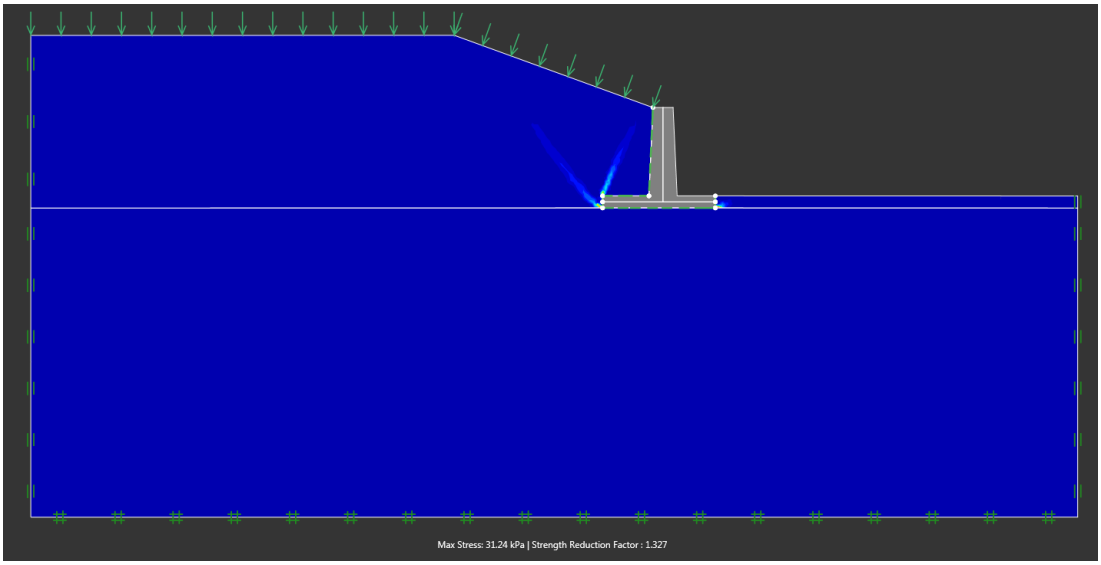

Figure 0.73 - Lower bound failure mode for case 37

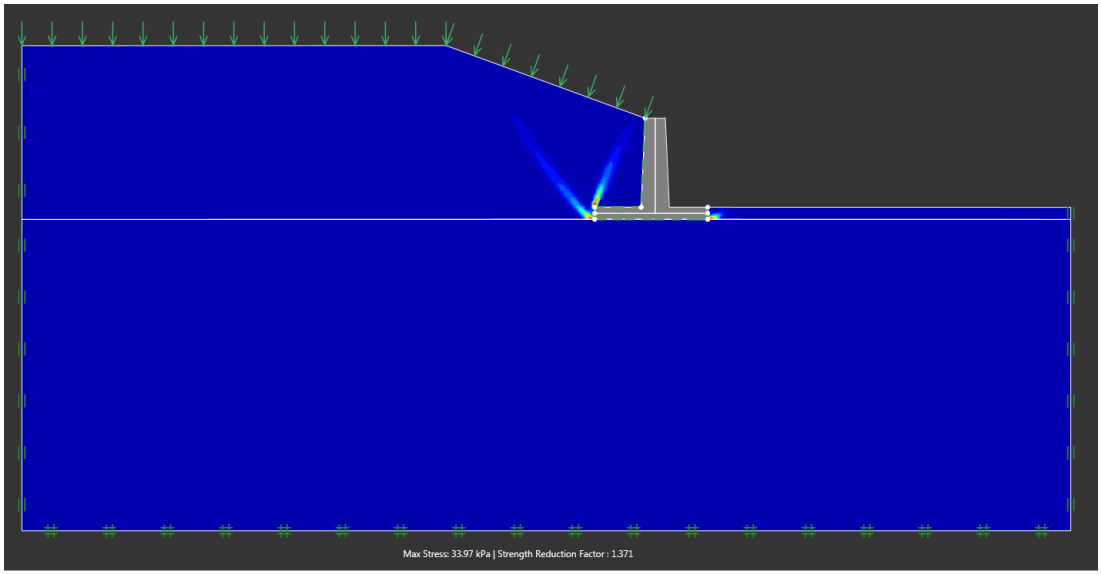

Figure 0.74 - Upper bound failure mode for case 37

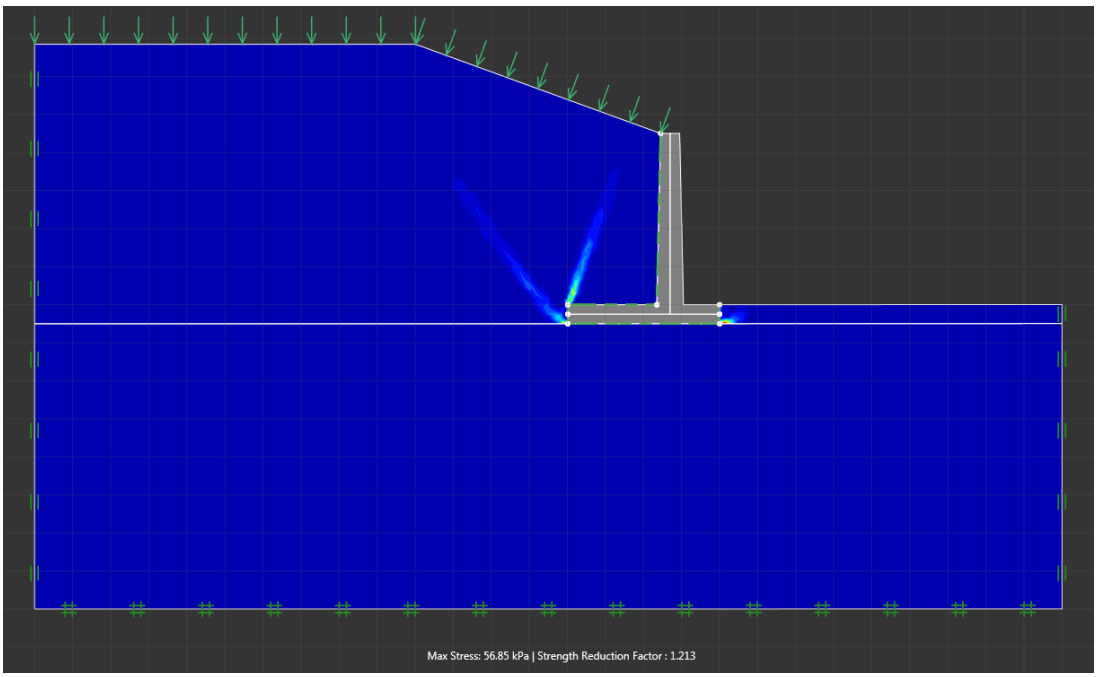

Figure 0.75 - Lower bound failure mode for case 38

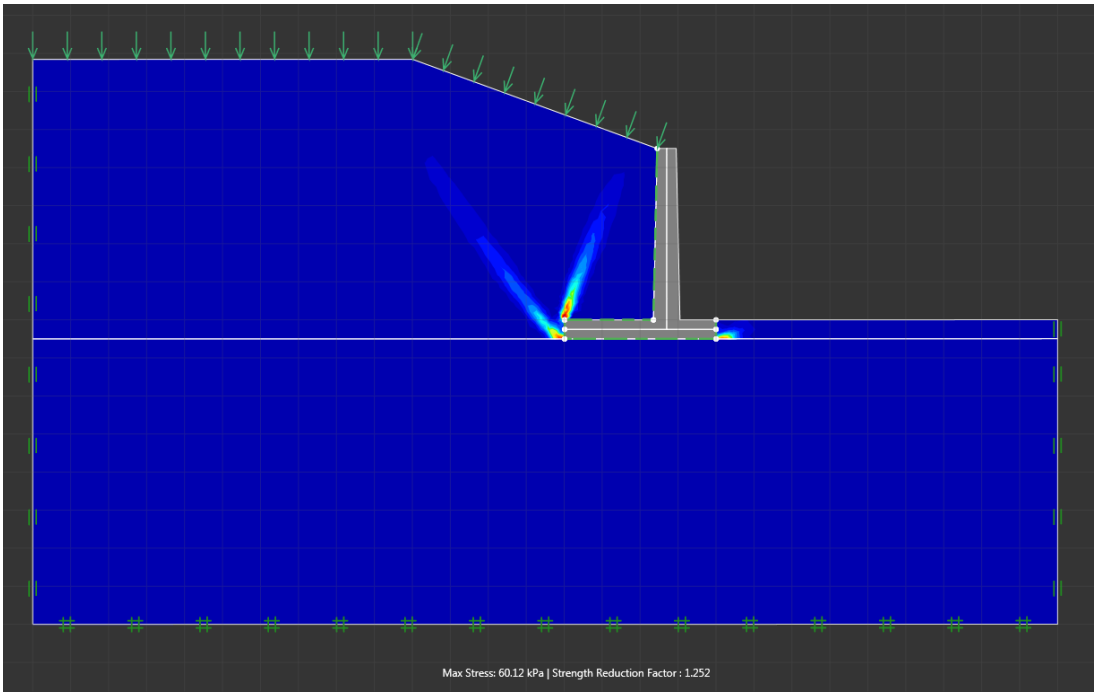

Figure 0.76 - Upper bound failure mode for case 38

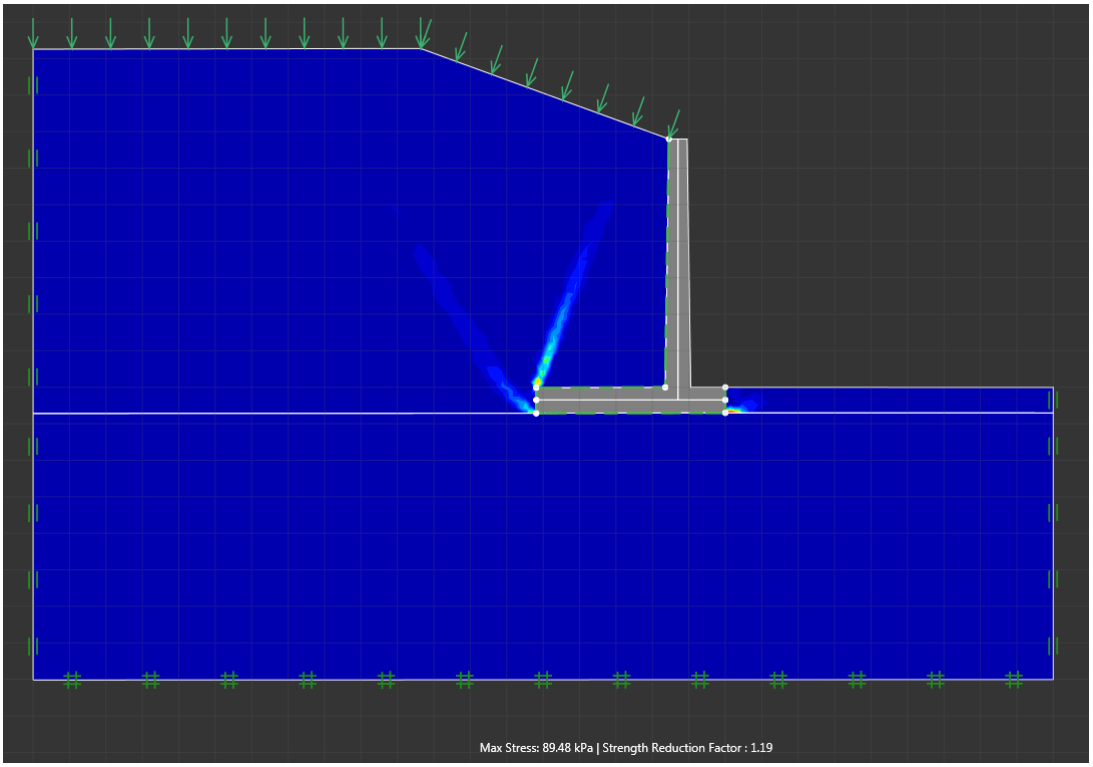

Figure 0.77 - Lower bound failure mode for case 39

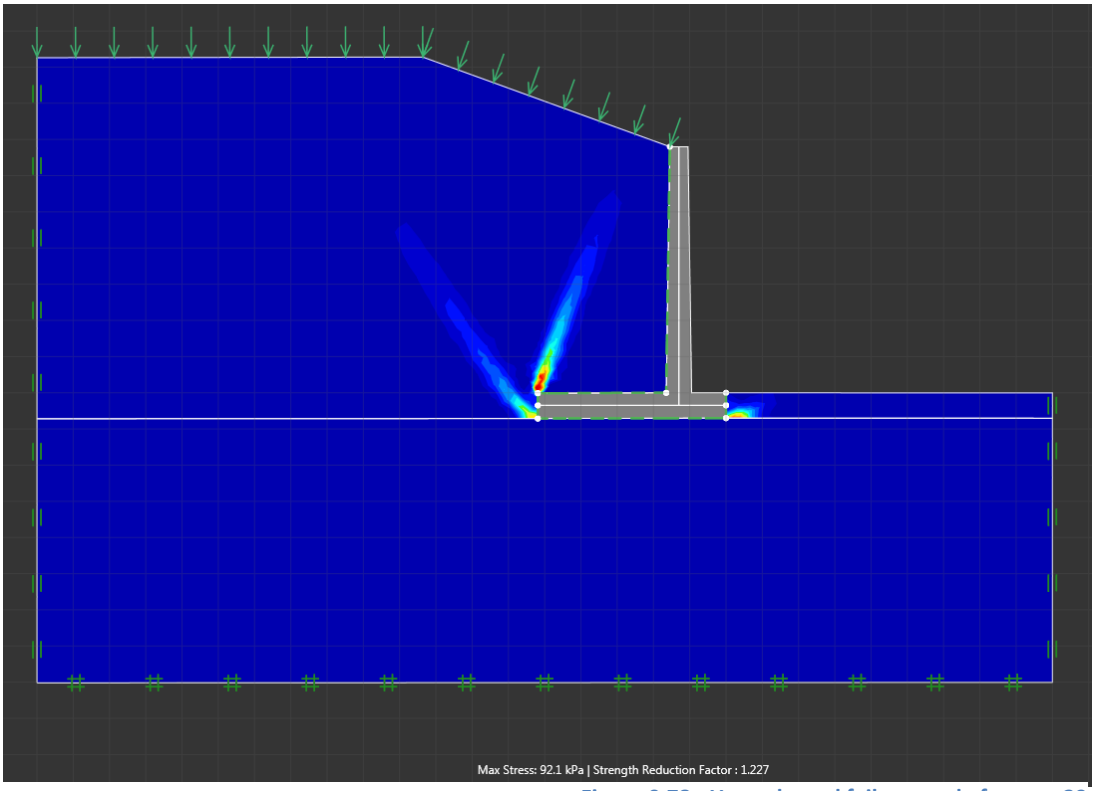

Figure 0.78 - Upper bound failure mode for case 39

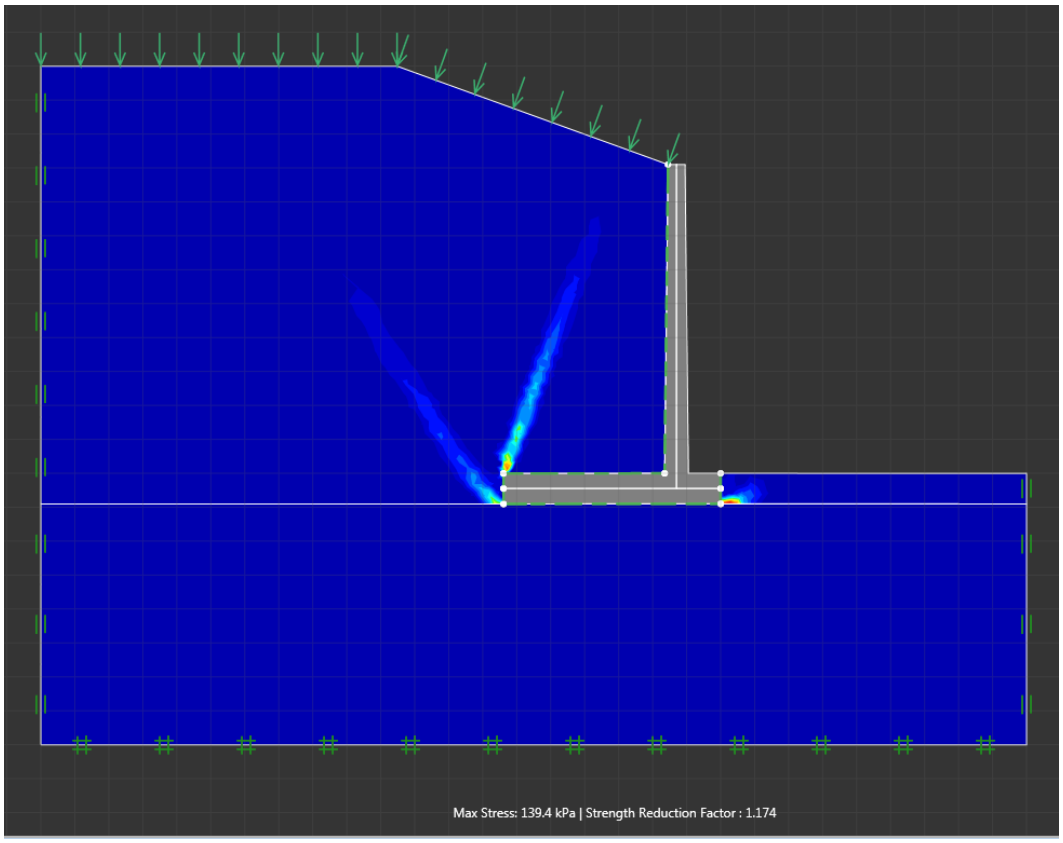

Figure 0.79 - Lower bound failure mode for case 40

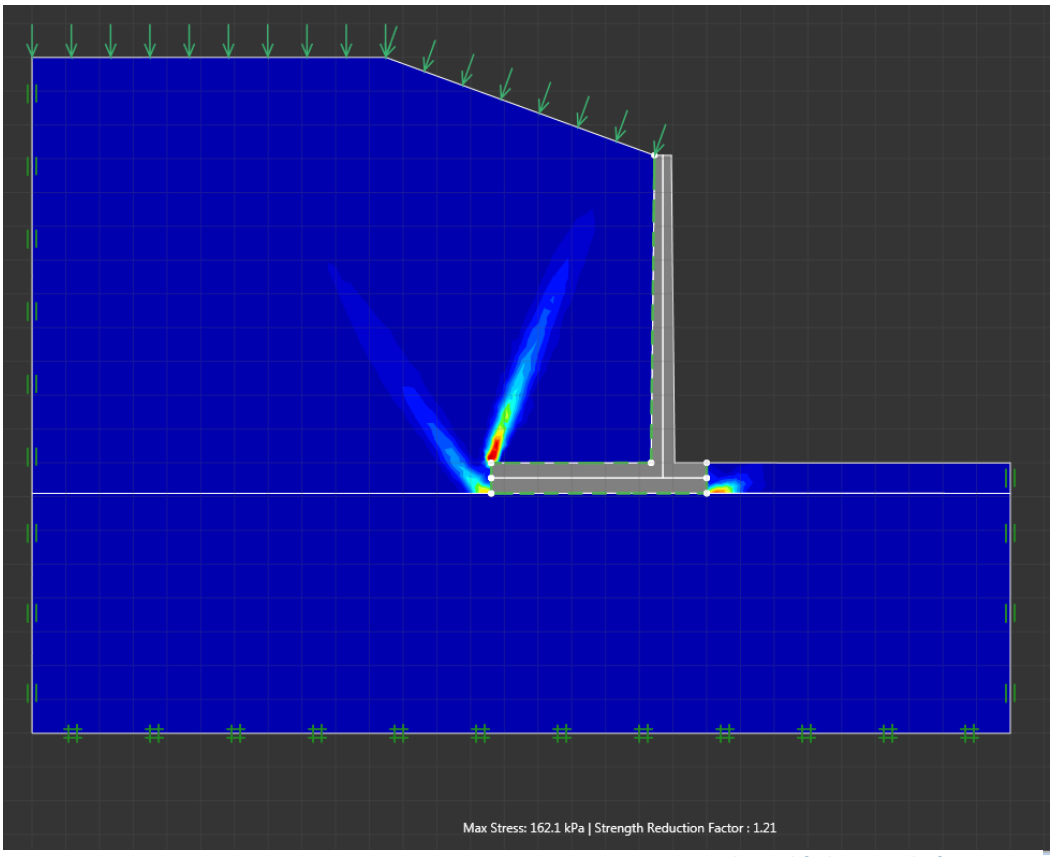

Figure 0.80 - Upper bound failure mode for case 40

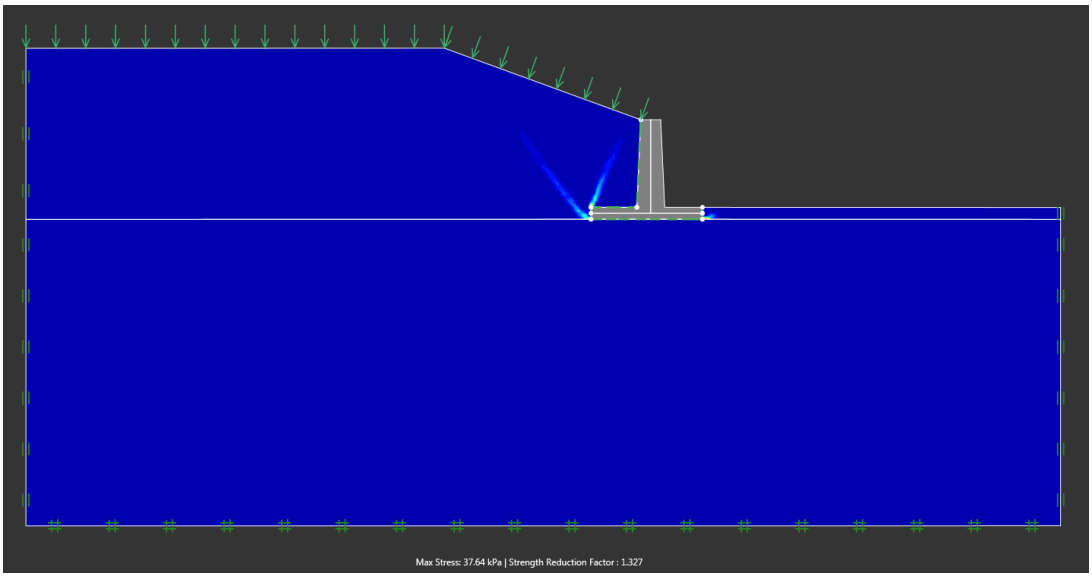

Figure 0.81 - Lower bound failure mode for case 41

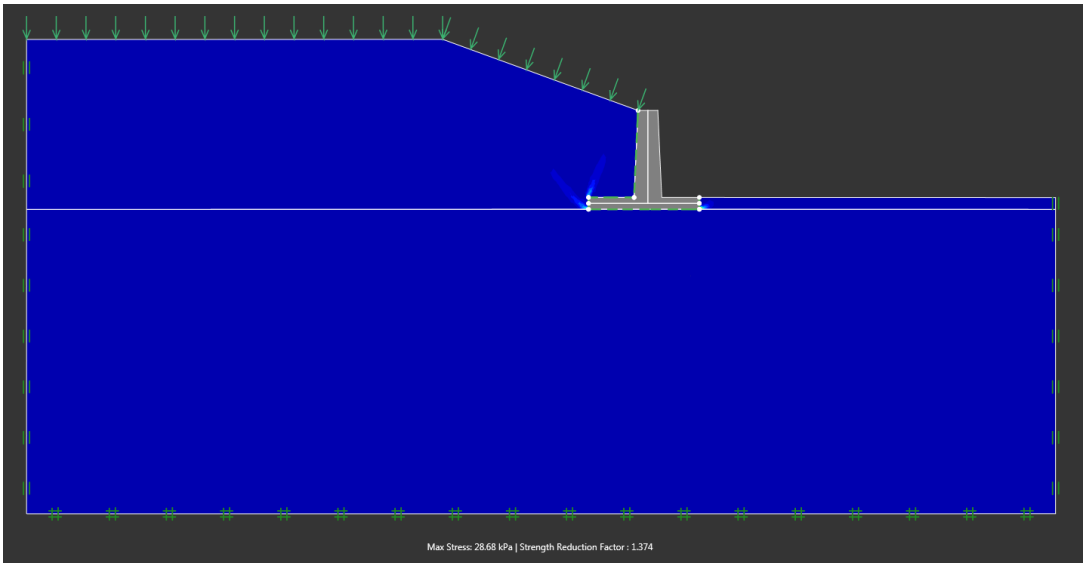

Figure 0.82 - Upper bound failure mode for case 41

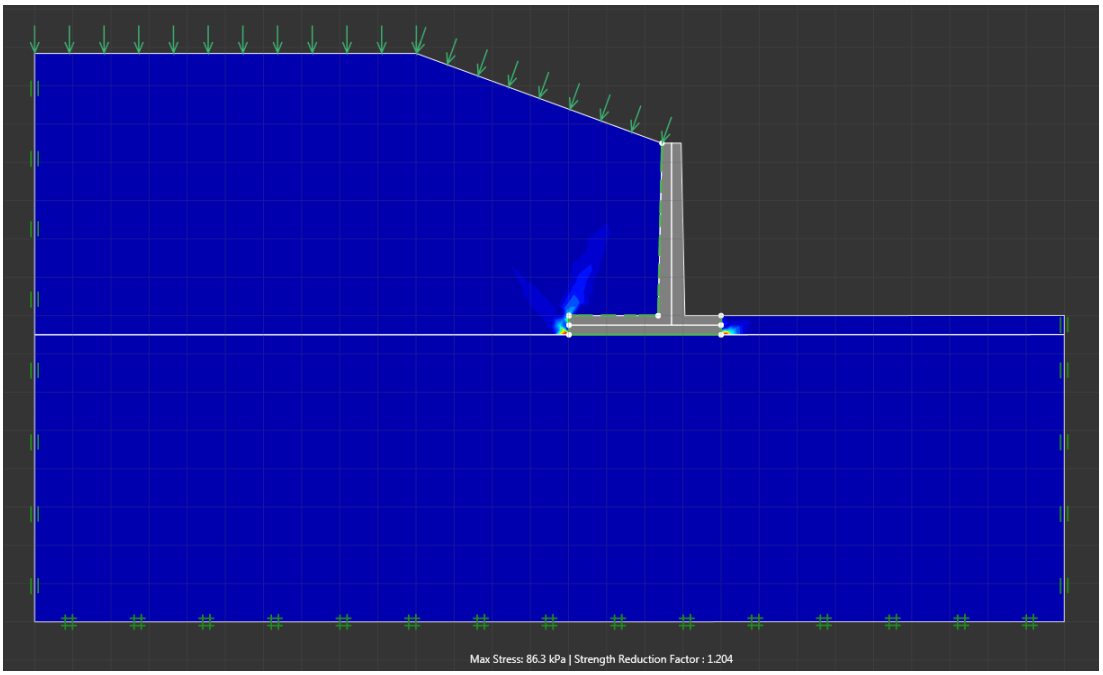

Figure 0.83 - Lower bound failure mode for case 42

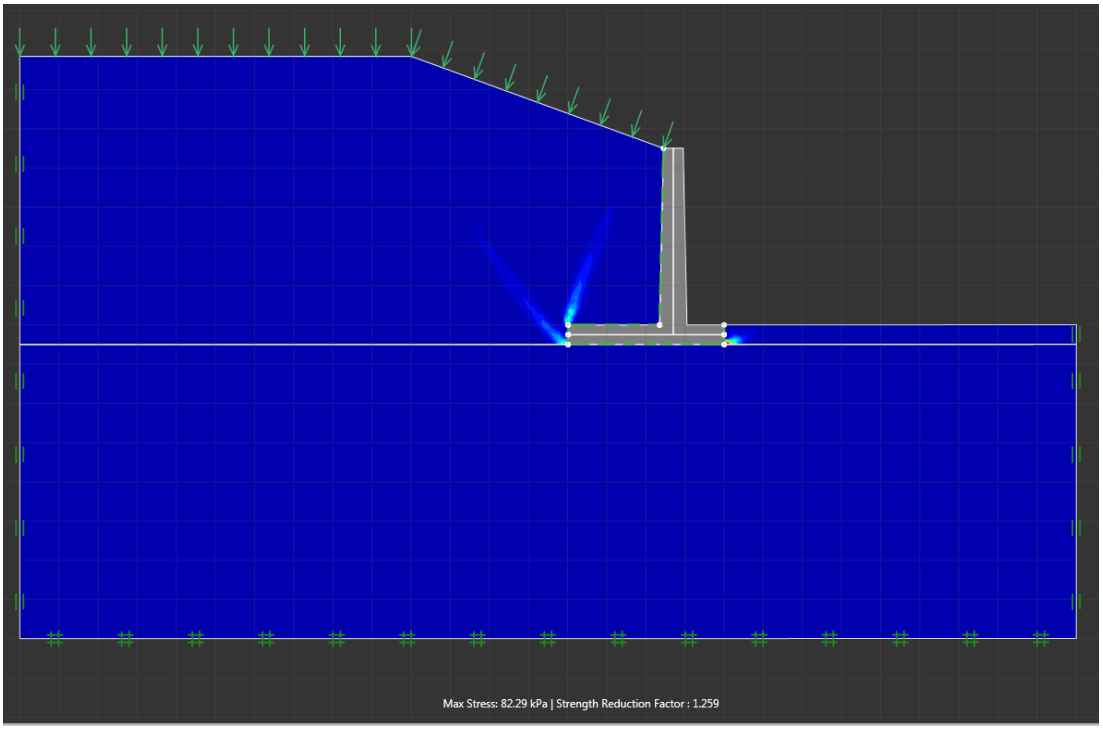

Figure 0.84 - Upper bound failure mode for case 42

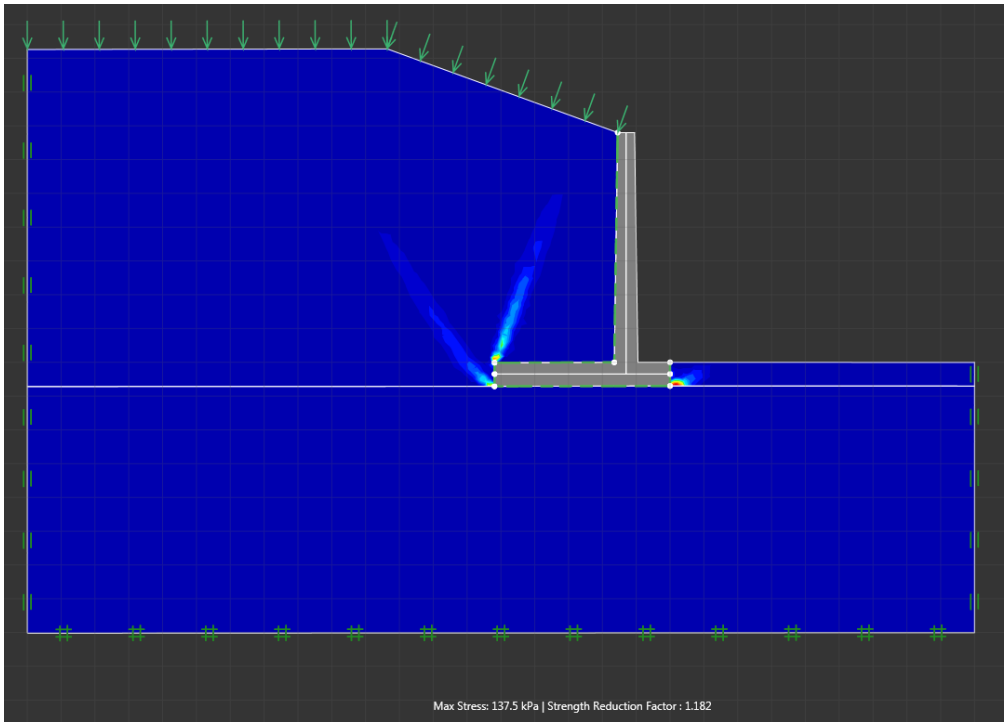

Figure 0.85 - Lower bound failure mode for case 43

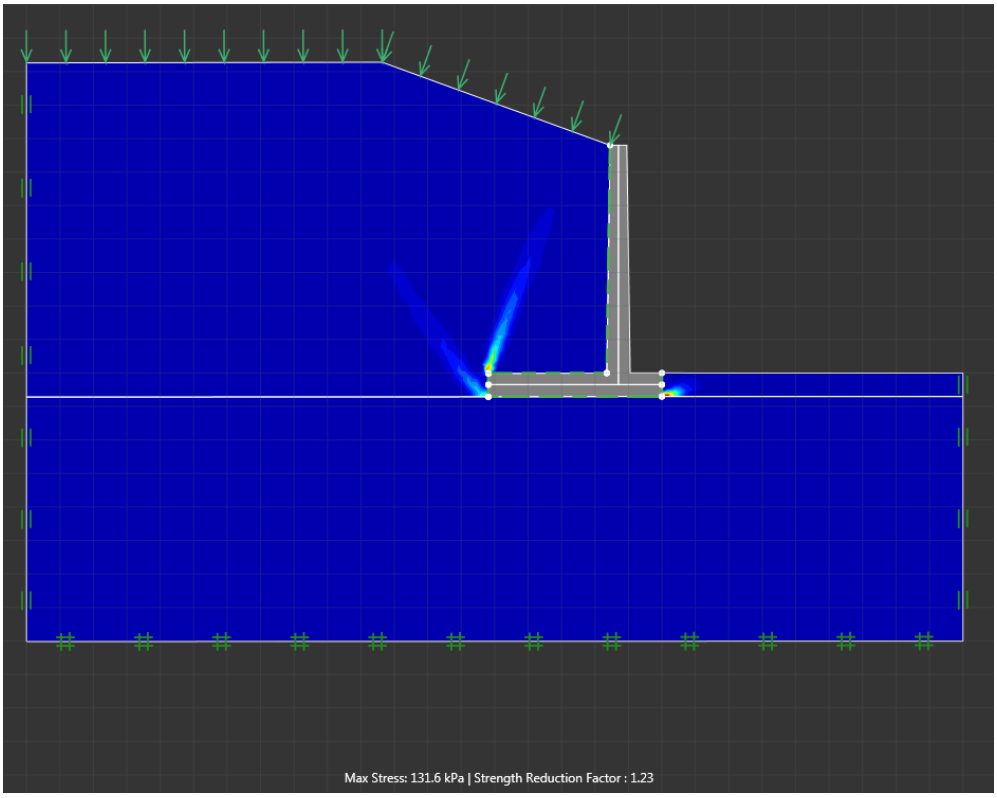

Figure 0.86 - Upper bound failure mode for case 43

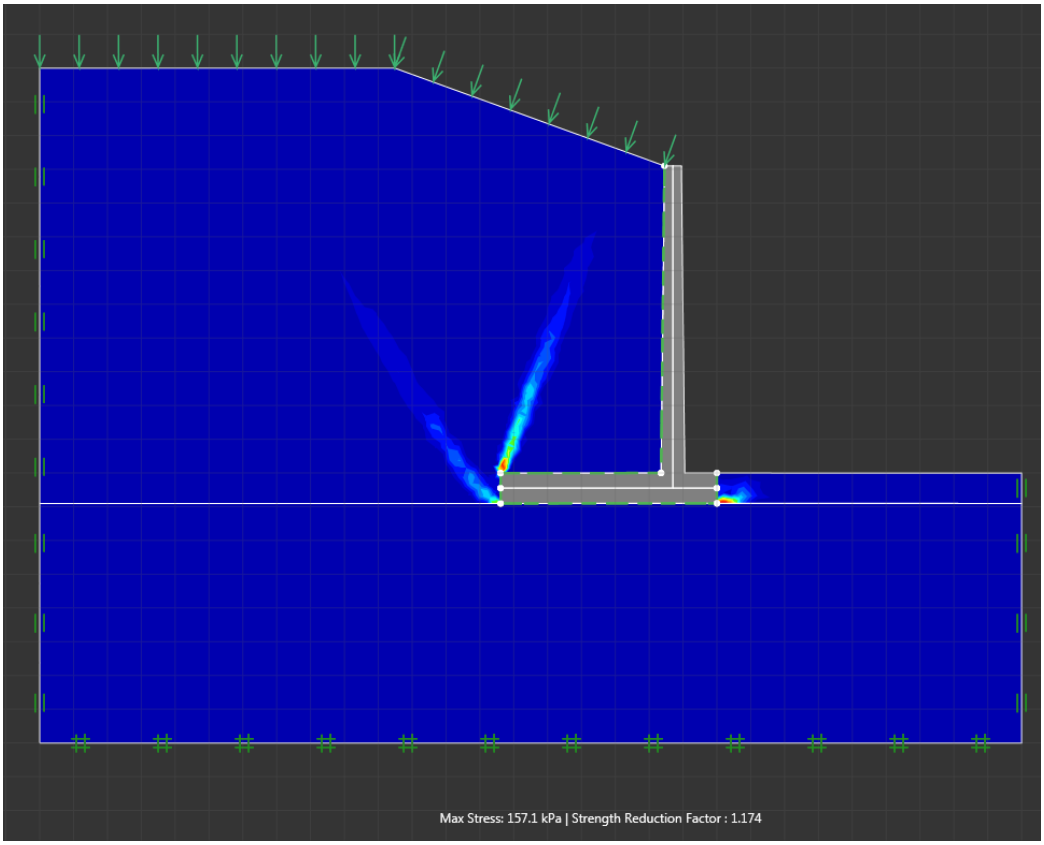

Figure 0.87 - Lower bound failure mode for case 44

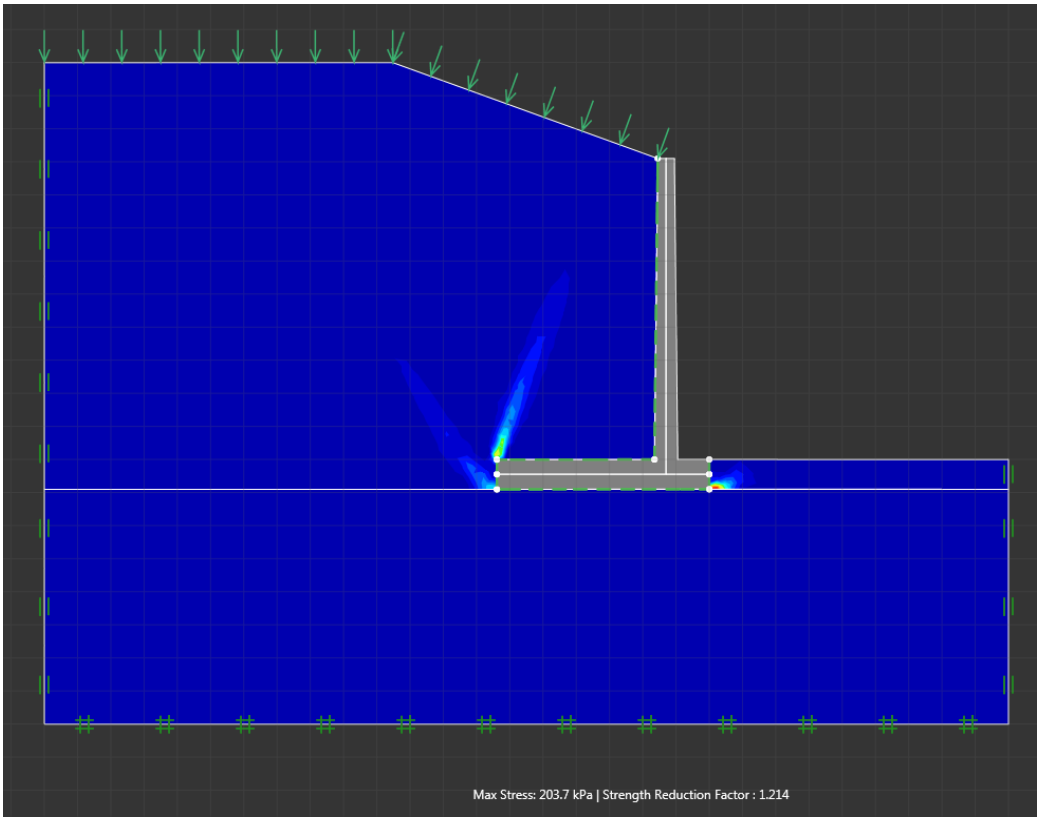

Figure 0.88 - Upper bound failure mode for case 44

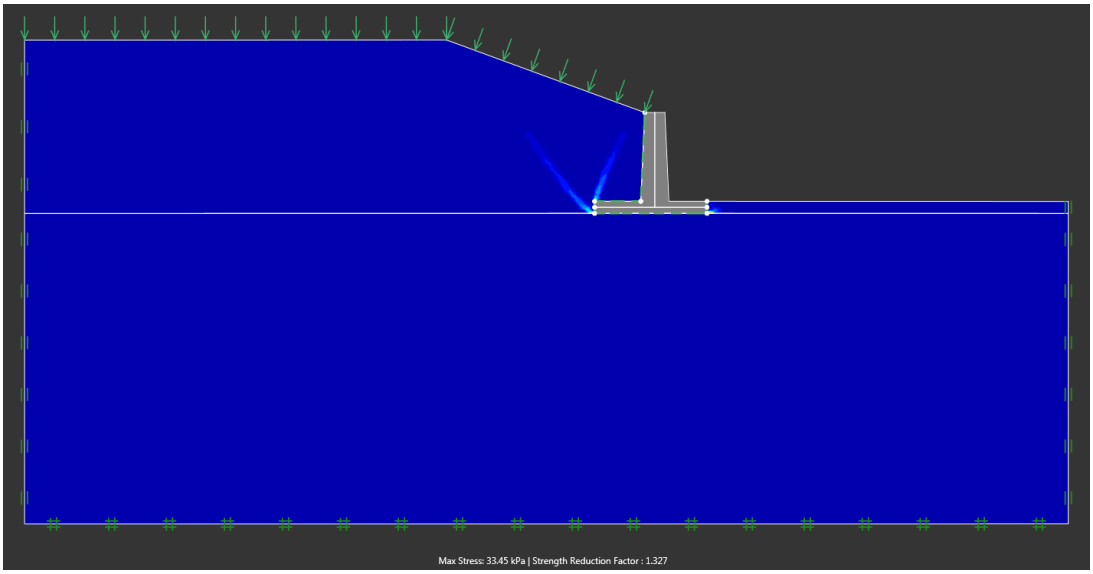

Figure 0.89 - Lower bound failure mode for case 45

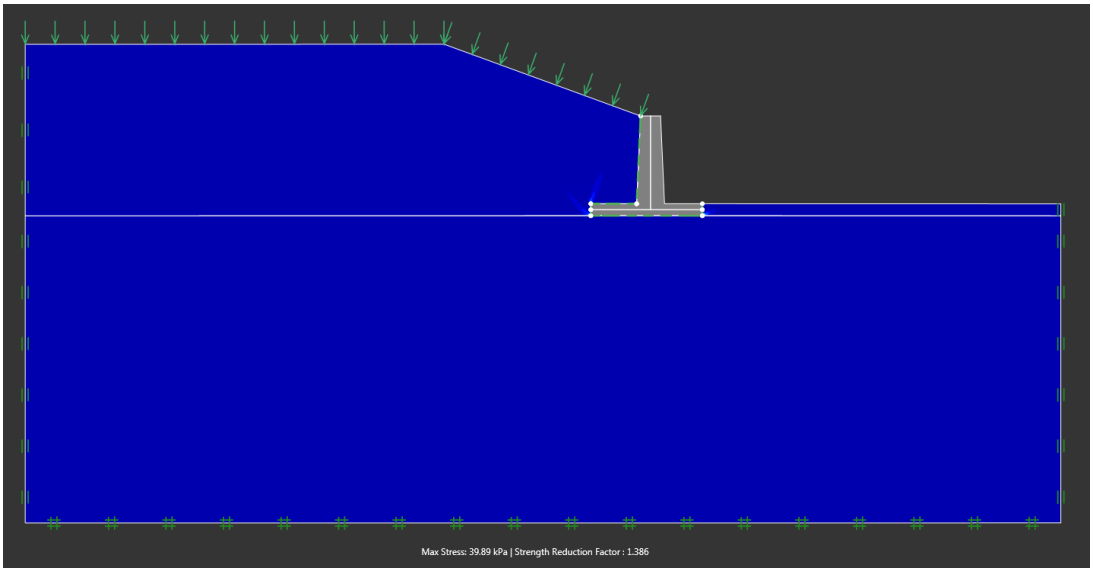

Figure 0.90 - Upper bound failure mode for case 45

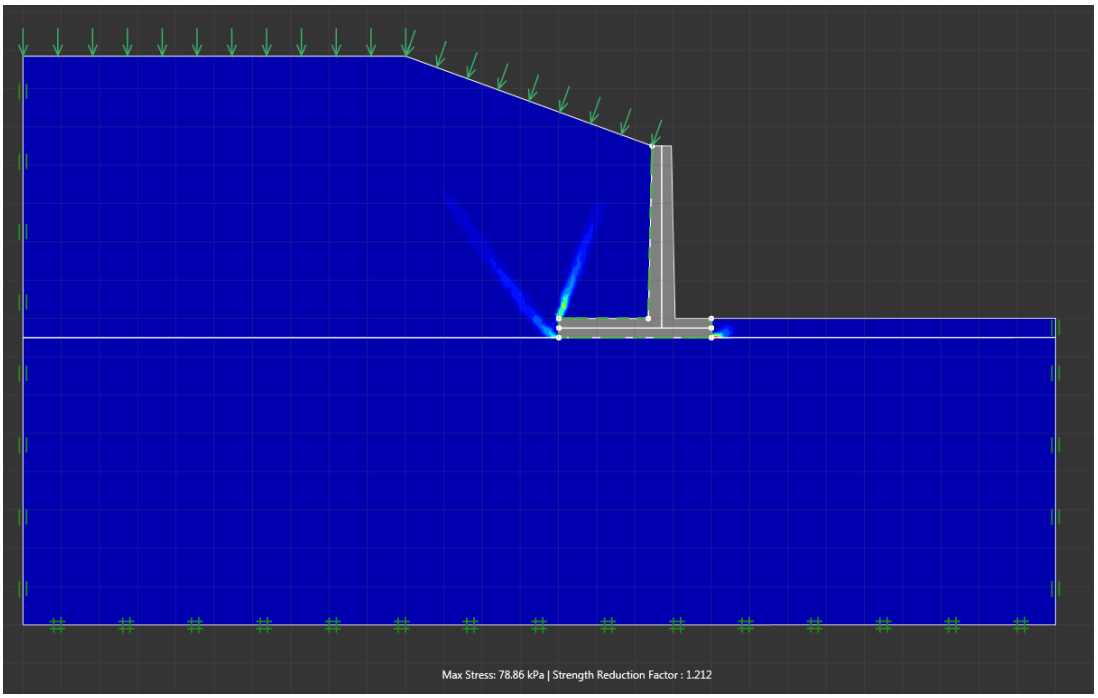

Figure 0.91 - Lower bound failure mode for case 46

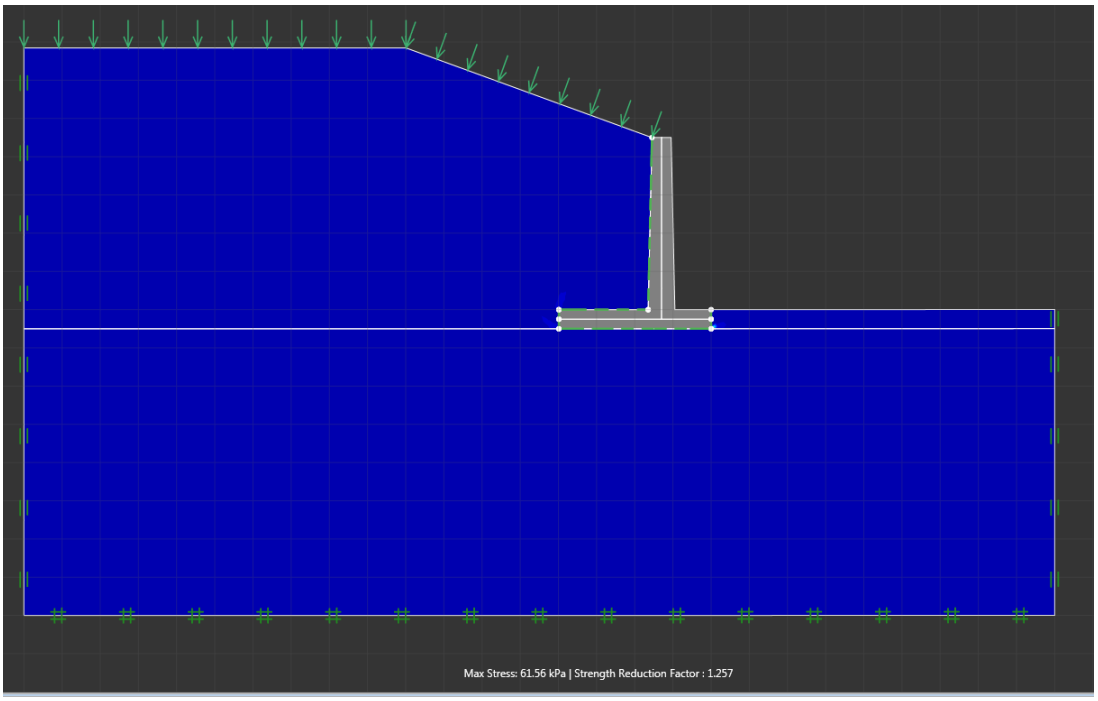

Figure 0.92 - Upper bound failure mode for case 46

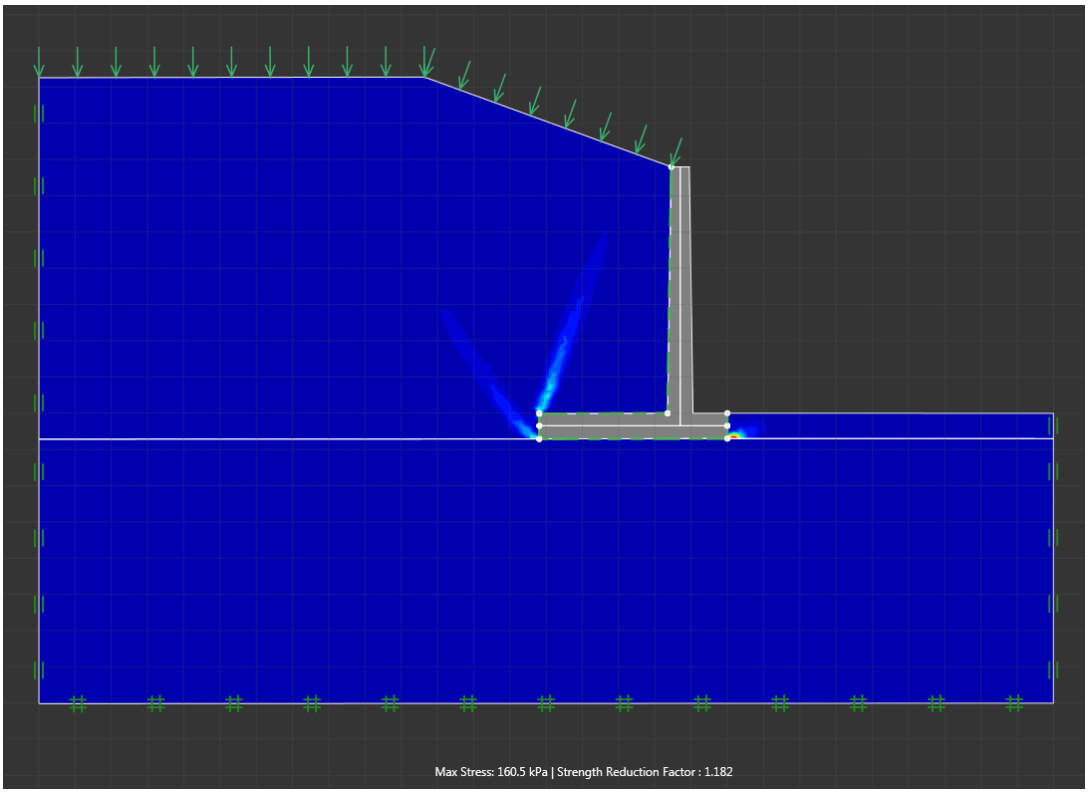

Figure 0.93 - Lower bound failure mode for case 47

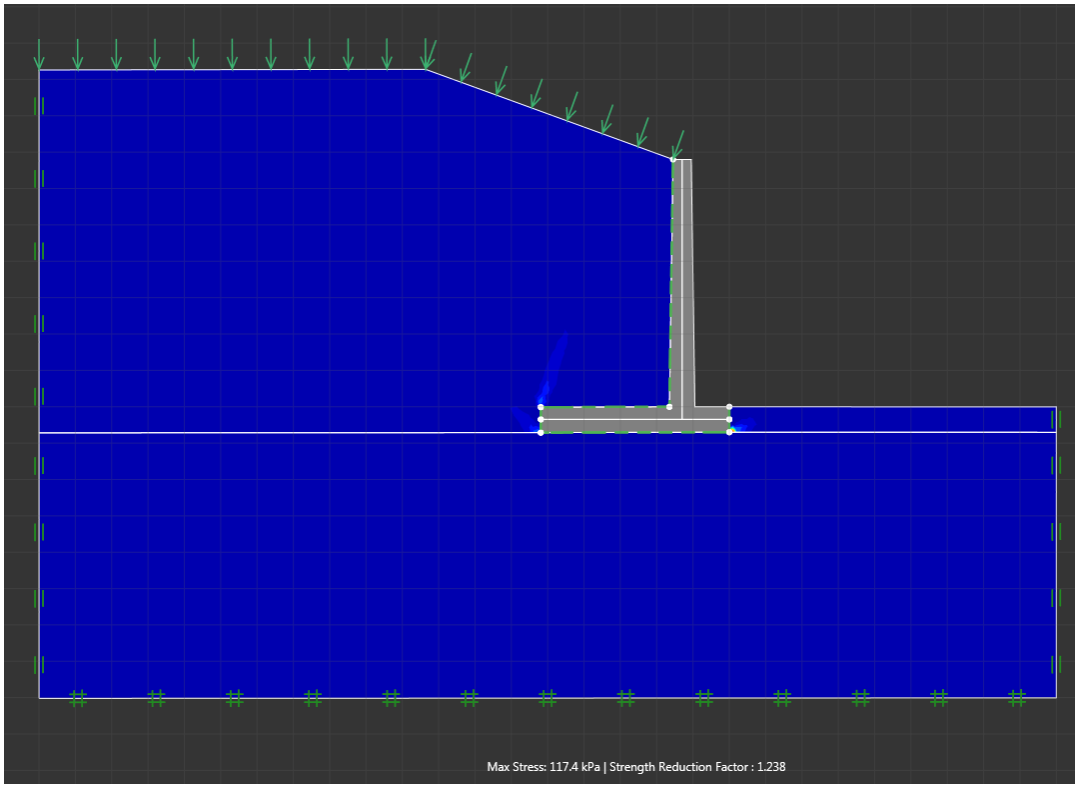

Figure 0.94 - Upper bound failure mode for case 47

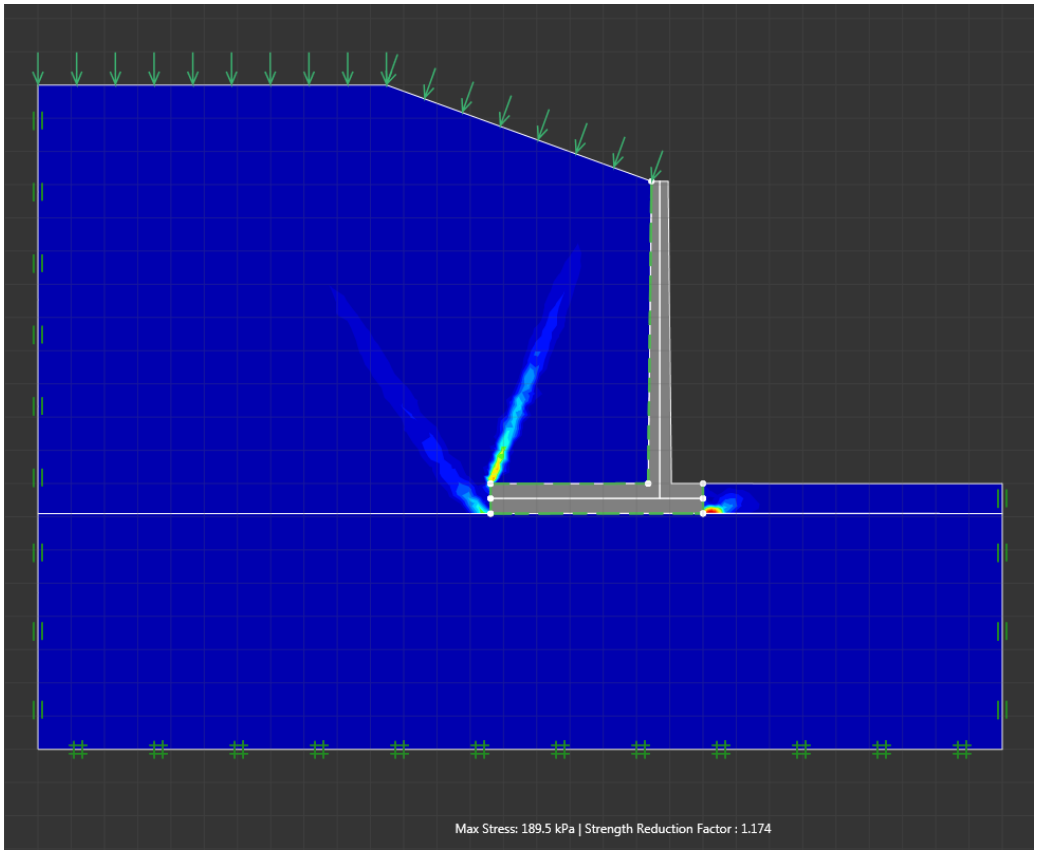

Figure 0.95 - Lower bound failure mode for case 48

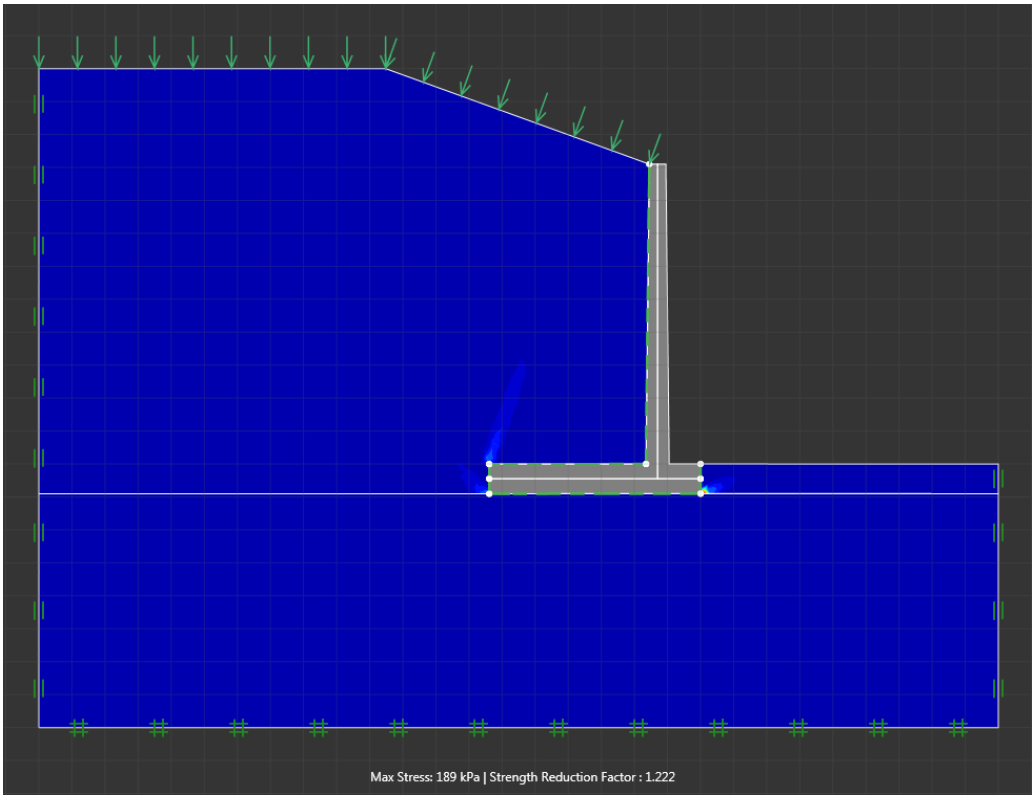

Figure 0.96 - Upper bound failure mode for case 48

Clay/Cl Silt Backfill

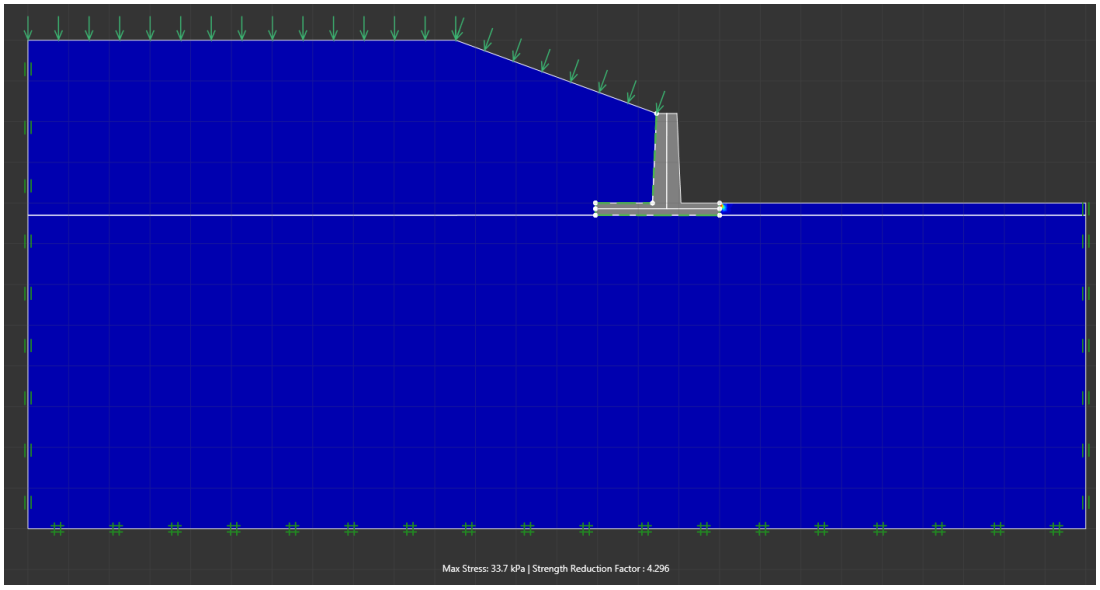

Figure 0.97 - Lower bound failure mode for case 49

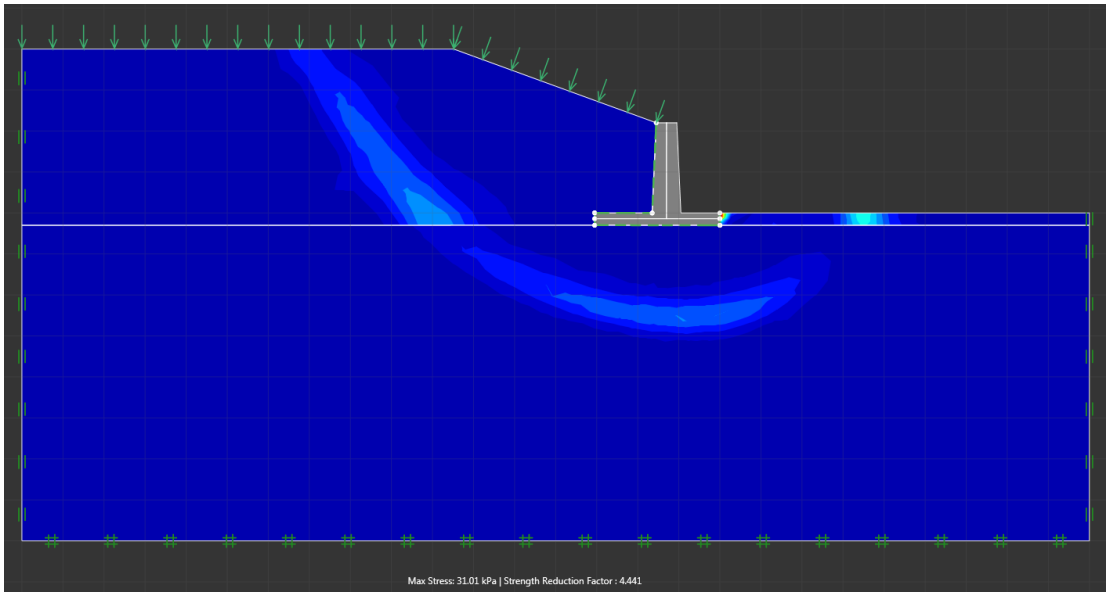

Figure 0.98 - Upper bound failure mode for case 49

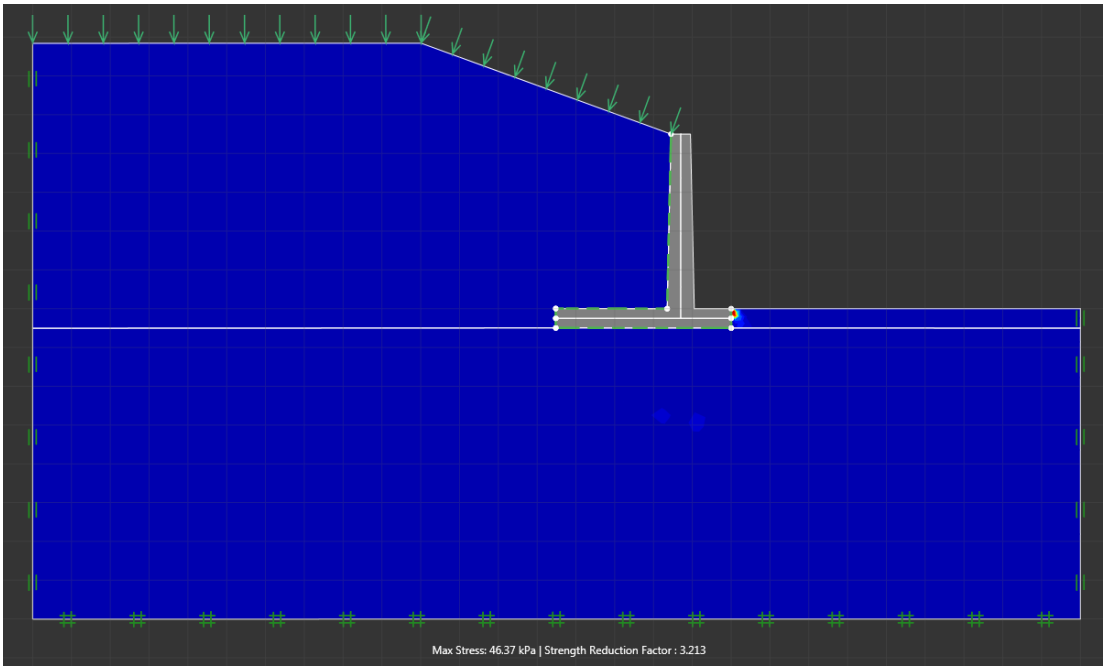

Figure 0.99 - Lower bound failure mode for case 50

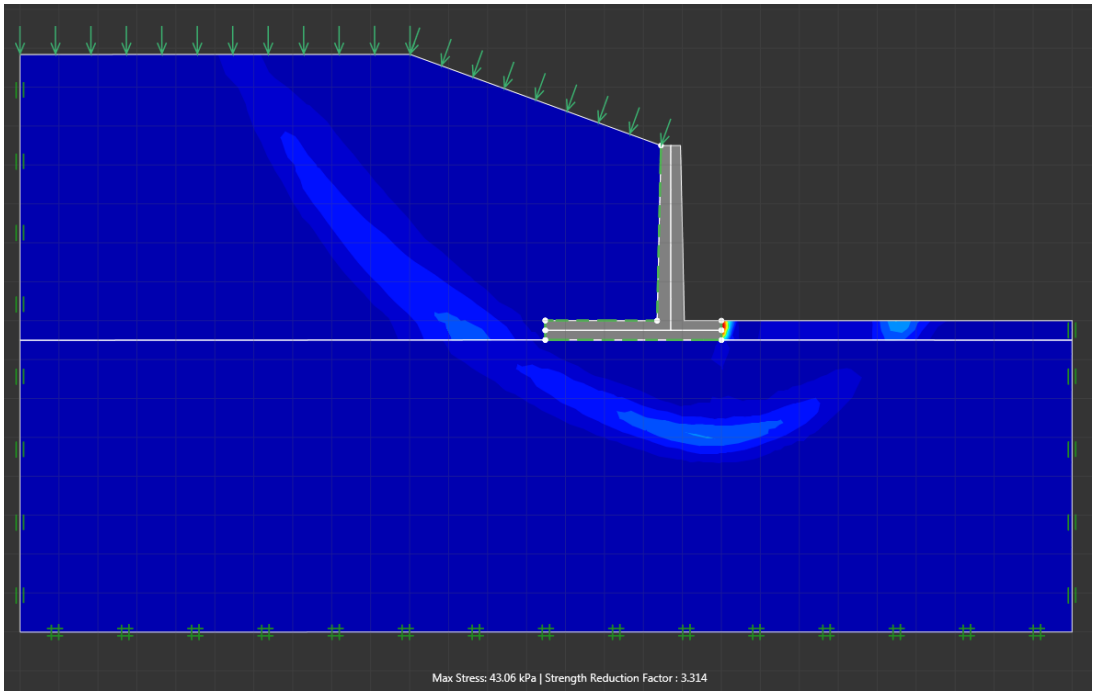

Figure 0.100 - Upper bound failure mode for case 50

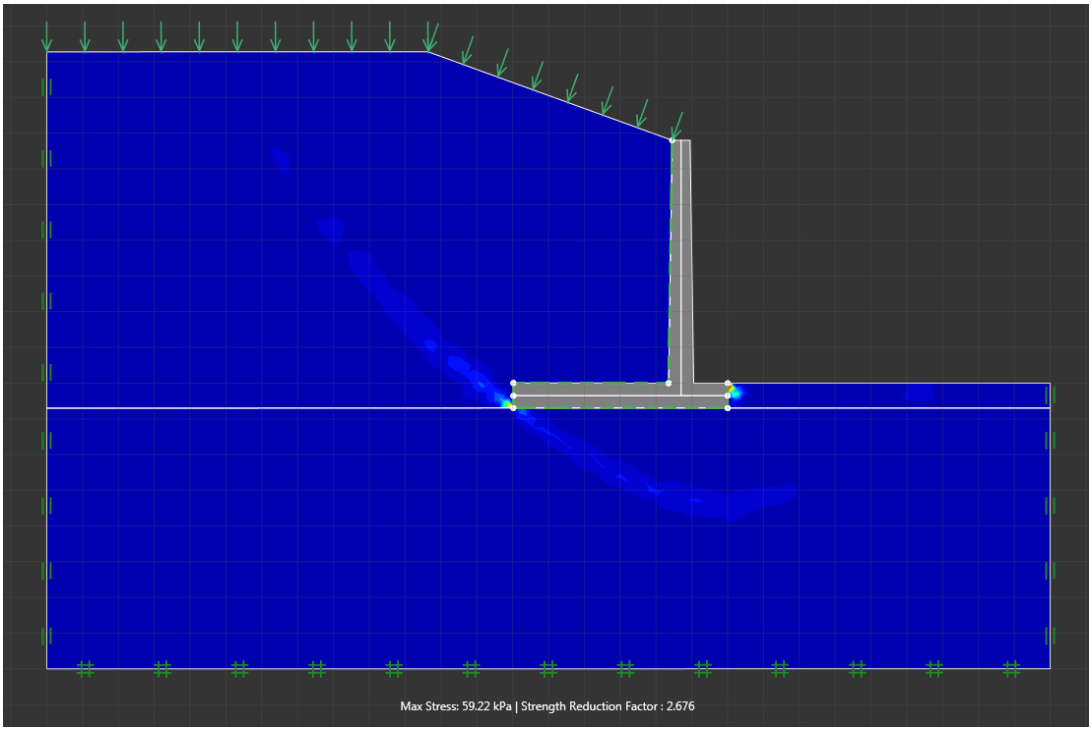

Figure 0.101 - Lower bound failure mode for case 51

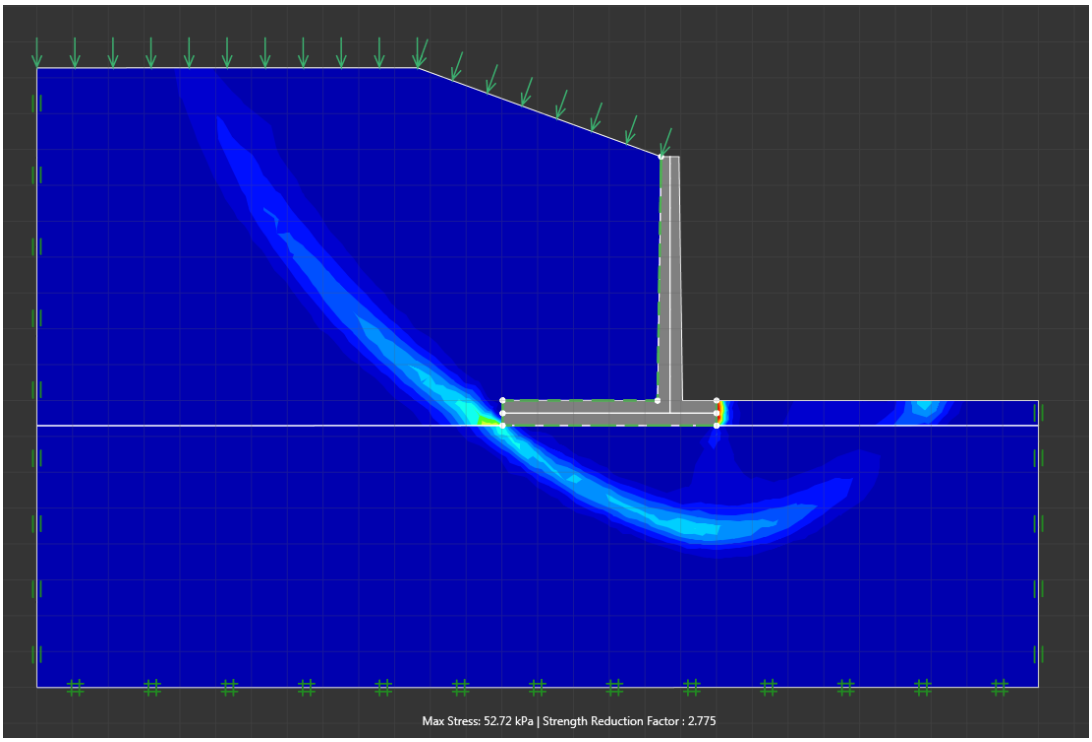

Figure 0.102 - Upper bound failure mode for case 51

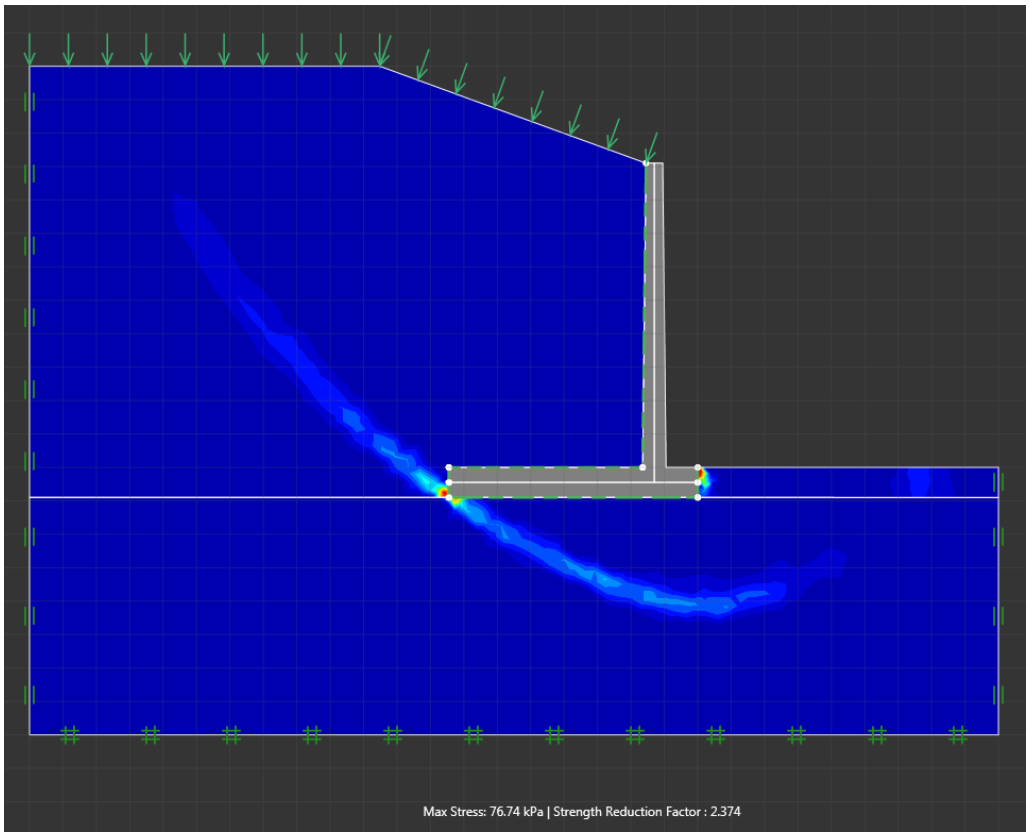

Figure 0.103 - Lower bound failure mode for case 52

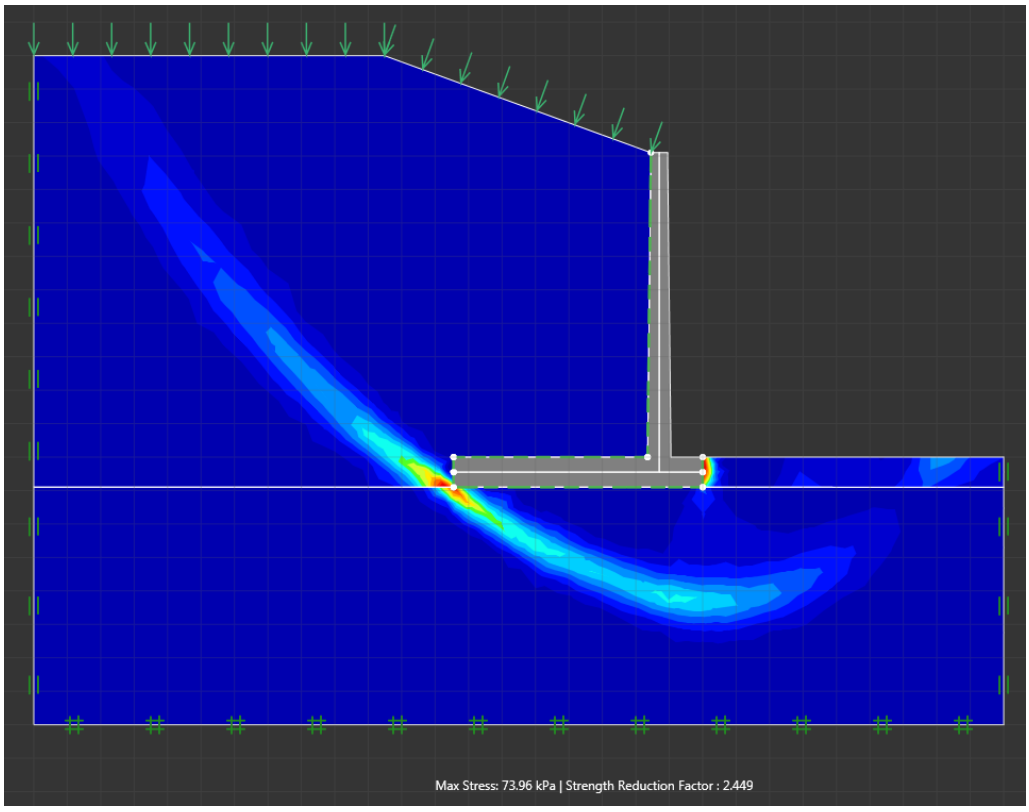

Figure 0.104 - Upper bound failure mode for case 52

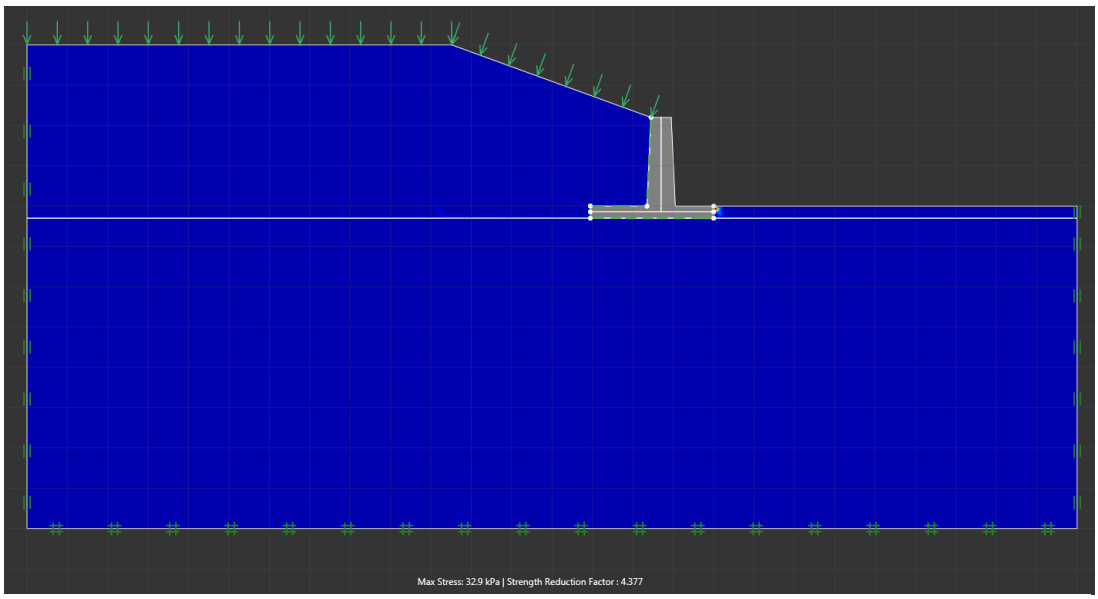

Figure 0.105 - Lower bound failure mode for case 53

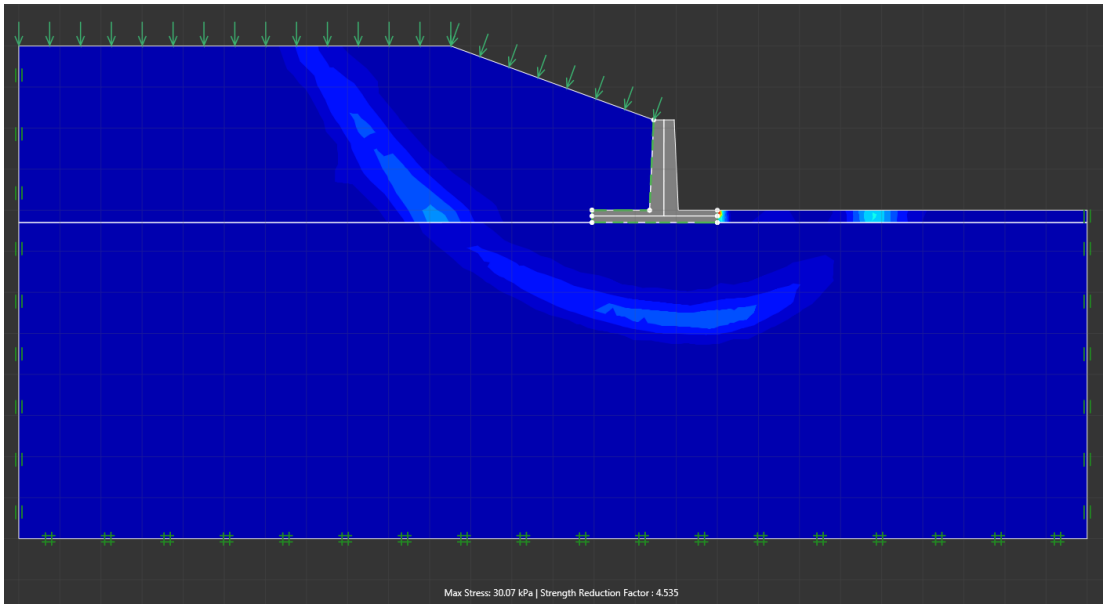

Figure 0.106 - Upper bound failure mode for case 53

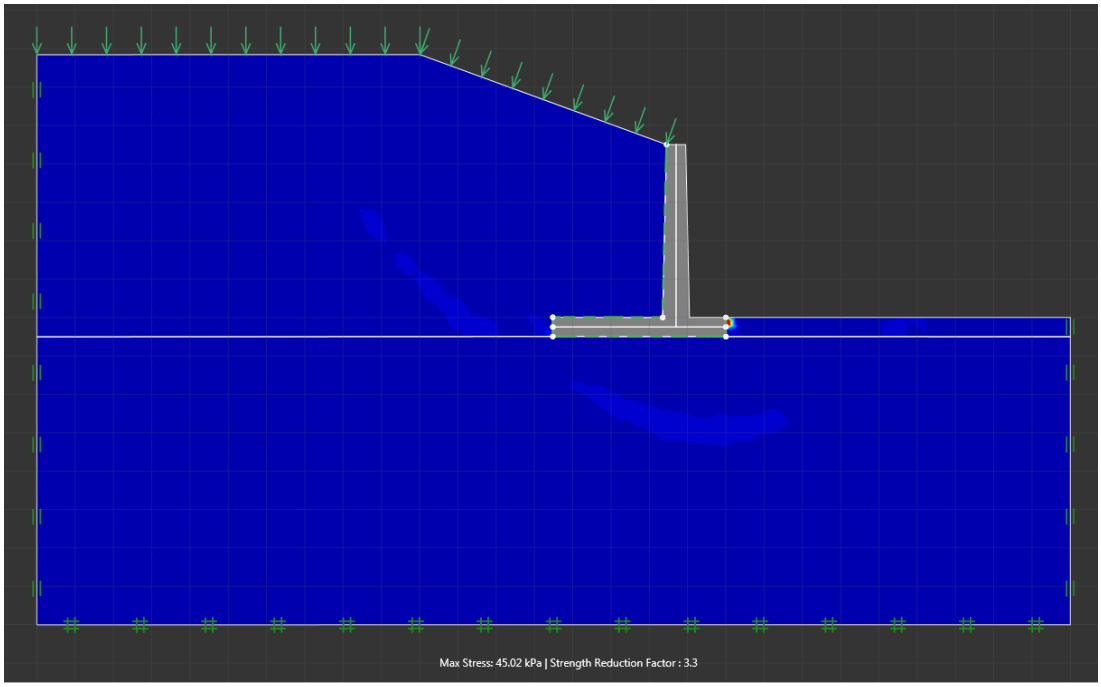

Figure 0.107 - Lower bound failure mode for case 54

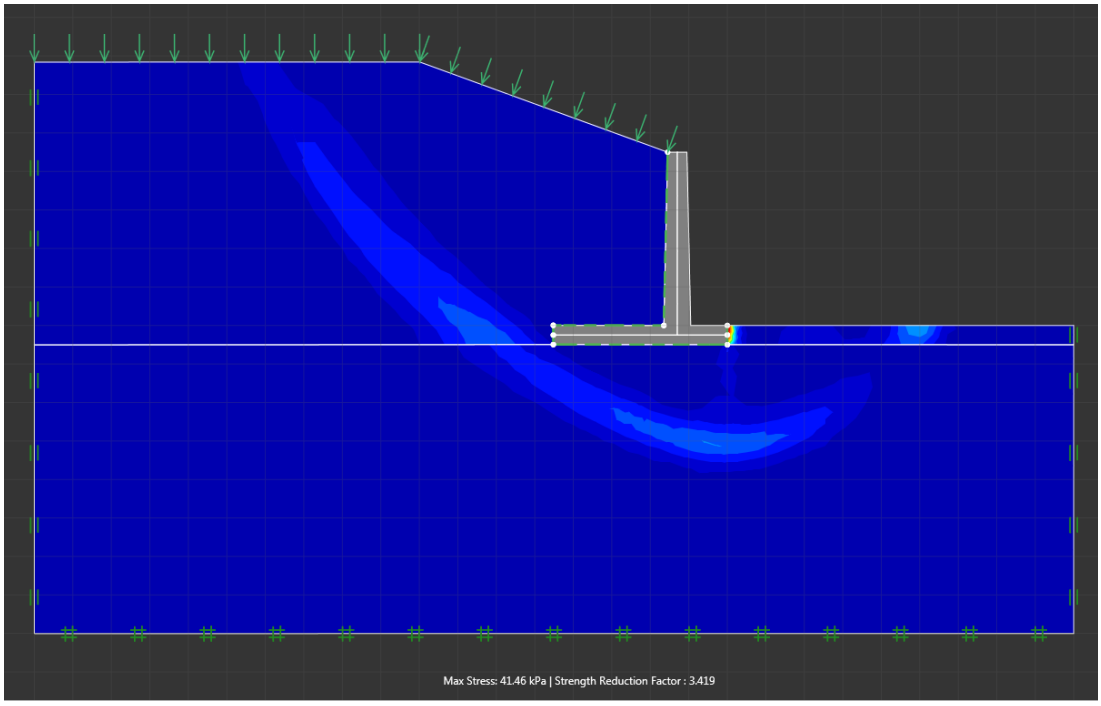

Figure 0.108 - Upper bound failure mode for case 54

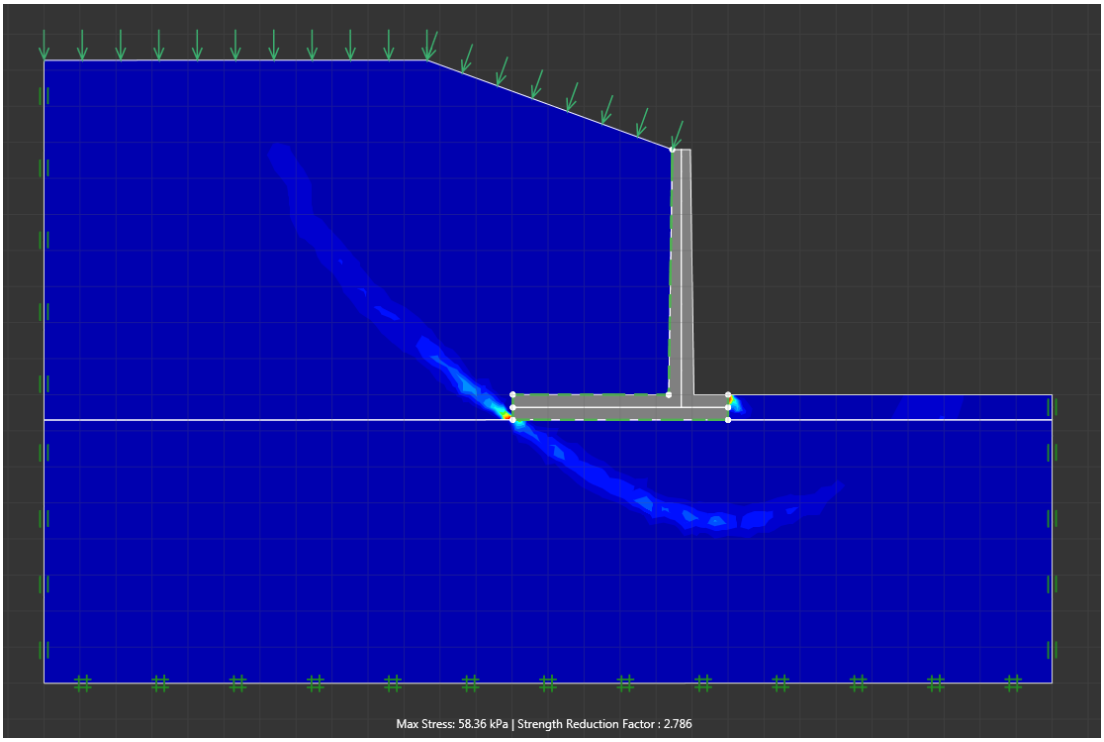

Figure 0.109 - Lower bound failure mode for case 55

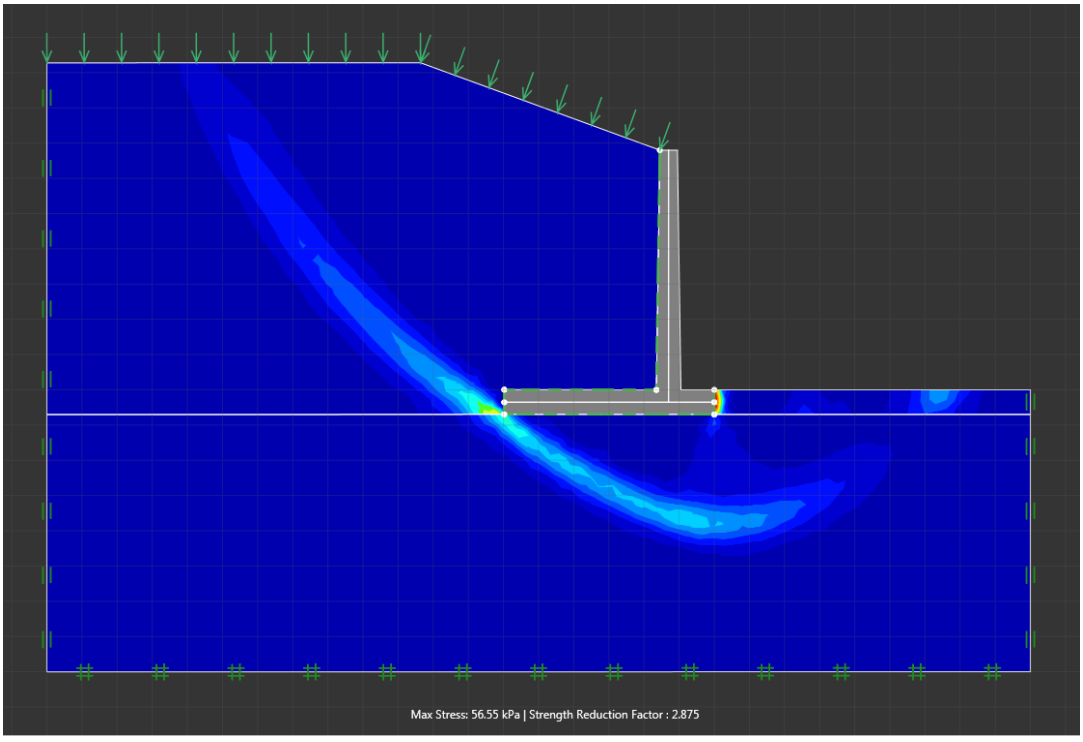

Figure 0.110 - Upper bound failure mode for case 55

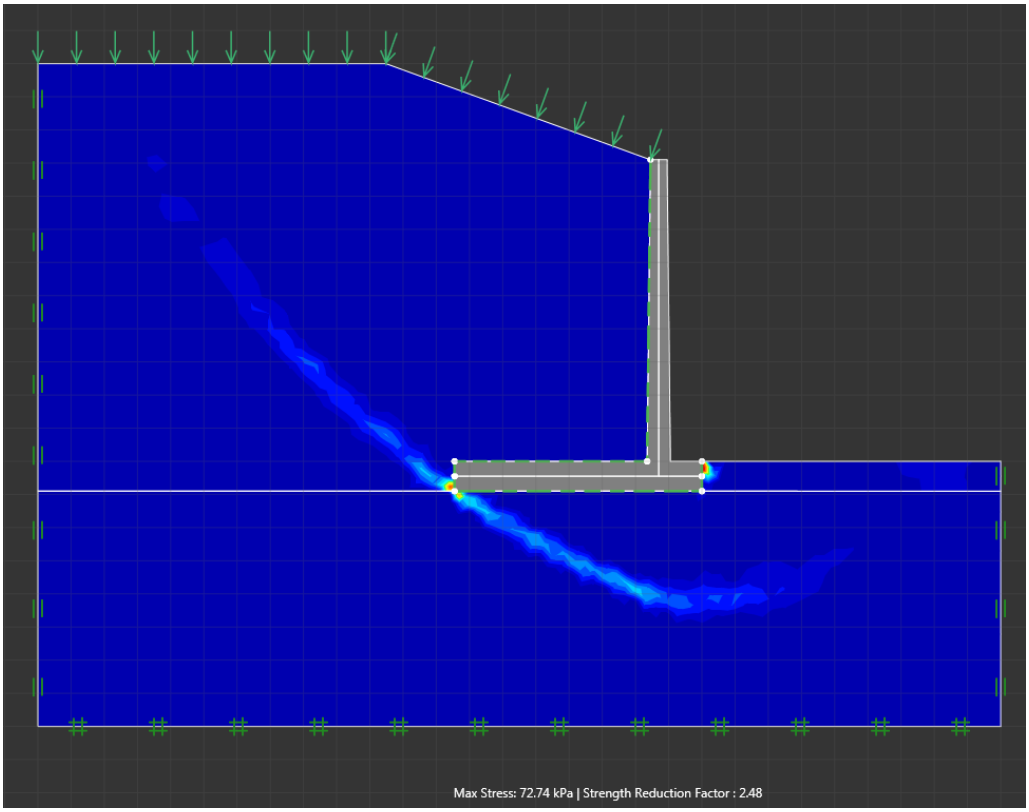

Figure 0.111 - Lower bound failure mode for case 56

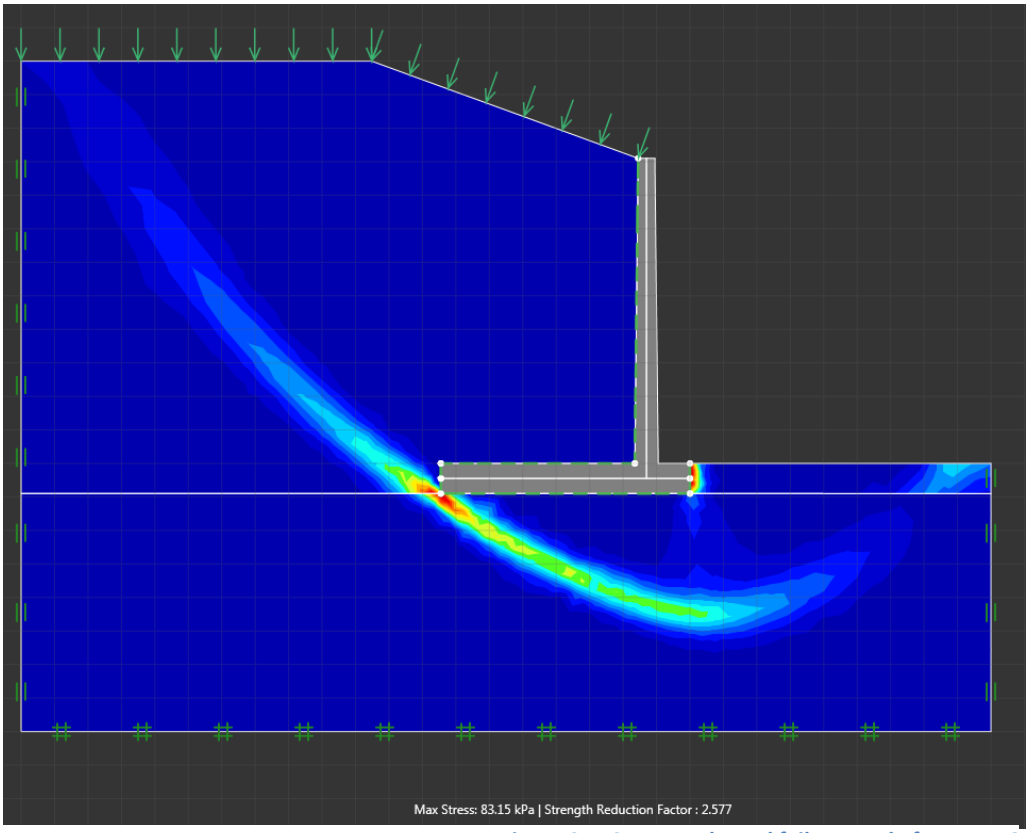

Figure 0.112 - Upper bound failure mode for case 56

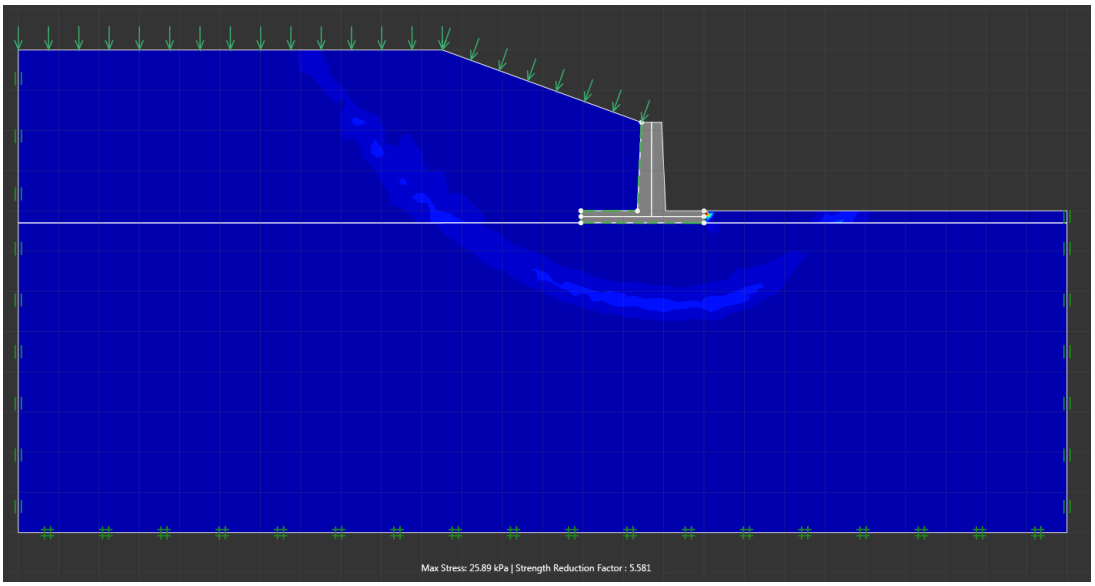

Figure 0.113 - Lower bound failure mode for case 57

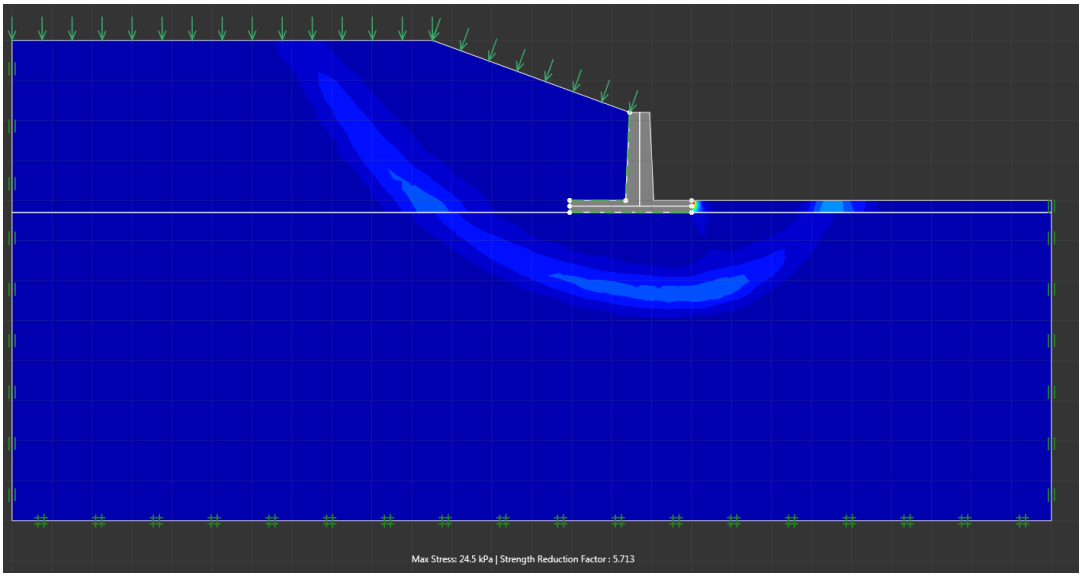

Figure 0.114 - Upper bound failure mode for case 57

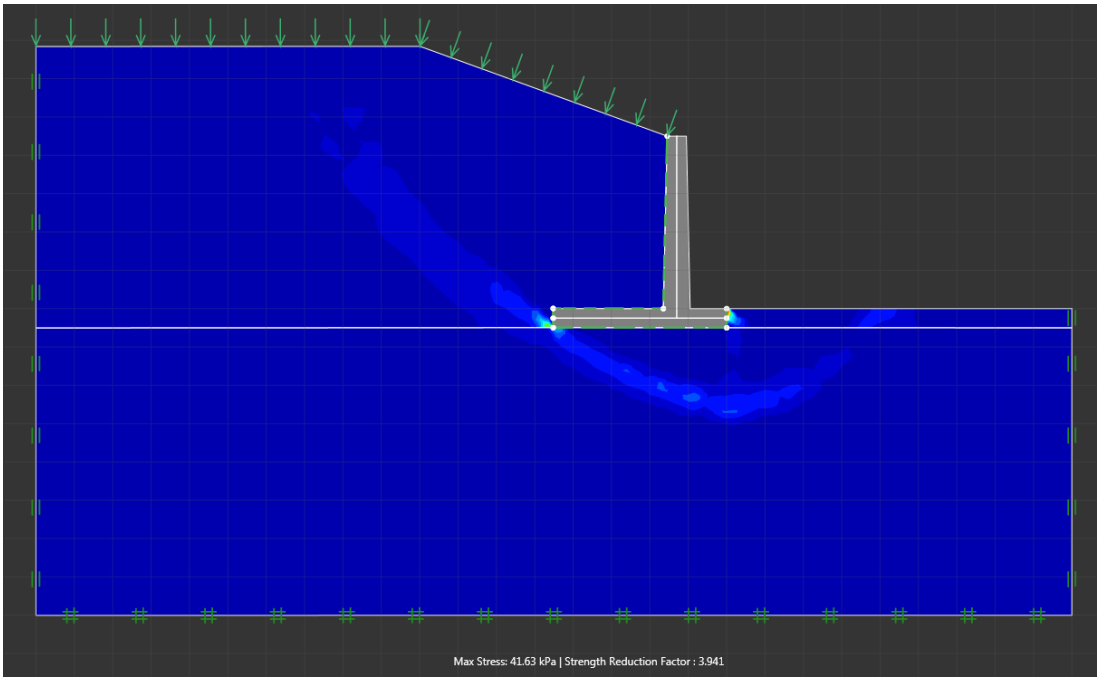

Figure 0.115 - Lower bound failure mode for case 58

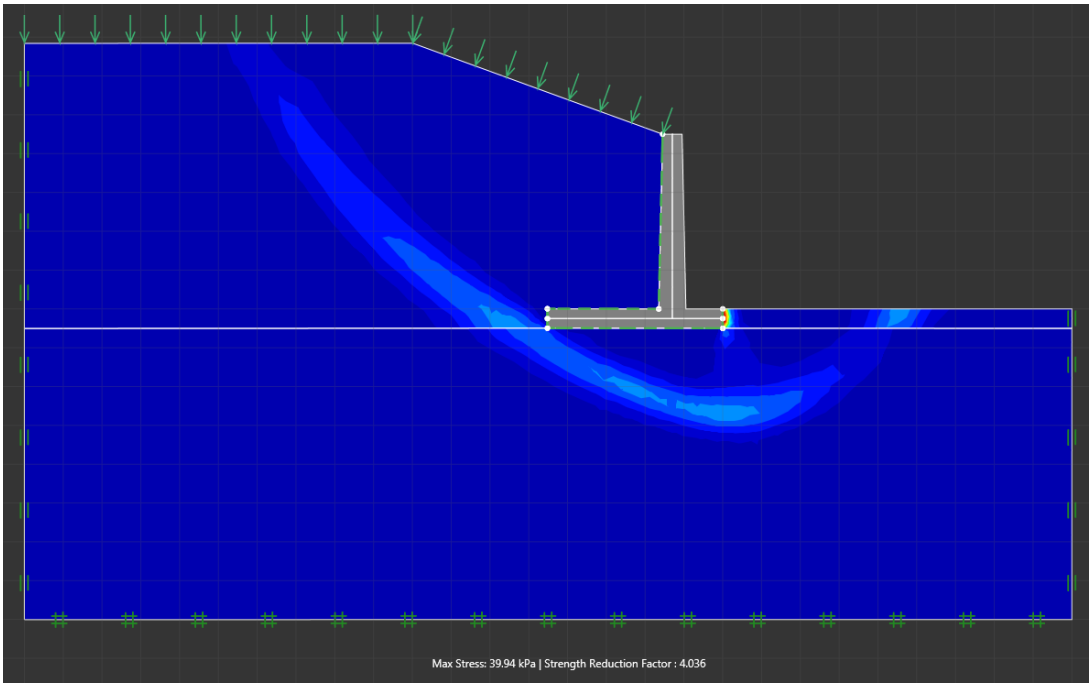

Figure 0.116 - Upper bound failure mode for case 58

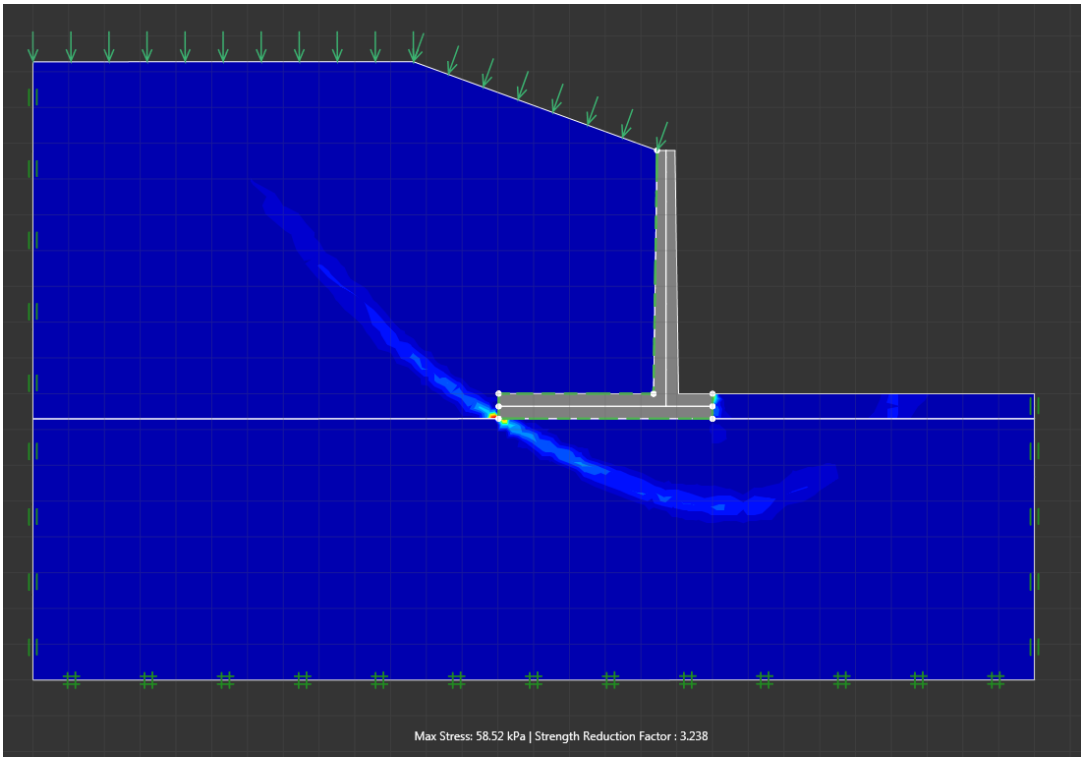

Figure 0.117 - Lower bound failure mode for case 59

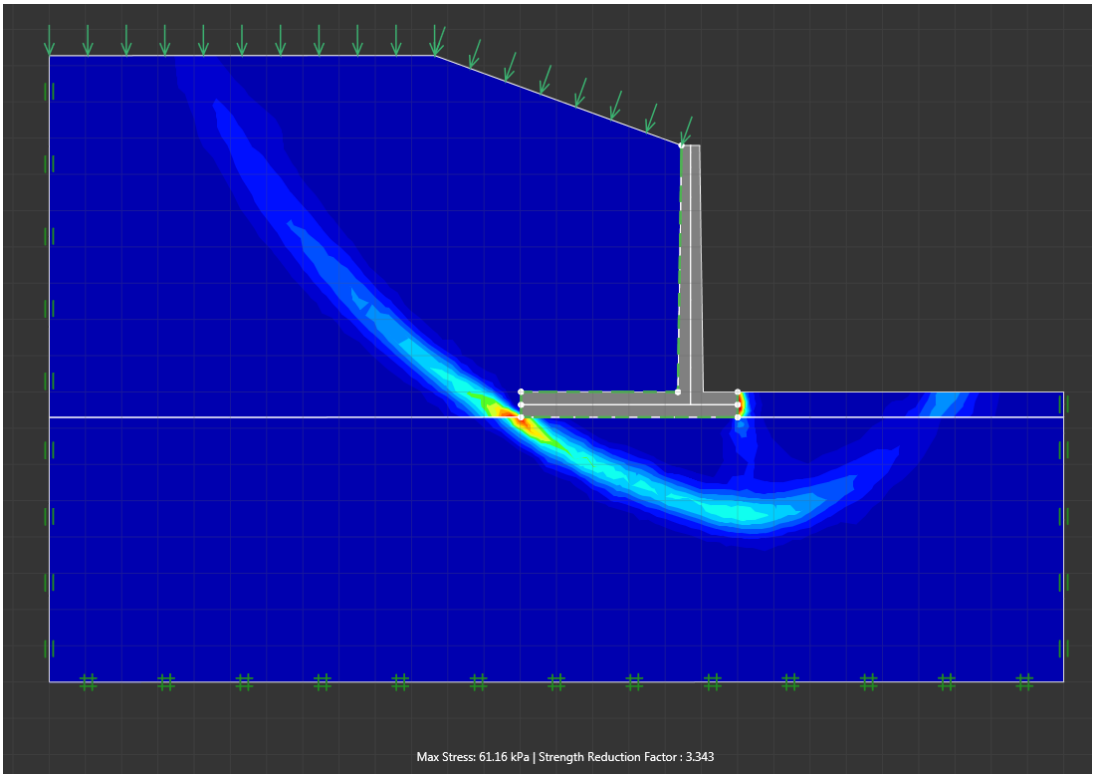

Figure 0.118 - Upper bound failure mode for case 59

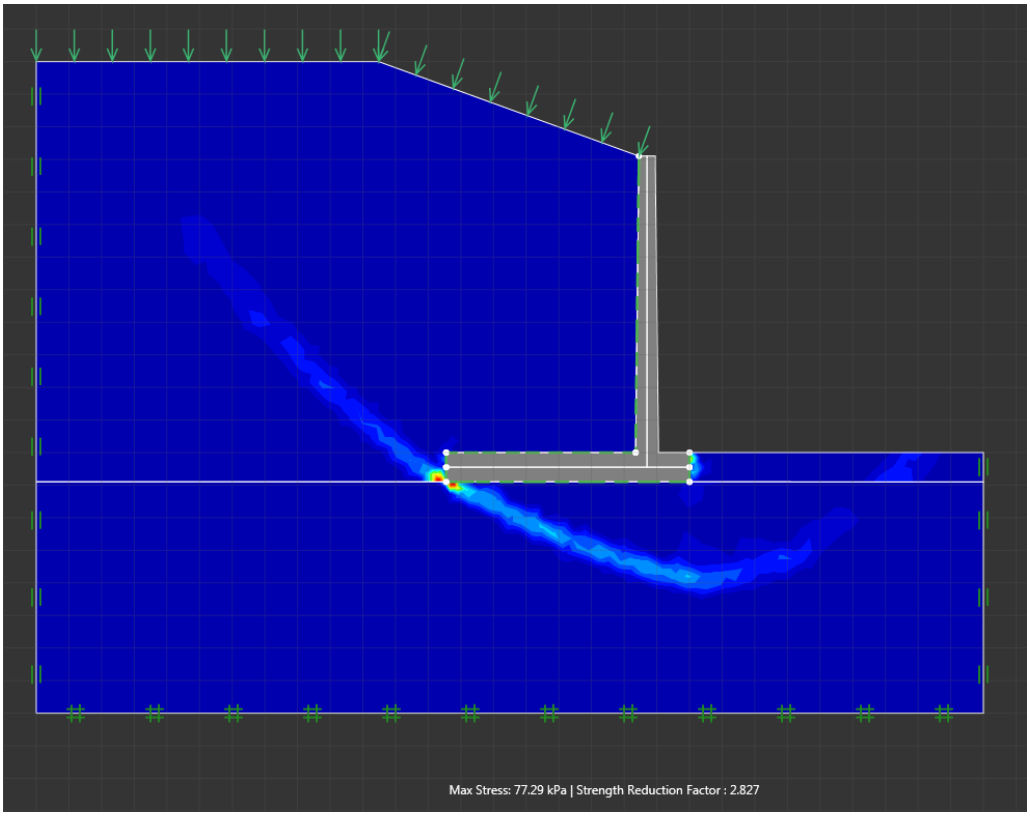

Figure 0.119 - Lower bound failure mode for case 60

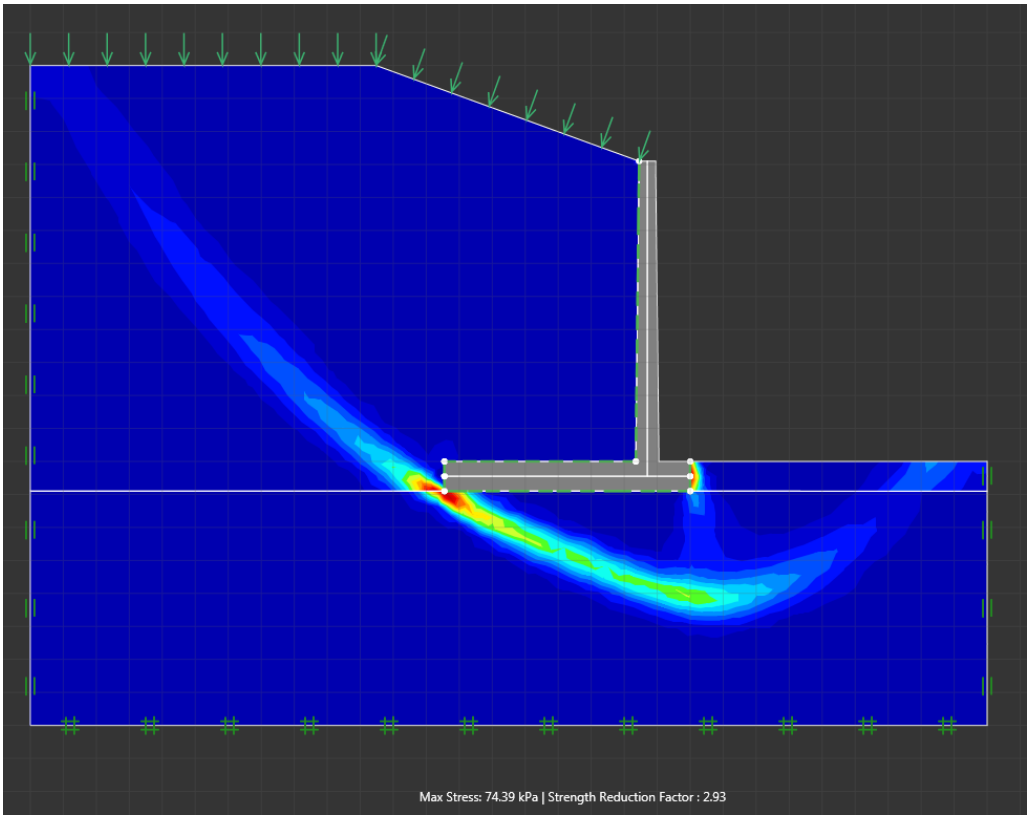

Figure 0.120 - Upper bound failure mode for case 60

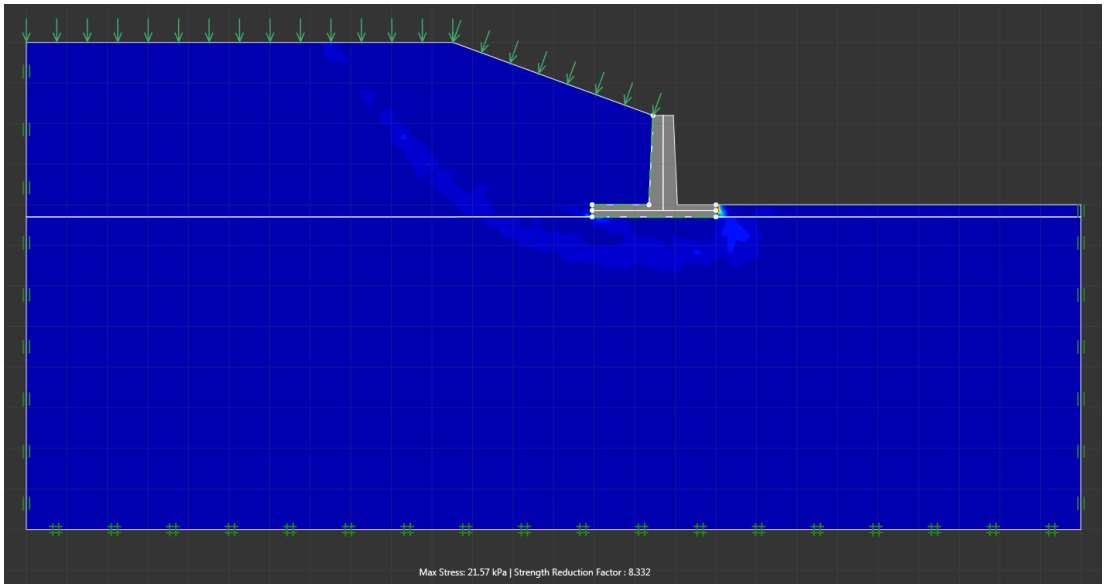

Figure 0.121 - Lower bound failure mode for case 61

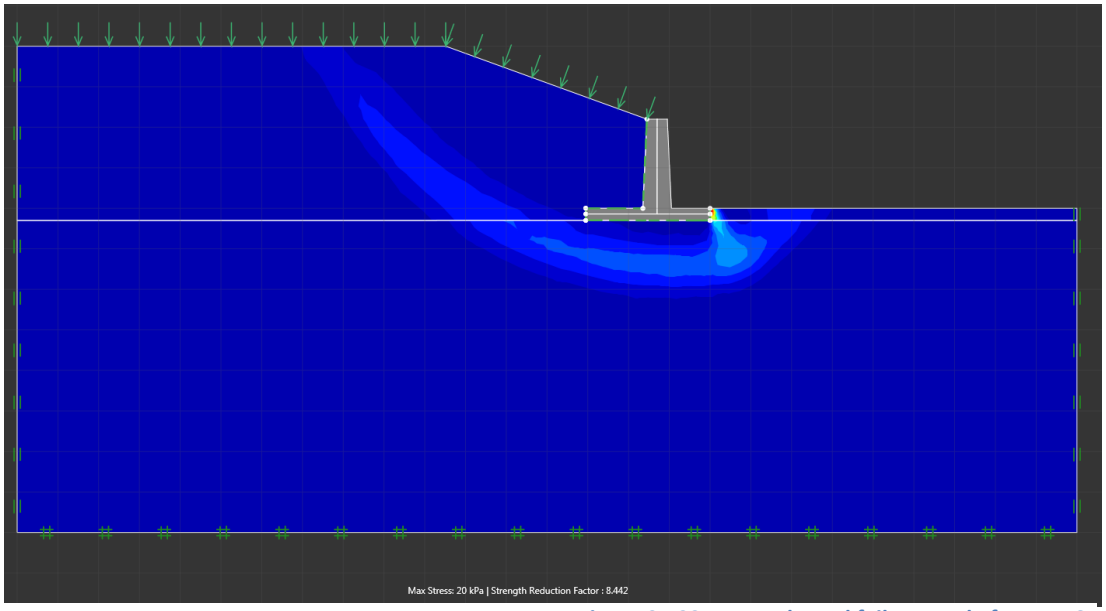

Figure 0.122 - Upper bound failure mode for case 61

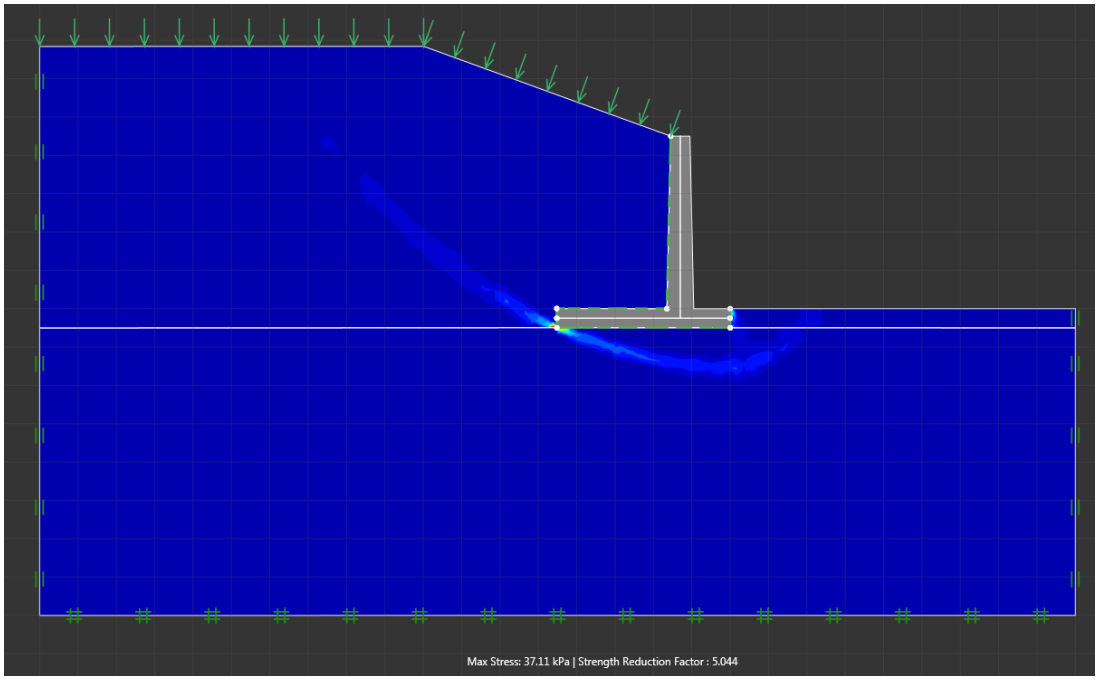

Figure 0.123 - Lower bound failure mode for case 62

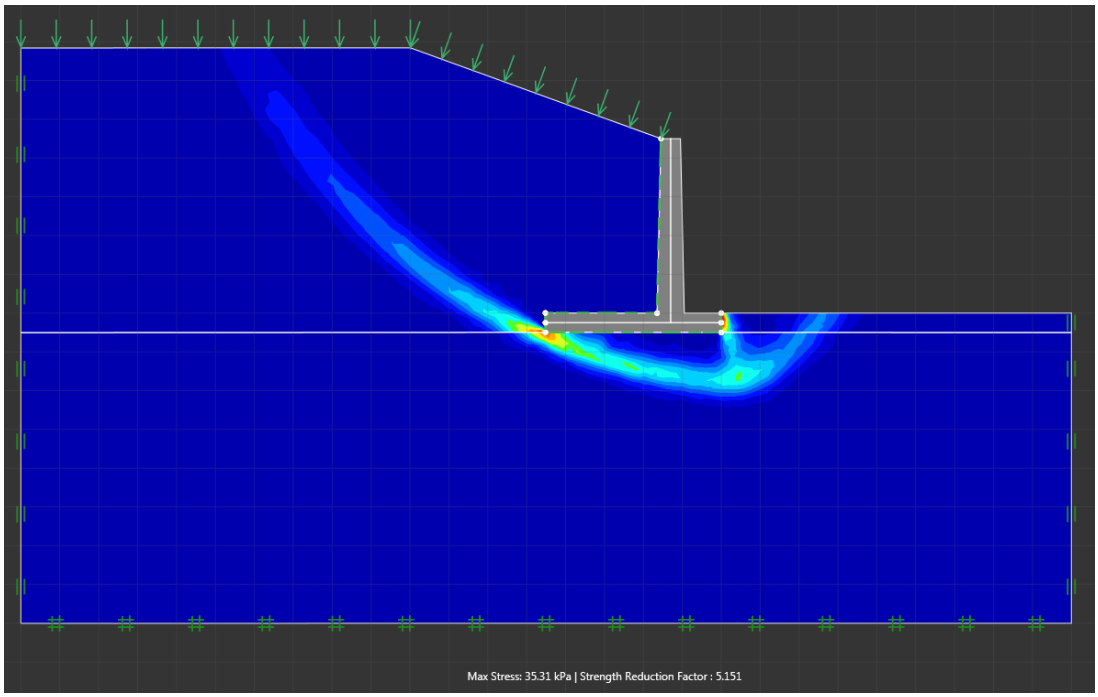

Figure 0.124 - Upper bound failure mode for case 62

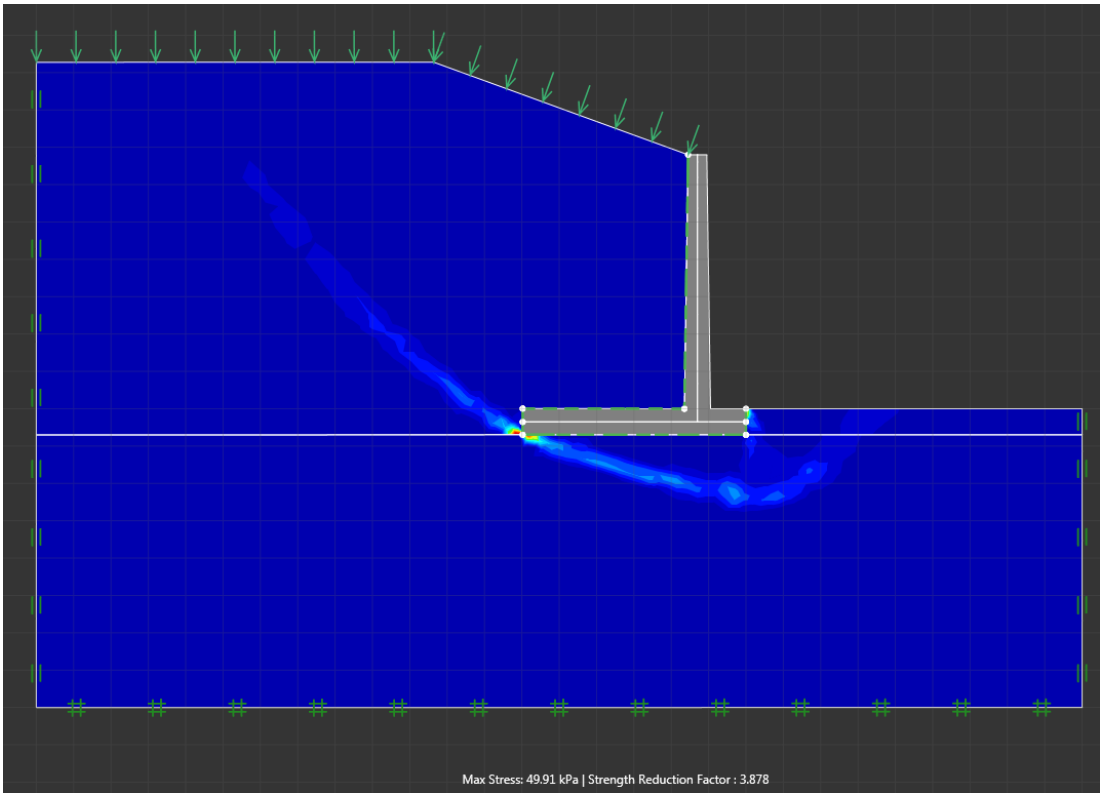

Figure 0.125 - Lower bound failure mode for case 63

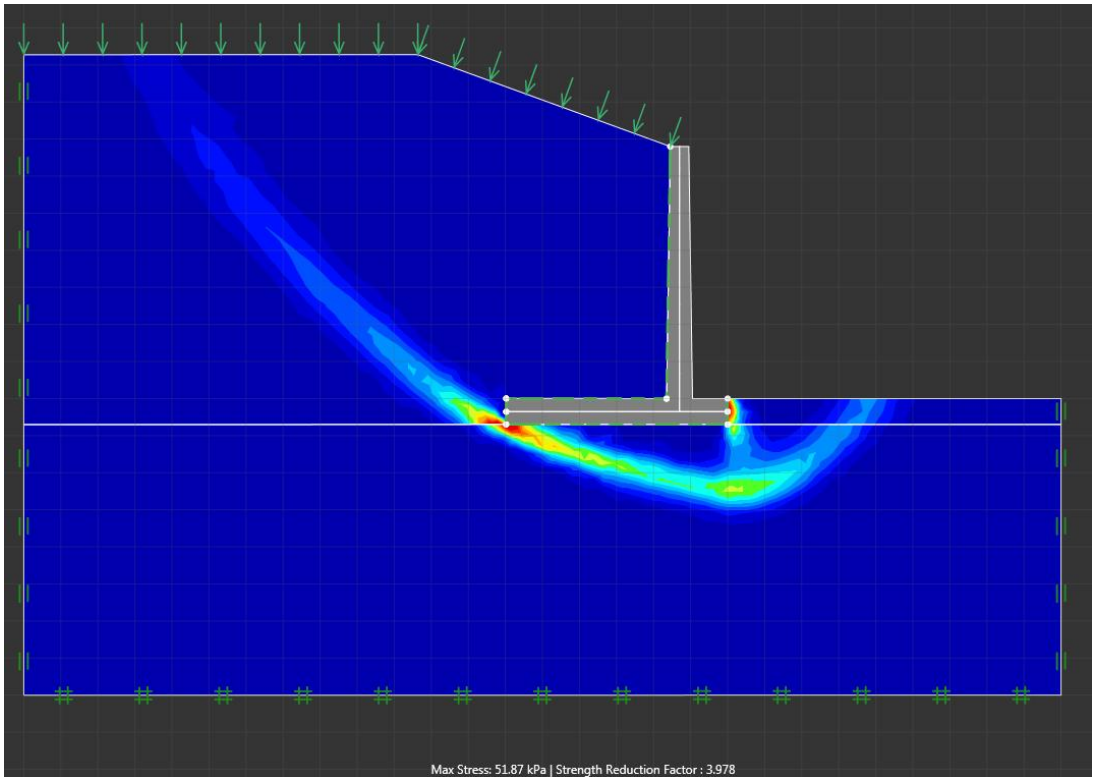

Figure 0.126 - Upper bound failure mode for case 63

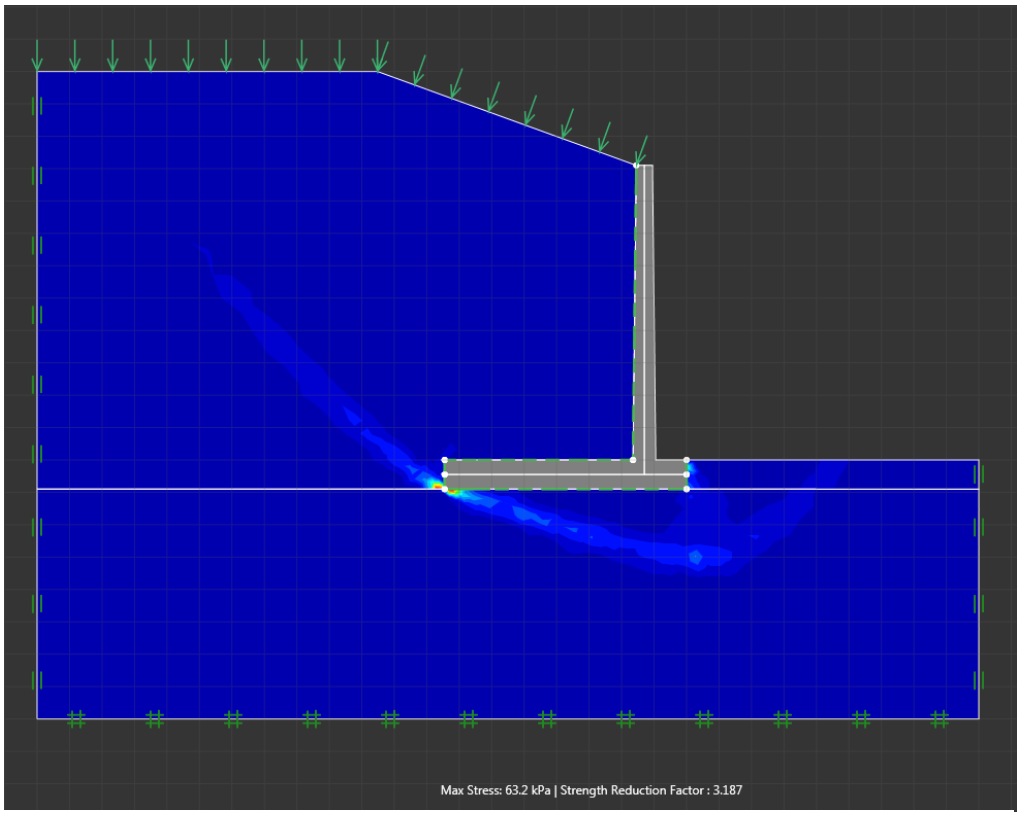

Figure 0.127 - Lower bound failure mode for case 64

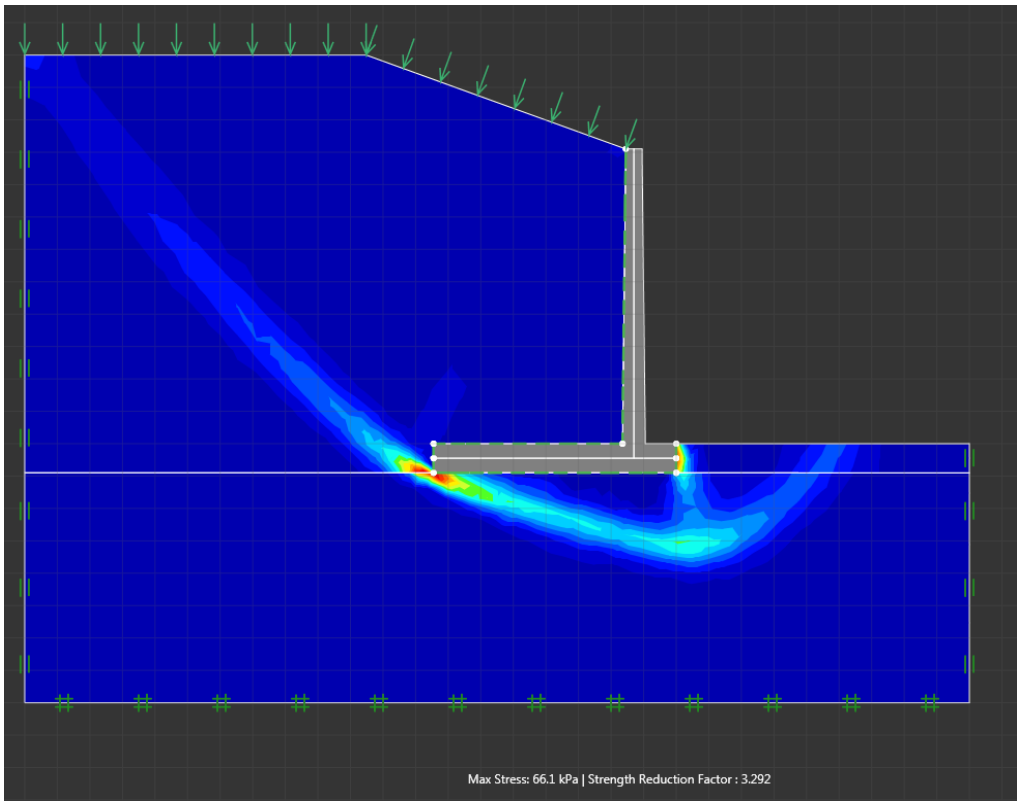

Figure 0.128 - Upper bound failure mode for case 64